TECHNISCHE UNIVERSITÄT MÜNCHEN
Lehrstuhl für Leichtbau

Structural Design Optimization Including Quantitative Manufacturing Aspects Derived from Fuzzy Knowledge

Martin Huber

Vollständiger Abdruck der von der Fakultät für Maschinenwesen der Technischen Universität München zur Erlangung des akademischen Grades eines

Doktor-Ingenieurs (Dr.-Ing.)

genehmigten Dissertation.

Vorsitzender: Univ.-Prof. Dr.-Ing. M. Lienkamp

Prüfer der Dissertation:

1. Univ.-Prof. Dr.-Ing. H. Baier

2. Univ.-Prof. Dr.-Ing. M. Zäh

Die Dissertation wurde am 15.09.2010 bei der Technische Universität München eingereicht und durch die Fakultät für Maschinenwesen am 07.12.2010 angenommen.

Bibliografische Information der Deutschen Nationalbibliothek
Die Deutsche Nationalbibliothek verzeichnet diese Publikation in der Deutschen Nationalbibliografie; detaillierte bibliografische Daten sind im Internet über
http://dnb.d-nb.de abrufbar.

ISBN 978-3-86853-806-9

Sternstr. 18, 80538 München
Tel.: 089/66060798
www.dr.hut-verlag.de

1. Auflage 2011

♦ Dedication ♦

This thesis is dedicated to my parents and my wife
for their love, endless support and encouragement.

Acknowledgments

I would like to express my gratitude to my supervisor Prof. Dr.-Ing. Horst Baier for his help and guidance. I am grateful for the trust he deposited in my work and his encouragement in different projects which finally resulted in this thesis. I would also like to thank the members of my committee Prof. Dr.-Ing. Michael Zäh and Prof. Dr.-Ing. Markus Lienkamp.
My thanks go to all colleagues at the Institute of Lightweight Structures at the Technische Universität München. Especially I would like to thank Ögmundur Petersson for the proofreading of my thesis and Max Wedekind and Thomas Kuhn for their advices in so many topics.

I would like to give my heartfelt appreciation to my parents, who always supported my interest in aeronautics and astronautics.

Finally I would like to give my admiration and gratitude to my wife Claudia, who has accompanied me with her love, unlimited patience, understanding and encouragement. Without her support, I wouldn't have been able to accomplish this work.

Unterschleißheim, December 2010 Martin Huber

Abstract

An innovative method for quantification of qualitative information within the framework of multidisciplinary structural optimization is presented in this thesis. The focus is on manufacturing aspects which are described by fuzzy data and expert knowledge. The method is applied to optimization of lightweight space frame parts. Manufacturing aspects change the optimal profile cross sections of extruded profiles and allow for trade-offs with respect to mass and manufacturability. The method is able to integrate otherwise neglected information into structural optimization, expand the problem formulation and finally gain additional insight into the optimal design.

Kurzfassung

Es werden Methoden zur Quantifizierung qualitativen Wissens in der Modellbildung zur multidisziplinren Strukturoptimierung untersucht, erweitert und an praktischen Beispielen umgesetzt. Insbesondere das Wissen ber Fertigungsaufwnde bei werkstoffhybriden Rahmenstrukturen wird damit in regelbasierten Typ-2-Fuzzy-Modellen abgebildet. Dadurch wird die Formulierung der Optimierungsaufgabe erweitert und vervollstndigt sowie das zugehrige Vorgehen zur Behandlung unscharfer Ziel- und Restriktionsinformationen vorgestellt. Aus diesem ganzheitlichen Prozess der Entwurfsoptimierung werden optimale Kompromisse und Hinweise bezglich der strukturmechanischen und fertigungstechnischen Aspekte gewonnen.

Contents

List of Figures

List of Tables

Nomenclatur

Acronyms

αCLO	α-cut level optimization
ANSYS®	Analysis System by ANSYS, Inc
Al	aluminum
ANN	artificial neural network
AZ31B	magnesium alloy AZ31B
AZ61A	magnesium alloy AZ61A
BBD	Box-Behnken designs of experiments
BHLS	bifocal hybrid laser welding
BoA	bisector of area
C1	crisp optimization run, with safety factor γ_1 in FLAME
C2	crisp optimization run, with safety factor γ_2 in FLAME
C3	crisp optimization run, with safety factor γ_3 in FLAME
CAD	computer aided design
CCD	central composite design of experiments
CCDi	circumscribed diameter
CE	composite extrusion
CER	cost estimating relationship
CFRS	carbon fiber reinforced silicone
CoA	center of area
CoG	center of gravity
CoS	center of support
CTE	coefficient of thermal expansion
CW-N440	composite wire with 50 Vol.% NEXTEL 440 fibers
CW-N610	composite wire with 60 Vol.% NEXTEL 610 fibers

CW-TP25 . . . . composite wire with 44 Vol.% Thornel P25 carbon fibers
CW-TP55 . . . . composite wire with 50 Vol.% Thornel P55 carbon fibers
CWR . . . . . Chen-Wang ranking for fuzzy numbers

DACE . . . . . Design and Analysis of Computer Experiments
DDO . . . . . deterministic design optimization
DFG . . . . . Deutsche Forschungsgemeinschaft - German Research Foundation
DLR . . . . . Deutsches Zentrum für Luft- und Raumfahrt - German Aerospace Center
DOE . . . . . design of experiments
DPR . . . . . Dubois-Prade ranking for fuzzy numbers
DSS . . . . . decision support system

E . . . . . Young's modulus
EBDO . . . . . evidence based design optimization
EKM . . . . . enhanced Karnik-Mendel algorithm
EN AW-2017 . . aluminum alloy EN AW-2017
EN AW-2024 . . aluminum alloy EN AW-2024
EN AW-2099 . . aluminum alloy EN AW-2099
EN AW-6056 . . aluminum alloy EN AW-6056
EN AW-6060 . . aluminum alloy EN AW-6060
EN AW-6082 . . aluminum alloy EN AW-6082
EN AW-7075 . . aluminum alloy EN AW-7075
ES . . . . . evolutionary strategy

FαLA . . . . . fuzzy α-level analysis
FEM . . . . . finite element method
FEMSP . . . . . finite element method for stochastic problems
FFD . . . . . full factorial design of experiments
FFD . . . . . fractional factorial design of experiments
FL . . . . . fuzzy logic
FLAME . . . . . Flexible Antenna Membrane Experiment
FORM . . . . . first order reliability method
FOU . . . . . footprint of uncertainty
FRBS . . . . . fuzzy rule-based system

FRM . . . . . fast recursive method
FSW . . . . . friction-stir welding

GαD . . . . . gradual α-level decreasing algorithm
GA . . . . . genetic algorithm
GAME . . . . . Genetic Algorithm for Multicriteria Engineering
GT2 FS . . . . . geometric type-2 fuzzy set

HAZ . . . . . heat affected zone

IA . . . . . interval analysis
IASCO . . . . . iterative algorithm with stop condition
IS . . . . . importance sampling
IT2 FS . . . . . interval type-2 fuzzy set
iTWFC . . . . . inverse of Tsai-Wu strength ratio index failure criterion

KGM . . . . . kriging method
KM . . . . . Karnik-Mendel algorithm

LDR . . . . . large deployable antenna reflector
LHS . . . . . latin hypercube sampling
LIA . . . . . level interval algorithm
LLB . . . . . Institute for Lightweight Structures - Technische Universität München
LoM . . . . . largest of maximum
LSA . . . . . limit state approximation
LSF . . . . . limit state function

MATLAB . . . . . MATrix LABoratory - commercial software from "The MathWorks, Inc."
MCS . . . . . Monte Carlo sampling
MF . . . . . membership function
Mg . . . . . magnesium
MoM . . . . . mean of maximum

ND . . . . . grade of necessity of dominance
NOVESPACE . . . owner and operator of Airbus A300 ZERO-G
NSD . . . . . grade of necessity of strict dominance

opTUM . . . . . algorithm for optimization with type-1 fuzzy uncertainties
opTUM-II . . . . algorithm for optimization with type-2 fuzzy uncertainties

PAEM . . . . . Padé approximants with extrema management
PBDO . . . . . possibility-based design optimization
PD . . . . . grade of possibility of dominance
PDF . . . . . probability density functions
PP . . . . . physical programming
PSD . . . . . grade of possibility of strict dominance

RBDO . . . . . reliability-based design optimization
RBF . . . . . radial basis function
RD . . . . . robust design
RDO . . . . . robust design optimization
RMS . . . . . root mean square error
RSA . . . . . response surface approximation
RSM . . . . . response surface method

SFB-TR10 . . . . Collaborative Research Center SFB Transregio 10
SFEM . . . . . stochastic finite element method
SHCBF . . . . . six-hump camel back function
SMART . . . . . shell membrane antenna reflector technology
SoM . . . . . smallest of maximum
SORM . . . . . second order reliability method
SPR . . . . . Sengupta-Pal ranking for interval numbers
SQP . . . . . sequential quadratic programming based optimization algorithm
SW-1.4310 . . . . steel wire 1.4310 (X10CrNi18-8)
SW-Nanoflex . . steel wire Nanoflex
SW-Nivaflex . . steel wire Nivaflex

T1-FRBS . . . . . type-1 fuzzy rule-based system
T1 FS . . . . . type-1 fuzzy set
T2-FRBS . . . . . type-2 fuzzy rule-based system
T2 FS . . . . . type-2 fuzzy set
TBT . . . . . ten bar truss

TEEM . . . . . Taylor's expansion with extrema management method

U1 . . . . . optimization run with uncertainties, two goals and six constraints

U2 . . . . . optimization run with uncertainties and four goals

VM . . . . . vertex method

VMgt . . . . . general transformation method

VMgtr . . . . . general transformation method with removed recurring points

VMo . . . . . optimized vertex method

VMrt . . . . . reduced transformation method

VMst . . . . . short transformation method

VMt . . . . . transformation method

Symbols

$\varnothing$ . . . . . empty set
a . . . . . acceleration
A . . . . . crisp set
$\tilde{A}$ . . . . . type-1 fuzzy set
$\tilde{\tilde{A}}$ . . . . . type-2 fuzzy set
α . . . . . threshold for α-cut level
α_{max} . . . . . maximum allowed possibility by α-cut level
b . . . . . wall thickness
B . . . . . width of cross section
β_i^{FSB} . . . . . fiber angle in layer i bottom face sheet
β_i^{FST} . . . . . fiber angle in layer i top face sheet
β . . . . . feasibility index in RDO
c_l . . . . . left boundary of centroid of interval type-2 fuzzy set
c_r . . . . . right boundary of centroid of interval type-2 fuzzy set
C . . . . . core of fuzzy set
C_c . . . . . centroid of fuzzy set
d_{fg}^1 . . . . . normal distance between crisp and fuzzy constraint boundary
$d_{L\mu}$ . . . . . distance measure left boundary of fuzzy set
$d_{R\mu}$ . . . . . distance measure right boundary of fuzzy set
d_S . . . . . distance of reinforcing element from stringer
ΔC . . . . . deviation of contour from designed contour
Δp_{rez} . . . . . deviation of position for reinforcing elements
ΔT . . . . . temperature difference
E . . . . . Young's modulus
E_c . . . . . Young's modulus composite material
ϵ_α^r . . . . . maximum error for comparison of real and surrogate system answer
ϵ_i^h . . . . . error boundary for equality constraint

f . . . . . objective function scalar
$\mathbf{f}$ . . . . . objective function vector
$\tilde{\mathbf{f}}$ . . . . . uncertain objective function vector
f_1 . . . . . reinforcement ratio in horizontal outer cross section
f_2 . . . . . reinforcement ratio in vertical outer cross section
f_P . . . . . focal length parabola
F . . . . . force
F_B . . . . . buckling load
g . . . . . inequality constraint function scalar
$\tilde{\mathbf{g}}$ . . . . . uncertain inequality constraint vector
G . . . . . shear modulus
G_c . . . . . shear modulus composite material
γ . . . . . safety factor for inequality constraint
γ_j^g . . . . . safety factor for inequality constraint of constraint j
γ^{FST} . . . . . slope angle of the top face sheet
h . . . . . equality constraint function scalar
H . . . . . height of profile cross section
I . . . . . indicator function
$\inf$ . . . . . infimum
λ . . . . . buckling factor for linear buckling analysis
$\tilde{\Lambda}$ . . . . . type-1 triangular fuzzy number
$\tilde{\tilde{\Lambda}}$ . . . . . type-2 triangular fuzzy number
m_D . . . . . mass of driver
m_B . . . . . mass of sandwich beam
m_P . . . . . mass of plate
m_P . . . . . mass of extruded profile
m_{RS} . . . . . mass of reflecting surface
M . . . . . moment
μ . . . . . membership value $0.0 \leq \mu \leq 1.0$
μ_f . . . . . mean of objective function f
μ_g . . . . . mean of constraint function g
M_{comb} . . . . . material combination of reinforced profile
n_α^I . . . . . number α-cut levels for primary membership function
n_α^{II} . . . . . number α-cut levels for secondary membership function
n_{ch} . . . . . number of chambers in extrusion die
n_e . . . . . number of embedded sets
n_f . . . . . number of objectives
n_g . . . . . number of inequality constraints
n_h . . . . . number of equality constraints
n_s . . . . . number of support points in DOE
ν . . . . . Poisson's ratio
ν_c . . . . . Poisson's ratio composite material
$\mathbf{p}$ . . . . . design parameter vector
$\tilde{\mathbf{p}}$ . . . . . uncertain design parameter vector
$\mathbf{p}_A$ . . . . . design parameter vector discipline A
$\mathbf{p}_{AB}$ . . . . . design parameter vector disciplines A and B
$\mathbf{p}_B$ . . . . . design parameter vector discipline B
Ψp_{rez} . . . . . uncertainty parameter for position of reinforcing elements

P . . . . . probability of failure
P_{cr} . . . . . critical buckling load computed by Euler buckling
p^1_{fg} . . . . . path along crisp constraint boundary for fg_1
$p^1_{d\,HAZ}$ . . . . . minimum distance reinforcements to HAZ profile 1
$p^2_{d\,HAZ}$ . . . . . minimum distance reinforcements to HAZ profile 2
p_{JT} . . . . . joining type of plate
p^1_{psM} . . . . . matrix material profile 1
p^2_{psM} . . . . . matrix material profile 2
p^1_{pt} . . . . . plate thickness profile 1
p^2_{pt} . . . . . plate thickness profile 2
p^1_{pw} . . . . . plate width profile 1
p^2_{pw} . . . . . plate width profile 2
p^1_{red} . . . . . diameter of reinforcing elements profile 1
p^2_{red} . . . . . diameter of reinforcing elements profile 2
$\mathbf{p}^1_{reE}$ . . . . . existence vector for all reinforcing elements profile 1
$\mathbf{p}^2_{reE}$ . . . . . existence vector for all reinforcing elements profile 2
p^1_{reM} . . . . . reinforcing element material profile 1
p^2_{reM} . . . . . reinforcing element material profile 2
p^1_{reN} . . . . . number of reinforcing elements profile 1
p^2_{reN} . . . . . number of reinforcing elements profile 2
p^1_{rez} . . . . . vertical position of reinforcing elements profile 1
p^2_{rez} . . . . . vertical position of reinforcing elements profile 2
p^1_{sft} . . . . . stringer flange thickness profile 1
p^2_{sft} . . . . . stringer flange thickness profile 2
p^1_{sfw} . . . . . stringer flange width profile 1
p^2_{sfw} . . . . . stringer flange width profile 2
p^1_{sh} . . . . . stringer height profile 1
p^2_{sh} . . . . . stringer height profile 2
p^1_{sN} . . . . . number of stringer profile 1
p^2_{sN} . . . . . number of stringer profile 2
p^1_{sT} . . . . . type of stringer profile 1
p^2_{sT} . . . . . type of stringer profile 2
p^1_{swt} . . . . . stringer web thickness profile 1
p^2_{swt} . . . . . stringer web thickness profile 2
PM_{res} . . . . . qualitative performance index for the residual stresses
P_{max} . . . . . maximum allowed probability of failure
π . . . . . possibility
q_{CWR} . . . . . limiting value for Chen-Wang Ranking
q_{DPR} . . . . . limiting value for Dubois-Prade Ranking
q_{SPR} . . . . . limiting value for Sengupta-Pal Ranking
r . . . . . system response, function value
$\tilde{r}$ . . . . . uncertain system response
$\tilde{\tilde{r}}$ . . . . . uncertain system response vector with type-2 fuzzy uncertainty
$\hat{r}$ . . . . . system response from surrogate model
$\hat{\tilde{r}}$ . . . . . uncertain system response from surrogates
$\hat{\overline{r}}_\alpha$ . . . . . max. system response from surrogate for given interval on α-cut level
$\hat{\underline{r}}_\alpha$ . . . . . min. system response from surrogate for given interval on α-cut level

$\tilde{\mathbf{r}}$ . . . . . uncertain system response vector
$\overline{\mathbf{r}}_\alpha$ . . . . . maximum system response vector for given interval on α-cut level
$\underline{\mathbf{r}}_\alpha$ . . . . . minimum system response vector for given interval on α-cut level
$\hat{\overline{\mathbf{r}}}_\alpha$ . . . . . maximum system response vector, surrogate model, given α-cut level
$\hat{\underline{\mathbf{r}}}_\alpha$ . . . . . minimum system response vector, surrogate model, given α-cut level
r_{all} . . . . . allowable system value
$\tilde{r}_{all}$ . . . . . allowable uncertain system value
$\hat{R}$ . . . . . radius ratio of profile cross section
ρ . . . . . density
ρ_c . . . . . density of composite material
$\sup$ . . . . . supremum
S . . . . . support of fuzzy set
S^l . . . . . support of interval type-2 fuzzy set, lower membership function
S^u . . . . . support of interval type-2 fuzzy set, upper membership function
s_L . . . . . minimum of support for lower membership function
s_R . . . . . maximum of support for lower membership function
s_{LL} . . . . . minimum of support for upper membership function
s_{RR} . . . . . maximum of support for upper membership function
S_k . . . . . skewness of fuzzy number
σ . . . . . stress
σ_{all} . . . . . allowable stress
σ_f . . . . . standard deviation objective function f
σ_g . . . . . standard deviation of constraint function g
t_{min} . . . . . minimum wall thickness
u . . . . . deformation in one direction
$\mathbf{u}$ . . . . . deformation vector
w_{HAZ} . . . . . width of heat affected zone
ω_1 . . . . . first eigenfrequency
Ω . . . . . sample space
$\mathbf{x}_{AB}$ . . . . . design variable vector disciplines A and B
$\mathbf{x}_A$ . . . . . design variable vector discipline A
$\mathbf{x}_B$ . . . . . design variable vector discipline B
x . . . . . design variable
$\tilde{x}$ . . . . . uncertain or fuzzy design variable
$\mathbf{x}_u$ . . . . . upper bound design variable vector
$\mathbf{x}$ . . . . . design variable vector
$\tilde{\mathbf{x}}$ . . . . . uncertain or fuzzy design variable vector
x_Λ . . . . . nominal value of triangular fuzzy number $\mu_{\tilde{A}}(x) = 1$
$\mathbf{x}_\Lambda$ . . . . . nominal value vector of triangular fuzzy numbers
$\mathbf{x}_l$ . . . . . lower bound design variable vector
$\mathbf{y}_A$ . . . . . system answers discipline A
$\mathbf{y}_B$ . . . . . system answers discipline B
φ . . . . . reinforcement ratio

Indices

$\tilde{A}$ . . . . . type-1 fuzzy set
$\tilde{\tilde{A}}$ . . . . . type-2 fuzzy set
x . . . . . scalar
x_α . . . . . on α-cut level
$\overline{x}$ . . . . . maximum within interval
$\underline{x}$ . . . . . minimum within interval
$\hat{x}$ . . . . . value from surrogate
x^* . . . . . values in optimum
$[x]$ . . . . . interval variable
$\mathbf{x}$ . . . . . vector
$\tilde{\mathbf{x}}$ . . . . . uncertain or fuzzy vector
$\mathbf{X}$ . . . . . matrix
$[\cdot]^T$ . . . . . transpose of $\cdot$

1. Introduction

1.1. Motivation

Today global markets require fast and flexible product development processes. This need is met in engineering by increasingly integrated simulation schemes for multiple disciplines used extensively in early design stages. To find the best design with respect to requirements arising from several disciplines structural optimization methods are gaining more importance. Optimization is applied on different levels of structural design which are outlined in figure 1.1. In general, the overall structural topology is determined first, followed by part and detailed design. On structural level, typical loads determine the design whereas manufacturing aspects become more important on part and detailed level.
An example is given in figure 1.1 for the generic space frame investigated in the Collaborative Research Center SFB Transregio 10 (SFB-TR10). On a the structural level the shape of the profiles defines load paths. From those loads, single parts are designed and optimized. On a detailed level, material selection, extrusion, machining and joining are main drivers for design.

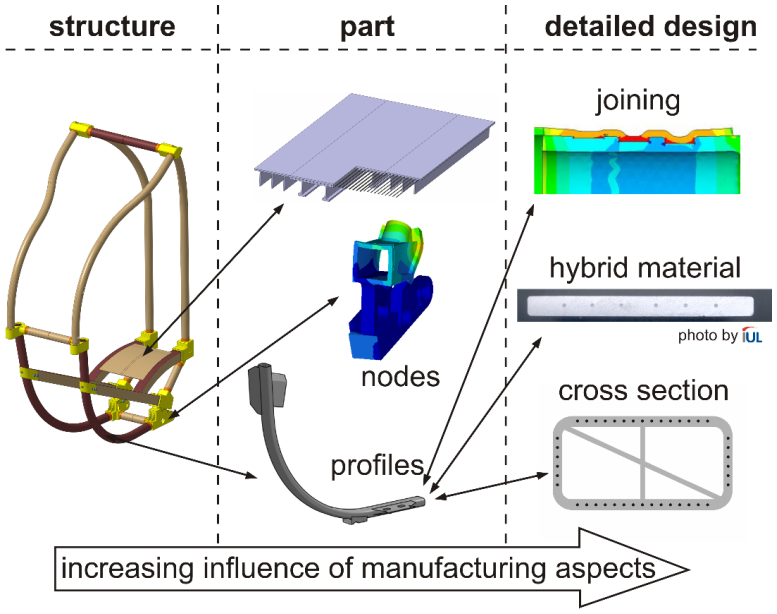

Figure 1.1.: Design and optimization on different structural levels

The information on manufacturing processes on detailed level is mostly based on numerical simulations. In this thesis a complementary approach is suggested. Information is available in a qualitative way by expert knowledge, which allows the inclusion of manufacturing influences on detailed, part and even on structural level already in an early design

phase. Manufacturing influences for example describe geometric relations for a given manufacturing process in order to ensure process reliability, correlations between material and part geometry, and manufacturing effort for a given design.
The advantage of multidisciplinary optimization with manufacturing aspects is shown in a simple example first presented in Huber and Baier (2006). It represents the typical problem formulation handled in this thesis. An extruded cantilever I-beam is optimized with respect to mass and deformation. Composite extrusion is used which allows the introduction of reinforcing elements. Stress constraints and geometric manufacturing constraint are present together with manufacturing effort evaluation. The latter is characterized by fuzzy models for production time. Optimization runs for three different settings of allowed manufacturing effort are summarized in figure 1.2.

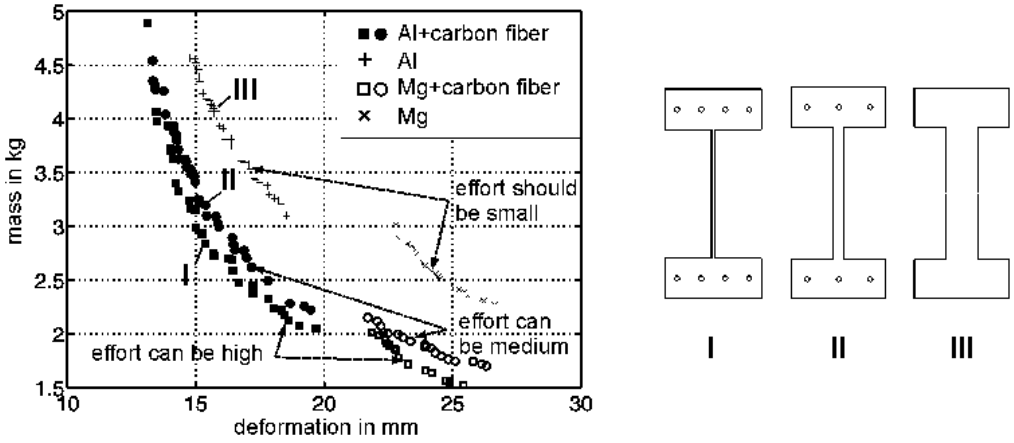

Figure 1.2.: Trade-off for mechanical properties and manufacturing effort, Huber and Baier (2006)

The three curves represent Pareto-optimal designs for three different settings of allowed manufacturing effort. Three designs named "I", "II" and "III" have a deformation of 16 mm. The solution for lowest manufacturing effort is design "III". The wall thickness ratio between web and flange is nearly one and reinforcing elements are missing. Design "II" has a medium amount of reinforcing elements and a typical web to flange ratio. Mass is reduced compared to design "III". Design "I" has again a slightly lower mass but the difference between the wall thicknesses can't be manufactured by extrusion. This example shows that the inclusion of models based on qualitative manufacturing knowledge can lead to designs with much better manufacturability. The penalty on mass and deformation for good process suitability is low in this example. A more complex version of an extruded profile will be outlined throughout the thesis.
Three main challenges, namely imprecision in manufacturing expert knowledge, model availability for manufacturing aspects and suitable optimization methods can be identified from the I-beam problem.

- **Imprecision in qualitative knowledge for mechanical and manufacturing aspects.** Early in the product development process many uncertainties and imprecisions arise for all disciplines of an engineering problem. Most established approaches to handle

uncertainties use statistics based on probability theory to find suitable designs, for example robust design (RD) methods. This is valid for aleatory uncertainty only, which describes the inherent variability of the system.[1] On the other hand epistemic uncertainty reflects lack of information or scarce data[2]. An example is the qualitative nature of expert knowledge on manufacturing aspects such as models for manufacturing time used in the I-beam example. Epistemic uncertainty can be reduced by additional information and may become aleatory uncertainty. More detailed classifications can be found in Nikolaidis et al. (2005). For epistemic uncertainty several evaluation methods are listed in Ayyub (2001). One of them is possibility theory, which is often interpreted in terms of fuzzy sets as described in Klir (1999).

- **Model availability.** Most integrated simulation schemes in structural engineering use numerical models based on the finite element method (FEM) and computer aided design (CAD) representing objective knowledge of the problem. In general these models require a lot of effort for implementation and a high amount of information.
  For epistemic expert knowledge Yoo (2000), Shehab and Abdalla (2002) and others suggest fuzzy rule-based systems (FRBSs) for modeling of experience and rule-based information. Mainly type-1 fuzzy sets (T1 FSs) are used for FRBSs at the moment. An example is manufacturing time in the I-beam problem taking into account the profile wall thicknesses, and number and diameter of reinforcing elements. Due to limitations of T1 FSs, Mendel (2001) suggests type-2 fuzzy sets (T2 FSs) for fuzzy rule-based systems, which allow for a continuous propagation of uncertainties in expert's information throughout the modeling process.

- **Design optimization.** Optimization methods, manual and automated ones, are part of nearly every product development process in engineering. An efficient algorithm for multidisciplinary and multiobjective optimization from Gleichmar (2004) and Langer (2005) is utilized in the I-beam problem. It can handle continuous as well as discrete design variables, and allows for multiple objectives. For manufacturing aspects discrete design variables are important for material and process selection, and for selection of part feature such as reinforcing elements. Multiple goals arise from structural and manufacturing needs. Examples are mass, eigenfrequency, manufacturability and manufacturing effort.
  If uncertainties are present in the problem formulation, system responses are not crisp values but statistical distributions, intervals or fuzzy numbers. A mapping has to be performed in order to evaluate goals and constraints in the optimization algorithm.

In this thesis an integrated approach for typical engineering optimization problems taking into account expert knowledge especially for manufacturing aspects is developed and evaluated. Uncertainty in expert knowledge is addressed by a fuzzy modeling approach. Knowledge-based, type-2 fuzzy models for qualitative manufacturing information are generated and utilized together with type-2 fuzzy system answers for uncertain structural responses in structural optimization. A literature review is given in section 1.2 followed by detailed objectives in section 1.3 and scope of the thesis in section 1.4.

[1] This kind of uncertainty is often referred to as irreducible, stochastic or random uncertainty.
[2] This kind of uncertainty is often referred to as subjective or reducible uncertainty.

1.2. Structural optimization with manufacturing aspects - a survey

The focus of this survey is on the modeling of manufacturing aspects especially, on evaluation of systems with uncertain input parameters and finally, on optimization approaches. An important term in this context is manufacturability which is often used for physical as well as economic manufacturing aspects. The definition of manufacturability is according to Shankar and Jansson (1993):

"Manufacturability is defined as the ability to manufacture a product to obtain the desired quality and rate of production while minimizing cost."

Different aspects have to be addressed with respect to optimization in this context. First, different criteria for the evaluation of designs have to be defined. To classify manufacturing and structural aspects Kumar and Bauer (2009) suggests three criteria. These are economic criteria, technological criteria and performance criteria. The first criterion is related to detailed cost estimations and overall manufacturing effort criteria, the second addresses the physical manufacturing process and its restrictions, and the third criterion assesses properties and performance of structures such as mass, stresses and eigenfrequencies. A detailed overview is given in section 1.2.1.
The handling of two types of uncertainty, aleatory or epistemic, in structural optimization is reviewed in section 1.2.2. The type of uncertainty, which is present in the problem at hand, defines the types of system equations. Commonly, the finite element method (FEM) is used to evaluate performance criteria. Different approaches for the handling of uncertain parameters in FEM models are discussed. Expert knowledge is another source for system equations in optimization. The fuzzy approach for modeling of expert knowledge is presented in detail in chapter 2. Finally design optimization problems with structural and manufacturing aspects are evaluated in section 1.2.3 followed by a summary in 1.2.4.

1.2.1. Design Criteria

Economic Criteria. Mainly cost estimations are included in this category. Niazi et al. (2006) provides a detailed survey for general product cost estimation. Qualitative and quantitative techniques are distinguished. Quantitative techniques utilize detailed analysis of a product design, the product features and manufacturing processes. Qualitative techniques, on the other hand, are primarily based on experience and comparison of new products with previously manufactured ones. Qualitative techniques utilizing fuzzy logic, rules and expert systems are grouped within decision support systems (DSSs). They are useful in early phases of the product design process. Curran et al. (2004) gives a review of cost modeling in aerospace engineering. He also classifies rule-based fuzzy logic as an advanced technique. A limited scope and application is identified due to the knowledge acquisition process. The model can handle only information provided by the experts.
A typical method in conceptual design phases are cost estimating relationships (CERs). Cost is expressed as a dependent variable of one or more design parameters such as weight, dimensions and others. Examples can be found in Bao and Samareh (2000) and also in Kundu et al. (2002), Curran et al. (2006a) and Pantelakis et al. (2009). Historical data are needed to build CERs. Therefore the predicting performance for innovative designs is limited. Also,

uncertainties of the models are not the focus of research in most literature sources.
As an qualitative alternative to cost estimations manufacturing effort can be used. Most effort estimations are related to production time and geometrical manufacturing aspects, the latter are described in the next paragraph. Yoo (2000) presents a fuzzy addition to a simulation-based model for production time. He adds a knowledge-based model for down time to a given analytical model. This down time is due to necessary tool change for small radii in a composite wing. A similar method is suggested by Shehab and Abdalla (2002). In both sources fuzzy rule-based models are built and crisp production times are computed. Menzel (2001) use fuzzy logic arithmetic for the modeling of production rates and gives figures for the uncertain production rate over time.

Technological criteria. This class of criteria summarizes the physical manufacturing process and its properties. For example Hug et al. (1983) shows the influence of the extrusion process for aluminum alloys on the optimal geometric design of a bridge reinforced with carbon fibers. An optimal combination of materials well suited for extrusion and carbon fiber reinforcements can lead to better design than high strength aluminum alloys.
Gupta et al. (1997) provides an overview of different automated manufacturability analyses. Rule-based systems are suggested for near-net-shape processes (e.g., casting, stamping, sheet metal working).
Subramaniam and Ulrich (1998) divide the processes into trajectory dominated and process-physics-dominated processes. Machining and laser cutting are examples for the first category, casting, stamping and extrusion for the second, respectively. An approach is provided which defines a producibility metric[3] from expert knowledge. This approach is fast and less costly than physical experiments and can be linked to cost models.
Alberti et al. (1998) use fuzzy logic and artificial neural networks (ANNs) for cold forging process planning. From 60 simulations rules for two antecedents are generated with a high prediction accuracy of 90%. In Yin et al. (2006), Yin et al. (2004) and Li et al. (2007) an approach for knowledge acquisition from metal forming simulations is presented in order to build rules from Fuzzy Rough Sets. For a deep drawing process 52 simulations with five design parameters are computed and nine rules are found to identify cracks and wrinkling.
In Coelho (2004) and Coelho and Bouillard (2005) "PAMUC II" is introduced, which handles expert knowledge directly by expert rules for optimization. Analytical test problems are discussed.
Menzel (2001) accounts for the uncertainties in expert knowledge. He presents a hybrid fuzzy rule-based approach for a technological analysis of single parts. Manufacturing aspects for high-pressure-metal-forming are described via T1-FRBS with respect to geometrical parameters. Menzel shows advantages compared to Neural Networks and he emphasizes the applicability of the approach for innovative manufacturing processes.
The optimization of structural and manufacturing aspects for composite structures is an upcoming field of interest. For example ply drop-off and angle discontinuity are described in Liu and Butler (2007), complex paths for fiber placement machines are discussed in Schumacher (1995) and Blom et al. (2008).

Performance criteria. The performance of a lightweight structure is defined primarily by its physical properties. Typical criteria for structural optimization are mass, eigenfrequencies, stresses, deformations and responses to dynamic loads. In the majority of structural

[3] "Producibility" and "manufacturability" are used interchangeable in this thesis.

optimization problems and in this thesis, the properties are computed with FEM. The handling of uncertainties with FEM models can be classified into two main approaches. The first one uses modified FEM codes, the second works with standard FEM but utilizes several computations of the same model with slightly changed input parameters.
Elishakoff and Ren (1999) and in more detail Elishakoff and Ren (2003) and Stefanou (2009) provide a general discussion about uncertainties handled directly by modified finite element codes. They present finite element method for stochastic problems (FEMSP)[4]. FEMSP provides mean and covariance for structural behavior with respect to variations in material properties, geometrical parameters and loads. Random variables and random fields can be mapped. A standard approach for FEMSP is a combination of deterministic FEM and perturbation techniques. Sudret and Der Kiureghian (2000) expand this overview and compare different methods. The probabilistic system answers obtained by FEMSP are used especially for reliability analysis. Moens and Vandepitte (2005a) and Moens and Vandepitte (2006) present an overview for non-probabilistic methods for uncertainty treatment in finite element analysis. They suggest that these methods are especially helpful in early design stages, when subjective information has to be quantified. In Moens and Vandepitte (2005b) a method for the computation of uncertain frequency-responses due to fuzzy inputs for damped structures is introduced and numerical case studies are given by De Gersem et al. (2005). Moens and Vandepitte conclude, that fuzzy methods are complementary to probabilistic methods rather than competitive. Another important contribution to this topic based on a fuzzy approach using interval analysis is introduced by Rao and Sawyer (1995) and further developed in Rao and Berke (1997), Rao et al. (1998) and Rao and Cao (2001). Fuzzy finite element equations are solved and fuzzy numbers for the system outputs are generated. The fuzzy mechanics of composites are analyzed in Rao and Liu (2004) and Liu and Rao (2005) for uncertain Young's moduli of fiber and matrix and uncertain fiber volume content.
An overview for evaluation of probabilistic uncertainties with classic finite element method is given in Choi et al. (2006). Sampling methods such as Monte Carlo sampling (MCS), importance sampling (IS) and latin hypercube sampling (LHS) are used to directly gain probabilistic information. The drawback of Monte Carlo sampling (MCS) is a very high number of computations needed, which increases with the number of random variables. Latin hypercube sampling (LHS) is a standard sampling method in engineering design for the computation of approximation functions. For reliability analysis, the first order reliability method (FORM) and second order reliability method (SORM) are established approaches.
So called fuzzy α-level analysis (FαLA) computes the fuzzy output of a system for fuzzy input parameters. Based on interval analysis (IA) one of the first implementations of fuzzy α-level analysis (FαLA) called vertex method (VM) is introduced by Dong and Shah (1987). The original VM can handle only monotonic functions and needs 2^n system evaluations for n uncertain parameters. An optimized vertex method (VMo) is described by Smith et al. (2002). The optimized vertex method reduces the required system evaluations by applying an optimization with bounded input parameters in order to find minimum and maximum system answers. Massa et al. (2006) introduce a procedure called Taylor's expansion with extrema management method (TEEM) to compute fuzzy system answers. The computational efficiency of TEEM is high compared to original extension principle of which VM is an implementation. In Massa et al. (2008) the authors suggest Padé approximants with extrema management (PAEM) for fuzzy modal analysis. Law (1996) introduces a level interval algorithm (LIA) to find the boundaries of the response parameters in FαLA. A linear approx-

[4]This method is also known as stochastic finite element method (SFEM).

imation based on fractional factorial design of experiments (FFD) and Powell's method for extrema search is proposed. Law states that this scheme is acceptable for design decisions in preliminary design stages. A method based on sparse grid interpolation is introduced in Klimke et al. (2004). More details on the interpolation scheme are given in Klimke and Wohlmuth (2005) and dimension-adaptive sparse grids are introduced in Klimke et al. (2006) which further reduce computational effort. A frequency response function of a truck cabin is analyzed for 27 uncertain parameters. In Klimke (2006) the approach is combined with a spectral element method from Nunes et al. (2006). Sparse-grid based sensitivity analysis is discussed in Klimke (2007). In Möller and Beer (2004) the authors summarize their extensive research on FαLA. In Beer and Liebscher (2008) the approach is extended to the highly nonlinear problem of crash analysis. Another algorithm for FαLA and its application to engineering examples is given in Degrauwe (2007). For T2 FS fuzzy α-level analysis is a new concept, only few literature sources can be found which will be introduced in the next chapter.

1.2.2. Design Optimization with Uncertainty Handling

In order to characterize uncertainties with the methods described before the number of system evaluations in optimization has to be increased. The main challenge is to keep the additional numerical effort limited. Today mainly statistical uncertainties are taken into account. Uncertainty handling is often summarized by the term robust design (RD). Thorough surveys can be found in Antonsson (ed.) (2001), Tsompanakis et al. (2008) and Beyer and Sendhoff (2007).

Optimization methods for aleatory uncertainties. Schuëller and Jensen (2008) identify the three most relevant contributions. System identification, reliability-based design optimization and robust design optimization. The latter is revised in more detail by Park et al. (2006) and Beyer and Sendhoff (2007) including many references to engineering applications. Robust and reliability-based optimization methods are successors of Taguchi's robust design methodology, which is not suitable for optimization due to very high computational effort. Robust design optimization minimizes the mean and variance of the objectives whereas reliability-based design optimization utilizes limit state functions in order to ensure a predefined failure probability, for details see Tsompanakis et al. (2008).
To reduce the computational effort, surrogate models are essential. For robust design optimization (RDO) often the response surface method (RSM) is used to model mean and variance of the systems answers[5]. Shaibu and Cho (2009) discuss three modeling approaches and show differences in the obtained optimal solution. Jin et al. (2003) suggest kriging method (KGM) or radial basis functions (RBFs) as better alternatives. Koch et al. (2002) provide an example with KGM surrogate models. Rais-Rohani and Singh (2004) compare global and local surrogate models in reliability-based problems and show an advantage of local response surface methods (RSMs) for computational effort.
Physical programming (PP) developed by Messac is used in Chen et al. (2000) and Messac and Ismail-Yahaya (2002) for RDO. PP transforms multiobjective trade-offs between a minimum mean value and minimum variance into a single objective problem. The method allows for subjective preferences defined by the engineer.

[5]This is also called dual response surface.

A comparison of a probabilistic and a fuzzy set approaches is given in Chen (2000). Different situations are investigated for available sample size and information on the true type of statistical distribution. Chen concludes that for small sample sizes and an unknown distribution of uncertain parameters, the aforementioned possibilistic methods should be used together with probabilistic ones.
The main challenge with above-mentioned methods is the generation of probability density functionss (PDFs) for input parameters. A quotation from Elishakoff (1995) emphasize this situation:

"In modern probabilistic codes and in most, if not all, studies the necessary probabilistic information on uncertain quantities is assumed rather than appropriately substantiated through statistical analysis of extensive experimental data. After numerous assumptions are made, some new numerical approaches, often sophisticated ones, are tested on simple examples. On the other hand the accuracy of the experimental data (if at all present) is not discussed."

Optimization methods for epistemic uncertainties. He and Qu (2008) and Mourelatos and Zhou (2008) provide a good overview, a short history is given in the following.
In the mid 1980s optimization of fuzzy structural systems was introduced by Guang-Yuan and Wen-Quan (1985) and Rao (1987). Rao transforms the original crisp objective and constraint function into fuzzy ones. The fuzzified constraints reflect the subjective engineering information about constraint relaxation. One design variable is added to the problem called λ which accounts for the level of satisfaction for all fuzzified objectives and constraints. The influence of different membership functions (linear, hyperbolic, logarithmic etc.) for fuzzy objectives and constraints is investigated by Dhingra et al. (1992) for a 25-bar truss. In Rao and Chen (1996) the authors extend the method by Dampster-Shafer theory and Yager's rule in order to merge different belief structures into one single design criterion and to evaluate a satisfaction function for multiple design criteria. Shih et al. (2003) and Shih and Lee (2006) extend the method to double and multi-α-level-cuts approaches.
Jensen (2001) introduces approximation models to decrease the number of expensive system evaluations. He also discusses different optimal designs due to different defuzzification techniques. Mourelatos and Zhou (2005) compare vertex, discretization and optimization methods for the computation of fuzzy system outputs for mathematical and engineering examples. In Zhou and Mourelatos (2008) and Mourelatos and Zhou (2008) the authors introduce evidence based design optimization (EBDO) and show for a cantilever beam and pressure vessel example, that the optimal designs by EBDO are more conservative than reliability-based design optimization (RBDO) solutions but less conservative than possibility-based design optimization (PBDO) optimal designs.
Uncertainties based on intervals can also be solved by so called anti-optimization which was introduced by Elishakoff et al. (1994). It describes the search for a worst case scenario for a given design. A six bar truss example is given in McWilliam (2001). By integrating anti-optimization into a system level structural optimization a computationally expensive, nested problem is created. Different methods to counter the high number of system evaluations are described in Lombardi and Haftka (1998) and tested on three engineering examples with load uncertainties. A combined approach for probability, fuzziness and anti-optimization is proposed in Tonon et al. (2001).
Jiang et al. (2007) transforms uncertainty given by intervals for constraints into satisfaction degrees. A ten-bar truss is optimized with a genetic algorithm, a penalty function approach and for different restricted satisfaction degrees. In Jiang et al. (2008) the computational effort of the approach is enhanced by a polynomial response surface approximation (RSA).

A Fuzzy analysis method for PBDO derived from RBDO is introduced in Choi et al. (2004). In Youn et al. (2005) the objective is formulated by different quality loss functions and the resulting optima are discussed. Massa et al. (2009) utilize Padé approximants with extrema management (PAEM) described in Massa et al. (2008) for the multiobjective optimization of a drop-tower impactor sled. The fuzzy input parameters are updated in order to find the feasible design space and simultaneously optimize the objectives.

1.2.3. Multidisciplinary design optimization with structural and manufacturing aspects

A general overview can be found in Saitou et al. (2005). A very detailed method to characterize aerospace design with respect to manufacturing is introduced in Rais-Rohani (1996) and Rais-Rohani (1998). It is based on a classification scheme defined in Shankar and Jansson (1993). Rais-Rohani and Huo (1999) optimize different wing spar designs by this method. A preliminary manufacturability analysis provides insight into the complexity and efficiency of the designs, the results of a subsequent optimization with cost constraints can be used for trade-off decisions. In Martinez et al. (2001) this method is used together with physical programming developed by Messac on the same wing spar optimization problem. The manufacturability indices in Martinez et al. (2001) for three different concepts are 0.6109, 0.6240 and 0.6095, respectively. The index variation is 2.4%, manufacturing cost variation 2.7%, and weight variation 6.9%.
A detailed description of a combined structural and cost optimization is given in Kassapoglou (1999a) and Kassapoglou (1999b) for metal and composite fuselage frames. In Kassapoglou (1997) the authors discuss trade-off between panel weight and manufacturing cost for a composite panel with manual lay-up.
Curran et al. (2006b) analyze and optimize weight-cost trade-offs for aluminum stiffened panels. The optimization of a large-scale civil aircraft wing is presented in Gantois and Morris (2004). Details for RDO of a wing spar with manufacturability and cost aspects are given in Rais-Rohani and Xie (2005).
Cristello and Kim (2007) present the optimization of a vehicle chassis for crash, stiffness, mass and hydroformability. A sophisticated decomposition-based assembly synthesis for space frames described in Cetin and Saitou (2004) is used in Cetin and Saitou (2005) for manufacturing cost minimization. In Lyu and Saitou (2005) a body-in-white is optimized for stiffness and manufacturability. A radar chart is used to evaluate optimal designs and to chose one which balances all three objectives.

1.2.4. Summary of literature review

Manufacturing aspects are often represented by manufacturing cost models in multidisciplinary design optimization. These models are expensive to generate and have to use available data. The advantage of knowledge-based models is emphasized by some author because they can be generated relatively quickly together with experts and because they are available already in early design stages.
If knowledge-based models are used in general type-1 fuzzy rule-based systems are utilized

and a single crisp value is derived from the model for evaluation in the optimization process. This neglects available information which was generated by numerically expensive schemes to derive system answers for fuzzy input parameters.

1.3. Objectives of work

In this thesis an integrated approach for the quantification and handling of qualitative manufacturing aspects for multidisciplinary, structural optimization is developed, implemented and evaluated. The methods are focused on T2 FSs, which are used for knowledge-based models as well as for uncertainty characterization for typical performance criteria. The approach should allow the decision maker to interpret and rank optimized structural designs with respect to typical performance measures such as masses and stresses. The following subgoals will be addressed in course of this thesis:

- Implementation of exemplary knowledge-based models representing manufacturing knowledge by type-1 fuzzy rule-based systems (T1-FRBSs) and type-2 fuzzy rule-based systems (T2-FRBSs).
- Handling of fuzzy input parameters derived from manufacturing influences and load uncertainties. Development, implementation and evaluation of a computationally efficient algorithm based on α-cut level optimization (αCLO) for evaluation of complex numerical models with respect to T2 FSs fuzzy input parameters. A speed up of computation by parallelization of system evaluations should be possible.
- Evaluation of fuzzy structural indices as well as fuzzy manufacturability indices for goal and constraint computation in standard optimization algorithms. Subgoals are:
  - The implementation and evaluation of defuzzification methods for T2 FSs.
  - Modeling of different levels of information content.
  - Evaluation of fuzzy constraint boundaries.
- Evaluation of methods for analytical and engineering examples. The latter are multidisciplinary problems with aerospace and automotive background.

A graphical overview with respect to the structural optimization process is given in a generalized flowchart in figure 1.3 on the next page.

1.4. Scope of thesis

In chapter 2, basics for engineering optimization, knowledge acquisition and representation are given. An engineering example is introduced and optimization, knowledge and uncertainty aspects are demonstrated. In chapter 3, type-1 fuzzy sets are extended to type-2 fuzzy sets. Evaluation methods for type-2 fuzzy sets are developed, implemented and discussed. An analytical function is used in chapter 4 to demonstrate the characteristics of evaluation methods for goal and constraint handling of fuzzy system properties. The methods are demonstrated on two different fields of application. First, extruded aluminum profiles are

optimized in chapter 5 in two examples. A structural part of an antenna demonstrator for satellites is optimized in chapter 6. The thesis is summarized in chapter 7 and an outlook is given.

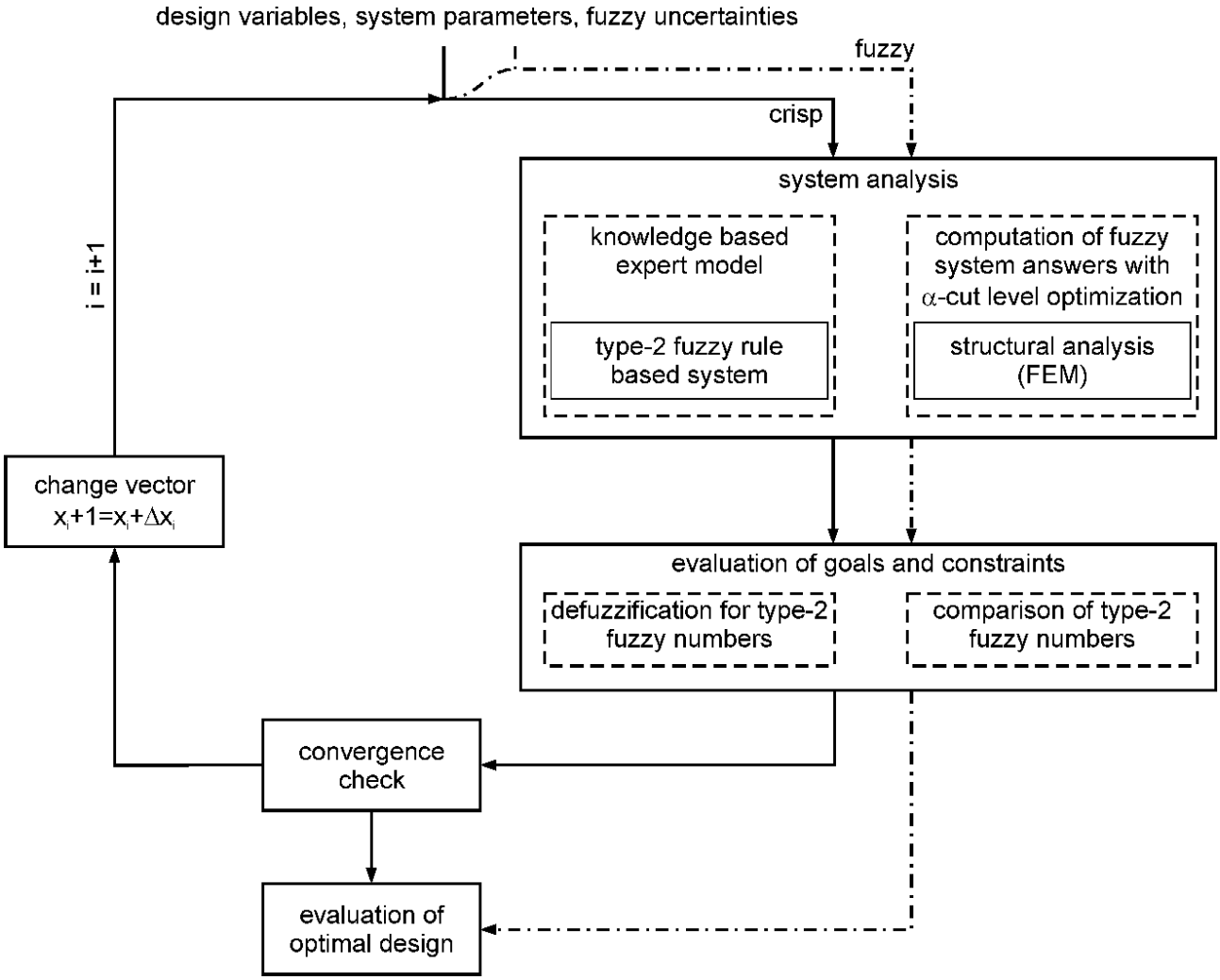

Figure 1.3.: Objectives of work with respect to engineering optimization flowchart

2. Basic definitions and introductory engineering example

The basics for structural optimization, knowledge-based fuzzy models and their handling in multidisciplinary optimization are given in this chapter. The optimization of an extruded profile is introduced in section 2.2. Generation and evaluation of knowledge-based information is given for the example.

2.1. Definition of optimization problem

The standard definition of a deterministic design optimization problem is:

$$\begin{aligned} min \quad & f(\mathbf{x},\mathbf{p}) \\ subject\ to: \quad & h_i(\mathbf{x},\mathbf{p},\epsilon_i^h) = 0 \qquad i = 1\ldots n_h \\ & g_j(\mathbf{x},\mathbf{p},\gamma_j^g) \leq 0 \qquad j = 1\ldots n_g \\ with: \quad & \mathbf{x}_l \leq \mathbf{x} \leq \mathbf{x}_u \end{aligned} \tag{2.1}$$

The objective f to be minimized is a function of the design variables $\mathbf{x}$ which can be varied within the boundaries from $\mathbf{x}_l$ to $\mathbf{x}_u$, and the design parameters $\mathbf{p}$. The latter are constants in deterministic design optimization (DDO), for example material properties and loads. An equality constraint h_i is often fulfilled if it is smaller than a given error boundary ϵ_i^h. Equality constraints are not present in this thesis and won't be discussed. The inequality constraint g_i is a functions of $\mathbf{x}$, $\mathbf{p}$ and the safety factor γ_j^g.
For multiobjective and multidisciplinary optimization problems the formulation is:

$$\begin{aligned} min \quad & \mathbf{f}(\mathbf{x}_A,\mathbf{x}_B,\mathbf{x}_{AB},\mathbf{p}_A,\mathbf{p}_B,\mathbf{p}_{AB},\mathbf{y}_A,\mathbf{y}_B) = min\,(f_1,f_2,\ldots,f_{n_f}) \\ subject\ to: \quad & g_j(\mathbf{x}_A,\mathbf{x}_B,\mathbf{x}_{AB},\mathbf{p}_A,\mathbf{p}_B,\mathbf{p}_{AB},\mathbf{y}_A,\mathbf{y}_B) \leq 0 \qquad j = 1\ldots n_g \\ with: \quad & \mathbf{x}_l \leq \mathbf{x} \leq \mathbf{x}_u \end{aligned} \tag{2.2}$$

The objective function vector $\mathbf{f}$ contains several function values f from one or more disciplines. Different methods are known to handle multiobjective optimization problems, the most prominent ones are weighted sum methods for gradient based algorithms and Pareto-optimality for evolutionary strategies (ESs) and genetic algorithms (GAs), see Langer (2005). Multiple disciplines A and B have design variables and parameters $\mathbf{x}_A$, $\mathbf{x}_B$, $\mathbf{p}_A$, and $\mathbf{p}_B$ and the ones present in both disciplines ($\mathbf{x}_{AB}$, $\mathbf{p}_{AB}$). The latter define the design coupling of the problem. A physical coupling of the disciplines is given by the appearance of the system

answer $\mathbf{y}_A$ of discipline A in the systems equations of system B and vice versa.
Uncertainties can appear in different ways within an optimization problem. Some or all design variables and/or parameters may be subject to statistical variations or given in intervals, $\tilde{\mathbf{x}}$ and $\tilde{\mathbf{p}}$ respectively. This leads to non-crisp system answers, objectives and constraints $\tilde{\mathbf{f}}$ and $\tilde{\mathbf{g}}$. In order to use standard optimization algorithms, the $\tilde{\mathbf{f}}$ and $\tilde{\mathbf{g}}$ have to be transformed to scalar values f and g.
For design optimization with uncertain parameters, different problem formulations are known. The most important ones will be shown in the following. Let's start with RDO:

$$\begin{aligned} min \quad & \mathbf{f}(\tilde{\mathbf{x}}, \mathbf{x}, \tilde{\mathbf{p}}, \mathbf{p}) && = \quad min\,[\mu_f(\tilde{\mathbf{x}}, \mathbf{x}, \tilde{\mathbf{p}}, \mathbf{p}), \ldots \\ & && \qquad \sigma_f(\tilde{\mathbf{x}}, \mathbf{x}, \tilde{\mathbf{p}}, \mathbf{p})] \\ subject\ to: \quad & \mu_{g_j}(\tilde{\mathbf{x}}, \mathbf{x}, \tilde{\mathbf{p}}, \mathbf{p}) + \beta_j \sigma_{g_j}(\tilde{\mathbf{x}}, \mathbf{x}, \tilde{\mathbf{p}}, \mathbf{p}) && \leq \quad 0 \qquad j = 1 \ldots n_g \\ with: \quad & \mathbf{x}_l \leq \tilde{\mathbf{x}}, \mathbf{x} \leq \mathbf{x}_u \quad and \quad \tilde{\mathbf{p}}, \mathbf{p} \end{aligned} \tag{2.3}$$

The two goals are the mean and standard deviation of the objective function μ_f and σ_f. In case of gradient based algorithms the multiobjective problem is transformed by a weighted sum into a single objective optimization. The behavior of constraints is controlled by the factor β. In general, RDO controls lower order statistical moments of system responses. Equation 2.3 can be also formulated without uncertainties in the constraints following the constraint formulation in equation 2.1.
For RBDO the formulation of the optimization problem includes probability P and the so called limit state function (LSF) g:

$$\begin{aligned} min \quad & \mathbf{f}(\tilde{\mathbf{x}}, \mathbf{x}, \tilde{\mathbf{p}}, \mathbf{p}) \\ subject\ to: \quad & P(g_j(\tilde{\mathbf{x}}, \mathbf{x}, \tilde{\mathbf{p}}, \mathbf{p}) > 0) - P_{max} \quad \leq \quad 0 \qquad j = 1 \ldots n_g \\ with: \quad & \mathbf{x}_l \leq \tilde{\mathbf{x}}, \mathbf{x} \leq \mathbf{x}_u \quad and \quad \tilde{\mathbf{p}}, \mathbf{p} \end{aligned} \tag{2.4}$$

The probability that g is higher than zero has to be smaller than a given, maximum probability P_{max}. This formulation is used on the component level of a structure. For engineering problems the limit state function has to be approximated due to computational effort by a limit state approximation (LSA). The first order reliability method (FORM) and second order reliability method (SORM) are such approximations. For highly non-linear or high dimensional limit state functions (LSFs) FORM and SORM exhibit limitations which are countered by sophisticated approximation methods, see for example Jurecka (2007).
Whereas for RDO the region of interest of the resulting PDF is in the area of $\mu_g \pm 2\sigma_g$ the region of interest for RBDO is determined commonly by a very small $P_{max} \leq 10^{-6}$. The latter needs accurate computation or approximation of the PDF. Even small deviations from the true PDF can lead to high deviations in P.
The original formulation of a possibility-based design optimization (PBDO) problem is given in equation 2.5. The possibility of an event π is compared with a given maximum possibility described by the α_{max}-cut level.

$$\begin{aligned} min \quad & \mathbf{f}(\tilde{\mathbf{x}}, \mathbf{x}, \tilde{\mathbf{p}}, \mathbf{p}) \\ subject\ to: \quad & \pi(g_j(\tilde{\mathbf{x}}, \mathbf{x}, \tilde{\mathbf{p}}, \mathbf{p}) \geq 0) - \alpha_{max} \quad \leq \quad 0 \qquad j = 1 \ldots n_g \\ with: \quad & \mathbf{x}_l \leq \tilde{\mathbf{x}}, \mathbf{x} \leq \mathbf{x}_u \quad and \quad \tilde{\mathbf{p}}, \mathbf{p} \end{aligned} \tag{2.5}$$

2.2. Definition of typical engineering problem with manufacturing aspects

An extruded profile shown in figure 2.1 which is produced by composite extrusion is optimized with respect to mass and stiffness. Composite extrusion is an innovative manufacturing process which allows the extrusion of already reinforced lightweight profiles. Composite extrusion is investigated within the Collaborative Research Center SFB Transregio 10 (SFB-TR10) "Integration of forming, cutting, and joining for the flexible production of lightweight space frame structures". This research is set up by Deutsche Forschungsgemeinschaft - German Research Foundation (DFG) at the universities of Dortmund, Karlsruhe, and Munich. A flexible, integrated process chain is investigated which includes the following production techniques described in Weinert et al. (2008).

- extrusion of continuously reinforced profiles
- three-dimensional rounding during extrusion
- cutting on the fly
- five-axis machining
- hybrid laser welding and friction stir welding
- joining by electromagnetic high speed forming or high pressure tube forming

In addition to experimental work, simulations for extrusion, machining and joining are investigated in order to complete the virtual process chain in parallel to the real one. All of the afore mentioned manufacturing processes and their virtual simulations are innovative and only sparse data and few models are available. To evaluate the potential of those manufacturing processes mainly expert knowledge is available in this early state of process development.

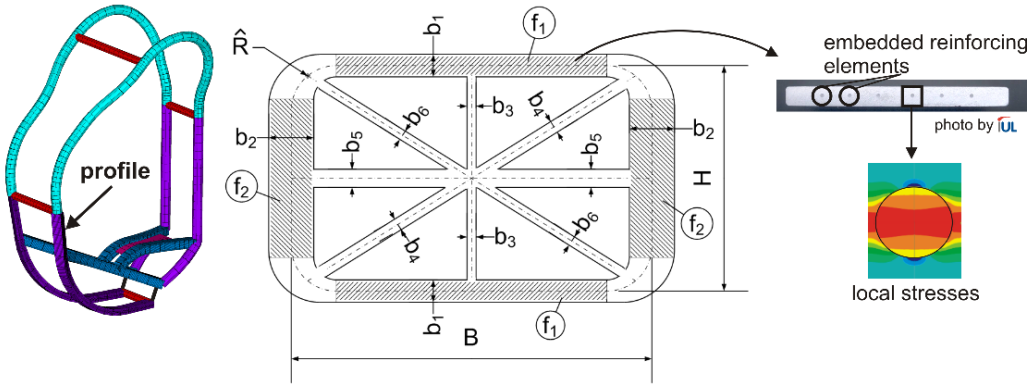

Figure 2.1.: Geometry properties of the reinforced profile optimization, Huber et al. (2008)

Apart from typical geometric design variables of the cross section also the reinforcement ratios f_1 and f_2 in different parts of the cross section can be changed. The reinforcement wires induce additional local residual stresses in the profile, which can lead to problems in subsequent production processes, such as drilling, milling, and joining. A heat treatment for reduction of residual stresses is not possible because of the curved shape of the profile as

described in Huber et al. (2008).
Two optimization problems are formulated in the following. The first takes goals and stress constraints together with some basic geometry constraints into account as shown in equation 2.6.

$$
\begin{array}{rlcll}
min & \mathbf{f}(\mathbf{x}) & = & [m_P, u] & \\
 & & & & \\
with: & \mathbf{x} & = & \left[H, B, \hat{R}, b_{1\ldots6}, f_1, f_2, M_{comb}\right] & \\
subject\ to: & g_{1,4,7}(\mathbf{x}) & = & \sigma_{i\ 1st\ p}/\sigma_{all\ m\ t} - 1 & \leq 0 \quad , i = [1,2,3] \\
 & g_{2,5,8}(\mathbf{x}) & = & \sigma_{i\ 3rd\ p}/\sigma_{all\ m\ c} - 1 & \leq 0 \quad , i = [1,2,3] \\
 & g_{3,6,9}(\mathbf{x}) & = & 50/\lambda - 1 & \leq 0 \quad , i = [1,2,3] \\
 & g_{10}(\mathbf{x}) & = & u_1/7.5 - 1 & \leq 0 \\
 & g_{11}(\mathbf{x}) & = & 40/\omega_1 - 1 & \leq 0 \\
 & g_{12}(\mathbf{x}) & = & \frac{max(b_1,b_2)/min(b_1,b_2)}{3} - 1 & \leq 0 \\
 & g_{13}(\mathbf{x}) & = & \frac{max(b_1,b_3)/min(b_1,b_3)}{3} - 1 & \leq 0 \\
 & g_{14}(\mathbf{x}) & = & \frac{max(((b_1+b_2)/2),b_4)/min(((b_1+b_2)/2),b_4)}{3} - 1 & \leq 0 \\
 & g_{15}(\mathbf{x}) & = & \frac{max(b_2,b_5)/min(b_2,b_5)}{3} - 1 & \leq 0 \\
 & g_{16}(\mathbf{x}) & = & \frac{max(((b_1+b_2)/2),b_6)/min(((b_1+b_2)/2),b_6)}{3} - 1 & \leq 0
\end{array}
\tag{2.6}
$$

In the second problem a qualitative performance index for the residual stresses PM_{res} is introduced as a third goal to be minimized in equation 2.7. The design variables and constraints are the same as in the two goal optimization.

$$
min \quad \mathbf{f}(\mathbf{x}) = [m_P, u, PM_{res}] \tag{2.7}
$$

PM_{res} is computed by a knowledge-based fuzzy model. In the next sections the building of such models and the evaluation of uncertain input parameters $\tilde{\mathbf{x}}$ and $\tilde{\mathbf{p}}$ are outlined theoretically and shown for the engineering problem at hand.

2.3. Quantification of qualitative manufacturing knowledge

In addition to simulation based models, for example FEM, knowledge based models can be used to map input parameters to system outputs in order to characterize engineering properties. Knowledge acquisition and representation are the first steps in quantifying expert knowledge. Many approaches are discussed in literature, thorough overviews can be found in Durkin (1994), Hoffman et al. (1995) and Ayyub (2001). The rule-based approach chosen for this thesis is introduced in the following, the mathematical representation in section 2.4. In the knowledge acquisition phase the input and output parameters of the model and their relations are identified. An expert or a group of experts provide the necessary information. Afterwards this knowledge is transferred with the help of knowledge representation into a quantitative model. A MATLAB interface for knowledge acquisition was developed by Daniilidis (2007) and implemented by the author for extruded and curved profiles in Huber et al. (2008). It follows a scheme introduced by Wagner and Zubey (2005).

- First card or concept sorting techniques are used to structure experts' knowledge. Previously defined objects, experiences, and rules are written on cards and the knowledge expert sorts them into groups.
- Second the expert describes what each group has in common. The groups are hierarchically organized.
- Finally a structured interview can be derived from the card sorting results to develop the rule base.

2.3.1. Rule-base basics

A rule-based system consists of facts, rules and an engine which derives actions. In the context of this thesis rules represent domain knowledge whereas facts represent data. The general description of a rule according to Durkin (1994) is given in equation 2.8.

$$\begin{aligned} antecedent &\rightarrow consequence \\ situation &\rightarrow action \end{aligned} \tag{2.8}$$

This general description is expressed by the following formulation.

$$IF\ situation\ \ THEN\ \ action \tag{2.9}$$

For several input parameters AND and OR relations have to be defined.

$$IF\ \ x_1\ IS\ A\ \ AND\ \ x_2\ IS\ B\ \ OR\ \ x_3\ IS\ C\ \ THEN\ \ f\ IS\ D \tag{2.10}$$

In this example x_1, x_2 and x_3 are the input parameters which are checked against the constants A, B and C and f is the output parameter which will be set to value D.

2.3.2. Example of knowledge acquisition for manufacturing aspects

An innovative extrusion process is used to manufacture the profile optimized in equation 2.6. Different defects which influence structural properties are recorded for the extrusion process, they are called *events*. In order to avoid rejects due to defects, the profile design should meet basic standards for manufacturability. For the extrusion process of composite aluminum profiles with embedded continuous reinforcing elements events are identified in table 2.1 on page 18.
The first event *residual stresses in profile after extrusion* is in the focus of this example. Manufacturing parameters influencing this event are identified and hierarchically ordered by their importance in table 2.2. Design variables from problem formulation in equation 2.6 are assigned to the parameters. This links the knowledge based model to the optimization problem.

Table 2.1.: Events for extrusion process of composite aluminum profiles, Huber et al. (2008)

event	effects on structural properties
residual stresses in profile after extrusion	suitability for subsequent manufacturing steps, σ_{all}
debonding - loss of adhesion between fibers and base material	reject due to defects, σ_{all}
deformation of profile cross section	cross section area, section modulus, tolerances
profile contour deviation	overall geometry, tolerances
torsion of the profile	overall geometry, tolerances

Table 2.2.: Parameters for event "residual stresses in profile after extrusion"

parameter	importance	corresponding design variable x
cooling conditions	very high	no
geometry of extrusion die	high	yes, profile cross section
number of reinforcing elements	above average	yes, reinforcement ratio
base material	average	yes
reinforcement material	average	yes
contour of the profile	below average	yes, topology of structure
reinforcement coating	low	no
reinforcement configuration	low	no

The identified parameters are now classified with respect to the structural optimization problem. The first parameter in table 2.2 has no equivalent design variable in the the optimization problem. It is assumed that optimal cooling settings are used. The second parameter, *geometry of extrusion die*, take into account the design variables of the cross section. The third parameter, *number of reinforcing elements*, is related to the reinforcement ratios f_1 and f_2. The sixth parameter, *contour of the profile*, is changed only in topology optimization of the overall space frame structure. *Matrix and reinforcement material* are set by discrete design parameter M_{comb}. The last two parameters are again not part of the problem formulation, because they are often fixed due to process reliability.
From the knowledge gained by knowledge acquisition, a qualitative performance index PM_{res} can be approximated. A structured interview is derived from the parameters listed in table 2.2. This interview is the basis of a type-1 fuzzy rule-based system which will be discussed in section 2.4.3.

2.4. Fuzzy sets and fuzzy rule-based systems

Fuzzy logic (FL) was introduced by Zadeh (1965) in order to find a mathematical formulation for human perception. The focus of FL is the description and handling of fuzzy sets[1]. In

[1]The basic concept was described in Bellman et al. (1964) for the formulation of a class problem in pattern classification.

contrast to crisp sets, a sample can have a degree of membership in fuzzy sets and therefore be part of several sets. The basic formulation of fuzzy sets has no physical meaning in terms of possibility or probability.

2.4.1. Definitions and set operations for type-1 fuzzy sets

The membership function gives the mathematical representation of the membership of a sample x in a fuzzy set $\tilde{A}$. The membership function $\mu_{\tilde{A}}(x)$ maps the samples from a sample space Ω to the their respective degree of membership.

$$\mu_{\tilde{A}}(x) \; : \; \Omega \to \mathbb{R} \mid x \to \mu_{\tilde{A}}(x) \tag{2.11}$$

A crisp interval set can be described by the membership function in equation 2.12.

$$\mu_A(x) = \begin{cases} 1 & \text{if } \; x \in A \\ 0 & \text{if } \; x \notin A \end{cases} \tag{2.12}$$

Commonly normalized and convex fuzzy sets are used, the first property defined in equation 2.13a, the second in 2.13b, respectively.

$$\mu_{\tilde{A}}(x) \quad \in [0,1] \tag{2.13a}$$
$$\mu_{\tilde{A}}(x_2) \geq \; \min\left[\mu_{\tilde{A}}(x_1), \mu_{\tilde{A}}(x_3)\right] \forall x_1, x_2, x_3 \in \Omega \;\; with \;\; x_1 \leq x_2 \leq x_3 \tag{2.13b}$$

The support S of a fuzzy set $\tilde{A}$ is defined in equation 2.14a, the core C in equation 2.14b.

$$S(\tilde{A}) = \{x \in \Omega \mid \mu_{\tilde{A}}(x) > 0\} \tag{2.14a}$$
$$C(\tilde{A}) = \{x \in \Omega \mid \mu_{\tilde{A}}(x) = 1\} \tag{2.14b}$$

A *fuzzy number* is a convex and normalized fuzzy set with at least piecewise continuous membership function. $\mu_{\tilde{A}}(x) = 1$ holds for precisely one of the x values. This point is referred to as *mean value of the fuzzy number*.
A *fuzzy interval* is a convex and normalized fuzzy set with at least piecewise continuous membership function, but $\mu_{\tilde{A}}(x) = 1$ holds for an interval $x \in [x_1, x_2]$ and not only a single value.
For fuzzy sets triangular or trapezoid membership functions are common. The first is a fuzzy number, the second a fuzzy interval with linear membership functions. Triangular fuzzy numbers are often characterized by their support interval $S(\tilde{A})$ with $\underline{x} \mid_{\mu_{\tilde{A}}(x)=0}$, $\overline{x} \mid_{\mu_{\tilde{A}}(x)=0}$ and their nominal value $x_\Lambda = x \mid_{\mu_{\tilde{A}}(x)=1}$. A short notation is $\tilde{\Lambda}\,(\underline{x}, x_\Lambda, \overline{x})$.

An example is given in figure 2.2 for the Young's modulus (E) of aluminum. In 2.2a the nominal single value[2] of 70 GPa and an interval $E \in [68, 70]\ GPa$ are shown. In 2.2 a triangular and trapezoidal fuzzy set is displayed. The triangular fuzzy number is $\tilde{\Lambda}(68, 69, 70)$.
The most important set operations union, intersection and complement are given in equation 2.15a, 2.15b and 2.15c, respectively.

$$\mu_{\tilde{A} \cup \tilde{B}}(x) = max\left(\mu_{\tilde{A}}(x), \mu_{\tilde{B}}(x)\right) \tag{2.15a}$$
$$\mu_{\tilde{A} \cap \tilde{B}}(x) = min\left(\mu_{\tilde{A}}(x), \mu_{\tilde{B}}(x)\right) \tag{2.15b}$$
$$\mu_{\tilde{A}^C}(x) = 1 - \mu_{\tilde{A}}(x) \tag{2.15c}$$

The *De Morgan's laws* can be proved for fuzzy sets and are stated in equation 2.16.

$$\left(\tilde{A} \cup \tilde{B}\right)^C = \tilde{A}^C \cap \tilde{B}^C \tag{2.16a}$$
$$\left(\tilde{A} \cap \tilde{B}\right)^C = \tilde{A}^C \cup \tilde{B}^C \tag{2.16b}$$

Also all other operations on classic sets hold for fuzzy sets, except the *excluded-middle laws*. The formulation for fuzzy sets is given in equation 2.17.

$$\tilde{A} \cap \tilde{A}^C \neq \varnothing \tag{2.17a}$$
$$\tilde{A} \cup \tilde{A}^C \neq \Omega \tag{2.17b}$$

The extension principle already defined in Zadeh (1965) is the mathematical basis for the mapping of fuzzy sets into a result space by $y = f(x)$.

$$\mu_{\tilde{B}}(y) = \sup_{x\,:\,y=f(x)} \mu_{\tilde{A}}(x) \tag{2.18}$$

For a given threshold $\alpha \in [0, 1]$ the α-cut for a convex fuzzy set is a crisp subset of the support $S(\tilde{A})$ defined by equation 2.19 and shown in figure 2.2c.

$$[A]_\alpha = \{x \mid \mu_{\tilde{A}}(x) \geq \alpha\} \tag{2.19}$$

From a number n_α^I of given known α-cuts the membership function $\mu_{\tilde{B}}(x)$ can be constructed to achieve a α-cut based representation.

[2] In set theory a set with exactly one element is called singleton.

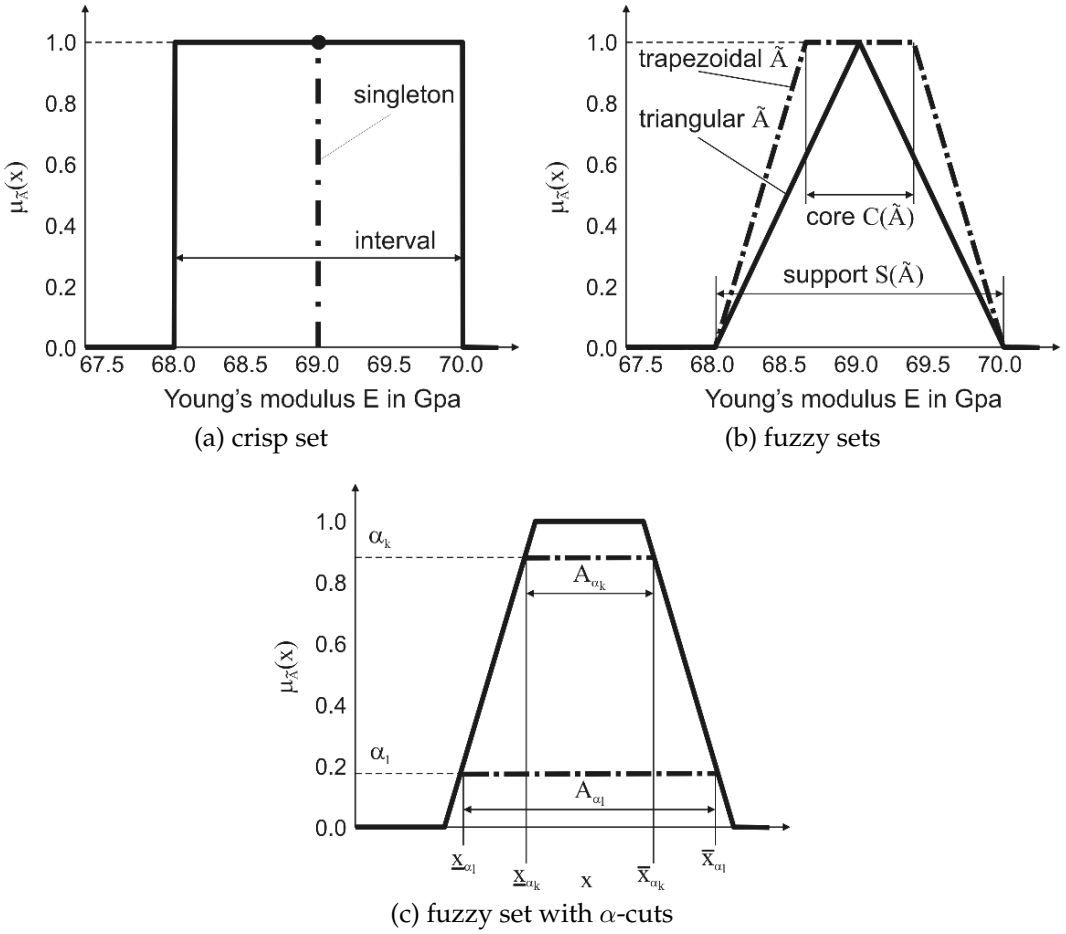

(a) crisp set (b) fuzzy sets

(c) fuzzy set with α-cuts

Figure 2.2.: Definition of different sets

2.4.2. Fuzzy rule-based systems

Knowledge representation can be handled by type-1 fuzzy rule-based system (T1-FRBS) or type-2 fuzzy rule-based system (T2-FRBS). After a knowledge acquisition according to section 2.3 has been performed, the following parts of a fuzzy rule-based system have to be defined.

- inputs: They have to be discretized over their respective universe of discourse.
- outputs: The outputs are discretized in a similar way. Depending on the available information the output can be a physical quantity or a generic number. The latter represents the qualitative nature better but is more difficult to evaluate with respect to the design.
- rule base and inference engine: The rule base connects the inputs with the outputs. This is the most important part of the knowledge-based model. The rules are evaluated by the inference engine. In this thesis the *Mamdani inference method* is used which is provided in MATLAB.

- defuzzification method: The final step is defuzzification[3]. For type-1 fuzzy rule-based systems a crisp output is generated by different means, for example center of area (CoA), bisector of area (BoA) and mean of maximum (MoM). For type-2 fuzzy rule-based systems the defuzzification has two steps. First, a so called type reduction computes a type-1 fuzzy set. Second, the generated set can be reduced further by already mentioned methods to a single crisp output.

2.4.3. Example for fuzzy rule-based system for manufacturing aspects

Two fuzzy submodels for manufacturability index PM_{res} are implemented. The first model represents the influence of the geometry of the extrusion die. The difference between maximum and minimum wall thickness b_{max}/b_{min} has a high influence followed by H/B with medium influence. If stiffeners and reinforcement are utilized, different material strands have to join in the die. Consequently a die with several chambers has to be used resulting in seam weld lines which have a high influence on PM_{res}. The chamber count of the die n_{ch} is the third parameter. For each input parameter of the model three membership functions "small", "medium" and "large" are utilized resulting in 27 rules.
The output is modeled with eleven membership functions. The input and output membership functions are shown in figure 2.3, the model output PM_1 in figure 2.3e on page 23.
The second model takes both reinforcement ratios f_1 and f_2 equally into account. Local residual stresses around reinforcing elements are high. Because material properties are homogenized a qualitative measure for resulting stresses is used. The input and output parameters are shown together with PM_2 in figure 2.4 on page 24.
The overall performance measure PM_{res} is calculated by equation 2.20. The weighting factors a_i reflect the influence of the submodels on PM_{res}.

$$PM_{res} = a_1 * PM_1 + a_2 * PM_2 \qquad a_1 = a_2 = 1 \tag{2.20}$$

[3]This part holds only for *Mamdani* fuzzy rule-based systems. For *Sugeno* fuzzy rule-based systems please refer to literature.

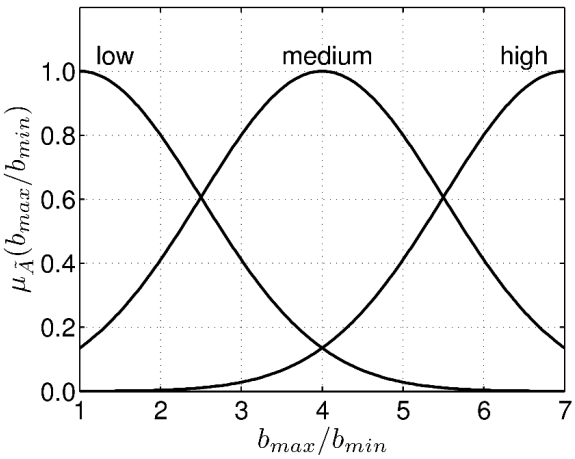

(a) membership function for input 1

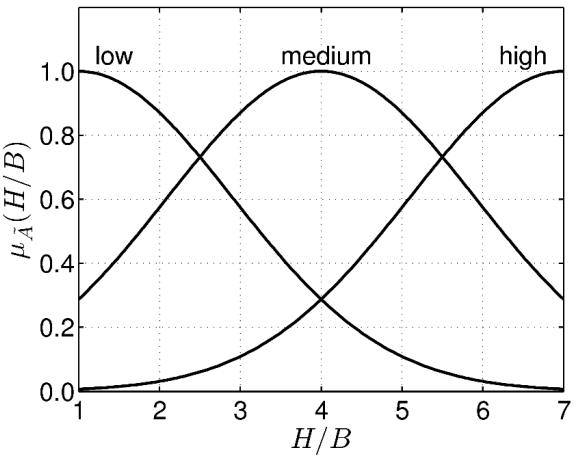

(b) membership function for input 2

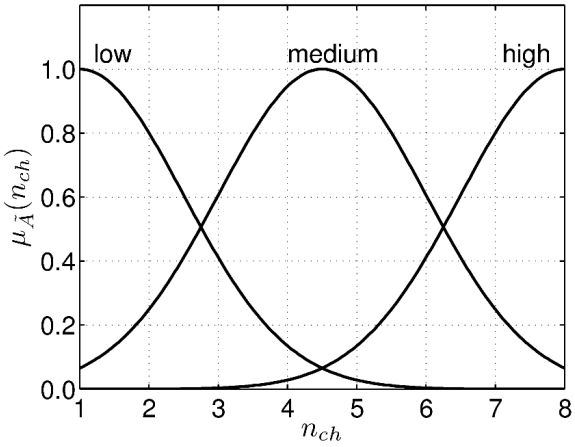

(c) membership function for input 3

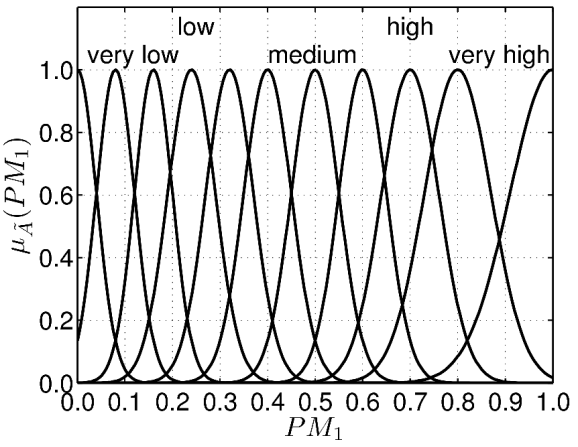

(d) membership function for output

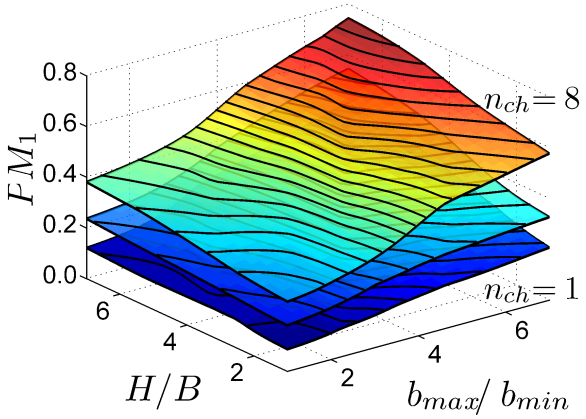

(e) output of knowledge-based model

Figure 2.3.: First fuzzy submodel for influence of die geometry

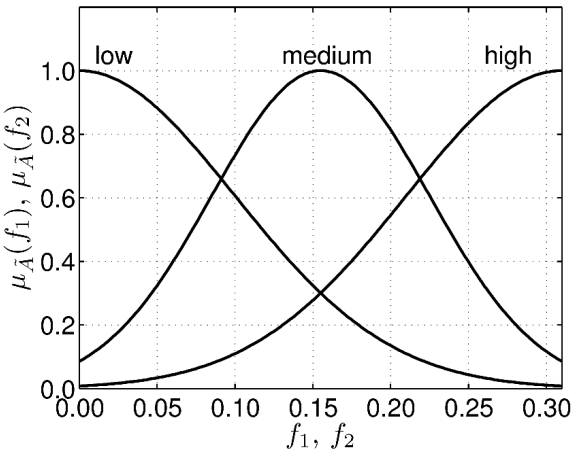

(a) membership function for input 1 and 2

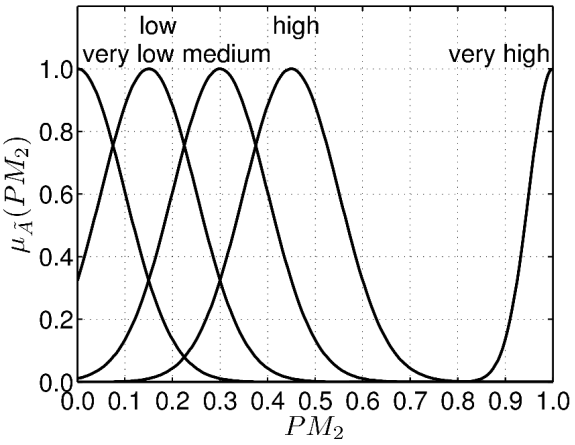

(b) membership function for output

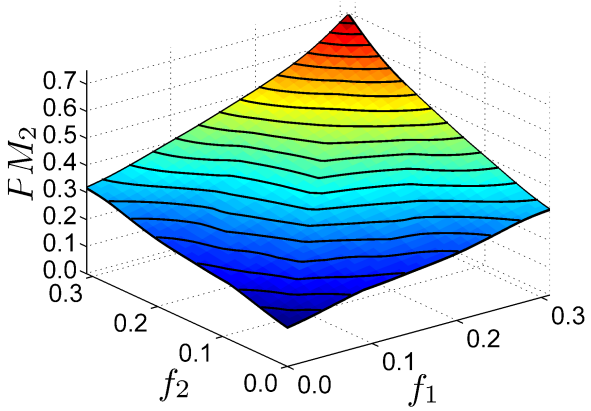

(c) output of knowledge-based model

Figure 2.4.: Second fuzzy submodel for influence of reinforcement ratios

2.5. Handling of fuzzy system and design parameters in structural optimization

Evaluation of design variables $\tilde{\mathbf{x}}$ and parameters $\tilde{\mathbf{p}}$ subjected to uncertainties is a major challenge in optimization. Depending on the uncertainties present in the problem formulation different approaches are known which are shortly discussed in the literature survey. In this thesis uncertainties are represented by fuzzy numbers which is in accordance with fuzzy information available from expert knowledge.
In this section, first a short literature overview together with an analytical example is given followed by the introduction of an algorithm developed in Wehrle (2008) under supervision of the author. An engineering example for allowed tolerances in profile extrusion is presented in section 2.5.3.

2.5.1. α-cut level optimization

First, a basic mathematical definition is necessary. From the definitions in section 2.4.1 and equation 2.19 the fuzzy analysis can be transformed into multiple interval computations in equation 2.21a. It can be expressed as constrained global optimization problems in equation 2.21b.

$$\tilde{\mathbf{r}} = f(\tilde{\mathbf{x}}) \quad \Leftrightarrow \quad [\tilde{\mathbf{r}}] = f([\tilde{\mathbf{x}}]_\alpha) \quad , \quad \forall \alpha \in [0,1] \tag{2.21a}$$

$$f([\tilde{\mathbf{x}}]_\alpha) \quad \Leftrightarrow \quad \begin{cases} \overline{\mathbf{r}}_\alpha = \sup f(\mathbf{x}) \\ \underline{\mathbf{r}}_\alpha = \inf f(\mathbf{x}) \end{cases} \quad , \quad with\ x_i \in [\tilde{x}_i]_\alpha \tag{2.21b}$$

This equation states that the computation of a fuzzy output can be substituted by n_α^I computations on α-cut levels. On each α-cut level the *infimum* inf and *supremum* sup of the system answer has to be found. The problem stated in equation 2.21 is easy to solve if monotonic functions are evaluated. For engineering problems this assumption is often not possible, especially for non-linear system behavior. Another challenge is the utilization of deterministic system equations such as FEM, which are commonly used in engineering design. The methods for α-cut level optimization (αCLO) are classified according to Degrauwe (2007). For more details see Braibant et al. (1999) and Klimke (2003).

Methods based on VM. The first approach computes the system output at predefined design points. Based on the vertex method (VM) introduced in Dong and Wong (1987) and Dong and Shah (1987) many derivatives of this method can be found in literature: level interval algorithm (LIA) by Wood et al. (1992), transformation method (VMt) by Hanss (2002), short transformation method (VMst) by Donders et al. (2004). Klimke (2003) developed several applications, for example reduced transformation method (VMrt) and general transformation method (VMgt) and general transformation method with removed recurring points (VMgtr).
Basically these methods compute the system answer at the corner points of the α-cut levels resulting in an approximation of the vertices of the fuzzy output. The original implementation needs 2^n system evaluations for n uncertain parameters on every α-cut level. An assumption for VM are monotonic functions, which also limits its use for engineering problems.
In addition to corner points, internal points are evaluated on each α-cut level for methods based on the transformation method (VMt). The evaluation of *supremum* and *infimum* are based on the computed support points only. Piecewise continuous and non-monotonic functions can be handled with high enough discretization. The general transformation method with removed recurring points (VMgtr) deletes recurring points from the computation scheme especially for $\tilde{x}$ with symmetric $\mu_{\tilde{A}}(x)$. With increasing number of fuzzy parameters the computational effort increases for afore mentioned methods.

Methods based on global optimization with surrogates. The system answer is approximated by surrogates based on design of experiments (DOE) and *supremum* and *infimum* are found by two optimizations. This overcomes the restrictions to monotonic functions with reasonable computation effort. Implementations can be found for the level interval algorithm (LIA) in Law (1996), for optimized vertex method (VMo) in Smith et al. (2002), gradual α-level decreasing algorithm (GαD) in Degrauwe (2007) and global optimization

with sparse grid interpolation in Klimke (2006). A book on this topic combines methods with evolutionary strategy, gradient method and Monte Carlo sampling in Möller and Beer (2004). An algorithm for optimization with type-1 fuzzy uncertainties (opTUM) was developed under supervision of the author in Wehrle (2008).
Stochastic algorithms can be utilized directly, gradient based ones need multiple starting points in order not to stop in a local minimum or maximum, respectively. The optimization problem is restricted only by the boundaries of the design variables $\mathbf{x}_l$ and $\mathbf{x}_u$ on a given α-cut level $[\tilde{\mathbf{x}}]_\alpha$. Different surrogate schemes can be found in literature.

The following example will give information on the advantages and disadvantages of different methods. The evaluated function is *peaks* provided by MATLAB. The function has two input variables x_1 and x_2 and one output r and is given in equation 2.22. The uncertainty is described by symmetric, triangular fuzzy membership functions $\tilde{x}_1 = \tilde{x}_2 = \tilde{\Lambda}(-2, 0, 2)$. The function has several local maxima and minima in the defined range.

$$r = 3 * (1 - x_1)^2 * e^{\left(-(x_1^2)-(x_2+1)^2\right)} - 10 * \left(\frac{x}{5} - x_1^3 - x_2^5\right) * e^{\left(-x_1^2-x_2^2\right)} - \frac{1}{3} * e^{\left(-(x_1+1)^2-x_2^2\right)} \tag{2.22}$$

The contours of the function are given in figure 2.5. Also the five α-cut levels are given together with the starting points for multiple gradient based optimization runs.

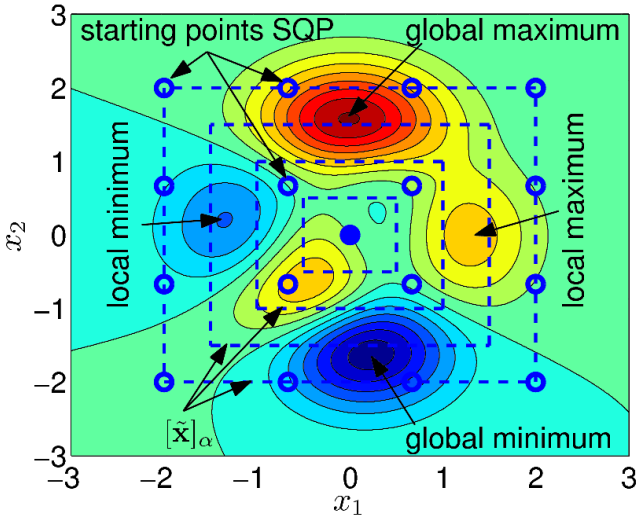

Figure 2.5.: Function *peaks* with α-cut levels

The fuzzy output $\tilde{r}$ is computed with the help of VM, VMrt, VMgt and VMgtr. The programming code in MATLAB for the last three methods can be found in Klimke (2003). The following methods from opTUM based on optimization[4] are utilized: method with gradient based SQP and single starting point at $\mathbf{x}_\Lambda$ (OM-SQP SSP), method with gradient based SQP and multiple starting points (OM-SQP MSP) and finally a method with a genetic algorithm (OM-GA).

[4]No surrogates are used for this simple example.

The fuzzy output $\tilde{r}$ computed by these methods is given in figure 2.6. On the left side in figure 2.6a the problem of VM with nonlinear functions can be seen, because the resulting fuzzy number $\tilde{r}$ for VM does not fulfill the definition of a fuzzy number. VMrt overcomes this problem but fails to give the true fuzzy output. VMgt and VMgtr give the same result for $\tilde{r}$, which still does not represent the true shape. At least 10 α-cut levels are needed for these two methods to achieve a proper representation.
On the right side in figure 2.6b the results for optimization based methods are given. A gradient based algorithm with a single starting point (OM-SQP SSP) runs into local extrema and can not provide the right answer. Only with multiple starting points (OM-SQP MSP) or with a stochastic algorithm (OM-GA), the true shape of $\tilde{r}$ is found correctly within the limitations of the α-cut discretization.

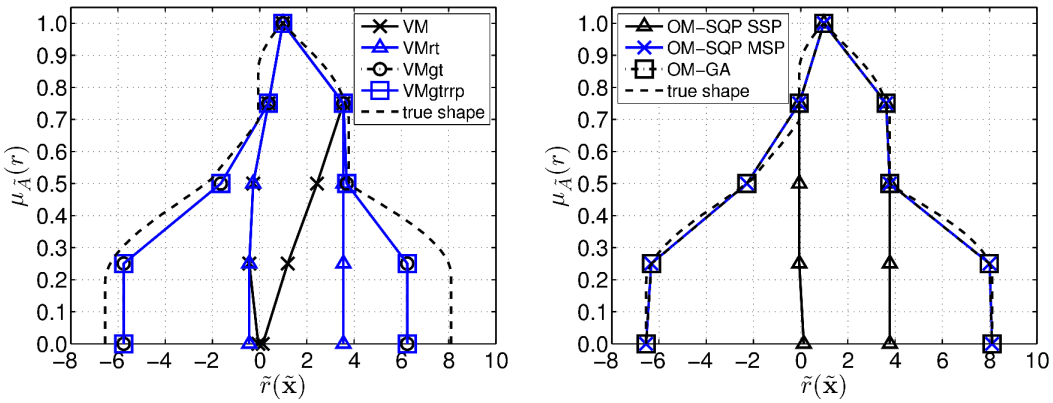

Figure 2.6.: Fuzzy number generated by different α-cut level optimization methods

Beside the ability of the different methods to find the true shape of $\tilde{r}$, the number of necessary function evaluations is crucial for engineering applications. For this example with only two uncertain input parameters $\tilde{x}$ the number of α-cut levels is varied $n_\alpha^I \in [3, 100]$ and the number of necessary function evaluations is given on a logarithmic scale in figure 2.7.

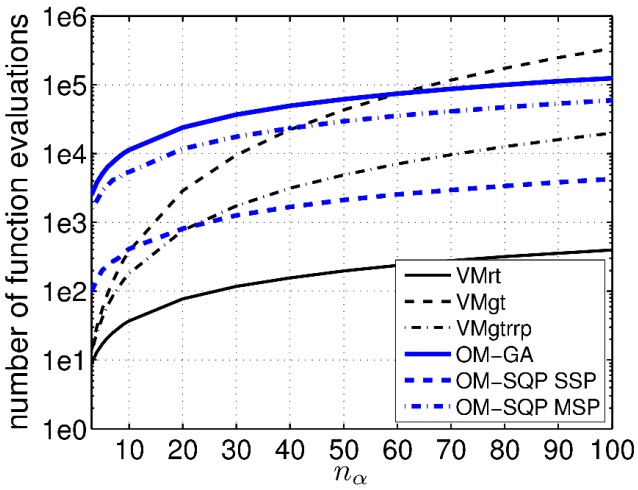

Figure 2.7.: Number of function evaluations for different α-cut level optimization methods

For only two uncertain design variables $\tilde{x}$ methods based on optimization need much more function evaluations for a small number of α-cut levels then methods based on vertex method. It is very important to note, that the settings for the optimization based methods are not optimized. For example 16 starting points are used for OM-SQP MSP, which could be reduced. No evaluation of the GA settings is performed with respect to population size and number of generations. With increasing number of α-cut levels the methods based on optimization are better compared to VM methods with respect to computational effort.

2.5.2. Algorithm opTUM – description and flowchart

The first implementation for type-1 fuzzy parameters was done in the master thesis Wehrle (2008) under supervision of the author. The algorithm is named algorithm for optimization with type-1 fuzzy uncertainties (opTUM)[5]. It utilizes surrogate based α-cut level optimization (αCLO) together with parallelization of system evaluation in order to reduce computation time. opTUM was tested in Wehrle (2008) with analytical functions and a ten bar truss (TBT) example. Together with the author the algorithm was enhanced and the influence of contour deviations of three dimensional curved profiles on structural performance was investigated in Huber et al. (2009).
The single steps of algorithm opTUM are shown in figure 2.9 on page 30 and described in the following.

- define uncertain design variables and parameters $\tilde{\mathbf{x}}$, $\tilde{\mathbf{p}}$:
  The shapes and ranges of the fuzzy membership function for $\tilde{\mathbf{x}}$ and $\tilde{\mathbf{p}}$ are defined.

- α-cut level discretization:
  The number of α-cut levels n_α^I is defined. Depending on the expected nonlinearity of the system three to six levels should be considered for engineering problems.
  $3 \leq n_\alpha^I \in \mathbb{N} \leq 6$

- DOE in interval boundaries for $\mu = 0$:
  A design of experiments scheme is used to define designs for the building of surrogates. The DOE are within the intervals of the $\mu = 0$ α-cut of $\tilde{\mathbf{x}}$ and $\tilde{\mathbf{p}}$. The number of support points n_s depends on the expected nonlinearity and the necessary computation time.

[5] Acronym from german name: **Opt**imierung unter **U**nsicherheiten mit der **M**öglichkeitstheorie

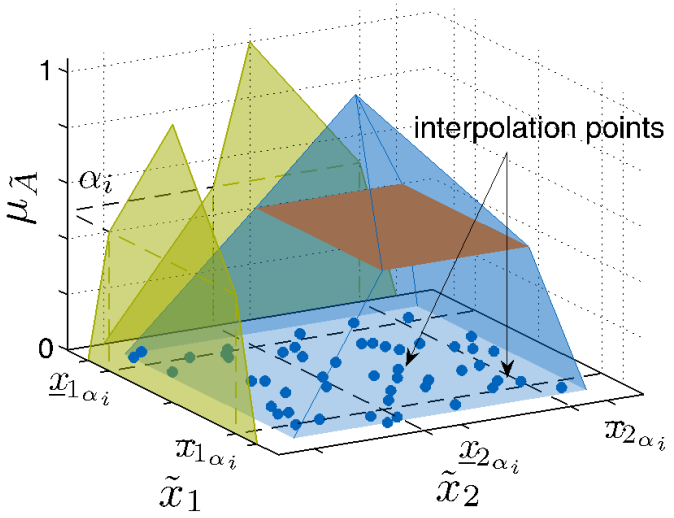

Figure 2.8.: DOE in parameter space

- system analysis r:
  Designs are computed according to DOE.

- surrogate model $\hat{r}$:
  A surrogate model is built for the system answer $\hat{r}$. Different modeling approaches can be used, for example KGM and RSM.

- interval analysis for each α-cut level $\hat{\overline{r}}_\alpha$, $\hat{\underline{r}}_\alpha$:
  The maximum and minimum value of the surrogate output $\hat{\overline{r}}_\alpha$ and $\hat{\underline{r}}_\alpha$ are computed on given α-cut levels. For engineering examples with local maxima and minima simple stochastic optimization algorithms or gradient based algorithms with multiple starting points can be utilized. Only side constraints have to be considered which limit the feasible range of $\tilde{\mathbf{x}}$ and $\tilde{\mathbf{p}}$ with respect to the α-level.

- result verification:
  The maximum and minimum have to be checked. Compute r for $(\tilde{\mathbf{x}}^*, \tilde{\mathbf{p}}^*)|_{\hat{\overline{r}}_\alpha}$ and for $(\tilde{\mathbf{x}}^*, \tilde{\mathbf{p}}^*)|_{\hat{\underline{r}}_\alpha}$.

- error smaller then bound?
  If the difference between $r|_{\hat{\overline{r}}_\alpha}$ and $\hat{\overline{r}}_\alpha$ or $r|_{\hat{\underline{r}}_\alpha}$ and $\hat{\underline{r}}_\alpha$ is bigger then given error bound ϵ^r_α add these points to surrogate and reevaluate model.

- α-cut level system response $\hat{\overline{r}}_\alpha$, $\hat{\underline{r}}_\alpha$

- generate possibilistic system response $\tilde{r}$ with $\hat{\overline{\mathbf{r}}}_\alpha$ and $\hat{\underline{\mathbf{r}}}_\alpha$ for all α-cut levels[6]

[6] $\tilde{r}$ is assumed to be very close to the real system answer and therefore the notation for surrogate results $\hat{\tilde{r}}$ is not used.

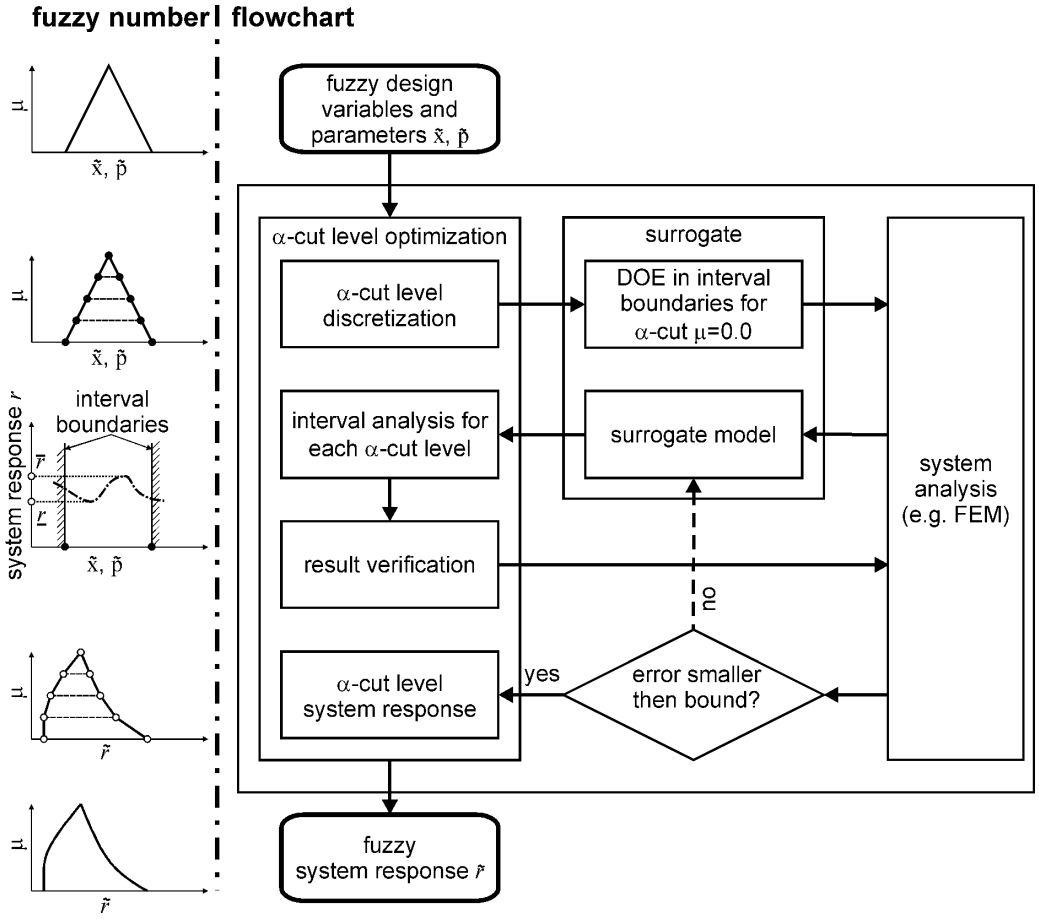

Figure 2.9.: Flowchart opTUM

2.5.3. Example for uncertain parameters arising from manufacturing processes

This example is not directly related to the one defined in equation 2.6 on page 16. Here a deviation of the profile contour ΔC from the designed geometry as shown in figure 2.10a is investigated. A detailed description can be found in Huber et al. (2009). The deviation of the contour ΔC is modeled by the fuzzy number in figure 2.10b.
Elastic-plastic material properties are assumed and a compression load is applied to the curved profile. A nonlinear FEM model is evaluated with opTUM. The resulting structural system answers are shown in figure 2.11. On the left hand side deformation is shown in figure 2.11a. For the nominal profile contour a deformation of 43.6 mm is computed. With increasing deviation ΔC the maximum deformation increases nearly linear to 45.7 mm. In figure 2.11b maximum stress is shown. Here a nonlinear behavior is observed. The stress in the profile reaches the yield strength of the material. To ensure a safety factor a critical α-cut level is identified at 0.68. This level restricts the allowed deviation of the contour ΔC to a maximum value of 6.7 mm. From this evaluation allowed tolerances for manufacturing processes with respect to structural properties can be found.

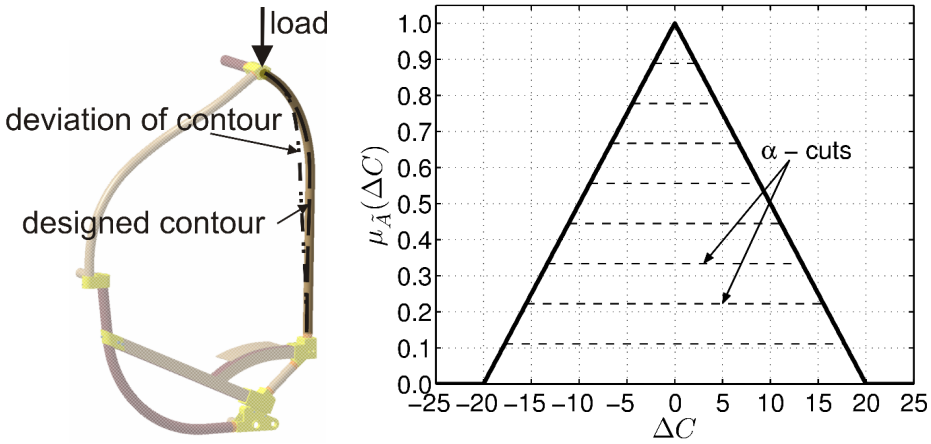

(a) space frame (b) fuzzy number for ΔC

Figure 2.10.: Deviation of profile contour due to manufacturing tolerances

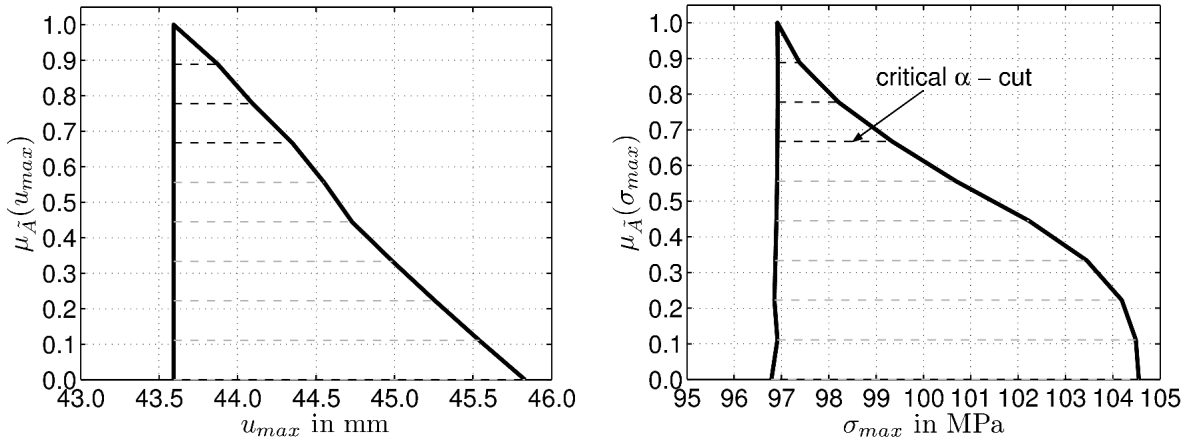

(a) deformation (b) maximum stress

Figure 2.11.: Mechanical properties as function of contour deviation ΔC

2.6. Summary of chapter

The basics for structural optimization, knowledge acquisition and knowledge representation are given in this chapter. The α-cut level optimization is introduced together with an efficient algorithm for its computation, opTUM. Starting with the definition of an engineering optimization problem the methods are utilized in an engineering context. Knowledge-based models are build from expert knowledge with a type-1 fuzzy rule-based system and system answers with respect to type-1 fuzzy set fuzzy input parameters are computed.

3. Advanced methods for the handling of qualitative manufacturing knowledge

The methods presented in chapter 2 are extended in order to handle uncertainties in expert knowledge described by type-2 fuzzy sets (T2 FS). For rule-based systems the single membership functions related to verbal expressions such as "small", "big", etc. are extended to type-2 fuzzy sets in order to account for uncertainties in the definition of verbal terms. This enhances the quantification of qualitative manufacturing information.
Type-2 fuzzy sets are mainly used for control applications. In the last years they gained more importance also in other fields of research. New methods for type-2 fuzzy uncertainties are developed in this chapter, the focus is on α-cut level optimization, defuzzification, and comparison methods for goal and constraint handling.
The basics of type-2 fuzzy sets are given in section 3.1, α-cut level optimization is extended in section 3.2. Advanced evaluation methods for goal and constraint handling are presented in sections 3.3 and 3.4. Finally consequences for structural optimization are summarized in section 3.5.

3.1. Basics of type-2 fuzzy systems

The basics of type-2 fuzzy sets can be found in Mendel (2001) and Castillo and Melin (2008). Type-2 fuzzy sets are a generalization of type-1 fuzzy sets adding a third dimension to the membership function.
A triangular type-1 membership function as shown in figure 2.2b is blurred by shifting the membership function to the left and right. The resulting set of membership functions is displayed in figure 3.1a on page 34. For a given x the vertical line intersects now not only one membership function with a single membership value $\mu_{\tilde{A}}(x)$ but several membership functions. The shifted membership functions do not necessarily have the same weight. By assigning an amplitude distribution to the membership function as indicated by the thinning and graying lines in figure 3.1b a three dimensional membership function is created. This is a type-2 membership function $\mu_{\tilde{\tilde{A}}}$ characterizing a type-2 fuzzy set $\tilde{\tilde{A}}$. Note the change in the notation of the y-axis from $\mu_{\tilde{A}}(x)$ to u.
The original membership function is called the *primary membership function*, the additional one the *secondary membership function*[1]. The latter is another type-1 membership function.
A type-2 fuzzy set denoted by $\tilde{\tilde{A}}$, is defined by a membership function $\mu_{\tilde{\tilde{A}}}(x,u)$, where $x \in X$ (universe of discourse), $u \in J_x^u \subseteq [0,1]$ and $0 \leq \tilde{\tilde{A}}(x,u) \leq 1$. The mathematical definition is given in equation 3.3 for continuous X.

$$\tilde{\tilde{A}} = \{(x, u, \mu_{\tilde{\tilde{A}}}(x,u)) \mid \forall x \in X, \forall u \in J_x^u \subseteq [0,1]\} \tag{3.1}$$

[1] For an exact definition please refer to Mendel (2001).

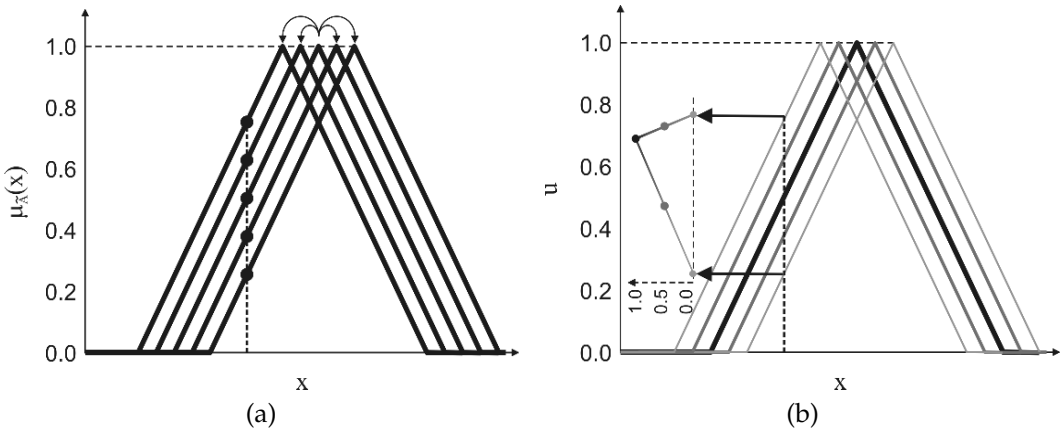

Figure 3.1.: Stepwise extension of type-1 fuzzy set to type-2 fuzzy set

For operations on type-2 fuzzy sets and defuzzification purposes, a definition for a discretized universe of discourse X with N discretization points is given in 3.2.

$$\tilde{\tilde{A}} = \sum_{i=1}^{N} \left[\sum_{u \in J_{x_i}} f_{x_i}(u)/u \right] \Big/ x_i \tag{3.2}$$

Most recently the well known α-cut level representation for type-1 fuzzy sets was also introduced to type-2 fuzzy sets in Liu (2008), Mendel and Liu (2008), Mendel et al. (2009) and Hamrawi and Coupland (2009). Wagner and Hagras (2008) and a few others basically introduced the same idea but named it differently, for example "zSlices" in Wagner and Hagras (2008).
An α-cut for a general type-2 fuzzy set is the union of all primary memberships of $\tilde{\tilde{A}}$, whose secondary grades are greater than or equal to α.

$$\tilde{\tilde{A}}_{\alpha} = \{(x, u, \mu_{\tilde{\tilde{A}}}(x, u)) \geq \alpha \mid \forall x \in X, \forall u \in J_x^u \subseteq [0, 1]\} \tag{3.3}$$

If the secondary membership function has the properties of an interval set as defined in equation 2.12 it is called interval type-2 fuzzy set (IT2 FS). Those are used for computational reasons and because they reflect an uniform uncertainty at the primary membership functions of x. This uncertainty is present especially for knowledge-based models, when the experts are not sure about the boundaries of a fuzzy set.
An interval type-2 membership function is shown in three dimensions in figure 3.2 together with its footprint of uncertainty (FOU). The footprint of uncertainty (FOU) is the union of all primary memberships and is defined in equation 3.4.

$$FOU\left(\tilde{\tilde{A}}\right) = \bigcup_{x \in X} J_x \tag{3.4}$$

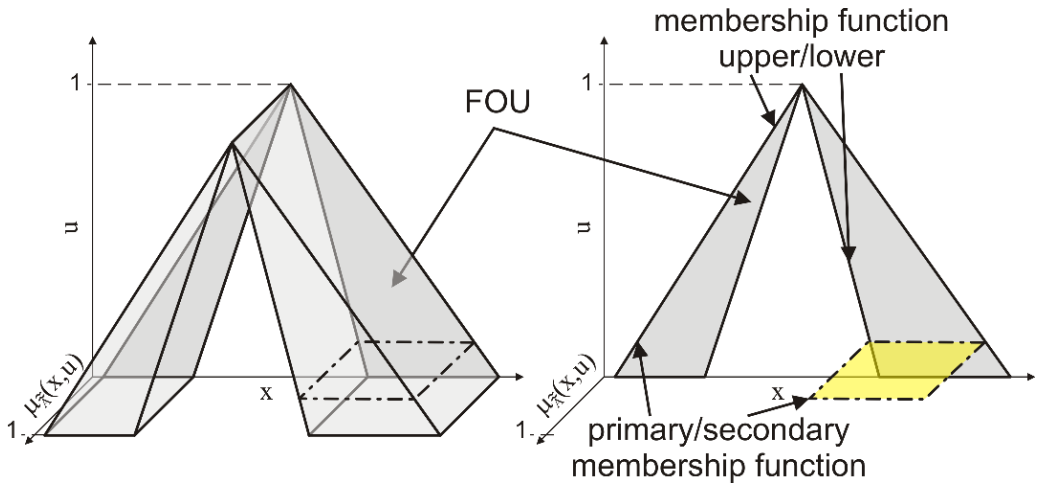

Figure 3.2.: Type-2 fuzzy set with footprint of uncertainty

The upper membership function is the upper boundary, the lower membership function the lower boundary of the FOU respectively. For general T2 FSs in α-cut level representation the footprint of uncertainty is given in equation 3.5.

$$FOU\left(\tilde{\tilde{A}}\right) = \tilde{\tilde{A}}_0 \tag{3.5}$$

With an indicator function $I_{\tilde{\tilde{A}}_\alpha}$ for $\tilde{\tilde{A}}_\alpha$ shown in equation 3.6 the α-cut representation of a general T2 FS is given in equation 3.7.

$$I_{\tilde{\tilde{A}}_\alpha}(x,u \mid \alpha) = \begin{cases} 1 & \text{if } (x,u) \in \tilde{\tilde{A}}_\alpha \\ 0 & \text{if } (x,u) \notin \tilde{\tilde{A}}_\alpha \end{cases} \tag{3.6}$$

$$\tilde{\tilde{A}} = \bigcup_{\alpha \in [0,1]} FOU\left(\tilde{\tilde{A}}_\alpha\right) \tag{3.7}$$

Basically the definitions and operations for type-2 fuzzy numbers, type-2 fuzzy sets and for type-2 fuzzy rule-based systems are similar to type-1 ones. Please refer to Mendel (2001) for details. Also general type-2 fuzzy sets are discussed in this literature source. In this thesis the Interval Type-2 Fuzzy Logic Toolbox for MATLAB used in Castillo and Melin (2008) kindly provided by Professor Oscar Castillo from the Tijuana Institute of Technology in Mexico is applied for type-2 fuzzy rule-based systems. The latter is used for knowledge-based expert models.

3.2. Extension of α-cut level optimization for type-2 fuzzy sets

The methods for αCLO presented in the last chapter have to be extended in order to handle T2 FSs. A new tool called algorithm for optimization with type-2 fuzzy uncertainties (opTUM-II) is developed, implemented and evaluated. The most important options for opTUM-II are shortly described. First T2 FS parameters and their definition are introduced followed by DOE schemes and surrogate methods. Finally optimization algorithms for α-cut level optimization are introduced.

3.2.1. Parameters of type-1 and type-2 fuzzy sets

The type-1 and type-2 fuzzy sets are defined by typical parameters. The shape of the primary and secondary MF for type-2 fuzzy set can be set independently. Table 3.1 provides an overview and figure A.1 in the appendix a geometric definition.

Table 3.1.: Parameters for type-1 and type-2 fuzzy sets in opTUM-II

fuzzy type	shape	subtype	number of parameters p	note
1	Gaussian	-	2	
	trapezoid	-	4	triangular for $p_2 = p_3$
2	Gaussian	primary	4	uncertain mean for $p_1 = p_3$
				uncertain σ for $p_2 = p_4$
	trapezoid	primary	8	triangular for $p_2 = p_3 = p_6 = p_7$
	triangular	secondary	2	location of core for FOU cut
				as ratio $\in [0, 1]$ for left
				and right boundary

3.2.2. Design of experiments and surrogate models

The αCLO can be based on the original system equations or on surrogate models. The former is feasible only if the computation time for one system equation is reasonable or a computer cluster is available. The latter will be commonly used for engineering examples with computation times for system equations ranging from several minutes to hours. In order to build a surrogate model, a design of experiments has to be performed. opTUM-II offers the following design of experiments schemes: LHS–DACE described in Lophaven et al. (2002a) and Lophaven et al. (2002b), FFD, FFD, CCD, BBD and LHS from MATLAB. Sampling points provided by the user can be integrated by simple text files.
Optionally the corner points of the α-cut levels can be evaluated. This adds 2^n system evaluations for n uncertain parameters. The sampling points are generated in the parameter intervals for $\mu(\tilde{x}) = 0$. Depending on the chosen design of experiments scheme the number of sampling points can be set manually or is given automatically.

Surrogate models have to be able to map local extrema in order to handle engineering problems. Mainly the kriging method implemented in DACE described in Lophaven et al. (2002a) is utilized for engineering problems in this thesis. A check of the surrogate quality is performed for second order polynomial regression model. The regression model is switched automatically to first or zero order if quality problems arise and a warning is issued to the user. In principal, every surrogate scheme provided by MATLAB can be used too.

3.2.3. Optimization algorithms for α-Cut Level Optimization

The optimization algorithm for αCLO has to be chosen carefully with respect to the properties of the system answers and, if used, the properties of the surrogate. The algorithm must find local extrema for given side constraints. The latter define the bounded parameter space. Optimization algorithms implemented are gradient based *fmincon* from MATLAB with a single and multiple starting points (generated by LHS design), a genetic algorithm from MATLAB and finally a simple evolutionary strategy based on the lecture *Multidisciplinary Design Optimization* available from Baier et al. (2008).

3.2.4. Extension of α-cut level optimization to type-2 fuzzy sets

The primary membership function is discretized into n_α^I, the secondary into n_α^{II} α-cut levels[2]. This leads to an overall number of $n_\alpha^I \bullet n_\alpha^{II}$ α-cut levels. This discretization is shown in figure 3.3a. For the primary membership function the levels are α_{1i} with $i = 1 \ldots n_\alpha^I$, for the secondary α_{2j} with $j = 1 \ldots n_\alpha^{II}$.
On every α-cut level two α-cut level optimizations are carried out. The first with the outer boundaries of the input parameters $x^{LL}_{\alpha 1 i 2 j}$ and $x^{RR}_{\alpha 1 i 2 j}$ as side constraints. The second with the inner boundaries $x^{L}_{\alpha 1 i 2 j}$ and $x^{R}_{\alpha 1 i 2 j}$.
After the results of all αCLOs are available, the fuzzy output $\tilde{r}$ is checked for convexity. Non-convex fuzzy sets are transformed in convex ones as shown in figure 3.3b for primary and secondary membership function.

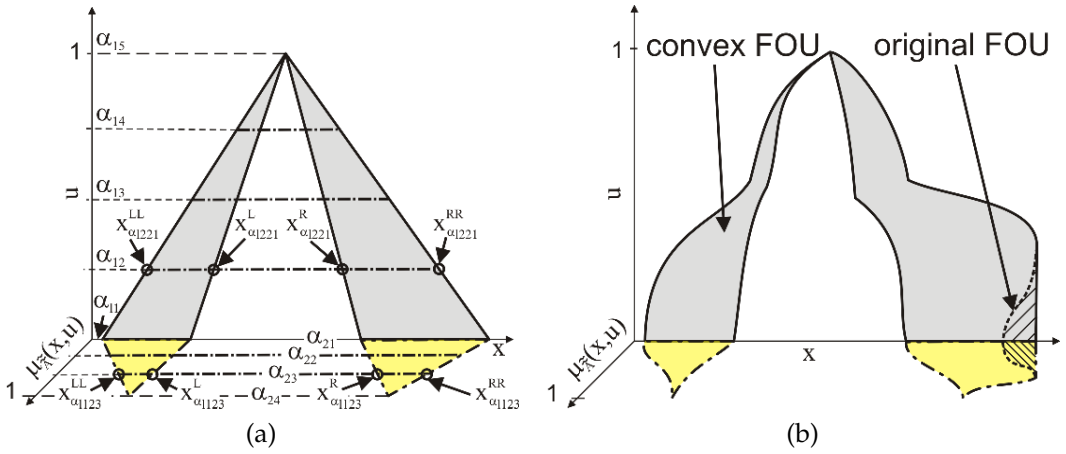

Figure 3.3.: Discretization of type-2 fuzzy set

[2]For interval type-2 fuzzy sets $n_\alpha^{II} = 1$.

3.2.5. Analytical example

For the example given in chapter 2.5.1 with results displayed in figure 2.6 the inputs x_1 and x_2 are changed to type-2 fuzzy sets:

$$\tilde{\tilde{x}}_1 = \tilde{\tilde{x}}_2 = \tilde{\tilde{\Lambda}}\left(-2.5, 0, 2.5; -2, 0, 2; -1.5, 0, 1.5\right) \tag{3.8}$$

The first three entries define the upper MF, the fourth to sixth entry the core of the type-2 fuzzy set and the seventh to ninth entry the lower MF. This definition represents a symmetrical uncertainty of 0.5 for the boundaries of the input parameters with the most possible value for the original type-1 fuzzy number. The FOU of the inputs is shown in figure 3.4a, $\mu_{\tilde{\tilde{A}}}(x, u)$ is given in figure 3.4b.

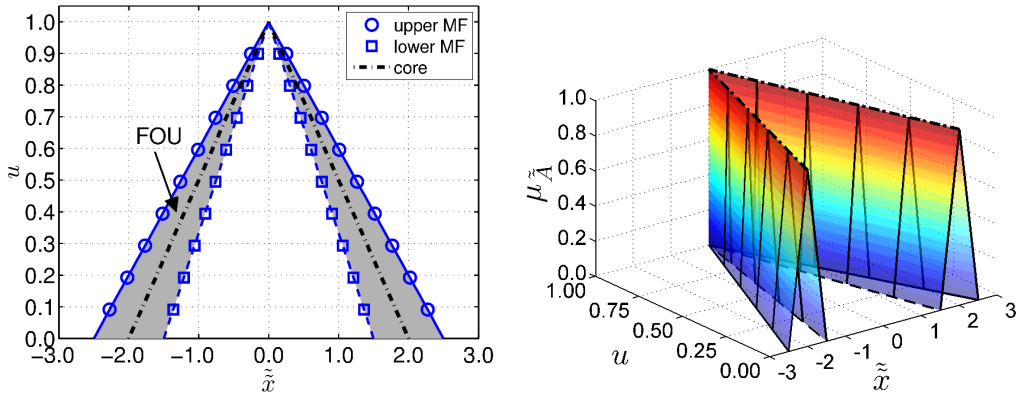

(a) (b)

Figure 3.4.: Type-2 fuzzy set for input parameters

The resulting output is shown in figure 3.5. On the left side the FOU of $\tilde{\tilde{r}}$ together with the core is displayed. The latter is exactly the same as the result of opTUM in figure 2.6 on page 27. On the right side in figure 3.5b $\mu_{\tilde{\tilde{A}}}(r, u)$ is shown.

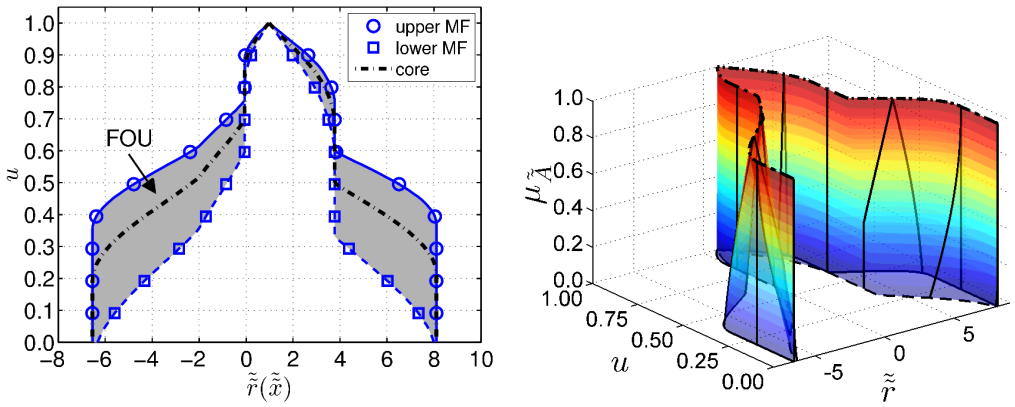

(a) (b)

Figure 3.5.: Type-2 fuzzy set for system output

3.3. Defuzzification methods for goals

For goal handling in standard optimization algorithms characteristic scalar values have to be computed for fuzzy sets. The following three considerations are important for selection of such methods.

- scalar values representing the physical measure of the engineering goal
- measures for uncertainty
- an estimate for nonlinear behavior

If additional effort is put into uncertainty analysis an important influence in optimization is assumed. This leads to multiobjective optimization problems which minimize the physical goals and uncertainty characteristics in parallel.
Methods for the above listed measures for T1 FSs and T2 FSs are presented in this section. For T1 FS known techniques are used, for IT2 FS and T2 FS sophisticated approaches are implemented and extended.

3.3.1. Goal handling for type-1 fuzzy sets

Several methods are well established for mapping T1 FS to a scalar value. This process is referred to as defuzzification. In order to minimize the loss of information by defuzzification not only one but several scalar values can be extracted from one T1 FS. Possible measures are given in figure 3.6, most of them can be extracted via opTUM-II.

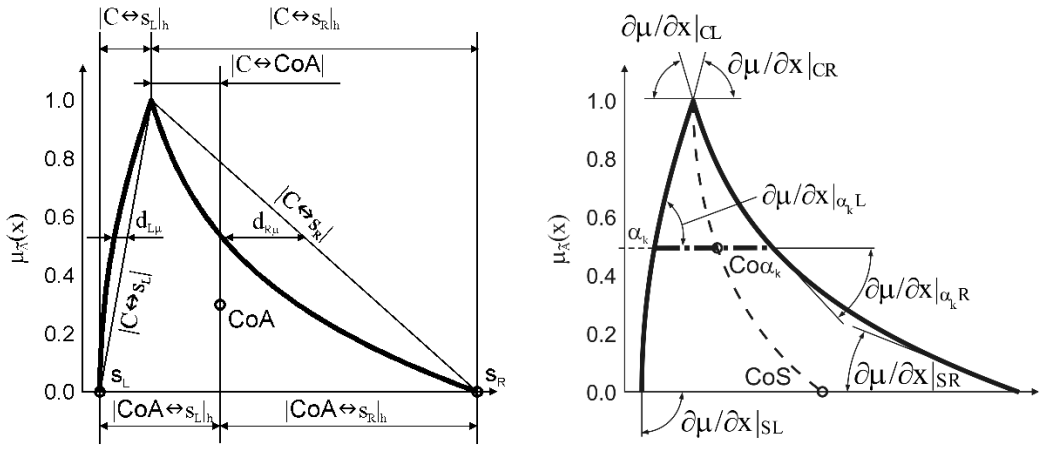

(a) (b)

Figure 3.6.: Information in a fuzzy number

Main physical goal. From an engineering point of view, this scalar should represent the main physical property to be minimized such as mass, deformation or eigenfrequencies. Core C, center of area (CoA) and center of support (CoS) are obvious choices with CoA as the by far mostly used scalar value for defuzzification. Also bisector of area (BoA), largest

of maximum (LoM), mean of maximum (MoM) and smallest of maximum (SoM), which are not shown in figure 3.6, can be found in literature, for example in Castillo and Melin (2008). CoA and CoS depend also on nonlinearities in the system answer.
For goals which are generally minimized the left most point of the support s_L can also be interesting.

Goal for uncertainty evaluation. Information about uncertainty for the main goals is essential for the following optimizations. The uncertainty is represented by support S or representative α level cuts. Also distances between core C, CoA, and CoS or boundaries of support s_L and s_R can be used.

Goal for nonlinearity evaluation. It can be measured by distances between the connection of C and s_L, s_R, $d_{L\mu}$ and $d_{R\mu}$ respectively. Also the ratio of gradients of the membership function at C, s_L and s_R are measures for nonlinearity.

Goal for skewness evaluation. The symmetry of the fuzzy number is evaluated. A possible measures is the absolute distance between core and CoS: $|C - CoS|$. It is similar to the skewness measure $S_k(\tilde{A})$ suggested in Subasic and Nakatsuyama (1997).

Different settings for main and secondary goals and their combination are discussed in chapter 4 for an analytical example.

3.3.2. Goal handling for type-2 fuzzy sets

The methods described in the previous section can be utilized also for upper and lower membership functions in IT2 FSs and on every α-cut level for general T2 FSs. To gain additional measures taking into account characteristics of IT2 FS and T2 FS enhanced methods are presented The evaluation with respect to optimization follows at the end of this section.

Defuzzification methods

Type-2 fuzzy sets hold more information than type-1 fuzzy sets. The defuzzification process commonly has two steps. In the first step the type-2 fuzzy set is mapped into a type-1 fuzzy set, in the second this type-1 fuzzy set is transfered into a crisp value by methods listed in section 3.3.1. This process is also shown in figure 3.7.

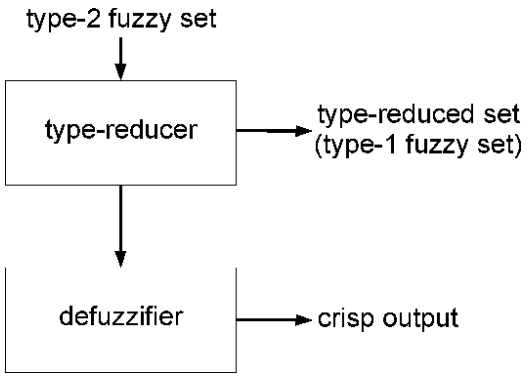

Figure 3.7.: Defuzzification process for type-2 fuzzy sets

In literature only few defuzzification methods for type-2 sets are used. The centroid type-reduction is the most popular one. The definition of the centroid $C_{c_{\tilde{A}}}$ of a general type-2 fuzzy set with N discretization points in the universe of discourse X (primary membership function) and M discretization points for the secondary membership function is given in equation 3.9a and for an interval type-2 fuzzy set in equation 3.9b.

$$C_{c_{\tilde{A}}} = \sum_{j=1}^{n} \left[\bigstar_{i=1}^{N} \mu_{\tilde{A}_e^j}(x_j, u_j) \right] \Big/ \frac{\sum_{i=1}^{N} x_i u_i}{\sum_{i=1}^{N} u_i} \tag{3.9a}$$

$$C_{c_{\tilde{A}}} = \int_{\theta_1 \in J_{x_1}} \cdots \int_{\theta_N \in J_{x_N}} 1 \Big/ \frac{\sum_{i=1}^{N} x_i \theta_i}{\sum_{i=1}^{N} \theta_i} = [c_l, c_r] \tag{3.9b}$$

$\bigstar_{i=1}^{N} \mu_{\tilde{A}_e^j}(x_j, u_j)$ is the t-norm of all embedded sets $\tilde{A}_e$ from 1 to N. Note that the centroid C_c for an interval type-2 fuzzy set is an interval bounded by c_l and c_r.
Equation 3.9a is computationally very expensive as stated in Coupland and John (2008), because the number n of embedded sets $\tilde{A}_e$ increase exponentially with increasing N and M. For $N = 21$ and $M = 2$ the number of embedded sets is $\tilde{A}_e = 2097152$ according to Mendel (2001). The computational effort for this method is too high for engineering applications.

Only a few approaches can be found in literature to overcome this problem. The three most prominent ones are implemented in opTUM-II and a short overeview is given in the following.

- defuzzification based on α-cut representation of a general T2 FS
- defuzzification based on embedded sets
- defuzzification based on geometric type-2 fuzzy set (GT2 FS)

α-cut representation of a general T2 FS. This approach was introduced by Liu (2008). On each of the n_α^{II} levels a defuzzification is performed for the IT2 FS in the corresponding n_α^{II} plane. For IT2 FS different algorithms are known to compute the centroid $C_{c_{\tilde{A}}\alpha}(x) = [c_l, c_r]$. The ones implemented in opTUM-II are the Karnik-Mendel algorithm (KM) from Karnik and Mendel (2001), enhanced Karnik-Mendel algorithm (EKM) from Wu and Mendel

(2008), fast recursive method (FRM) from Melgarejo (2007) and iterative algorithm with stop condition (IASCO) from Duran et al. (2008). The algorithms were successfully tested on IT2 FS provided in Mendel (2005).
Finally an overall centroid $C_{c\tilde{\tilde{A}}}(x)$ is computed by equation 3.10 resulting in a type-1 fuzzy set for the centroid of a T2 FS. This type-1 fuzzy set can be defuzzified to a crisp value.

$$C_{c\tilde{\tilde{A}}}(x) = \bigcup_{\alpha\in[0,1]} \alpha / C_{c\tilde{\tilde{A}}\alpha}(x) \tag{3.10}$$

The algorithms EKM, FRM and IASCO originate from IT2 FS control applications and are therefore very fast. They are computationally efficient even for repeated computations on n_α^{II} levels and several outputs.

Embedded sets. In this method described by Greenfield et al. (2005) the complete T2 FS is taken into account. According to the discretization a user provided number of so called embedded sets in equation 3.11a is selected. The number of all embedded sets n_e depends on the number of sampling points N in X and M_i, the number of secondary membership levels at every domain point x_i. As can be seen from equation 3.11b n_e is very high even for small N and M_i. The T2 FS is defined by $\tilde{\tilde{A}}_e$ in equation 3.11c.

$$\tilde{\tilde{A}}_e = \sum_{i=1}^{N} [f_{x_i}(u_i)/u_i] / x_i \; ; \qquad u_i \in J_{x_i} \subseteq U = [0,1] \tag{3.11a}$$

$$n_e = \prod_{i=1}^{N} M_i \tag{3.11b}$$

$$\tilde{\tilde{A}} = \sum_{j=1}^{n_e} \tilde{\tilde{A}}_e \tag{3.11c}$$

For the selected $\tilde{\tilde{A}}_e$ the centroid is determined according to Mendel (2001). The disadvantage is, that the computation has to be performed several times with different randomly chosen $\tilde{\tilde{A}}_e$ in order to get the true $C_{c\tilde{\tilde{A}}}(x)$. Therefore two runs with different sets generate different results and the method is computationally less effective than the first one.

Geometric type-2 fuzzy set (GT2 FS). Coupland and John (2008) introduced a method where the volume properties of the whole T2 FS are utilized. The so called geometric type-2 fuzzy set (GT2 FS) is bounded by polygons, an example is given in figure 3.8.

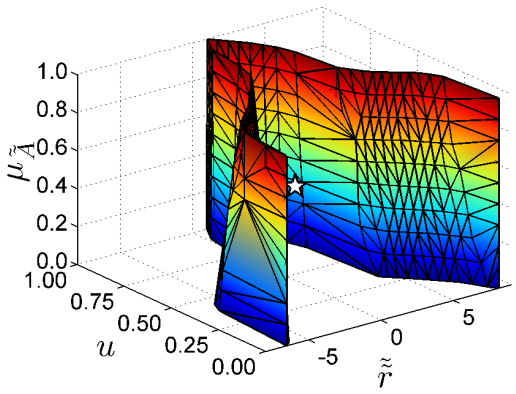

Figure 3.8.: Geometric type-2 fuzzy set defined by polygons

From this representation the CoG of the GT2 FS can be easily computed. For the example in figure 3.8, it is marked with a white star. The meaning of this CoG with respect to fuzzy uncertainty is viewed critically in Mendel et al. (2009).

Evaluation of defuzzification methods

The response shown in figure 3.5 is analyzed with the three methods for $n_\alpha^I = 10$ and $n_\alpha^{II} = 5$. The discretization of the universe of discourse X is parameterized $N \in [10, 100, 1000]$ in order to find the sensitivity of the methods to this value. For the second method with embedded sets the number of sample sets is $n_e \in [10, 100, 1000]$ and the mean of 100 runs is given in table 3.2. The computational effort is given as ratio of the computation time with respect to the time needed for EKM with $N = 1000$.

Table 3.2.: Comparison of different defuzzification methods for T2 FS

	EKM		embedded sets			GT2 FS	
N	C_c	t/t_{ref}	n_e	C_c[1]	t/t_{ref}[2]	CoG	t/t_{ref}
10	0.9492	0.04	10	0.9056	0.01	no value[3]	no value[3]
			100	0.9236	0.02		
			1000	0.9321	0.07		
100	0.9405	0.13	10	0.9436	0.06	0.5176	0.93
			100	0.9417	0.08		
			1000	0.9406	0.18		
1000	0.9435	1.00	10	0.9452	0.54	0.5168	7.77
			100	0.9437	0.61		
			1000	0.9454	1.46		

[1] mean from 100 runs
[2] mean from 100 runs for one embedded set
[3] unable to generate GT2 FS for $N = 10$

α-cut representation of a general T2 FS. This method is very fast and gives quite constant results. A deviation in the C_c can be seen in table 3.2, which is a result of the dis-

cretization N. A detailed analysis shows that especially for low N high fluctuations occur as displayed in figure 3.9. It is suggested to use $N > 400$ for this method.

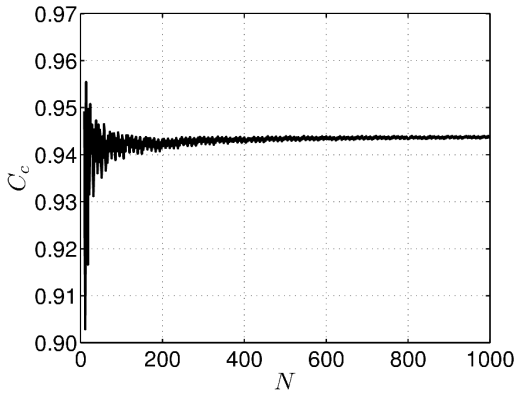

Figure 3.9.: Convergence of centroid for α-cut level method with EKM

Embedded sets. Multiple runs have to be performed in order to compute the mean value of C_c. $N = 10$ is too small for this method. For $N = 100$ the standard deviation of C_c can be reduced by nearly 50% for $n_e = 1000$ sampled embedded sets compared to $n_e = 10$. For $N = 1000$ even 10 embedded sets provided good results. As already pointed out, 100 runs where performed for every parameter combination of N and n_e. For a single embedded set with $N = 10$ the difference between the true C_c (set to 0.9435) and the value generated by one embedded set can be up to +13%/-21%, for $N = 100$ up to +6%/-7% and for $N = 1000$ approximately ±2%.

Geometric type-2 fuzzy set (GT2 FS). The derived values for CoG are quite different from the other two methods. For a discretization with $N = 10$ the utilized algorithm was not able to build a GT2 FS. There is clearly a lower bound for discretization in order to gain a proper geometric representation. If this precondition is met, a higher N does not provide better results but much higher computational effort. A compromise between minimum discretization and computation time depends also on the shape of the T2 FS and therefor a priori setting of N is difficult.

The α-cut representation with EKM and the embedded set method provide nearly the same value for C_c. The higher computational effort of the latter suggests that the α-cut representation should be used for further studies.

Evaluation of goal handling methods

How the goals are evaluated in detail for T2 FSs has to be defined together with the findings of the last section. In addition to measures already mentioned for T1 FSs, additional ones are shown in figure 3.10 for IT2 FSs. They also apply for general T2 FSs if executed for a single α-cut level for a secondary membership function. The advantage of IT2 FSs and T2 FSs is the possibility to evaluate the differences between upper and lower MFs.

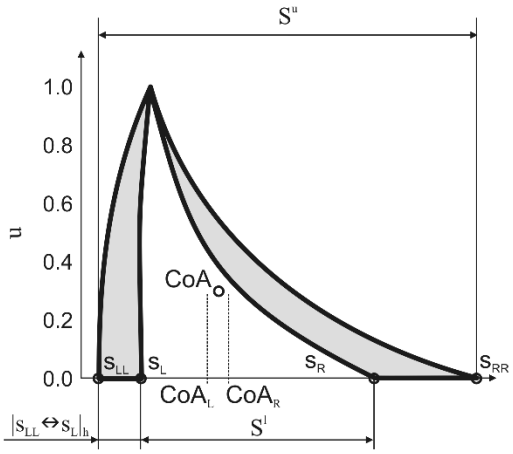

Figure 3.10.: Additional information in type-2 fuzzy number

Main physical goal. Centroids computed by methods described at the beginning of this section which are similar to center of area are mainly utilized. center of support for upper and lower MFs can be used too.

Goal for uncertainty evaluation. Differences in the support of upper and lower MF provide additional information. Two examples are the ratio of $|s_{LL} \leftrightarrow s_{RR}|_h$ and $|s_L \leftrightarrow s_R|_h$ and distance between s_L and s_{LL}.

Goal for nonlinearity evaluation. The same measures as for type-1 fuzzy sets are utilized for upper membership functions. Additionally, the distance between the CoS of upper and lower MFs $|CoS_{S^u} - CoS_{S^l}|$ can be utilized.

Goal for skewness evaluation. This measure is similar to the one for T1 FSs. The upper MF is used in $|C - CoS_{S^u}|$. Another measure for skewness of IT2 FSs, which is not evaluated in this work, is given in Wu and Mendel (2007).

3.4. Evaluation methods for constraints

The evaluation of constraints in structural optimization is commonly based on crisp numbers. The fuzzy outputs generated by opTUM-II can not used directly in standard algorithms such as gradient based or stochastic ones. A simple way to handle T2 FSs, IT2 FSs and T1 FSs is type-reduction and defuzzification, which generates a crisp number. Another way are ranking, comparison and similarity measures based on possibility or evidence theory for which numerous approaches are known for T1 FSs. Ranking of IT2 FSs and T2 FSs has been increasingly investigated in recent years. The following constraint handling schemes are discussed and evaluated in this work.

- distance of center of areas (CoAs)
- distance of center of supports (CoSs)
- Dubois-Prade ranking for fuzzy numbers (DPR)

- Adapted Sengupta-Pal ranking for interval numbers (SPR)
- Chen-Wang ranking for fuzzy numbers (CWR)

Provided that the system answer, which has to be constrained, is given as a interval type-2 fuzzy set or type-2 fuzzy set the cases shown in figure 3.11 for different types of allowable values have to be considered.

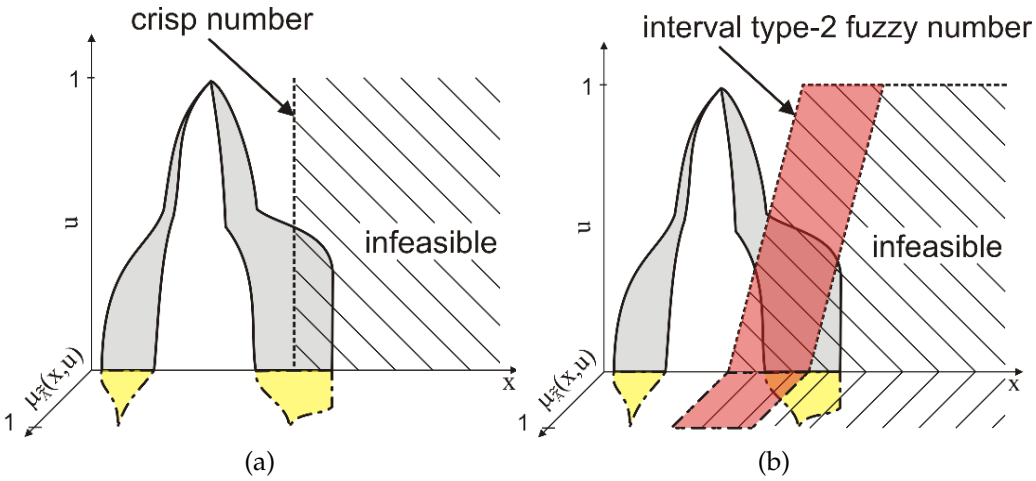

Figure 3.11.: Comparison of type-2 system response with constraint

Distance of CoAs. This scheme is very common and can be used for all types of comparisons shown in figure 3.11. Given a constant allowable value in crisp or fuzzy form the CoA of the allowable value is a crisp number. Also for different symmetrical shapes of fuzzy allowable values CoA is constant. Although uncertainty and nonlinearity in the system answer will generate differences to the standard crisp approach, the decision maker's preference can be included only by safety factors.

Distance of CoSs. The basic concept of this distance already includes up to four comparisons for different combinations of upper and lower MFs for system answer and allowable value. Not only the lowest α-cut levels but also all other can be compared with each other for n_α^I and n_α^{II}. This results in a vector or matrix of distances, respectively.
Different crisp constraint schemes can be utilized. First, the minimum or mean distance for all α-cut levels can be calculated. Second, several constraints can be generated representing a comparison on every α-cut level. This can be done for all four possible combinations of comparisons mentioned above. A compromise between available information and usefulness in engineering problems has to be found.

Dubois-Prade ranking for fuzzy numbers (DPR). This ranking scheme was developed for T1 FS and is described in Dubois and Prade (1983). The relative location of two fuzzy numbers $\tilde{A}_i$ and $\tilde{A}_j$ is evaluated by DPR. The result is in the range of $\in [0, 1]$. It was identified in Pan (2009) under the supervision of the author as a favorable scheme for constraint evaluation based on given requirements. DPR includes four measures, grade of possibility of dominance (PD), grade of possibility of strict dominance (PSD), grade of necessity of dominance (ND) and grade of necessity of strict dominance (NSD). From these measures a combined one or representative ones have to be found.

$$PD\left(\tilde{A}_i, \tilde{A}_j\right) = \sup_{\substack{x_i, x_j \\ x_i \geq x_j}} \min\left(\tilde{A}_i(x_i), \tilde{A}_j(x_j)\right) \tag{3.12a}$$

$$PSD\left(\tilde{A}_i, \tilde{A}_j\right) = \sup_{x_i} \inf_{\substack{x_j \\ x_i \leq x_j}} \min\left(\tilde{A}_i(x_i), 1 - \tilde{A}_j(x_j)\right) \tag{3.12b}$$

$$ND\left(\tilde{A}_i, \tilde{A}_j\right) = \inf_{x_i} \sup_{\substack{x_j \\ x_i \geq x_j}} \min\left(1 - \tilde{A}_i(x_i), \tilde{A}_j(x_j)\right) \tag{3.12c}$$

$$NSD\left(\tilde{A}_i, \tilde{A}_j\right) = 1 - \sup_{\substack{x_i, x_j \\ x_i \leq x_j}} \min\left(\tilde{A}_i(x_i), \tilde{A}_j(x_j)\right) \tag{3.12d}$$

Sengupta-Pal ranking for interval numbers (SPR). This approach is based on comparison of interval numbers described by Sengupta and Pal (2000). The comparison has to be evaluated for all α-cut levels resulting in a vector and matrix for IT2 FSs and T2 FSs, respectively. The intervals of system output and allowed value are compared on each α-cut level. SPR offers the possibility to take into account the decision maker's preference (optimistic, neutral, pessimistic).
An interval $A = [\underline{a}, \overline{a}]$ and $B = [\underline{b}, \overline{b}]$ can be described by the following properties.

$$m(A) = \frac{1}{2}(\underline{a} + \overline{a}) \tag{3.13a}$$

$$w(A) = \frac{1}{2}(\overline{a} - \underline{a}) \tag{3.13b}$$

A fuzzy relation which is slightly changed to the formulation in Sengupta and Pal (2000) for the distance of two intervals is given in equation 3.14.

$$\mu_{A \Leftrightarrow B} = \begin{cases} 1 & \text{if } m(A) \geq m(B) \\ \max\left\{0, \frac{m(A) - (\underline{b} + w(A))}{m(B) - (\underline{b} + w(A))}\right\} & \text{if } m(B) \geq m(A) \geq \underline{b} + w(A) \\ 0 & \text{otherwise} \end{cases} \tag{3.14}$$

If $\mu_{A \Leftrightarrow B} = 1$ than interval B is definitely rejected, if $\mu_{A \Leftrightarrow B} = 0$ than interval B is definitely accepted. The changes from the original definition result in a rejection of B as soon as $m(A) \geq m(B)$ regardless of the spreads $w(A)$ and $w(B)$.
The decision maker's preference is included via factor M in equation 3.15 for $\pi_{A \Leftrightarrow B}$. $M < 1$ for optimistic decisions, $M = 1$ for neutral and $M > 1$ for pessimistic ones.

$$\pi_{A \Leftrightarrow B} = \left(\mu_{A \Leftrightarrow B}\right)^{1/M} \tag{3.15}$$

$\pi_{A \Leftrightarrow B,i}$ is computed on every α-cut level i, a final measure has to be generated. This can be done by mean or maximum of all $\pi_{A \Leftrightarrow B,i}$.

Chen-Wang ranking for fuzzy numbers (CWR). Originally used for fuzzy risk analysis, CWR described by Chen and Wang (2009) has been investigated. This measure is similar to SPR because intervals are compared on each α-cut level. For CWR these comparisons are than weighted by the according α-cut level.
In order to compute CWR the overall left and right boundaries of all considered fuzzy numbers $\tilde{A}_1, \tilde{A}_2, \ldots,$ and $\tilde{A}_m$ have to be defined.

$$U = \max\left\{x \mid x \in \tilde{A}_{\alpha,i}, i = 1, 2, \ldots, m\right\} \tag{3.16a}$$

$$L = \min\left\{x \mid x \in \tilde{A}_{\alpha,i}, i = 1, 2, \ldots, m\right\} \tag{3.16b}$$

The so called signal/noise ratio $\hat{\eta}_{i,k}$ of the kth α-cut level is defined in equation 3.17 using mean $m(A)$ and spread $w(A)$ from equation 3.13.

$$\hat{\eta}_{i,k} = \frac{m_{i,k} - L}{2w_{i,k} + c} \tag{3.17}$$

Parameter $c > 0$ is used to avoid numerical problems if $w_{i,k} = 0$ for crisp numbers. According to Chen and Wang (2009) $c = U - L + 1$ is used. The ranking index $RI\left(\tilde{A}_i\right)$ is calculated in equation 3.18.

$$RI\left(\tilde{A}_i\right) = \frac{\sum_{k=1}^{n_\alpha^I} \alpha_k \times \hat{\eta}_{i,k}}{\sum_{k=1}^{n_\alpha^I} \alpha_k} \tag{3.18}$$

The larger $RI\left(\tilde{A}_i\right)$ the better the ranking of $\tilde{A}_i$. From equation 3.18 it can also be seen that the α-cut level for $\alpha = 0$ does not effect $RI\left(\tilde{A}_i\right)$. A small n_α^I neglects the lower part of $\tilde{A}_i$ if α-cut levels are evenly distributed. In Chen and Wang (2009) $n_\alpha^I = 10$ is suggested.

3.5. Summary of chapter

For knowledge based type-2 fuzzy rule-based systems the Interval Type-2 Fuzzy Logic Toolbox kindly provided by Professor Oscar Castillo is applied. The algorithm opTUM is extended to opTUM-II which can handle T2 FSs input parameters. The defuzzification and comparison of T2 FSs output parameters from opTUM-II is discussed in the second part of chapter 3. Defuzzification for T2 FSs can be performed by EKM for IT2 FSs which is extended to general T2 FSs, embedded sets or a geometric representation of general T2 FSs. Only the first approach gives good defuzzification results with reasonable computation effort.
Comparison of T2 FSs is performed by different methods. Simple methods for T2 FS, which take only the center of area into account and sophisticated comparison methods for T1 FSs which are extended to T2 FSs are introduced. All of these comparison methods are evaluated in the next chapter in order to find approaches suited for engineering optimization.

4. Evaluation of advanced knowledge-handling methods

In order to find approaches suited for engineering optimization the methods described in chapter 3 are evaluated with the help of an analytical optimization example. The evaluation is limited to interval type-2 fuzzy sets due to practical considerations for engineering problems.
First, goal handling with single and multiple objectives is analyzed in section 4.1 followed by constraint handling in 4.2. An analytical optimization problem is solved for different combinations of goals and constraints in section 4.3. Finally, conclusions are drawn for engineering problems in section 4.4.

4.1. Evaluation of goal handling methods

In this section different methods for goals handling under uncertainty are presented. A tilted version of the well known six-hump camel back function (SHCBF) described in equation 4.1 is minimized by different means.

$$f = \left(4 - 2.1x_1^2 + \frac{x_1^4}{3}\right) \cdot x_1^2 + x_1 x_2 + \left(-4 + 4x_2^2\right) \cdot x_2^2 + \frac{x_1}{3} + \frac{x_2}{2} \tag{4.1}$$

The design variables are $x_1 \in [-2, 2]$ and $x_2 \in [-1, 1]$. The function has one global optimum at x_1^{opt} =0.051, x_2^{opt} =-0.739 with f^{opt} =-1.371 and five local ones. They are listed in table 4.1.

Table 4.1.: Global and local optima of tilted six-hump camel back function

type	$\mathbf{x}^{opt}$		f^{opt}
global	[0.051,	-0.739]	-1.371
local	[-0.129,	0.683]	-0.719
local	[-1.719,	0.774]	-0.393
local	[1.686,	-0.817]	-0.054
local	[-1.633,	-0.621]	1.266
local	[1.578,	0.477]	2.900

The contours of the function are given in figure 4.1a together with global and local optima. Note the local optima in the right upper corner in a very flat area. In figure 4.1b the sum of derivatives given in equation 4.2 is displayed.

$$f_\partial = \left|\frac{\partial f}{\partial x_1}\right| + \left|\frac{\partial f}{\partial x_2}\right| \tag{4.2}$$

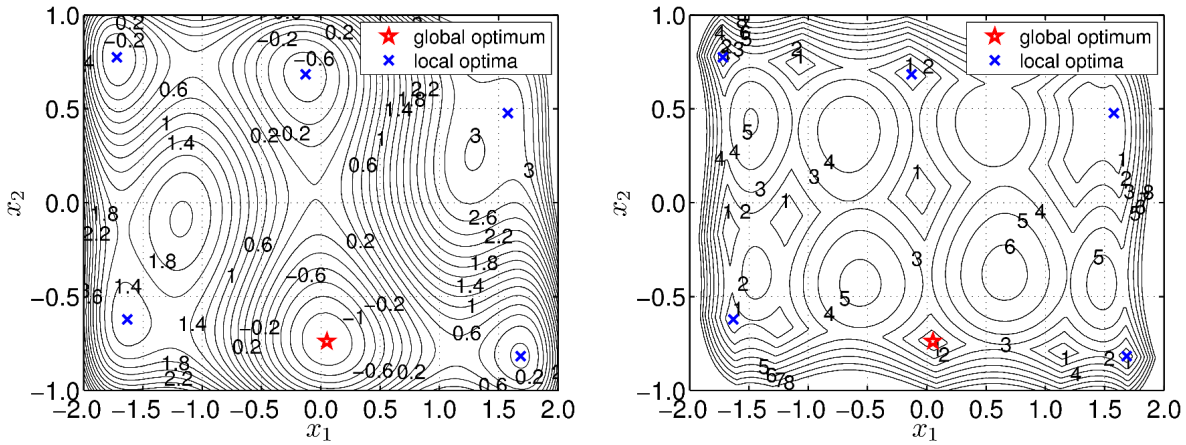

(a) contours of function

(b) contours of sum of derivatives

Figure 4.1.: Contours of goal and derivative sum for six-hump camel back function

Two parameters are varied for each problem. The first is the number of α-cut levels, which influences the shape of the resulting fuzzy set but also the computation effort. The second is the level of uncertainty which is present in the problem.

4.1.1. Methods for main physical goals

Triangular interval type-2 fuzzy sets are used to model uncertainty in the design variables x_1 and x_2. The uncertainty is varied in $S^u(\tilde{x}) \in [2, 4, 10, 20]\%$ of design space $\mathbf{x}_u - \mathbf{x}_l$ for the upper membership function. $S^l(\tilde{x})$ is half of these values. The number of α-cut levels is also changed $n_\alpha^I \in [2, 3, 4, 5, 10]$ in order to see dependencies of results on this parameter. GAME is used for optimization which results in slight deviations in the optimized results due to randomness in the optimization process.
For triangular IT2 FSs the core C gives the same result as the deterministic optimization and is not evaluated. center of area of interval type-2 fuzzy sets and center of support which are shown in figure 4.2 are discussed in the following.

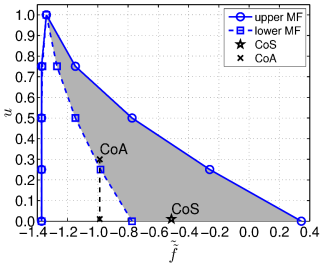

Figure 4.2.: Difference between CoA and CoS for type-2 fuzzy set

Center of area (CoA). This objective is influenced by nonlinearities of the fuzzy output. With increasing uncertainty in $\tilde{x}$ the difference from the original problem also increases. Figure 4.3a for $S^u(\tilde{x}) = 4\%$ resemble the original problem. In figure 4.3b the high uncertainty of $S^u(\tilde{x}) = 20\%$ has a smoothing effect which mask some of the local optima.
The number of α-cut levels n_α^I introduce differences in the contours. For $n_\alpha^I = 2$ and $n_\alpha^I = 10$ with $S^u(\tilde{x}) = 4\%$ a comparison is shown in figure 4.4a in percent with basis $n_\alpha^I = 10$. In areas where the function value passes through zero the differences are very high. For $n_\alpha^I = 5$ and $n_\alpha^I = 10$ these differences are much smaller as displayed in 4.4b. The additional computational effort for $n_\alpha^I = 10$ is not necessary for a good approximation of the fuzzy number for this example.

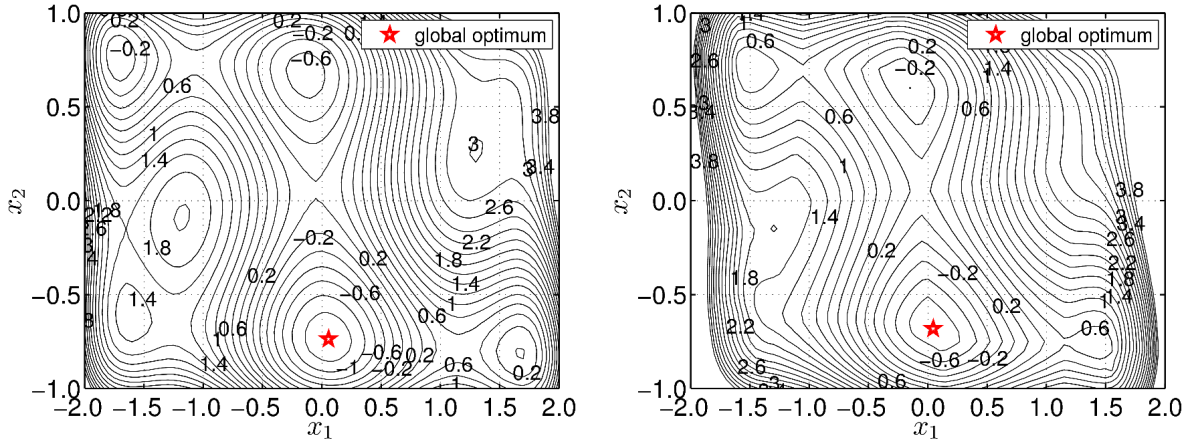

(a) $n_\alpha^I = 5$, $S^u(\tilde{x}) = 4\%$ (b) $n_\alpha^I = 5$, $S^u(\tilde{x}) = 20\%$

Figure 4.3.: Effect of different uncertainty settings for evaluation with CoA

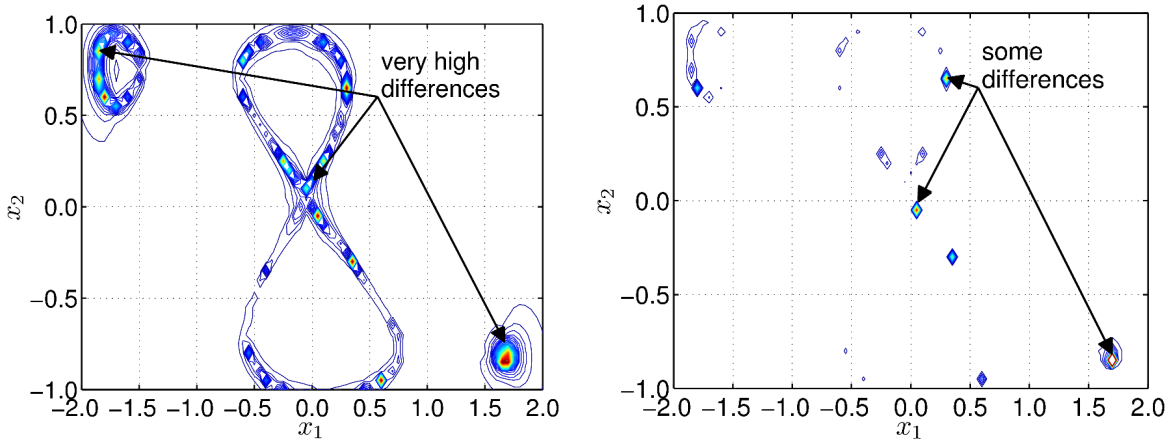

(a) difference $CoA\left(n_\alpha^I = 2\right)/CoA\left(n_\alpha^I = 10\right)$ (b) difference $CoA\left(n_\alpha^I = 5\right)/CoA\left(n_\alpha^I = 10\right)$

Figure 4.4.: Differences in system answers due to n_α^I

Center of support (CoS). The support S of the resulting fuzzy number is not influenced by the number of α-cut levels n_α^I. For $S^u(\tilde{x}) = 4\%$ the contours of the goal shown in figure 4.5a are very similar to the original function whereas for $S^u(\tilde{x}) = 20\%$ in figure 4.5b a significant distortion can be seen.
A version of this measure is $(\text{CoS}|_{S^u}+\text{CoS}|_{S^l})/2$ which represents the mean of CoS for upper and lower MFs. Distortion for high uncertainties is less than for CoS only. The results listed in table 4.2 lie in between the ones for CoA and CoS.

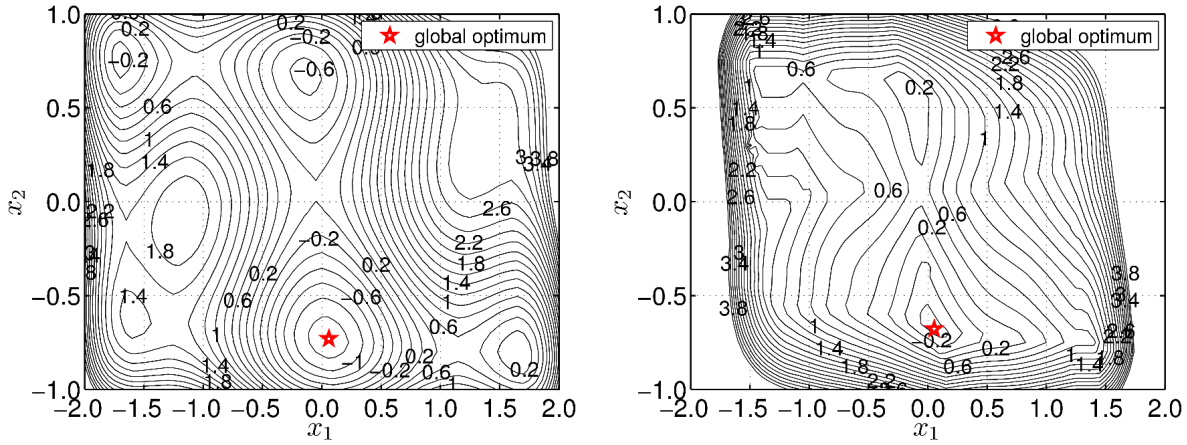

(a) $n_\alpha^I = 5$, $S(\tilde{x}) = 4\%$ (b) $n_\alpha^I = 5$, $S(\tilde{x}) = 20\%$

Figure 4.5.: Comparison of different algorithm settings for CoS

The resulting optimal designs are summarized in table 4.2. As already stated small deviations occur due to the random processes in GAME. For CoA the results for $S^u(\tilde{x}) \in [2, 4, 10]\%$ are quite similar, for $S^u(\tilde{x}) = 20\%$ the optimum shows different optimal design variables together with a shifted optimal function value.
For CoS optimal designs show a higher difference from the deterministic optimum than the ones generated by CoA. For high uncertainties the difference is significant. One reason for this behavior is the higher dependency of CoS on unsymmetric nonlinearities.

Table 4.2.: Global optima for different levels of uncertainty and evaluation methods

n_α^I	$S^u(\tilde{x})$ %	CoA $\mathbf{x}^{opt}$	CoA f^{opt}	CoS $\mathbf{x}^{opt}$	CoS f^{opt}	$\sum$CoS/2 $\mathbf{x}^{opt}$	$\sum$CoS/2 f^{opt}
2	2	[0.042, -0.740]	-1.367	[0.052, -0.741]	-1.364	[0.049, -0.738]	-1.365
	4	[0.048, -0.740]	-1.355	[0.047, -0.740]	-1.338	[0.051, -0.742]	-1.348
	10	[0.043, -0.732]	-1.275	[0.018, -0.732]	-1.174	[0.039, -0.714]	-1.219
	20	[0.020, -0.701]	-1.017	[0.113, -0.636]	-0.693	[0.022, -0.665]	-0.815
3	2	[0.050, -0.738]	-1.367	[0.047, -0.740]	-1.363	[0.051, -0.739]	-1.365
	4	[0.055, -0.734]	-1.356	[0.049, -0.738]	-1.338	[0.051, -0.737]	-1.347
	10	[0.037, -0.736]	-1.279	[0.070, -0.711]	-1.173	[0.043, -0.718]	-1.218
	20	[0.015, -0.705]	-1.035	[0.087, -0.653]	-0.676	[0.025, -0.657]	-0.802
4	2	[0.047, -0.739]	-1.367	[0.055, -0.735]	-1.363	[0.050, -0.738]	-1.365
	4	[0.054, -0.739]	-1.356	[0.062, -0.733]	-1.339	[0.051, -0.737]	-1.347
	10	[0.037, -0.726]	-1.278	[0.080, -0.708]	-1.179	[0.071, -0.735]	-1.219
	20	[0.025, -0.700]	-1.042	[0.090, -0.647]	-0.674	[0.006, -0.658]	-0.809
5	2	[0.050, -0.739]	-1.367	[0.050, -0.739]	-1.363	[0.049, -0.738]	-1.365
	4	[0.059, -0.738]	-1.356	[0.060, -0.731]	-1.338	[0.048, -0.735]	-1.347
	10	[0.040, -0.734]	-1.278	[0.073, -0.711]	-1.172	[0.046, -0.720]	-1.218
	20	[0.045, -0.681]	-1.041	[0.055, -0.678]	-0.659	[0.021, -0.657]	-0.803
10	2	[0.048, -0.738]	-1.367	[0.052, -0.738]	-1.363	[0.050, -0.738]	-1.365
	4	[0.044, -0.734]	-1.355	[0.050, -0.738]	-1.338	[0.056, -0.740]	-1.346
	10	[0.049, -0.718]	-1.275	[0.057, -0.722]	-1.171	[0.031, -0.715]	-1.220
	20	[0.031, -0.681]	-1.025	[0.052, -0.688]	-0.665	[0.056, -0.657]	-0.814
-	det. opt.			[0.051, -0.739]	-1.371		

4.1.2. Goals for uncertainty evaluation

To quantify the uncertainty in the goal three measures are introduced. An optimization with two goals is performed with minimized uncertainty as second goal. The diagrams can be found in appendix A.3.

Support S^u. Three areas are identified by Pareto-optimal solution for low uncertainty, see also figure 4.6a. First, the original global optimum already known from optimization of CoA. This point comes with a very wide S^u. Second, the area in the middle of the design space around $x_1 = x_2 \approx 0$ with medium S^u. Third, an area in the upper right corner of the design space has minimum S^u but a very high CoA of ≈ 3. The latter represents a flat area in CoA space with several local minima. With increasing uncertainty an optimal area is found around $x_1 = -0.13$ and $x_2 = 0.70$. For high $S^u(\tilde{x}) = 20\%$ another change in optimal designs is observed. Pareto-fronts for $S^u(\tilde{x}) \in [2, 4, 10, 20]\%$ clearly indicate the trade-off between small CoA and small $S^u(\tilde{f})$.
For engineering optimization S^u offers the ability for uncertainty minimization. A disadvantage are optimal designs for very small S^u in areas where the main physical goal is high.

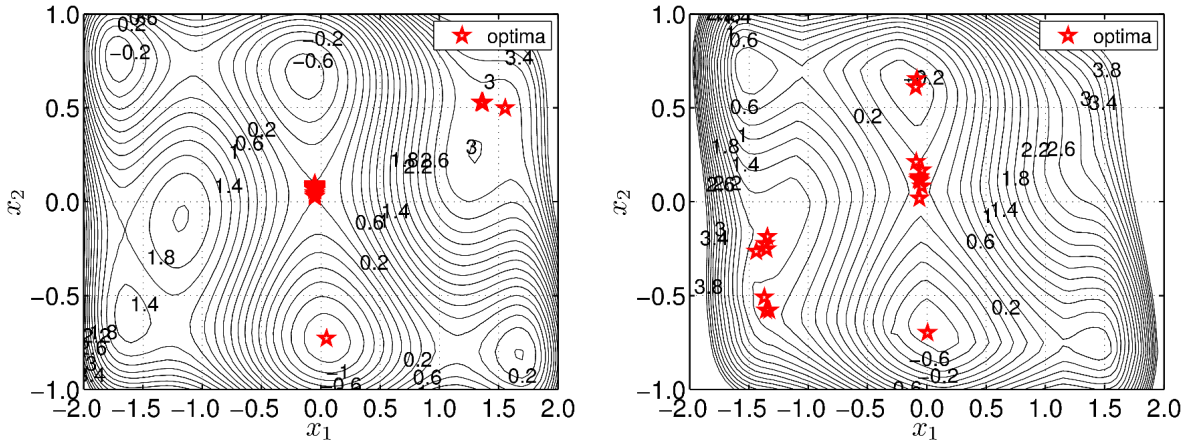

(a) $S^u(\tilde{x}) = 4\%$, goal=CoA (b) $S^u(\tilde{x}) = 20\%$, goal=CoA

Figure 4.6.: Goals CoA and S^u

Difference S^u-S^l. This measure minimizes the difference between upper and lower MFs. Designs found by this goal show minimal different behavior for maximum and minimum uncertainty of input parameters expressed by interval type-2 fuzzy sets. Results for $n_\alpha^I = 5$ are shown in appendix A.3.2. For small $S^u(\tilde{x})$ optima are similar to those found by S^u. For higher uncertainties additional optima are found in the lower left corner of the design space. For high uncertainties optima differ highly from the ones found by S^u. For $S^u(\tilde{x}) \in [4, 10, 20]\,\%$ these results are significant and $S^u - S^l$ is a valid goal for uncertainty characterization.

Relative difference $(S^u - S^l)/S^u$. This measure uses the ratio of the difference of $S^u - S^l$ with respect to S^u. This prevents the algorithm from converging to areas where the overall uncertainty in the system answer is very small in order to reduce the amount of $S^u - S^l$. Results are given in appendix A.3.3. Different optimal areas are identified by this method compared to $S^u - S^l$, the optimal design itself is nearly the same as for $S^u - S^l$.

4.1.3. Goals for nonlinearity and skewness evaluation

Nonlinearity in the fuzzy numbers of goals indicate a nonlinear correlation between input and output parameters.

Gradient measure $\partial\mu/\partial r|_{SL}$, $\partial\mu/\partial r|_{SR}$, $\partial\mu/\partial r|_{CL}$, $\partial\mu/\partial r|_{CR}$. Gradients of the upper membership functions S^u with respect to system output as shown in figure 3.6 on page 39 are evaluated with the following formula.

$$f_{grad} = \left|\left.\frac{\partial\mu}{\partial r}\right|_{SL} + \left.\frac{\partial\mu}{\partial r}\right|_{CL}\right| + \left|\left.\frac{\partial\mu}{\partial r}\right|_{SR} + \left.\frac{\partial\mu}{\partial r}\right|_{CR}\right| \tag{4.3}$$

The gradient at bottom and top have opposite signs due to definition of convex fuzzy numbers and therefore the + in the equation calculates the difference between top and bottom gradient. For $n_\alpha^I = 2$ no results can be computed.
The disadvantage of this measure is that the gradient can become infinite if core C and the respective point of support s_{LL} or s_{RR} have the same value of r which represents a vertical line.

Distance $d_{L\mu}$ **and** $d_{R\mu}$**.** The distances between the straight connection line $|C \leftrightarrow s_{LL}|$ and upper MF and between $|C \leftrightarrow s_{RR}|$ and upper MF are summarized.
The results are slightly influenced by n_α^I, but the differences are not significant for $n_\alpha^I \geq 5$. Diagrams can be found in appendix A.3.4. Some optimal designs are located on nearly straight lines near the global optimum for CoA. Areas with optimal solutions change slightly with increasing uncertainty in input parameters.

Distance $|CoS|_{S^u} - CoS|_{S^l}|$**.** This is a measure for nonlinearity only if S^u and S^l of the input parameters differ significantly. In the example this requirement is fulfilled by setting S^l to be half of S^u. Results in appendix A.3.5 show that this measure is less dependent on the level of uncertainty.

Distance $|C - CoS|_{S^u}|$**.** This is a very similar measure to the previous one. Results are given in appendix A.3.6.

4.2. Evaluation of constraint handling methods

The evaluation of constraints is based on three functions described in equation 4.4. The allowed crisp values r_{all} are also given.

$$fg_1^c = 5 * sin(x_1) - 12 * cos(1.5 * x_2^2) - 5 * (1.2 * x_1^2 x_2) + x_1 + x_2 + 50, \quad fg_1^c \leq 43.00 \tag{4.4a}$$
$$fg_2^c = x_1^3 + x_2^3, \quad fg_2^c \leq 3.40 \tag{4.4b}$$
$$fg_3^c = (4 - 3 * x_2^2 + \frac{x_2^6}{2}) * x_2^2, \quad fg_3^c \leq 1.35 \tag{4.4c}$$

In figure 4.7 the contours of the goal function f given in equation 4.1 are shown together with the crisp boundaries of fg_1^c, fg_2^c and fg_3^c. The feasible area is bounded on top, bottom

and right hand side. The boundaries cross most of the extrema and also limit the flat area of f in the upper right corner.

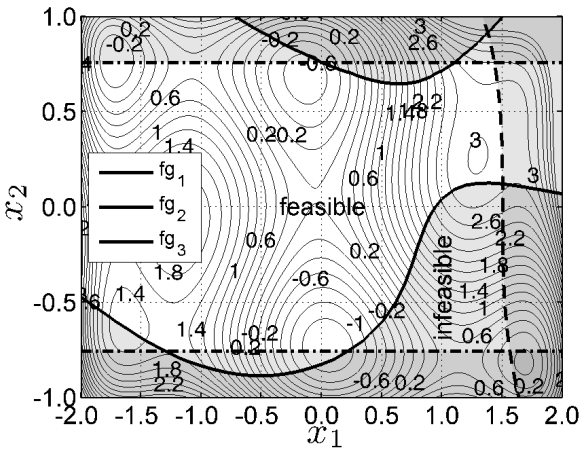

Figure 4.7.: Constraints and feasible design space

Constraint handling methods described in section 3.4 are tested with three different fuzzy numbers $\tilde{r}_{all}$ for each of the allowed values fg_1^{all}, fg_2^{all} and fg_3^{all}. These three versions represent decision maker's with different information levels. Parameters for the fuzzy allowed values are given in table 4.3 for primary MF. Fuzzy values are defined as IT2 FSs.

Table 4.3.: Parameters of fuzzy number for primary MF of allowed values

		primary upper MF				primary lower MF			
func.	version	p_1^p	p_2^p	p_3^p	p_4^p	p_5^p	p_6^p	p_7^p	p_8^p
fg_1^{all}	1	41.00	43.00	43.00	45.00	42.00	43.00	43.00	44.00
	2	41.00	42.00	44.00	45.00	42.00	43.00	43.00	44.00
	3	41.00	41.00	45.00	45.00	42.00	42.00	44.00	44.00
fg_2^{all}	1	3.00	3.40	3.40	3.80	3.20	3.40	3.40	3.60
	2	3.00	3.20	3.60	3.80	3.20	3.40	3.40	3.60
	3	3.00	3.00	3.80	3.80	3.20	3.20	3.60	3.60
fg_3^{all}	1	1.15	1.35	1.35	1.55	1.25	1.35	1.35	1.45
	2	1.15	1.25	1.45	1.55	1.25	1.35	1.35	1.45
	3	1.15	1.15	1.55	1.55	1.25	1.25	1.45	1.45

The first version shown in figure 4.8a for fg_1^{all} is extracted from a high amount of information. The most possible value is known by the expert and defined by a crisp core C for the upper and lower MF. The second version given in figure 4.8b shows a higher uncertainty than the first one. The most possible value is not known exactly which is stated via an interval core C. The third version has highest uncertainty and is basically an interval representation of the allowed value. It is displayed in figure 4.8c. The fuzzy allowed values are symmetric, CoAs and CoSs have the same value.

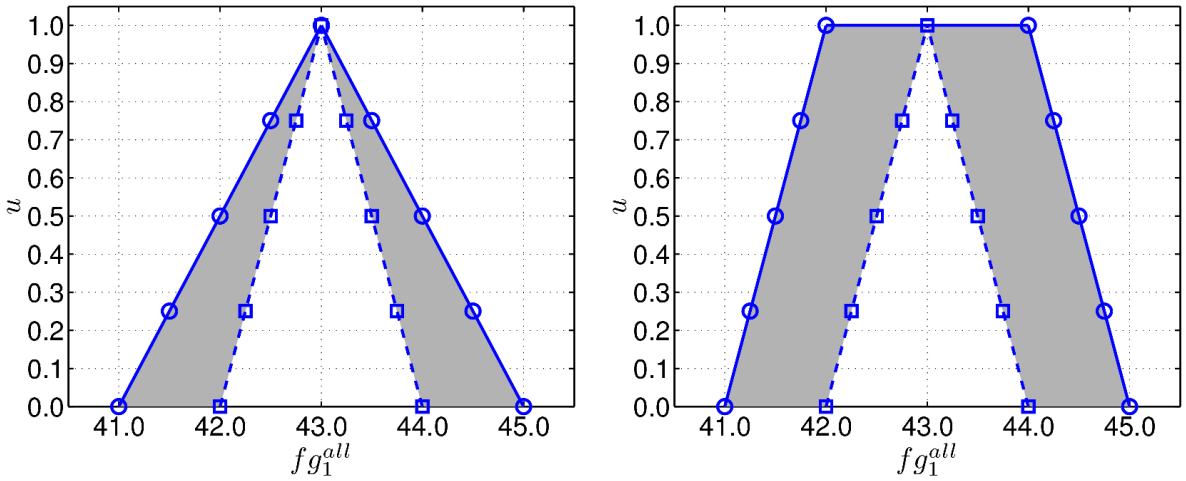

(a) version 1

(b) version 2

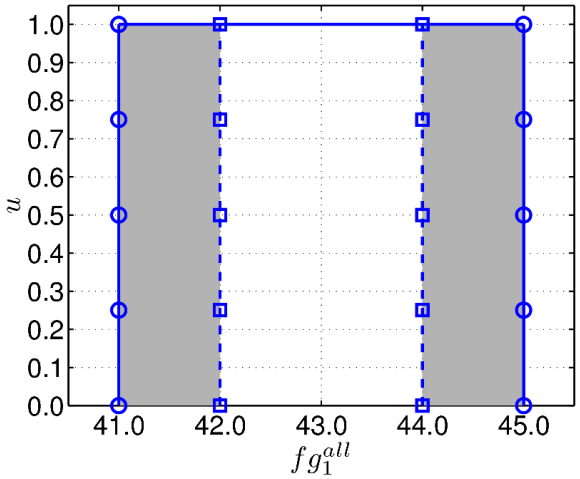

(c) version 3

Figure 4.8.: Allowed fuzzy values for fg_1^c

Resulting boundaries of the feasible design space are discussed in the following for constraint handling methods described in section 3.4. Feasible and infeasible design space always refer to the original crisp constraint formulation.

4.2.1. Distance of Center of Area and Center of Support

The two measures center of area and center of support are evaluated together due to their similarity. CoS is in the basic definition a measure for the upper membership function only. This definition can be expanded to all α-cut levels by equation 4.5.

$$CoS_\alpha = \frac{\underline{r}\,|_{\mu=\alpha} + \overline{r}\,|_{\mu=\alpha}}{2} \tag{4.5}$$

center of support for the upper and lower MFs, mean of CoS_α for $\alpha \in [0,1]$ and upper MF, and finally CoS_α for $\alpha = 0.5$ and upper MF are evaluated. The resulting boundaries

of the feasible design space for distance $CoA\,|_{\tilde{r}_{all}} - CoA\,|_{\tilde{r}=0}$ are shown in figure 4.9a, for $CoS\,|_{\tilde{r}_{all}} - CoS\,|_{\tilde{r}=0}$ in figure 4.9b.

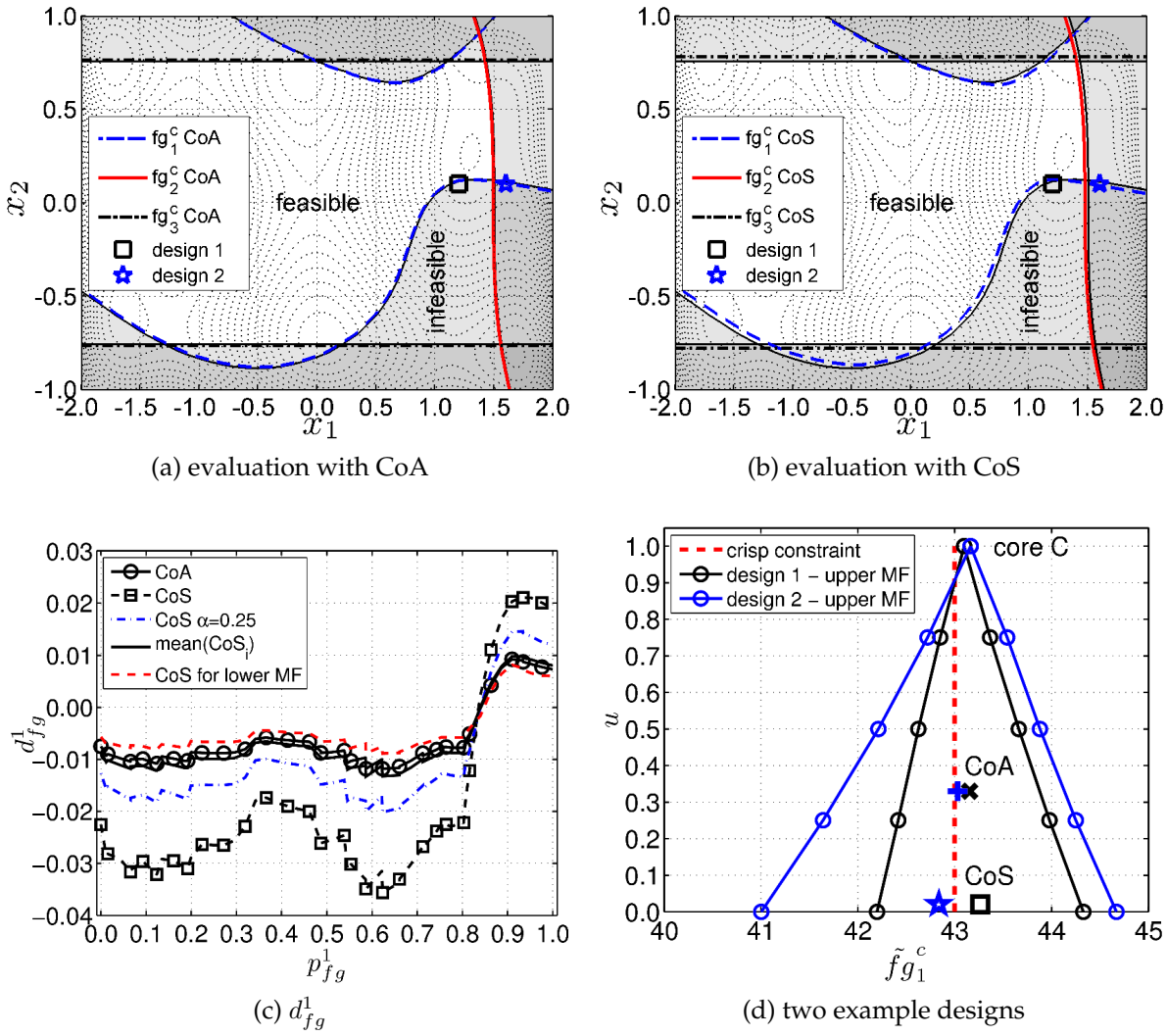

(a) evaluation with CoA

(b) evaluation with CoS

(c) d_{fg}^1

(d) two example designs

Figure 4.9.: Constraint boundaries for CoA and CoS

The differences between the original crisp boundaries and CoA approach are very small. For the center of support the differences are bigger and the boundaries can be clearly distinguished in figure 4.9b.
All other methods mentioned above show similar behavior and are not presented in the design space. To exemplify their characteristics, deviations from the original crisp boundary are shown by Euclidean distance d_{fg}^1 for selected points along the path of boundary p_{fg}^1. For for $d_{fg}^1 = 0$ the fuzzy constraint boundary is the same as the crisp one.
As an example, the lower part of boundary fg_1^c is investigated in figure 4.9c. For most of the path the fuzzy constraints are slightly shifted to the original feasible design space which is indicated by negative d_{fg}^1. At a ratio of approximately $p_{fg}^1 \approx 0.85$ the sign of d_{fg}^1 changes and the boundary given by fuzzy computation moves into originally infeasible design space. This is due to a skewness shift of the fuzzy number.
In order to show the influence of α-cut levels, the curve for $CoS_{\alpha=0.25}$ is also shown in figure 4.9c. It lies in between the curve for CoS and CoA.

The following conclusions are drawn for this approach:

- The influence of uncertainty and skewness are most prominent for evaluation of CoS.
- CoS allows for a decision makers preference by using CoS_α on a certain α-cut level.
- The higher computational effort for T2 FSs compared to IT2 FSs is not necessary for the presented example.

4.2.2. Dubois-Prade Ranking for fuzzy numbers

This approach offers four measures for the comparison of fuzzy system answers with fuzzy allowable values: grade of possibility of dominance (PD), grade of possibility of strict dominance (PSD), grade of necessity of dominance (ND) and grade of necessity of strict dominance (NSD). Type-1 fuzzy sets can be compared directly. For type-2 fuzzy sets only upper membership functions are evaluated. The individual measures are $\in [0, 1]$, therefore, a limit factor q_{DPR} has to be chosen. For fg_1^c contours are shown together with the boundary for $q_{DPR} = 0.5$. For fg_2^c and fg_3^c only the boundaries $q_{DPR} = 0.5$ are displayed.

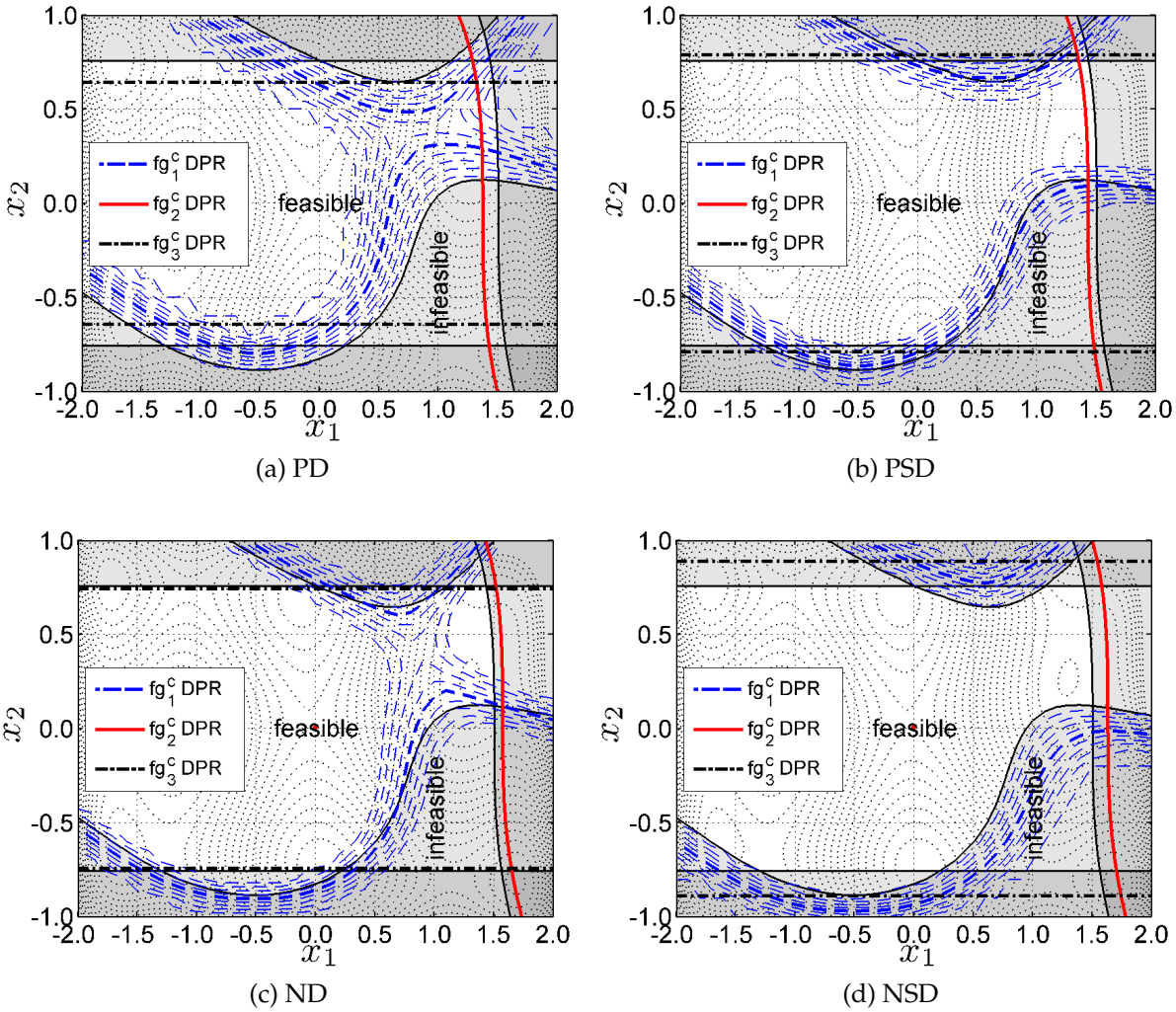

(a) PD

(b) PSD

(c) ND

(d) NSD

Figure 4.10.: DPR for upper MF and $q_{DPR} = 0.5$

In figure 4.10a $q_{DPR} = 0.5$ for PD lies within the feasible design space with varying distance to the crisp boundaries. For grade of possibility of strict dominance and $q_{DPR} = 0.5$ figure 4.10b shows indifferent behavior. For fg_2^c the fuzzy boundary lies in the feasible, for fg_3^c in the infeasible design space. The fg_1^c curve for $q_{DPR} = 0.5$ wavers between the feasible and infeasible design space with different intersection points compared to CoA and CoS. Grade of necessity of dominance (ND) in figure 4.10c gives similar results as PSD. Finally $q_{DPR} = 0.5$ for NSD in figure 4.10d lies completely in the infeasible design space.
The influence on the constraint boundary for the fuzzy constraints by the shape of the allowed value is investigated in figure 4.11. For $q_{DPR} = 0.5$ and grade of possibility of dominance the boundaries are shown for all three versions of allowed values. For fg_1^c different shapes have a high influence. The more conservative the assumption of the allowed value, the smaller the feasible design space is. For the second and third version the design space is additionally divided in the upper right corner.

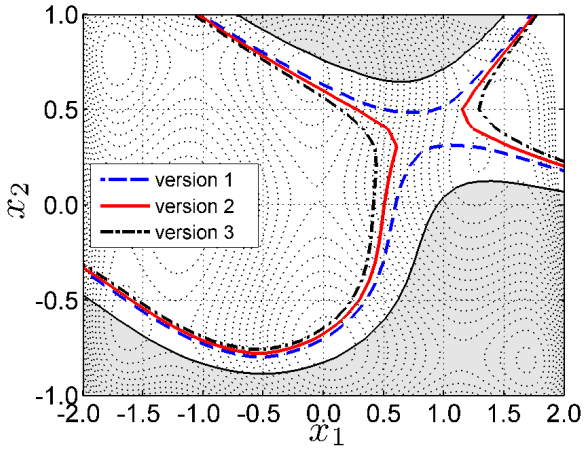

Figure 4.11.: DPR for the upper MF and $q_{DPR} = 0.5$ for different fuzzy numbers of fg_1^c

The sums of DPR measures are also investigated. This is interesting if constraints are treated as goals which have to be minimized. The properties of DPR are well suited to this task. First, a minimum value of zero allows search for designs for which the fuzzy system answers do not intersect the fuzzy allowable values at all. Second, a normalization of constraint violation is given.
In figure 4.12a the sum for upper MF PSD is given together with the boundary for $q_{DPR} = 0.5$. In figure 4.12b the sum for upper MF PD and lower MF PSD is displayed. For $q_{DPR} = 1.0$ the boundary stays well within the feasible design space.
For engineering examples the following conclusions for DPR are derived:

- Mean of grade of possibility of strict dominances for upper and lower MF is very similar to the original crisp boundary. In flat areas of the constraint function deviations from the latter can be seen.
- NSD is not suitable for engineering optimization if used as single measure.
- Information gained by type-2 fuzzy sets provides no decisive advantage compared to interval type-2 fuzzy sets.
- The sum of DPR for all constraints allows for multiobjective optimization.

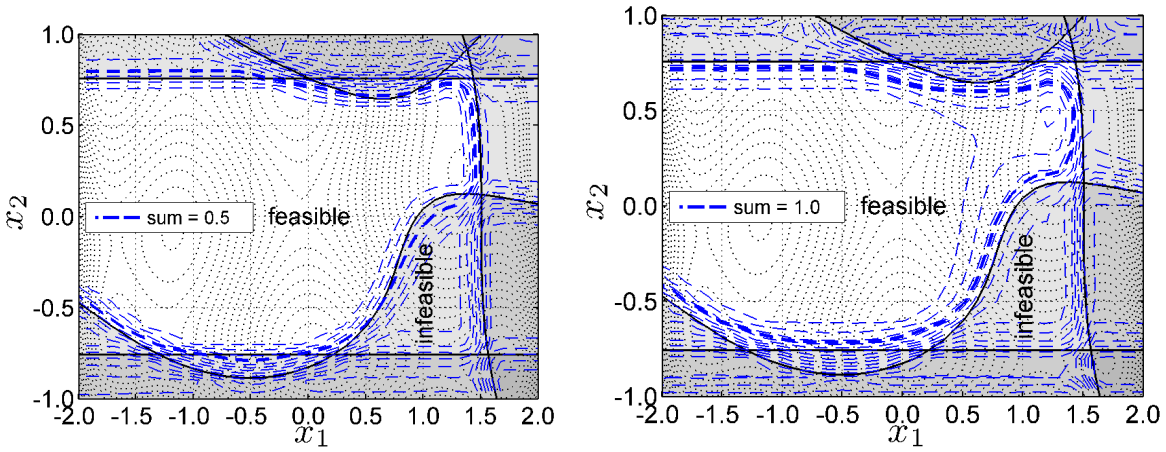

(a) sum for upper MFs PSD, $q_{DPR} = 0.5$

(b) sum for upper MFs PD and lower MFs PSD, $q_{DPR} = 1.0$

Figure 4.12.: Sum of mean DPR for upper and lower MFs

4.2.3. Sengupta-Pal Ranking for fuzzy numbers

This measure based on interval analysis shows a very sharp change between feasible and infeasible designs. Mean and maximum operations together with a limit factor $q_{SPR} = 0.5$ are utilized to gain a single value for constraint evaluation. The influence of decision maker's preference is minimal.
SPR depends strongly on the shape of the allowed fuzzy value fg^{all}. The evaluation of SPR may be affected if both intervals become small, which is often the case for α-cut levels with $\alpha \geq 0.8$. The sharp change in magnitude for this measure is a disadvantage in engineering optimization. The necessary normalization by mean or maximum introduce unwanted effects.

- SPR in the presented formulation presented in chapter 3 is not useful for engineering optimization.
- Only a very sharp boundary which basically follows the crisp constraints is computed.
- The choice of the decision maker has only marginal influence on the resulting boundary.

4.2.4. Chen-Wang Ranking for fuzzy numbers

Because of the definition of U and L in equation 3.16 different versions of allowed fuzzy values fg^{all} have no influence on Chen-Wang ranking for fuzzy numbers (CWR). U and L depend on the maximum and minimum values of the two fuzzy numbers which are compared. This extrema can always be found at the support S, which is the same for all versions of fg^{all}. The order of comparison is also important and gives different results.
In contrast to $DPR \in [0, 1]$ this measure has no fixed upper and lower bound for any of the three constraints. This makes it difficult to set a constant limit factor q_{CWR} a priori. The characteristic can be seen in 4.13a for $q_{CWR} = 0.3$. The boundaries for fg_1^c and fg_2^c are displayed,

the boundary for fg_3^c is missing, because the maximum value for the CWR measure of fg_3^c is $CWR = 0.25$. If the sequence of comparison is switched, the resulting boundaries change as shown in figure 4.13b.

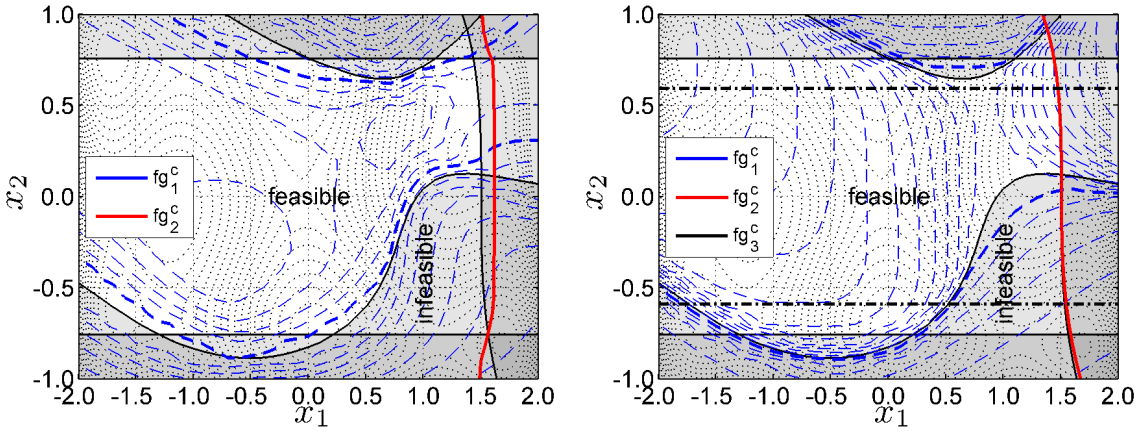

(a) order 1, fg^c upper MF $\Leftrightarrow$ fg^{all} upper MF (b) order 2, fg^c upper MF $\Leftrightarrow$ fg^{all} upper MF

Figure 4.13.: CWR for different MF combinations and $q_{CWR} = 0.3$

As for Dubois-Prade ranking for fuzzy numbers the sum of all constraints for Chen-Wang ranking for fuzzy numbers can be computed also and used as an additional goal. CWR is not so well suited in the basic definition due to different value ranges for single constraints. In figure 4.14 the resulting contours are shown. In figure 4.14a upper MFs are evaluated. Compared to similar measures for DPR in figure 4.12 on page 61 the contours of the sum of CWR for all constraints show different characteristics. Designs with a minimum sum of CWR can be found only far away from constraint boundaries in a roughly shaped oval centered at $x_1 \approx -0.25,\ x_2 \approx 0.0$. For $q_{CWR} = 0.5$ the fuzzy constraint boundary can be found in and outside of the original feasible design space.
If lower MFs are used to compute the sum of CWR, which is shown in figure 4.14b, the area with minimum sum enlarges and the fuzzy constraint boundary for $q_{CWR} = 0.5$ can be found mostly outside of the original feasible design space.

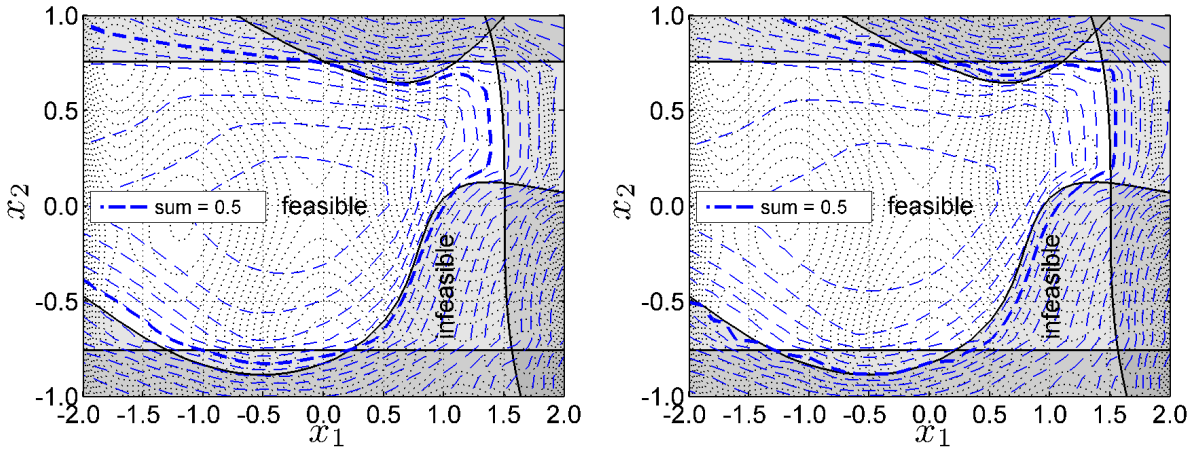

(a) for upper MFs, $q_{CWR} = 0.5$ (b) for lower MFs, $q_{CWR} = 0.5$

Figure 4.14.: Sum of mean CWR

The following conclusions for engineering examples can be drawn for CWR.

- Only if both ranking sequences are taken into account a general measure can be computed.
- The decision makers choice is introduced by q_{CWR}, different fuzzy fg^{all} do not influence the measure as long as the support S is the same.
- The sum of CWR for all constraints allows for multiobjective optimization, result interpretation is not obvious due to different ranges for the sum.

4.3. Optimization of analytical example

The optimization of the analytical example which is defined in equations 4.1 and 4.4 is slightly changed in order to have several of the optima for f in slightly infeasible design space. The crisp constraint values are changed according to equation 4.6, the fuzzy allowed values are shifted accordingly.

$$fg_1^c \leq 41.62 \tag{4.6a}$$
$$fg_2^c \leq \ 2.20 \tag{4.6b}$$
$$fg_3^c \leq \ 1.15 \tag{4.6c}$$

The new crisp allowed values result in a narrowed feasible design space, which is nearly separated by fg_1^c. Also the global optimum and the next best local one are now in infeasible design space.

4.3.1. Results for single crisp goal, CoA and CoS

The optimization of a single goal with constraints results in one optimal design. In table 4.4 these results are summarized for different uncertainty levels.

Table 4.4.: Optimization results for single goal optimization

	crisp	fuzzy							
	1a	2a				3a			
$S^u{}_x$	-	2%	4%	10%	20%	2%	4%	10%	20%
x_1	0.039	0.037	0.035	0.030	0.024	0.036	0.034	0.028	0.017
x_2	-0.640	-0.640	-0.641	-0.644	-0.656	-0.641	-0.642	-0.652	-0.654
goal	-1.294	-1.292	-1.287	-1.250	-1.125	-1.289	-1.274	-1.170	-0.832
Δx_1	0.0%	-5.5%	-9.2%	-21.9%	-38.4%	-7.2%	-13.0%	-26.7%	-55.5%
Δx_2	0.0%	0.0%	0.1%	0.5%	2.4%	0.1%	0.3%	1.8%	2.1%

The Lagrange multipliers in this point are $\lambda_1 = \lambda_2 = 0$ and $\lambda_3 = 0.7815$. The latter is due to the fact, that the optimal solution is restricted only by fg_3. The derivatives for f at the

optimal crisp design point are $\partial f/\partial x_1 = 0.0039$ and $\partial f/\partial x_2 = 1.4609$, the derivatives of the constraints are $\partial f g_1^c/\partial x_1 = 6.2939$, $\partial f g_1^c/\partial x_2 = -12.3131$, $\partial f g_2^c/\partial x_1 = 0.0045$, $\partial f g_2^c/\partial x_2 = 1.2303$, $\partial f g_3^c/\partial x_1 = 0$, $\partial f g_3^c/\partial x_2 = -2.1483$. Thus the optimal design is much more sensitive to changes in x_2 than to changes in x_1.
The results for fuzzy design variables reflect the information given by gradients for the crisp optimal solution. It can be seen from table 4.4 that Δx_1 increases approximately linearly with increasing uncertainty in the design variables. A change in x_1 has minimal influence on the goal and therefore Δx_1 is much higher than Δx_2.
Optimal designs for center of area are closer to deterministic optima than optimal designs for center of support. For high uncertainties in ${S^u}_x \geq 10\%$ the change in optimal design is significant.
For the three optimal designs generated by crisp and fuzzy evaluations resulting IT2 FSs for goal f and an uncertainty level of $S^u(\tilde{x}) = 10\%$ are compared by radar chart in figure 4.15.
The measures are core C, CoA, CoS, support S, difference between left most point of upper and lower MF s_{LL}-s_L, relative difference of S^u and S^l given by $(S^u - S^l)/S^u$ and finally a measure for nonlinearity $\sum d_{L\mu}/|C \leftrightarrow s_{LL}| + \sum d_{R\mu}/|C \leftrightarrow s_{RR}|$.
The axes of the radar chart always have the lower bound at the center and the upper bound outward. It is obvious from figure 4.15 that the optimal design generated by CoS always has the smallest and the crisp optimal design the highest values except for nonlinearity. The function value at the optimum f for CoA and CoS is smaller than f for the crisp optimum because these points are situated in the crisp infeasible design space. This is due to the skewness of the fuzzy constraint values. The axis boundaries for axes 1, 2 and 3 differ by 11.2%, which reflects nonlinearity and skewness of the fuzzy value for f.
The support S in axis 4 for the optimal CoS design is much smaller than the support of the crisp optimum. For nonlinearity measure in axis 7 the order is reversed. Lowest nonlinearity is achieved by the crisp optimal design, the highest one by CoS. This is due to the fact, that $\sum d_{L\mu}$ for the CoS optimal design is 2.2% greater than for the crisp optimal design and $|C \leftrightarrow s_{LL}|$ is 19.8% smaller. Therefore nonlinearity of the left hand side of the upper membership function for the CoS optimal design is higher than for crisp optimal design.

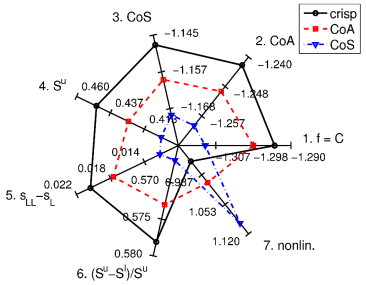

Figure 4.15.: Radar chart for properties of fuzzy f for different optimal designs

4.3.2. Results for optimization with three goals

In this section three goals are considered for optimization. First center of area and support S^u of f are minimized. The third goal is the sum of CWR constraint evaluation method. The higher goal three the higher the constraint violation for a given design.
In figure 4.16 optimal designs for different uncertainty levels are compared. The designs

are split into three groups. First, with a low value for the third goal, second with medium and third with a high value for the third goal. The global minimum for f is found only by violation of the first and third constraint. The global minimum and the next best local one are identified by this approach. Especially designs with a very low f are situated in the infeasible crisp design space. In figure 4.17 on page 67 the corresponding projected Pareto-fronts are shown.
For $S^u(\tilde{x}) = 4\%$ the minimum first and second goal can be reached simultaneously as shown in figure 4.17a whereas for $S^u(\tilde{x}) = 20\%$ very small S^u is found only for high f as displayed in figure 4.17b. The corresponding designs for the latter are in the lower left corner of the design space in figure 4.16b. For $S^u(\tilde{x}) = 4\%$ and $S^u(\tilde{x}) = 20\%$ designs with a low second goal around $f \approx 0$ can be found in fully feasible design space.
In figures 4.17c and 4.17d the trade-off between small f and small constraint violation is given. In figure 4.17e the findings from figure 4.17a are confirmed by converging designs for high values of goal number three on the y axis for small $S^u(\tilde{x}) = 4\%$.

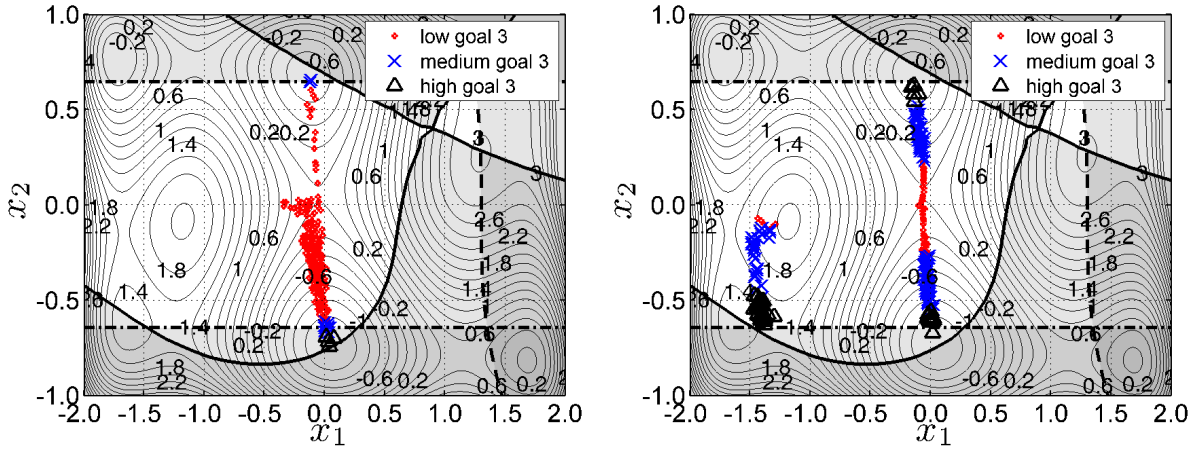

(a) design space for small S_x^u

(b) design space for large S_x^u

Figure 4.16.: Design space for optimization with three goals

4.4. Summary of chapter

From an engineering point of view the following conclusions can be drawn from the results presented in this chapter:

- IT2 FSs proved to be very useful for evaluation of uncertainties. They are computational more efficient than general T2 FSs. They can represent different levels of available information.
- The number of α-cut levels for primary membership functions n_α^I is set to five for the engineering examples. Lower numbers don't allow for proper evaluation of nonlinearities and higher numbers introduce a high computational effort.
- For evaluation of physical properties center of area is utilized.
- S^u will be used for characterization of overall uncertainty.

- For constraint handling, distance of center of area and Chen-Wang ranking for fuzzy numbers show good properties for engineering problems. The first depends on uncertainties as well as nonlinearities of system answers. The second is a very flexible measure with respect to the decision maker's preferences about pessimistic or optimistic situations.
- Radar charts allow for a quick comparison of different solutions with respect to given properties.

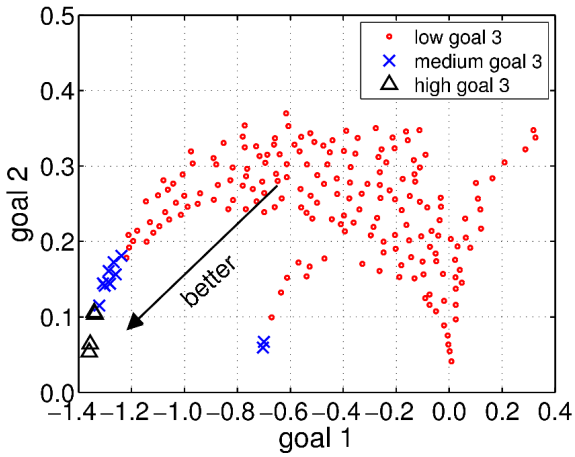

(a) $S^u(x)$ = 4%, goal 1 and goal 2

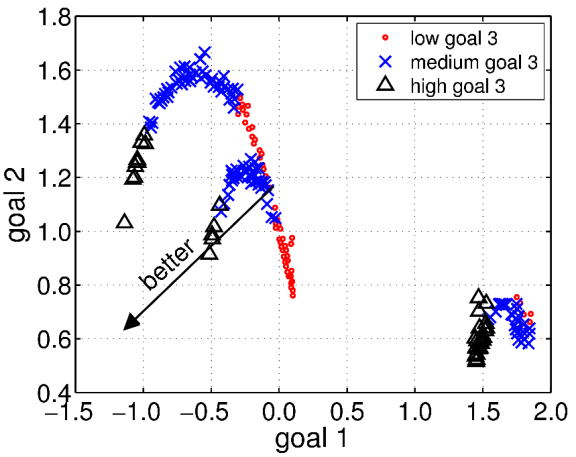

(b) $S^u(x)$ = 20%, goal 1 and goal 2

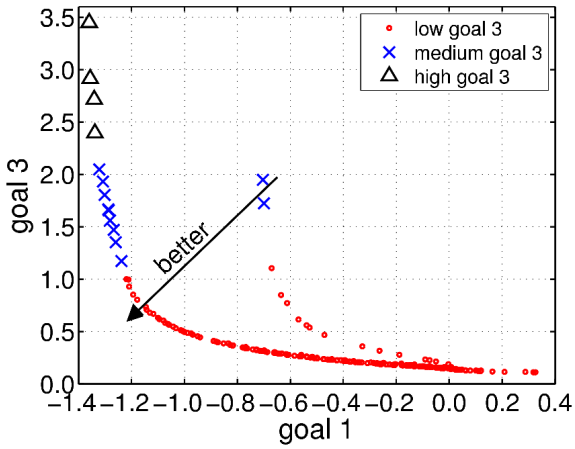

(c) $S^u(x)$ = 4%, goal 1 and goal 3

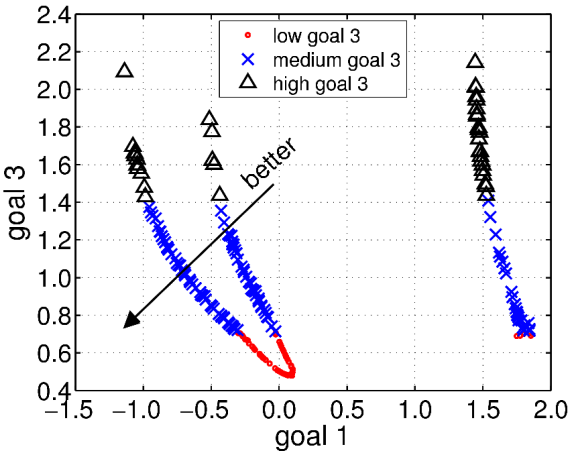

(d) $S^u(x)$ = 20%, goal 1 and goal 3

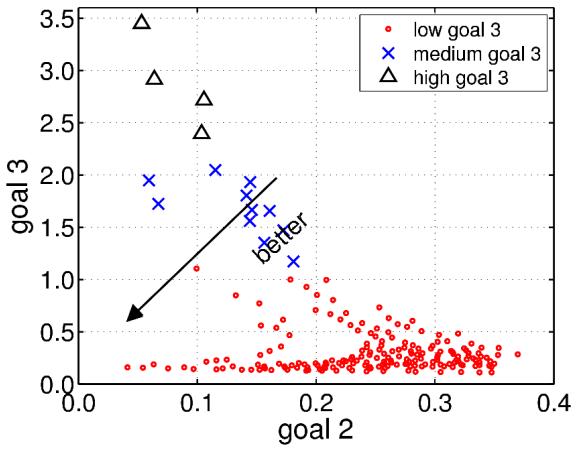

(e) $S^u(x)$ = 4%, goal 2 and goal 3

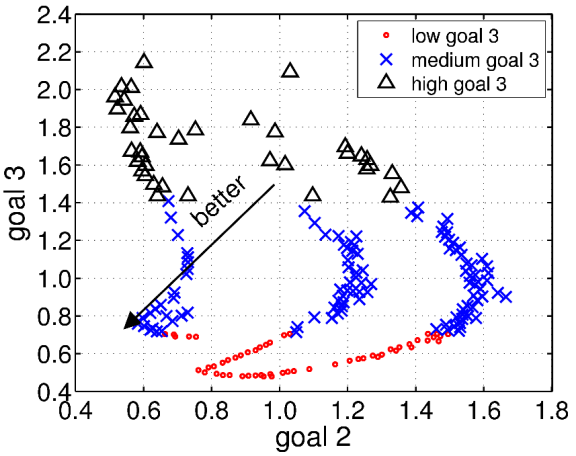

(f) $S^u(x)$ = 20%, goal 2 and goal 3

Figure 4.17.: Projected Pareto-fronts for different uncertainty settings

5. Optimization of extruded profiles for a generic vehicle space frame

The methods introduced in the last chapters are applied to two engineering problems related to extruded, lightweight profiles. The basis for the examples is a generic space frame shown in figure 5.1. The main focus in the examples is on manufacturing aspects introduced by typical manufacturing processes within the Collaborative Research Center SFB Transregio 10 (SFB-TR10) project. The project is already outlined in sections 2.2, 2.3.2 and 2.4.3. Additional information necessary for the presented optimization examples is given in section 5.1.
The optimization of a single profile manufactured by composite extrusion (CE) for reinforced profiles is evaluated first. The manufacturing knowledge is modeled with type-1 fuzzy sets in this example.
A plate built of such profiles is optimized in section 5.3. In this example manufacturing aspects are modeled with type-2 fuzzy sets. Uncertain system parameters are introduced. The first goal is to evaluate designs based on the possibilistic analysis introduced in this thesis. The second is an optimization with opTUM-II and the comparison of the resulting designs with deterministic optima. The most important results and conclusions are summarized and discussed in section 5.4.

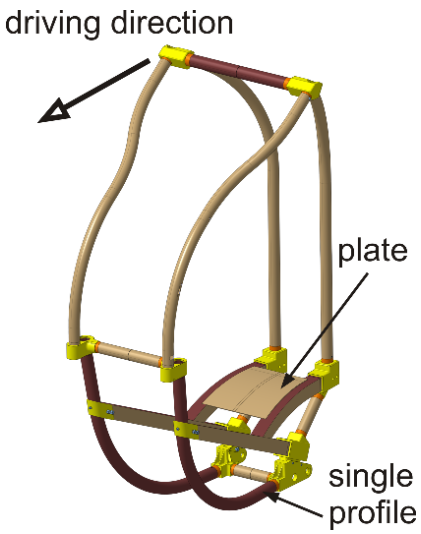

Figure 5.1.: Generic space frame with optimized profile and plate

5.1. Manufacturing aspects for extruded profiles of a generic space frame

A short overview of general manufacturing aspects for processes investigated within the Collaborative Research Center SFB Transregio 10 (SFB-TR10) project is given. Profiles manufactured by composite extrusion are in the focus of research. Those profiles are made from light metals together with strengthening and stiffening reinforcing elements. The combined materials influence not only the mechanical properties but also the extrusion and joining processes.

5.1.1. Materials

Up to now mainly aluminum EN AW-6060 is used as a matrix material combined with SW-1.4310, CW-N440 and CW-N610 reinforcing elements. Also EN AW-2099 and EN AW-6056 are tested with SW-Nanoflex and SW-Nivaflex reinforcing elements in Kloppenborg et al. (2008b). Smaller test batches are described within SFB-TR10 for EN AW-6060 with carbon fiber reinforcements CW-TP25 in Weidenmann et al. (2005b) and first results are available for magnesium matrix AZ31B with SW-1.4310.
Based on the experience of research in SFB-TR10 matrix materials and reinforcing elements selected for this optimization problem are listed in table 5.1 and table 5.2. Aluminum alloys which are widely used for structural applications are added. Also a higher strength magnesium alloy is utilized. Magnesium has different strength limits for tension and compression which has to be considered in the design. Details on this material behavior can be found for example in Swiostek (2008).

Table 5.1.: Mechanical properties of matrix materials

material	E	ρ	CTE	$Rp_{0.2}$ tension	$Rp_{0.2}$ compression	Extrudability index[1]
	GPa	kg/m^3	$10^{-6} * K^{-1}$	MPa	MPa	–
EN AW-2017	72.0	2800	23.0	230.0	230.0	5
EN AW-2024	73.0	2770	23.2	290.0	290.0	4
EN AW-6060	70.0	2700	23.4	160.0	160.0	7
EN AW-6082	70.0	2700	23.4	250.0	250.0	5
EN AW-7075	71.7	2850	23.6	450.0	450.0	4
AZ31B	45.0	1780	26.0	180.0	110.0	5[2]
AZ61A	45.0	1780	26.0	220.0	130.0	4[2]

[1] qualitative measure for extrudability: 1-not applicable,...,7-excellent according to experience and European Aluminium Association (2009)
[2] approximated values from literature research and experience

Reinforcing elements and their properties are listed in table 5.2. Within SFB-TR10 aluminum with steel wire, Al_2O_3 and carbon reinforcements CW-TP25 are investigated. Details can be found in Weidenmann et al. (2005b), Weidenmann et al. (2005a) and Merzkirch et al. (2009). Infiltrated wires with a aluminum or magnesium matrix are used for Al_2O_3 and carbon reinforcements. Measured mechanical properties for CW-N440 and CW-N610 reinforcements with aluminum matrix can be found in Merzkirch et al. (2009). The much

lower properties of CW-N440 with aluminum is due to different infiltration techniques, the one for CW-N440 is experimental, the one for CW-N610 already used for small batch production. Mechanical properties for CW-TP25 and CW-TP55 reinforced composite wires are computed by rule of mixture and evaluated by values available from literature, for example from Amateau (1976), Hayes et al. (1993), Neussl et al. (2000), Blucher et al. (2001) and Matsunaga et al. (2007). Mechanical properties of magnesium AZ91 with 38 Vol.% unidirectional P100 graphite fiber are discussed in Lee (1992). Alloys AZ91C and ZE41A with 40 Vol.% P55 fiber are listed in Tsangarakis and Taleghani (1992). Mechanical properties for magnesium AZ91D with 50 Vol.% and 60 Vol.% are given in Russell-Stevens et al. (2005). Magnesium with Al_2O_3 is also produced and tested, for example the compressive behavior of ZE41A alloy with 35 Vol.% α-Al_2O_3 fiber in Güden et al. (2006).

Table 5.2.: Mechanical properties of reinforcing elements

reinforcement	matrix material	volume ratio	E	ρ	CTE	$Rp_{0.2}$ tension	$Rp_{0.2}$ compression
		%	GPa	kg/m^3	$10^{-6} * K^{-1}$	MPa	MPa
SW-1.4310	-	-	195.0	7900	16.8	1484.0[1]	1635.0[1]
CW-N440	Al	50	80.0	2900	9.0	706.0	706.0
CW-N610	Al	60	231.0	3400	9.0	1455.0	1455.0
CW-TP55	Al	50	242.5	2350	2.3	930.0	450.0
CW-N440	Mg	50	71.8	2394	9.0	707.0	703.0
CW-N610	Mg	60	212.5	3035	9.0	1434.0	1430.0
CW-TP55	Mg	50	204.3	1869	1.3	815.0	359.0

[1] mean value for $Rp_{0.2}$ for wire diameters from 0.65-5.00 mm.

5.1.2. Composite extrusion

A critical aspect of the extrusion process for lightweight designs is minimum achievable wall thickness of the profile cross section. As already shown in Hug et al. (1983), high strength aluminum alloys are not necessarily optimal with respect to mass. In areas of the profile cross section, where only minimal loads have to be transfered lower strength aluminum alloys can achieve smaller wall thicknesses. From literature wall thickness data with respect to the aluminum alloy can be found in Hufnagel (1984), for magnesium in DIN (9711-2), Kainer (2003) and Friedrich and Mordike (2006). Three main parameters determine minimum achievable wall thicknesses. First is circumscribed diameter (CCDi) of the profile, second is the complexity of the cross section and here especially the classification into simple and hollow profiles and finally the extrusion material.
If reinforcing elements are introduced, the extrusion process is always as complex as for hollow profiles, because two or more material strands join around the reinforcing elements in the welding chamber. The overall CE is very complex and the position of the reinforcing elements with respect to the boundaries of the matrix materials is one parameter which determines the manufacturability. Defects as described for example in Kleiner et al. (2006) for a thin walled cross sections with 56 mm width and a wall thickness of 2 mm are now after several years of research under control. This shows the lightweight potential of the manufacturing process but also the necessity to asses this potential early in product development.

5.2. Optimization of profile made by composite extrusion

This example and the one discussed in section 5.3 are related to research work accomplished within the SFB-TR10 project. The profile optimized is shown in figure 5.2, the design variables are given in detail in table 5.3. The optimization problem at hand is formulated in section 2.2 in equations 2.6 and 2.7. The knowledge acquisition is described in section 2.3.2 followed by the resulting fuzzy rule-based models in section 2.4.3. This example has already been published in Huber et al. (2008).

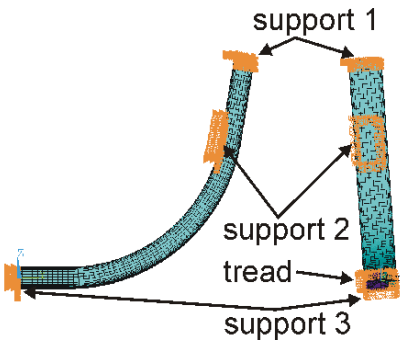

Figure 5.2.: Model of an extruded profile with supports

Table 5.3.: Design variables of the profile optimization problem

design variable	description	lower bound	upper bound	unit	stepsize	variable type
$\hat{R}$	radius ratio[1]	0.0	1.0	-		continuous
H	height	15.0	100.0	mm		continuous
B	width	15.0	100.0	mm		continuous
$b_{1,2}$	outer section	2.0	10.0	mm		continuous
$b_{3...6}$	stiffener[2]	0.0	3.0	mm		continuous
f_1, f_2	reinforcement ratios	0	0.3	-		continuous
M_{comb}[3]	material combination	1	4	-	AlSt, AlCF MgSt, MgCF	discrete

[1] this is only a scaling: $\hat{R} = 0 \rightarrow \hat{R}_{min}$ and $\hat{R} = 1 \rightarrow \hat{R}_{max}$
$\hat{R}_{min}$ and $\hat{R}_{max}$ are predefined by H, B and finite element discretization
[2] if $\leq 1.5\ mm$ the stiffener does not exist
[3] Al: Al6060 T4, Mg: AZ31HP, St: steel wire 1.4310, CF: Thornel 25

5.2.1. Load cases

Three static load cases are computed. Load cases 1 and 2 are related to a loading condition during normal use. The third load considers stresses due to thermal mismatch of matrix and reinforcements. To ensure the stability of the lightweight profile a linear buckling analysis is performed for each load case. The first eigenfrequency is computed by modal analysis.

Table 5.4.: Space frame profile - load cases

number of load case	description	load		unit
1	pothole - driver standing	F_{LC1}	2.94	kN
		M_{LC1}	220.50	Nm
2	pothole - driver seated	F_{LC2}	0.74	kN
		M_{LC2}	1102.50	Nm
3	temperature difference	ΔT	100.00	K

5.2.2. Discussion of optimization results for TR10 proflie

Optimal cross sections are shown on the right hand side of figure 5.3. Designs $2G_1$ and $2G_2$ correspond to the standard optimization formulation given in equation 2.6, designs $3G_{1-4}$ are optimal solutions for optimization with manufacturing aspects given in equation 2.7. Designs $2G_1$ and $2G_2$ from standard optimization have stiffeners in the cross section in combination with very low reinforcement ratios f_1 and f_2. This leads to high differences between wall thickness of outer cross sections and the stiffeners. A trade-off between mass and deflection is obvious from the Pareto-front shown on the left hand side of figure 5.3.
If manufacturing aspects are taken into account higher reinforcement ratios are preferred to stiffeners. The optimization with three goals is projected to the mass-deflection plane. This projection shows differences to the two goal optimization mainly for very lightweight designs. For a mass higher than 3 kg only minor differences can be seen in goals space for the two optimization formulations.

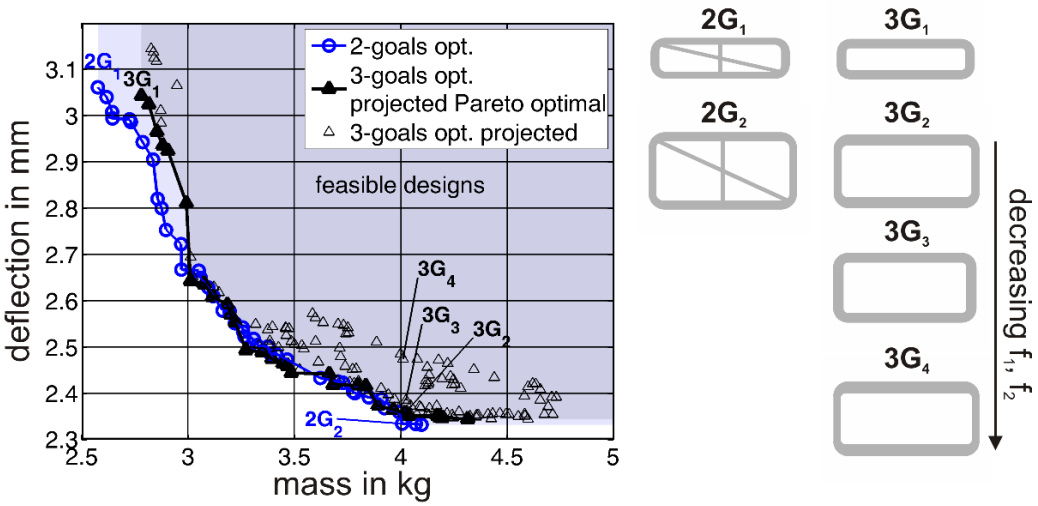

Figure 5.3.: Pareto-fronts for optimization with and without manufacturing aspects, Huber et al. (2008)

The design variables of the highlighted solutions are given in table 5.5. In the two goals optimization, a design with two stiffeners is generated for all Pareto-optimal solutions. To reach a comparable mechanical performance without stiffeners, design $3G_1$ has a high reinforcement ratio f_2 in the vertical walls of the cross section. It has a much smaller manufacturing performance measure than design $2G_1$ with two stiffeners.

For small deformations stiffeners and high reinforcement ratios offer a similar performance measure, for example see designs $2G_2$ and $3G_2$. Design $3G_3$ has a much smaller performance measure PM_{res} indicating a favorable residual stress situation. This reduction can be accomplished with slightly worse mechanical properties. Design $3G_4$ has no reinforcements at all leading to the smallest possible residual stress. This good suitability for subsequent manufacturing processes comes with a ~5% higher deflection.

Table 5.5.: Design variables and goals for six selected designs of the solution

parameter	$2G_1$	$2G_2$	$3G_1$	$3G_2$	$3G_3$	$3G_4$	unit
$\hat{R}$	0.697	0.109	0.269	0.048	0.000	0.000	1
H	23.400	48.200	22.100	45.700	45.200	44.400	mm
B	90.000	99.200	91.100	100.000	100.000	98.300	mm
b_1	4.700	6.200	6.600	8.100	7.300	8.600	mm
b_2	6.000	5.200	6.800	5.900	7.800	5.200	mm
b_3	3.000	2.600	-	-	-	-	mm
b_4	-	-	-	-	-	-	mm
b_5	-	-	-	-	-	-	mm
b_6	2.500	2.800	-	-	-	-	mm
f_1	0.018	0.031	0.017	0.228	0.153	0.000	mm
f_2	0.060	0.054	0.163	0.121	0.076	0.000	mm
material	Mg/CF	Mg/CF	Mg/CF	Mg/CF	Mg/CF	Mg/CF	
mass	2.618	4.007	2.781	4.021	4.025	4.011	kg
deflection	3.040	2.335	3.042	2.358	2.386	2.474	mm
PM_{res}	(0.554)[1]	(0.506)[1]	0.492	0.560	0.484	0.349	1

[1] not evaluated in optimization

5.3. Optimization of stringer stiffened, metal matrix composite plate

The optimization problem presented in this section is based on a plate shown in figure 5.4. Within the SFB-TR10 research project an exemplary motorcycle space frame is designed and produced in small numbers. At the moment a simple sheet metal connects the two halves of the space frame as shown in figure 5.1. The sheet metal should be replaced in this engineering task by a reinforced plate. The plate is made from two different types of profiles which are joined parallel to the reinforcing elements. The profiles cross sections and also reinforcing elements of the two basic profiles can be set independently.

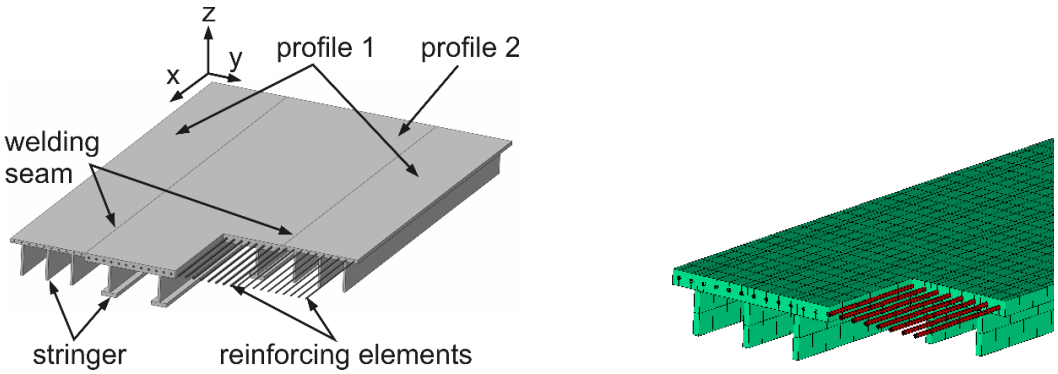

(a) configuration of plate made from two different profiles

(b) finite element numerical model

Figure 5.4.: Plate made from two extruded profiles

5.3.1. Load cases

Three load cases are computed for the given structure. The known prestress in reinforced profiles due to composite extrusion investigated in section 5.2 is neglected in this example. The detailed values for each load case can be found in table 5.6.

TR10 - Buckling load case

An Euler buckling analysis is performed in order to check stability under compressive loads. The buckling load is applied to the plate and local stresses in the plate and the stringers are checked. The plate and the stringers are supported so that global buckling of the top plate occurs first.
The load case is computed in three steps. First a small pressure load is applied to the front of the plate at $x = 600\ mm$ in negative x direction. This is the basis for the second step, the Euler buckling analysis. In the third step the pressure load is multiplied by the first buckling factor and divided by a factor in order to account for higher buckling loads computed in the linear analysis. First and third principal stresses (maximum and minimum stress) are determined for top plate, stringer web and stringer flange for both profiles, respectively.

TR10 - Pothole load case

This is a static load case which introduces a driver with a mass of 100 kg and acceleration loads in all three directions. In x direction the acceleration is -1.5 g, in y direction 1.0 g and in z direction 4.5 g. The forces of the drivers mass as a reaction of those accelerations are distributed to a portion of the plate. No load uncertainties are present in this example. The same stresses are evaluated as for buckling analysis.

TR10 - Temperature load case

The mix of different types of matrix and reinforcing materials leads to a mismatch of thermal expansion coefficient. For typical operating conditions with a temperature difference of 50 K the resulting stresses are computed. It is assumed that the connection between the plate and the rest of the structure elongates together with the plate in x direction.

Table 5.6.: Reinforced plate - load cases

load case	load	direction	value	unit
1	F_B	x	$P_{cr}/10$	N
2	m_D	-	100.0	kg
	a	x	-1.5	g
	a	y	1.0	g
	a	z	4.5	g
3	ΔT	-	50	K

5.3.2. Modeling

The numerical model itself, design variables and uncertain parameters are discussed together with performance measures in the following.

Numerical model

An ANSYS® FEM model with beam, shell and mass elements is utilized for the model of the plate. The matrix material of the profiles is represented by SHELL181 elements, reinforcing elements by BEAM188 elements, respectively. The stringers of the profiles are connected via coupled degrees of freedom to the top plate in order to simulate the wall thickness of the top plate. The beams are connected to shells via shared nodes as shown in figure 5.4b. Linear element definitions are used.
The plate is supported at its edges. For buckling analysis stringers are supported so that local buckling of the stringers at front and back is not the dominant failure mode. The driver in the pothole load case is simplified by an equivalent mass point situated above the plate. The forces due to acceleration loads are transfered to a portion of the plate only.

Design parameters and uncertain parameters

The profiles are characterized mainly by their width and their stringer height. Together with the type of stringer (with or without flange at the bottom) those dimensions determine the CCDi of the profile. Wall thicknesses of the top plate and the stringer complete the cross section definition. Additionally, up to 20 reinforcing elements can be switched on or off. The diameter and z positions of all reinforcing elements are also design variables. Geometrical design variables are shown in figure 5.5. The overall width of the plate is fixed to $p_W = p^1_{pw} + p^2_{pw} = 400 \ mm$ and the length to $p_L = 600 \ mm$. The maximum number of reinforcing elements is set to $p^1_{reN} = p^2_{reN} = 20$.

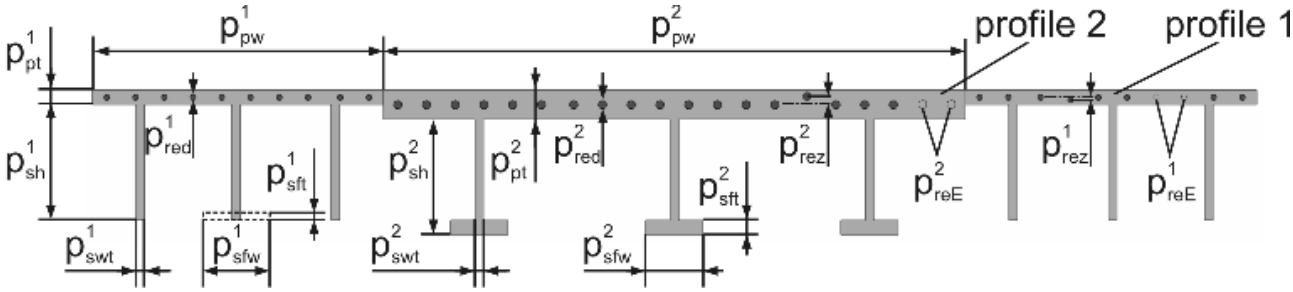

Figure 5.5.: Geometric design variables of profiles

Not all design variables are subject to uncertainties. They are listed in table 5.7 together with information about uncertainty bounds. Discrete choices are numbered, see table footnote for details.

Table 5.7.: Design variables with uncertainty bounds

design variable	nominal value	lower bound	upper bound	unit	variable type[1]
p^2_{pw}	133.3	-	-	mm	c
p^1_{pt},p^2_{pt}	7.0	from T2-FRBS	from T2-FRBS	mm	c
p^1_{sh},p^2_{sh}	20.0	-	-	mm	c
p^1_{swt},p^2_{swt}	3.0	from T2-FRBS	from T2-FRBS	mm	c
p^1_{sft},p^2_{sft}	3.0	from T2-FRBS	from T2-FRBS	mm	c
p^1_{sfw},p^2_{sfw}	0.4	-	-	-	c
p^1_{sN},p^2_{sN}	5	-	-	-	qc
p^1_{sT},p^2_{sT}	1	-	-	-	d
p^1_{red},p^2_{red}	2.0	-	-	mm	c
p^1_{rez},p^2_{rez}	0.0	from T1-FRBS[2]	from T1-FRBS[2]	mm	c
$\mathbf{p}^1_{reE}$,$\mathbf{p}^2_{reE}$	no reinf.	-	-	-	d
p^1_{psM},p^2_{psM}	EN AW-6060	-	-	-	d
p^1_{reM},p^2_{reM}	SW-1.4310	-	-	-	d

[1] c: continuous, qc: quasi continuous, d: discrete
[2] via additional system parameter Ψp_{rez}

For the nominal design the fuzzy input parameters are shown in figure 5.6. Because the wall thicknesses for top plates and stringers of profile 1 and 2 are the same, which result in repetitive fuzzy numbers, only exemplary ones are shown together with the uncertain parameter for reinforcing element position.

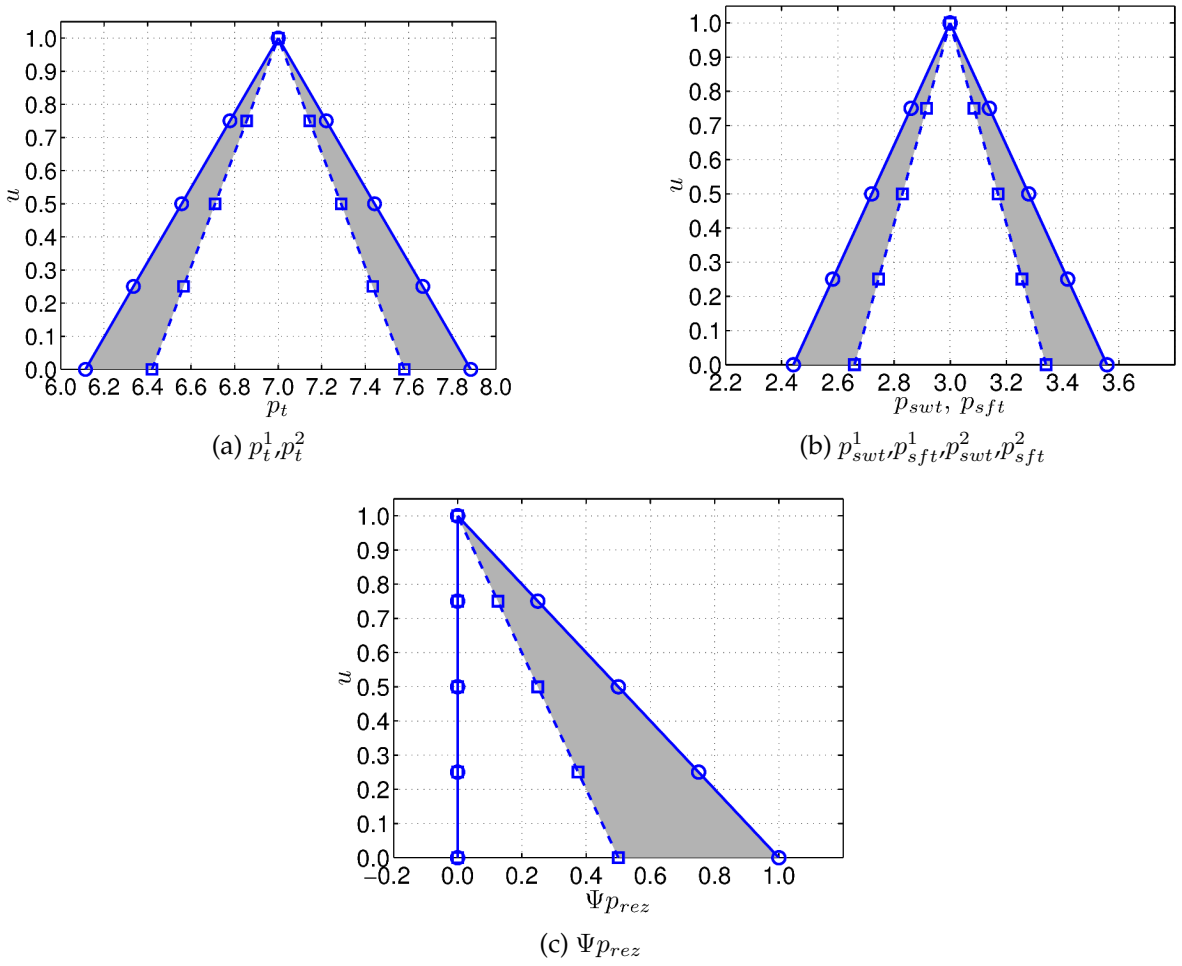

(a) p_t^1,p_t^2

(b) p_{swt}^1,p_{sft}^1,p_{swt}^2,p_{sft}^2

(c) Ψp_{rez}

Figure 5.6.: Uncertain input parameters

The boundaries of the fuzzy numbers are computed by T2-FRBS, which will be discussed in the following. The manufacturing processes involved in production of the plate are composite extrusion (CE) for single profiles, cutting, machining, joining of profiles and finally joining of the plate to space frame. These steps are shortly introduced.

Composite extrusion (CE). From literature sources and expert knowledge gathered by interviews within SFB-TR10, type-2 fuzzy rule-based systems for prediction of minimal allowable wall thicknesses are generated. Minimum wall thicknesses as a function of circumscribed diameter (CCDi) are displayed in figure 5.7 for aluminum and magnesium alloys. In figure 5.7a known values for different materials and complex profile cross sections are compared with each other. High strength materials need much higher wall thicknesses and also magnesium extrusion needs high wall thicknesses for reasonable profile dimensions. In figure 5.7b the knowledge-based model for aluminum alloy EN AW-6060 is shown. The nominal value follows the crisp values for complex cross section whereas the lower value

follows the values for simple profile cross sections. The upper value is symmetrical to the lower one and represents the uncertainty of minimum wall thickness for composite extrusion. The uncertainty varies for different materials with increasing CCDi due to available information. knowledge-based models for other matrix materials can be found in the appendix.

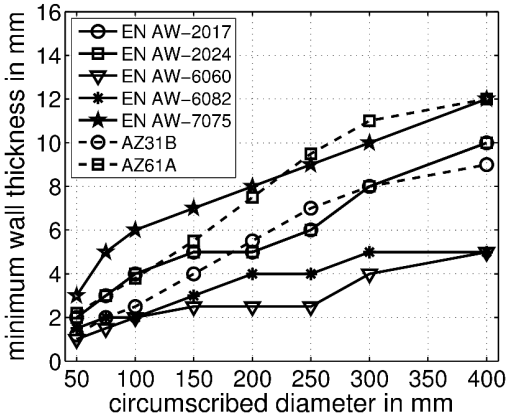

(a) crisp values for complex profiles and different matrix materials

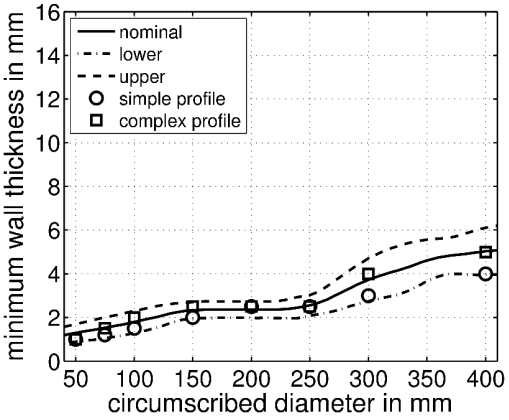

(b) knowledge-based model for EN AW 6060

Figure 5.7.: Minimum wall thickness as a function of circumscribed profile diameter

The rule-based system is based on interval type-2 fuzzy sets. The input parameter CCDi is described by nearly evenly distributed IT2 FSs with Gaussian shape. In this example the membership function and rules are defined initially. A basic numerical optimization of the MF for the output is performed in order to match given minimum wall thickness data. In the following, MFs for input and output are changed in order to include expert based manufacturing knowledge.
Exemplary model inputs, outputs and rules for EN AW-6060 are discussed in the following. One membership function for $CCDi \approx 250-300\ mm$ is wider which indicates the high priority of this class of profiles. The rule base is very basic and connects every input MF directly with one output MF.

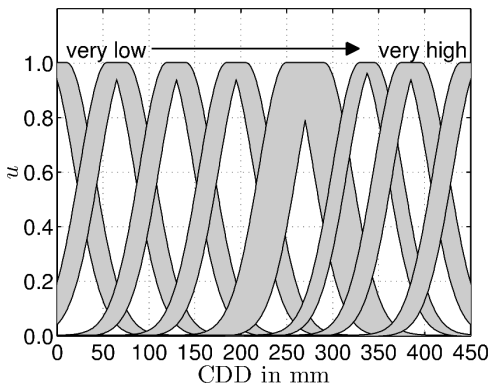

(a) input CCD

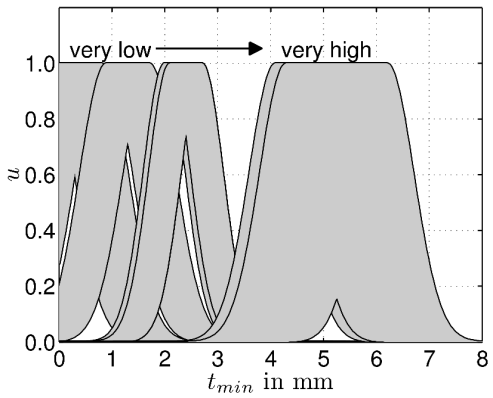

(b) output t_{min}

Figure 5.8.: Input and output membership functions for minimum wall thickness

Profiles produced by extrusion are subjected to different deviations in their cross section parameters and in their geometrical parameters in extrusion direction. Only wall thickness tolerances are considered in this example. A knowledge-based model is generated by EN (12020-2) and EN (755-9) for aluminum and by DIN (9711-3) for magnesium. Two parameters influence the model. First CCDi and second the local wall thickness t. The upper and lower bound of the IT2 FS are determined by tolerance values for simple and complex, such as hollow profiles. In figure 5.9 the output of the models is shown for different classes of materials. For EN AW-6060, which is well suited for extrusion, tolerances and their uncertainties shown in figure 5.9a are small. All other aluminum alloys in this example are represented by the model in figure 5.9b. For magnesium, uncertainties of tolerances in figure 5.9c are very high due to differing and mostly sketchy information provided by literature.

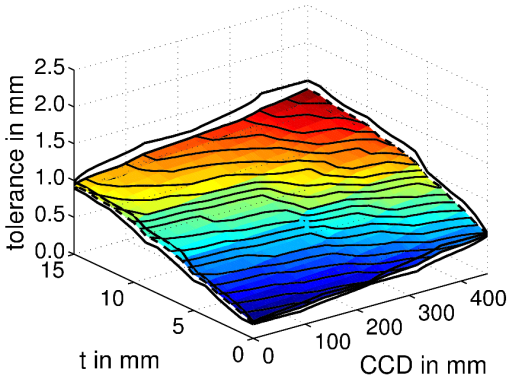

(a) EN AW 6060

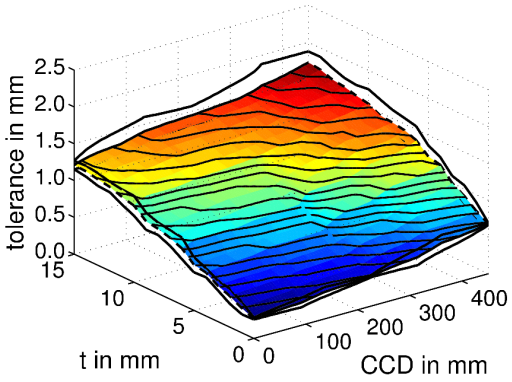

(b) EN AW 2017, 2024, 6082 and 7075

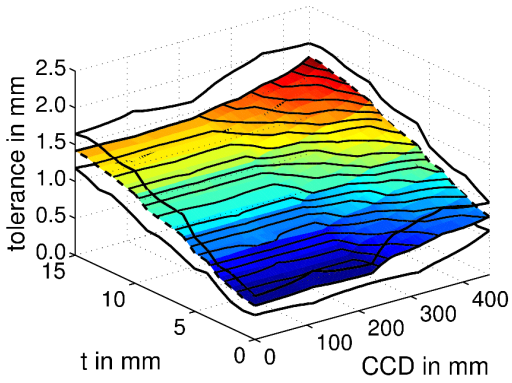

(c) AZ31B and AZ61A

Figure 5.9.: Tolerances of wall thickness as a function of CCD and t

Again the T2-FRBS for EN AW-6060 is shown in figure 5.10. In this model trapezoidal MFs are used. This model is not optimized numerically. Input and output MFs are changed in order to fit the given information.
The rules are listed in equation 5.1. For every combination of input parameters a single output membership function is used in this model. The output membership functions are numbered from MF_1 for low and MF_{15} for high tolerances according to figure 5.10c.

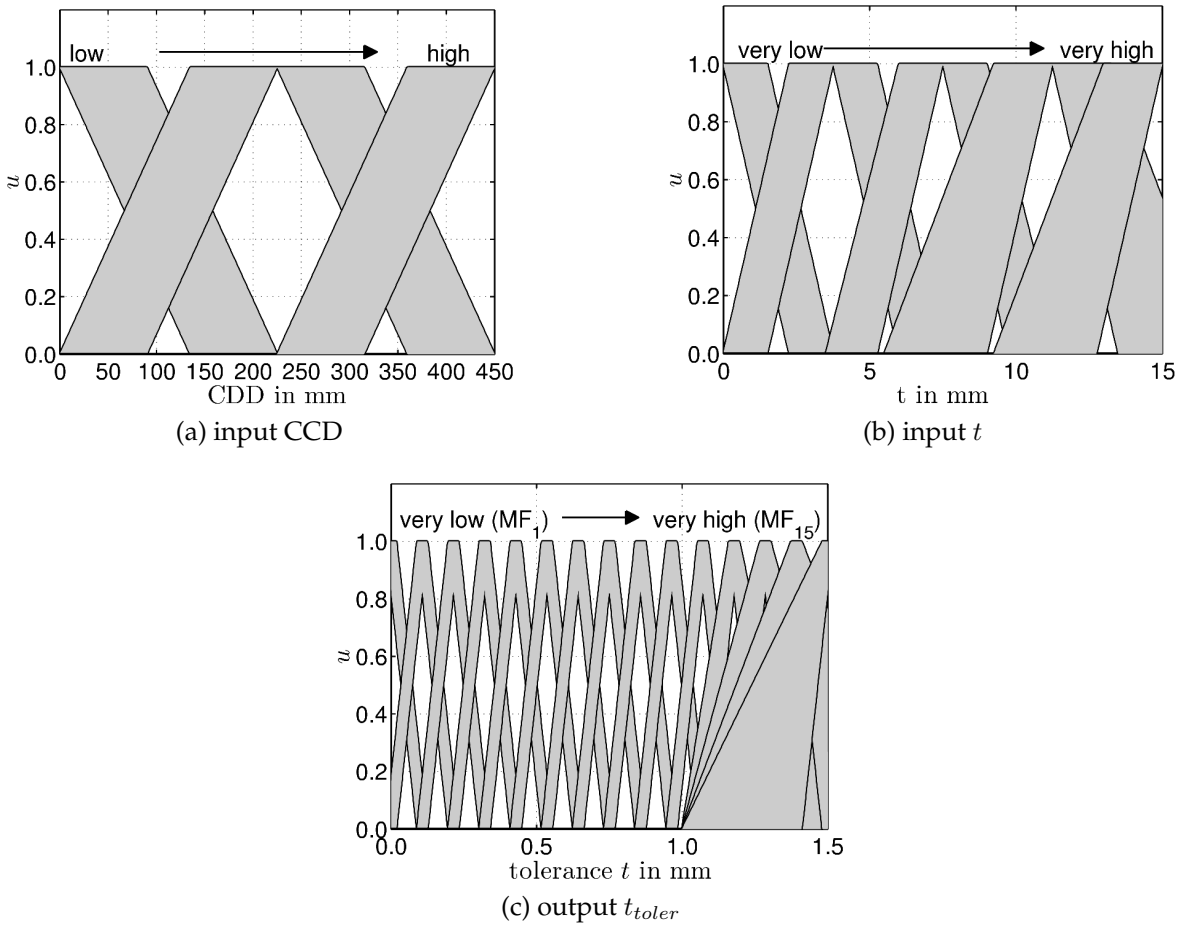

(a) input CCD

(b) input t

(c) output t_{toler}

Figure 5.10.: Input and output membership functions for tolerance of t

$$
\begin{array}{lllllllllll}
IF & CCD & IS & low & AND & t & IS & very\,low & THEN & t_{toler} & IS\ MF_1 \\
IF & CCD & IS & low & AND & t & IS & low & THEN & t_{toler} & IS\ MF_2 \\
IF & CCD & IS & low & AND & t & IS & medium & THEN & t_{toler} & IS\ MF_3 \\
IF & CCD & IS & low & AND & t & IS & high & THEN & t_{toler} & IS\ MF_4 \\
IF & CCD & IS & low & AND & t & IS & very\,high & THEN & t_{toler} & IS\ MF_5 \\
IF & CCD & IS & medium & AND & t & IS & very\,low & THEN & t_{toler} & IS\ MF_6 \\
IF & CCD & IS & medium & AND & t & IS & low & THEN & t_{toler} & IS\ MF_7 \\
IF & CCD & IS & medium & AND & t & IS & medium & THEN & t_{toler} & IS\ MF_8 \\
IF & CCD & IS & medium & AND & t & IS & high & THEN & t_{toler} & IS\ MF_9 \\
IF & CCD & IS & medium & AND & t & IS & very\,high & THEN & t_{toler} & IS\ MF_{10} \\
IF & CCD & IS & large & AND & t & IS & very\,low & THEN & t_{toler} & IS\ MF_{11} \\
IF & CCD & IS & large & AND & t & IS & low & THEN & t_{toler} & IS\ MF_{12} \\
IF & CCD & IS & large & AND & t & IS & medium & THEN & t_{toler} & IS\ MF_{13} \\
IF & CCD & IS & large & AND & t & IS & high & THEN & t_{toler} & IS\ MF_{14} \\
IF & CCD & IS & large & AND & t & IS & very\,high & THEN & t_{toler} & IS\ MF_{15}
\end{array}
\tag{5.1}
$$

Deviation of reinforcing element positions. Early in the SFB-TR10 project deflections of the reinforcing elements due to the extrusion process were found because of interaction of material flow and reinforcing elements as shown in figure 5.11. Details can be found for example in Kleiner et al. (2006). An important part of the SFB-TR10 project is the simultaneous development of numerical simulation tools for manufacturing processes. Also, composite extrusion is simulated and especially material flow, positioning and optimization of the seam welds in the profile cross section are investigated in Schikorra and Kleiner (2006), Kloppenborg et al. (2008a) and Kloppenborg et al. (2009). Much better position accuracy for reinforcing elements is achievable by now, but still horizontal and vertical deviations of the position can be observed.

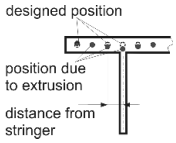

Figure 5.11.: deviation of reinforcing element position

Here only vertical deviations are modeled. Based on experience with an I-beam reinforcing elements are deflected most near the web. This behavior is approximated by the model described in figure 5.12 on page 83. The vertical deviation of a single reinforcing element Δp_{rez} is computed by the input variable d_S, which describes the distance from the nearest stringer. The resulting output shown in figure 5.12c predicts high negative deviations near the stringer and small positive deviations far away. Ψp_{rez} has to be multiplied with a ratio of the local wall thickness.
Again a simple rule base maps the three input MFs directly to the corresponding output MFs. The final position of each reinforcing element is computed by the following equation.

$$p_{rez\,i} = \Delta p_{rez\,i} * \Psi p_{rez} * p_{pt} \qquad i = 1 \ldots p_{reN} \tag{5.2}$$

Cutting and Machining. Suitability for cutting and machining of profiles depends mainly on the ratio and type of reinforcements. Adapted strategies for machining are discussed in Biermann et al. (2008). Reinforced profiles in general cause much higher tool wear and determine the quality of the machined surface.

Joining. Joining of profiles is accomplished by bifocal hybrid laser welding (BHLS) or friction-stir welding (FSW) of the base materials at the profile edges. A summary of research within SFB-TR10 on these processes for reinforced and not reinforced profiles can be found in Zäh et al. (2008). Mostly two parts with the same alloy of aluminum have been welded up to now in SFB-TR10. Both processes are capable of joining different alloys of the same material and also of joining different materials.
In this example it is assumed, that both BHLS and FSW are able to weld plates from 2 to 15 mm. BHLS is restricted to welds of same material, whereas FSW can also weld mixed magnesium and aluminum profiles. A short literature review supporting this assumption can be found in appendix A.6.1.
Process stability for both processes can be achieved if no reinforcing elements lay within a certain distance to the joining zone. For simplification reasons this zone is defined as heat

affected zone (HAZ). It is determined by experience from SFB-TR10 and literature research. In the HAZ reinforcing elements are not allowed in order to guarantee undisturbed welding processes. For BHLS the width of the HAZ is approximately double the wall thickness of the thinner profile. For FSW HAZ is assumed to be four times the wall thickness of the thinner profile.

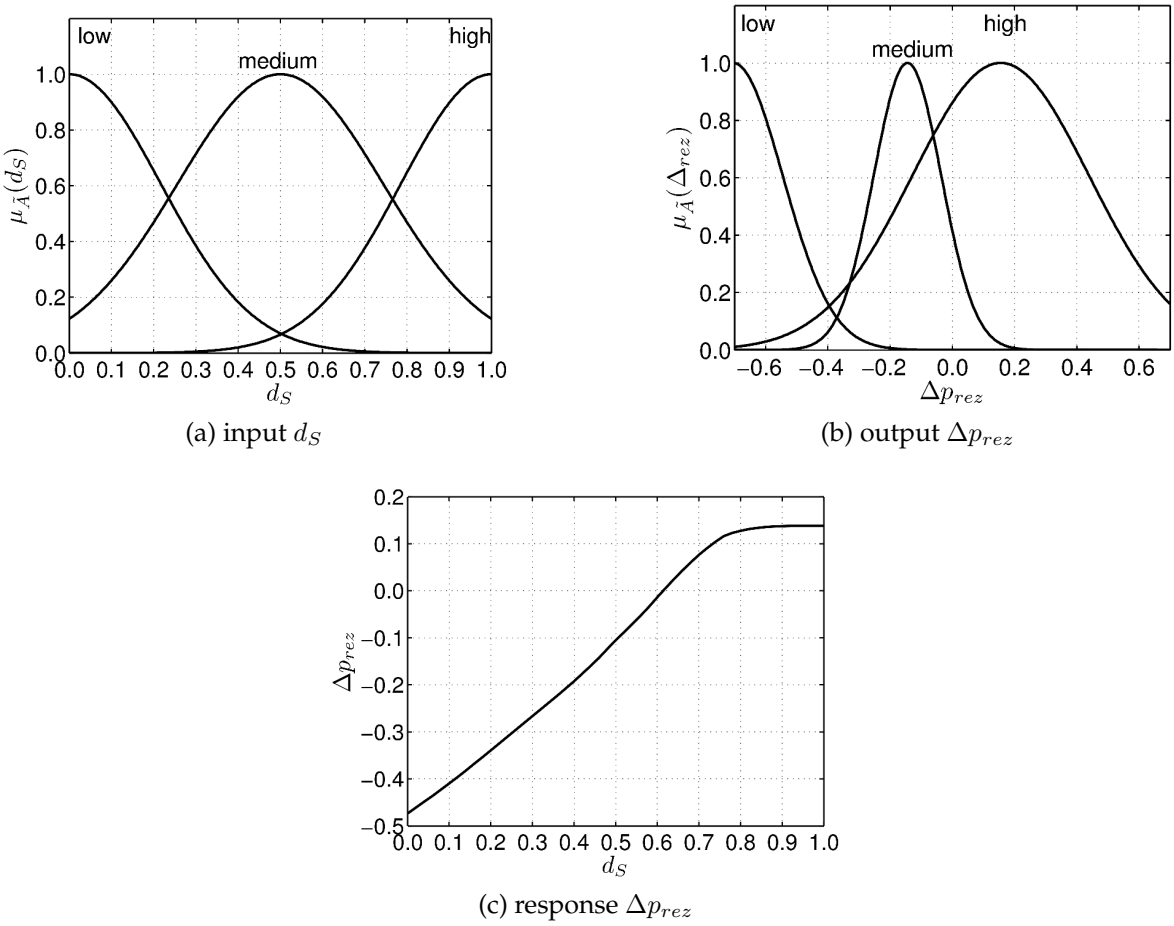

(a) input d_S

(b) output Δp_{rez}

(c) response Δp_{rez}

Figure 5.12.: Deviation of reinforcing elements from design position due to extrusion process

Performance measures

Typical structural properties and manufacturability indices are the focus of the engineering problem. They are listed below.

- mass of plate m_P: The mass of the plate should be as low as possible. Due to tolerances in wall thickness mass is a fuzzy output.
- P_{cr}: The buckling load has to be as high as possible. This is equal to minimization of negative buckling load $-P_{cr}$. Also the buckling load depends on uncertain parameters.
- stresses: Maximum and minimum principal stresses $\sigma_{i\,1st}$, $\sigma_{i\,3rd}$ are evaluated for different parts of the two profiles. This is done for the top plate, the stringers and the reinforcing elements separately. This is necessary because of different allowable stresses

for tension and compression for magnesium as well as some reinforcing materials. Stresses depend on local wall thicknesses and also on reinforcing position.

- manufacturability aspects:
  - position of reinforcing elements: Reinforcing elements have to maintain a minimum distance from a profile wall of 1 mm. This value was achieved in manufacture for simple profiles. The allowed value is uncertain for other materials than EN AW-6060.
  - stringer web thickness: Summarized stringer web thicknesses are not allowed to be wider than profile width.
  - minimum wall thicknesses: Depending on CCDi different minimum wall thicknesses have to be maintained. This is an important uncertainty parameter, because tolerances of wall thickness vary with profile parameters as well as allowed values.
  - heat affected zone: This zone depends mainly on the joining process. No reinforcing element should be positioned within the HAZ. The width of the HAZ is defined by the joining process and also introduces uncertainty to the problem.
  - material combination: FSW can join all material combinations. Bifocal hybrid laser welding (BHLS) can join only alloys of the same material but has the advantage of a smaller zone which is influenced by reinforcing elements.

Depending on the formulation of the optimization problem different performance measures are considered.

5.3.3. Evaluation of initial design

The design given in table 5.7 is evaluated. The reinforced plate shows slightly lower stresses in the matrix than without reinforcements. The efficiency of different means to increase the stiffness of the plate is shown in table 5.8. These numbers are of course valid only for the given initial design and may change for other designs. If reinforcing elements are introduced, mass increases by approximately 10% and buckling load by nearly 6%. If I shaped stringers are used without reinforcing elements a 9.3% increase in m_P and a 17.5% increase in P_{cr} is achieved. For both measures, stringer shape and reinforcing elements a nearly 20% increase in mass but also a 24% increase in buckling load can be achieved.
The fuzzy numbers for m_P and P_{cr} are nearly linear. S^u_{mass} and $S^u_{P_{cr}}$ show a wide spread of the system answers with respect to uncertain parameters. Diagrams can be found in appendix A.6.2.
Compression stresses for the different load cases show slight nonlinearities (see appendix A.6.2 for details). In general, advantages are gained by reinforcing elements and the second stringer type for load cases 1 and 2 whereas a negative impact occurs on load case 3 due to thermal load.

Consequences for optimization. Two primary goals are mass of the plate m_P and buckling load P_{cr}. Some basic constraints arise from geometric boundaries. For example the reinforcing elements have to be within the plate material and stringer width can not be higher than plate width. Additionally, stresses are evaluated for plate, stringers and reinforcing

Table 5.8.: Performance measures for initial designs

reinforcing elements	stringer type	m_P	Δm_P	P_{cr}	ΔP_{cr}
-	-	kg	%	N	%
no	simple	5.99	0.0	5.32e4	0.0
yes	simple	6.58	9.8	5.62e4	5.7
no	I stringer	6.55	9.3	6.25e4	17.5
yes	I stringer	7.14	19.1	6.60e4	24.0

elements in all three load cases.
Crisp optimization runs are performed without safety factor and multiple objectives. The optima of crisp and uncertain runs are compared with each other.
Results in Huber et al. (2010) show better convergence for problems with discrete variables if the mutation probability of the discrete variables is smaller. For crisp optimization mutation probability is set to 80% for both continous and discrete variables. In optimization with uncertainties the mutation probability is set to 80% for continous and to 20% for discrete variables.
It is very important to provide a proper initial population if manufacturing aspects are present. After random generation of the initial population certain parameters have to be changed in order to provide enough feasible designs from the beginning. In the case of the SFB-TR10 example, the outer two reinforcement elements were switched off and the reinforcement diameters $\mathbf{p}^1_{reE}$, $\mathbf{p}^2_{reE}$ and the position of the reinforcing elements p^1_{rez}, p^2_{rez} where limited.

5.3.4. Definition of optimization task

The mathematical definition of the crisp optimization task is given in equation 5.3 and 5.4. With uncertainties arising from the manufacturing process the optimization formulation changes. It is presented in equation 5.5. All necessary crisp values are derived by CoA evaluation.
Typical fuzzy constraints are given in figure 5.13 on page 88. Some are negative values for constraints where the present property of the design has to be larger than the allowed value, for example reinforcing element position in figure 5.13a or minimum wall thickness in figure 5.13d. Allowed stresses are derived from the materials used in the reinforced profiles, an example is given for an aluminum alloy in figure 5.13c.
Whereas several optimization runs with different initial populations were performed for crisp optimization, only two were performed for the problem formulation with uncertainties. The higher computational effort for the latter was compensated by restart of the optimization with the non-dominated designs as initial population after 30 generations.

$$
\begin{aligned}
min \quad & \mathbf{f}(\mathbf{x}) &&= [m_P, -P_{cr}] \\
with: \quad & \mathbf{x} &&= \big[p^1_{pt}, p^1_{sh}, p^1_{swt}, p^1_{sft}, p^1_{sfw}, p^1_{sN}, p^1_{sT}, p^1_{red}, p^1_{rez}, p^1_{reN}, \mathbf{p}^1_{reE}, \ \dots \\
& && \quad p^1_{psM}, p^1_{reM}, p^2_{pt}, p^2_{pw}, p^2_{sh}, p^2_{swt}, p^2_{sft}, p^2_{sfw}, p^2_{sN}, p^2_{sT}, p^2_{red}, \dots \\
& && \quad p^2_{rez}, p^2_{reN}, \mathbf{p}^2_{reE}, p^2_{psM}, p^2_{reM}\big] \\
subject\ to: \quad & g_1(\mathbf{x}) &&= \frac{abs(p^1_{rez}) + (p^1_{red}/2) + 0.5}{p^1_{pt}/2} - 1 \quad \leq 0 \\
& g_2(\mathbf{x}) &&= \frac{abs(p^2_{rez}) + (p^2_{red}/2) + 0.5}{p^2_{pt}/2} - 1 \quad \leq 0 \\
& g_3(\mathbf{x}) &&= \frac{p^1_{swt} * p^1_{sN}}{0.99 * (p_W - p^2_{pw})} - 1 \quad \leq 0 \\
& g_4(\mathbf{x}) &&= \frac{p^2_{swt} * p^2_{sN}}{0.99 * p^2_{pw}} - 1 \quad \leq 0
\end{aligned}
\tag{5.3}
$$

$$
\begin{aligned}
g_{5,17,29}(\mathbf{x}) &= \sigma^1_{i\,1st\,p} / \sigma^1_{all\,m\,t} - 1 \quad \leq 0 \quad , i = [1,2,3] \\
g_{6,18,30}(\mathbf{x}) &= \sigma^1_{i\,3rd\,p} / \sigma^1_{all\,m\,c} - 1 \quad \leq 0 \quad , i = [1,2,3] \\
g_{7,19,31}(\mathbf{x}) &= \sigma^1_{i\,1st\,s} / \sigma^1_{all\,m\,t} - 1 \quad \leq 0 \quad , i = [1,2,3] \\
g_{8,20,32}(\mathbf{x}) &= \sigma^1_{i\,3rd\,s} / \sigma^1_{all\,m\,c} - 1 \quad \leq 0 \quad , i = [1,2,3] \\
g_{9,21,33}(\mathbf{x}) &= \sigma^1_{i\,1st\,re} / \sigma^1_{all\,re\,t} - 1 \quad \leq 0 \quad , i = [1,2,3] \\
g_{10,22,34}(\mathbf{x}) &= \sigma^1_{i\,3rd\,re} / \sigma^1_{all\,re\,c} - 1 \quad \leq 0 \quad , i = [1,2,3] \\
g_{11,23,35}(\mathbf{x}) &= \sigma^2_{i\,1st\,p} / \sigma^2_{all\,m\,t} - 1 \quad \leq 0 \quad , i = [1,2,3] \\
g_{12,24,36}(\mathbf{x}) &= \sigma^2_{i\,3rd\,p} / \sigma^2_{all\,m\,c} - 1 \quad \leq 0 \quad , i = [1,2,3] \\
g_{13,25,37}(\mathbf{x}) &= \sigma^2_{i\,1st\,s} / \sigma^2_{all\,m\,t} - 1 \quad \leq 0 \quad , i = [1,2,3] \\
g_{14,26,38}(\mathbf{x}) &= \sigma^2_{i\,3rd\,s} / \sigma^2_{all\,m\,c} - 1 \quad \leq 0 \quad , i = [1,2,3] \\
g_{15,27,39}(\mathbf{x}) &= \sigma^2_{i\,1st\,re} / \sigma^2_{all\,re\,t} - 1 \quad \leq 0 \quad , i = [1,2,3] \\
g_{16,28,40}(\mathbf{x}) &= \sigma^2_{i\,3rd\,re} / \sigma^2_{all\,re\,c} - 1 \quad \leq 0 \quad , i = [1,2,3]
\end{aligned}
\tag{5.3}
$$

$$
\begin{aligned}
and: \quad & 2.00\ mm \leq p^1_{pt}, p^2_{pt} \leq 15.00\ mm \\
& 75.00\ mm \leq p^2_{pw} \leq 250.00\ mm \\
& 11.00\ mm \leq p^1_{sh}, p^2_{sh} \leq 80.00\ mm \\
& 0.50\ mm \leq p^1_{swt}, p^2_{swt} \leq 15.00\ mm \\
& 0.50\ mm \leq p^1_{sft}, p^2_{sft} \leq 10.00\ mm \\
& 0.05 \leq p^1_{sfw}, p^2_{sfw} \leq 0.90 \\
& 1.00 \leq p^1_{sN}, p^2_{sN} \leq 10.00 \\
& 0.50\ mm \leq p^1_{red}, p^2_{red} \leq 5.00\ mm \\
& -7.00\ mm \leq p^1_{rez}, p^2_{rez} \leq 7.00\ mm \\
& p^1_{reN}, p^2_{reN} = 20 \\
& p^1_{sT}, p^2_{sT} \in [1,2] \\
& \mathbf{p}^1_{reE}, \mathbf{p}^2_{reE} \in [0,1] \\
& p^1_{psM}, p^2_{psM} \in [1,2,3,4,5,6,7] \\
& p^1_{reM}, p^2_{reM} \in [1,2,3,4]
\end{aligned}
\tag{5.4}
$$

$$
\begin{aligned}
min \quad & \mathbf{f}(\mathbf{x},\tilde{\mathbf{x}},\tilde{\mathbf{p}}) && = [m_P, -P_{cr}] && \\
with: \quad & \mathbf{x} && = \begin{bmatrix} p^1_{sh}, p^1_{sfw}, p^1_{sN}, p^1_{sT}, p^1_{red}, p^1_{rez}, p^1_{reN}, \mathbf{p}^1_{reE}, \ \dots \\ p^1_{psM}, p^1_{reM}, p^2_{pw}, p^2_{sh}, p^2_{sfw}, p^2_{sN}, p^2_{sT}, p^2_{red}, \dots \\ p^2_{rez}, p^2_{reN}, \mathbf{p}^2_{reE}, p^2_{psM}, p^2_{reM}, p_{JT} \end{bmatrix} && \\
& \tilde{\mathbf{x}} && = \begin{bmatrix} p^1_{pt}, p^1_{swt}, p^1_{sft}, p^2_{pt}, , p^2_{swt}, p^2_{sft} \end{bmatrix} && \\
& \tilde{\mathbf{p}} && = [\Psi p_{rez}] && \\
subject\ to: \quad & g_1(\mathbf{x}) && = \frac{abs(p^1_{rez})+(p^1_{red}/2)+0.5}{p^1_{pt}/2} - 1 && \leq 0 \\
& g_2(\mathbf{x},\tilde{\mathbf{x}},\tilde{\mathbf{p}}) && = \frac{abs(p^2_{rez})+(p^2_{red}/2)+0.5}{p^2_{pt}/2} - 1 && \leq 0 \\
& g_3(\mathbf{x},\tilde{\mathbf{x}},\tilde{\mathbf{p}}) && = \frac{p^1_{swt} * p^1_{sN}}{0.99*(p_W - p^2_{pw})} - 1 && \leq 0 \\
& g_4(\mathbf{x},\tilde{\mathbf{x}},\tilde{\mathbf{p}}) && = \frac{p^2_{swt} * p^2_{sN}}{0.99*p^2_{pw}} - 1 && \leq 0 \\
& g_{5,17,29}(\mathbf{x},\tilde{\mathbf{x}},\tilde{\mathbf{p}}) && = \sigma^1_{i\ 1st\ p}/\sigma^1_{all\ m\ t} - 1 && \leq 0 \quad , i = [1,2,3] \\
& g_{6,18,30}(\mathbf{x},\tilde{\mathbf{x}},\tilde{\mathbf{p}}) && = \sigma^1_{i\ 3rd\ p}/\sigma^1_{all\ m\ c} - 1 && \leq 0 \quad , i = [1,2,3] \\
& g_{7,19,31}(\mathbf{x},\tilde{\mathbf{x}},\tilde{\mathbf{p}}) && = \sigma^1_{i\ 1st\ s}/\sigma^1_{all\ m\ t} - 1 && \leq 0 \quad , i = [1,2,3] \\
& g_{8,20,32}(\mathbf{x},\tilde{\mathbf{x}},\tilde{\mathbf{p}}) && = \sigma^1_{i\ 3rd\ s}/\sigma^1_{all\ m\ c} - 1 && \leq 0 \quad , i = [1,2,3] \\
& g_{9,21,33}(\mathbf{x},\tilde{\mathbf{x}},\tilde{\mathbf{p}}) && = \sigma^1_{i\ 1st\ re}/\sigma^1_{all\ re\ t} - 1 && \leq 0 \quad , i = [1,2,3] \\
& g_{10,22,34}(\mathbf{x},\tilde{\mathbf{x}},\tilde{\mathbf{p}}) && = \sigma^1_{i\ 3rd\ re}/\sigma^1_{all\ re\ c} - 1 && \leq 0 \quad , i = [1,2,3] \\
& g_{11,23,35}(\mathbf{x},\tilde{\mathbf{x}},\tilde{\mathbf{p}}) && = \sigma^2_{i\ 1st\ p}/\sigma^2_{all\ m\ t} - 1 && \leq 0 \quad , i = [1,2,3] \\
& g_{12,24,36}(\mathbf{x},\tilde{\mathbf{x}},\tilde{\mathbf{p}}) && = \sigma^2_{i\ 3rd\ p}/\sigma^2_{all\ m\ c} - 1 && \leq 0 \quad , i = [1,2,3] \\
& g_{13,25,37}(\mathbf{x},\tilde{\mathbf{x}},\tilde{\mathbf{p}}) && = \sigma^2_{i\ 1st\ s}/\sigma^2_{all\ m\ t} - 1 && \leq 0 \quad , i = [1,2,3] \\
& g_{14,26,38}(\mathbf{x},\tilde{\mathbf{x}},\tilde{\mathbf{p}}) && = \sigma^2_{i\ 3rd\ s}/\sigma^2_{all\ m\ c} - 1 && \leq 0 \quad , i = [1,2,3] \\
& g_{15,27,39}(\mathbf{x},\tilde{\mathbf{x}},\tilde{\mathbf{p}}) && = \sigma^2_{i\ 1st\ re}/\sigma^2_{all\ re\ t} - 1 && \leq 0 \quad , i = [1,2,3] \\
& g_{16,28,40}(\mathbf{x},\tilde{\mathbf{x}},\tilde{\mathbf{p}}) && = \sigma^2_{i\ 3rd\ re}/\sigma^2_{all\ re\ c} - 1 && \leq 0 \quad , i = [1,2,3] \\
& g_{41}(\mathbf{x},\tilde{\mathbf{x}},\tilde{\mathbf{p}}) && = t_{min}/p^1_{pt} - 1 && \leq 0 \\
& g_{42}(\mathbf{x},\tilde{\mathbf{x}},\tilde{\mathbf{p}}) && = t_{min}/p^1_{swt} - 1 && \leq 0 \\
& g_{43}(\mathbf{x},\tilde{\mathbf{x}},\tilde{\mathbf{p}}) && = t_{min}/p^1_{sft} - 1 && \leq 0 \\
& g_{44}(\mathbf{x},\tilde{\mathbf{x}},\tilde{\mathbf{p}}) && = t_{min}/p^2_{pt} - 1 && \leq 0 \\
& g_{45}(\mathbf{x},\tilde{\mathbf{x}},\tilde{\mathbf{p}}) && = t_{min}/p^2_{swt} - 1 && \leq 0 \\
& g_{46}(\mathbf{x},\tilde{\mathbf{x}},\tilde{\mathbf{p}}) && = t_{min}/p^2_{sft} - 1 && \leq 0 \\
& g_{47}(\mathbf{x},\tilde{\mathbf{x}},\tilde{\mathbf{p}}) && = w_{HAZ}/p^1_{d\ HAZ} - 1 && \leq 0 \\
& g_{48}(\mathbf{x},\tilde{\mathbf{x}},\tilde{\mathbf{p}}) && = w_{HAZ}/p^2_{d\ HAZ} - 1 && \leq 0
\end{aligned}
\tag{5.5}
$$

$$
g_{49}(\mathbf{x},\tilde{\mathbf{x}},\tilde{\mathbf{p}}) = \begin{cases} -1 & \text{if } p_{JT} = FSW \\ -1 & \text{if } p_{JT} = BHLS \ \& \ p^1_{psM} \in [1-5] \ \& \ p^2_{psM} \in [1-5] \\ -1 & \text{if } p_{JT} = BHLS \ \& \ p^1_{psM} \in [6,7] \ \& \ p^2_{psM} \in [6,7] \\ +1 & \text{if } p_{JT} = BHLS \ \& \ p^1_{psM} \in [1-5] \ \& \ p^2_{psM} \in [6,7] \\ +1 & \text{if } p_{JT} = BHLS \ \& \ p^1_{psM} \in [6,7] \ \& \ p^2_{psM} \in [1-5] \end{cases} \tag{5.6}
$$

$$
\begin{array}{lrlll}
and: & 2.00 \; mm & \leq & p^1_{pt}, p^2_{pt} & \leq 15.00 \; mm \\
& 75.00 \; mm & \leq & p^2_{pw} & \leq 250.00 \; mm \\
& 11.00 \; mm & \leq & p^1_{sh}, p^2_{sh} & \leq 80.00 \; mm \\
& 0.50 \; mm & \leq & p^1_{swt}, p^2_{swt} & \leq 15.00 \; mm \\
& 0.50 \; mm & \leq & p^1_{sft}, p^2_{sft} & \leq 10.00 \; mm \\
& 0.05 & \leq & p^1_{sfw}, p^2_{sfw} & \leq 0.90 \\
& 1.00 & \leq & p^1_{sN}, p^2_{sN} & \leq 10.00 \\
& 0.50 \; mm & \leq & p^1_{red}, p^2_{red} & \leq 5.00 \; mm \\
& -7.00 \; mm & \leq & p^1_{rez}, p^2_{rez} & \leq 7.00 \; mm \\
& & & p^1_{reN}, p^2_{reN} & = 20 \\
& & & p^1_{sT}, p^2_{sT} & \in [1, 2] \\
& & & \mathbf{p}^1_{reE}, \mathbf{p}^2_{reE} & \in [0, 1] \\
& & & p^1_{psM}, p^2_{psM} & \in [1, 2, 3, 4, 5, 6, 7] \\
& & & p^1_{reM}, p^2_{reM} & \in [1, 2, 3, 4] \\
& & & p_{JT} & \in [1, 2]
\end{array}
\tag{5.7}
$$

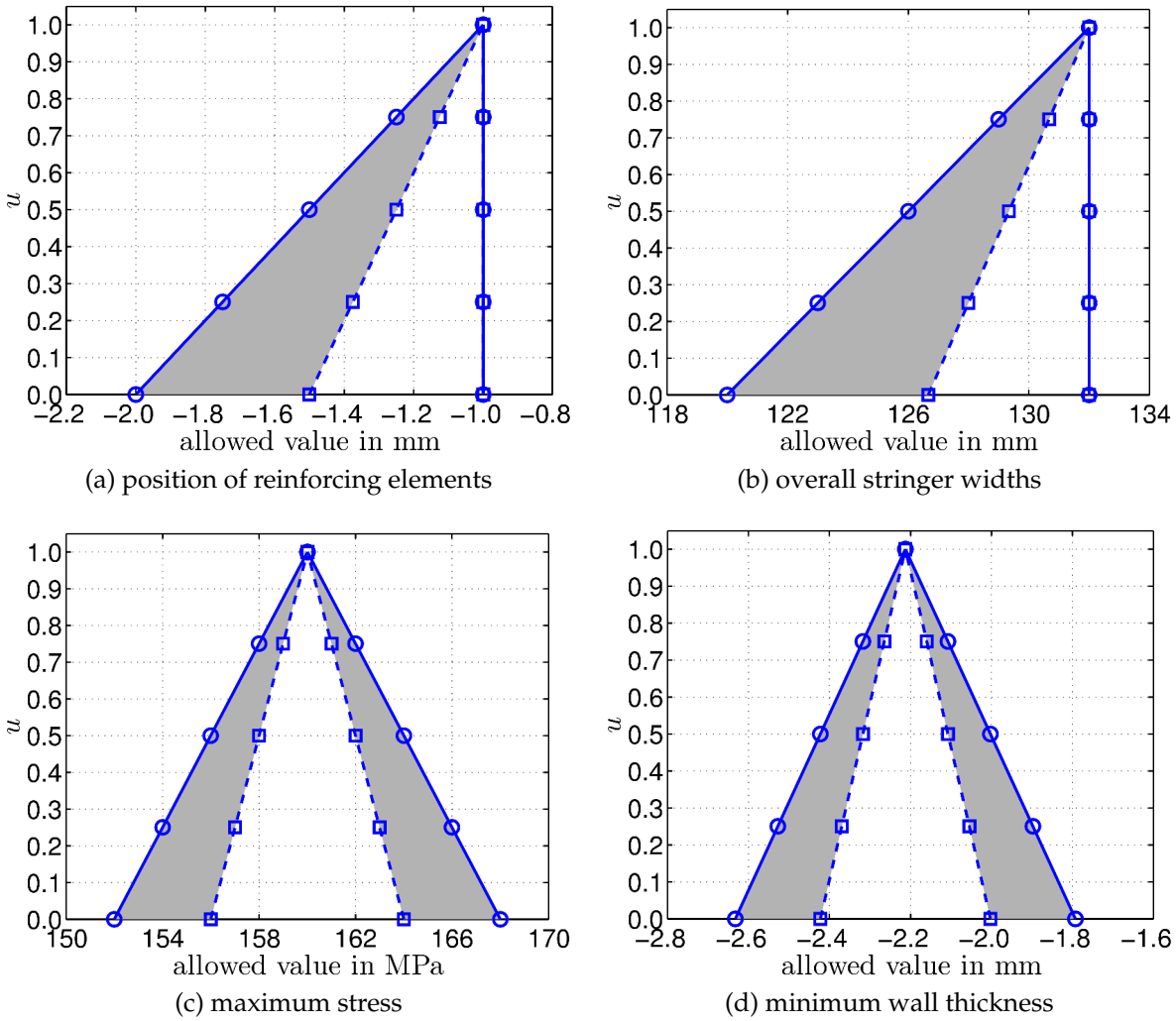

(a) position of reinforcing elements

(b) overall stringer widths

(c) maximum stress

(d) minimum wall thickness

Figure 5.13.: Exemplary allowed values for constraint evaluation

5.3.5. Discussion of optimization results for TR10 plate

The discussion of results will focus on different designs which originate from the optimization problems formulated in equations 5.3 and 5.5. Designs with low mass offer also small buckling loads and vice versa. This is shown in figure 5.14 where the ideal design could be found in the upper left corner. On the left hand side in figure 5.14a the overall Pareto-fronts are shown for crisp optimization marked by the letter "C" and for uncertainty driven optimization marked by "U". A nearly linear correlation between mass and buckling load is found for crisp optimal designs. If manufacturing uncertainties are taken into account the Pareto-front is slightly curved.
For designs with low buckling loads, masses are higher for optimal designs in the presence of uncertainties. For higher buckling loads a few better designs are found for problem formulation 5.5. A check showed, that those designs are also feasible in the crisp problem formulation. To assure convergence, several optimization runs were started with optimized designs as starting population. Minor enhancements could be achieved, the optimized designs discussed in the following are the summary of all optimization runs.
Optimal designs for crisp optimization are made from three material combinations for the two profiles. As can be seen in figure 5.14a and zoomed in on lightweight solution in figure 5.14b, aluminum profiles are chosen for high buckling loads. For low mass an aluminum-magnesium or magnesium-magnesium combination of the two profiles is selected.
Optimal designs with manufacturing aspects have only aluminum-aluminum or magnesium-magnesium material combinations. For high buckling loads EN AW-7075 and for medium ones EN AW-2024 or EN AW-6082 are utilized.
The Pareto-fronts for problem formulations in equations 5.3 and 5.5 include very different designs for the overall goal space. Selected ones are compared in figure 5.15 and table 5.9. On the left hand side in figure 5.15a the crisp optimal design with small mass is characterized by thin wall thicknesses and one stringer with a wide flange in the middle profile. The reinforcing elements have a diameter of 1.8 mm in the outer profiles and 1.2 mm in the middle profile, respectively. The design has a mass of 3.6 kg.
If manufacturing constraints are taken into account in figure 5.15b much greater wall thicknesses are needed. The stringer in the middle profile is not that high and the stringer flange is smaller. Reinforcing elements in the outer profile have 1.6 mm diameter, in the middle profile 5 mm. For the second profile a low strength magnesium alloy is chosen which allows smaller wall thicknesses. The design has a mass of 5.8 kg.
For high buckling loads additional stringers are needed together with higher wall thicknesses. An optimal design for problem formulation defined in equation 5.3 is given in figure 5.15c. High strength aluminum alloys are utilized together with reinforcing elements. If uncertainties are taken into account in figure 5.15d smaller stringers in profile 1 and a lower width of the second profile are the main characteristics. Also the second profile has no reinforcing elements.

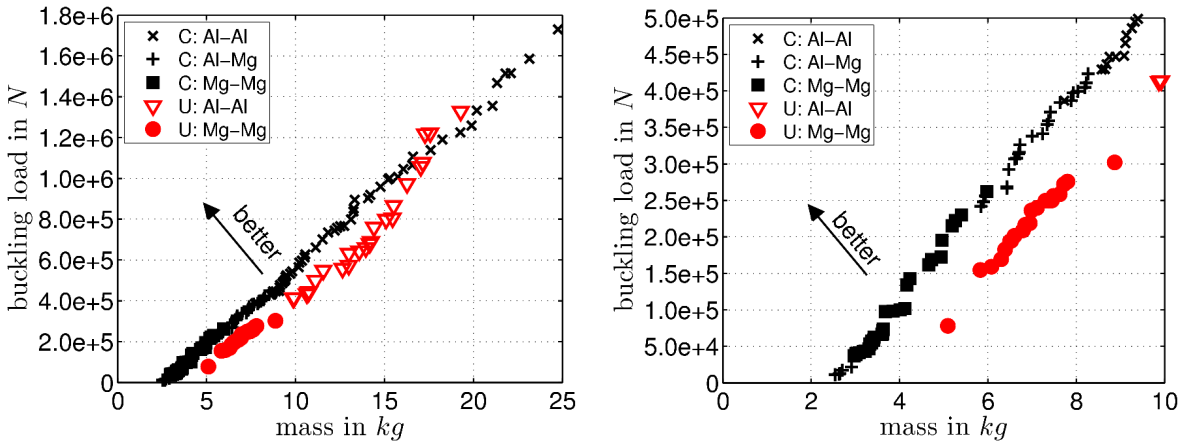

(a) overall solutions (b) optimal designs with less than 10 kg

Figure 5.14.: Pareto-optimal results with respect to material combination

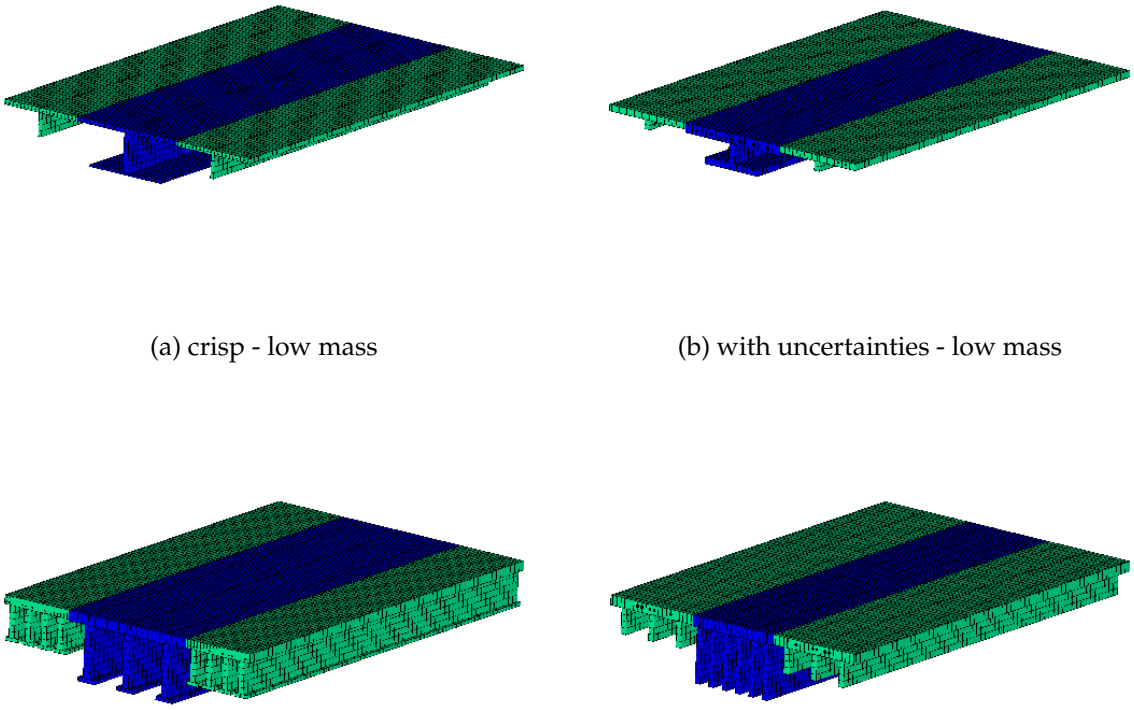

(a) crisp - low mass (b) with uncertainties - low mass

(c) crisp - high buckling load (d) with uncertainties - high buckling load

Figure 5.15.: Comparison of optimal designs

Table 5.9.: Design variables and goals of four selected designs of the solution

	crisp		with uncertainties		
	low	high	low	high	
parameter	mass	buckling load	mass	buckling load	unit
p^1_{pt}	6.40	12.30	8.80	13.50	mm
p^1_{sh}	32.30	49.20	12.80	35.50	mm
p^1_{swt}	5.00	8.60	8.70	8.30	mm
p^1_{sft}	3.10	4.70	8.30	10.00	mm
p^1_{sfw}	0.11	0.75	0.44	0.83	1
p^1_{sN}	1.00	4.00	1.00	3.00	1
p^1_{sT}	1.00	2.00	1.00	1.00	1
p^1_{red}	1.80	1.90	1.60	4.10	mm
p^1_{rez}	-0.40	-2.40	0.90	0.40	mm
p^1_{reN}	20.00	11.00	4.00	5.00	1
p^1_{psM}	AZ61A	EN AW-7075	AZ61A	EN AW-7075	-
p^1_{reM}	CW-TP55	SW-1.4310	CW-TP55	SW-1.4310	-
p^2_{pw}	161.00	191.00	153.00	131.00	mm
p^2_{pt}	5.40	14.00	13.20	15.00	mm
p^2_{sh}	57.10	78.70	35.40	76.80	mm
p^2_{swt}	7.30	10.00	9.30	8.00	mm
p^2_{sft}	2.30	5.50	8.70	7.40	mm
p^2_{sfw}	0.72	0.43	0.56	0.56	1
p^2_{sN}	1.00	3.00	1.00	6.00	1
p^2_{sT}	2.00	2.00	2.00	1.00	1
p^2_{red}	1.20	2.30	5.00	1.50	mm
p^2_{rez}	-1.10	3.50	-1.00	0.60	mm
p^2_{reN}	20.00	4.00	8.00	0.00	1
p^2_{psM}	AZ61A	EN AW-7075	AZ31B	EN AW-7075	-
p^2_{reM}	CW-N440	CW-N440	CW-N440	CW-N440	-
p_{JT}	BHLS	FSW	BHLS	BHLS	-
mass	3.63	20.19	5.83	19.30	kg
buckling load	0.73	13.33	1.55	13.27	N*10^5
figure	5.15a	5.15c	5.15b	5.15d	

Radar charts for the two goals are shown in figure 5.16 and 5.17 for the initial and minimum mass designs. For buckling load the initial design has the lowest absolute value but also a small overall uncertainty. Minimum mass design from crisp optimization shows high skewness and nonlinearity of the fuzzy system answer.
For mass the radar chart is displayed in figure 5.17. Each of the three designs is best for certain fuzzy properties. It depends on the decision maker which design is chosen.

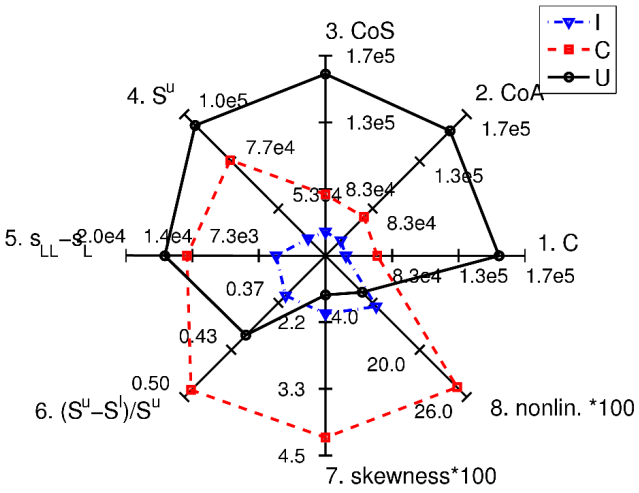

Figure 5.16.: Radar charts for minimal mass designs - buckling load

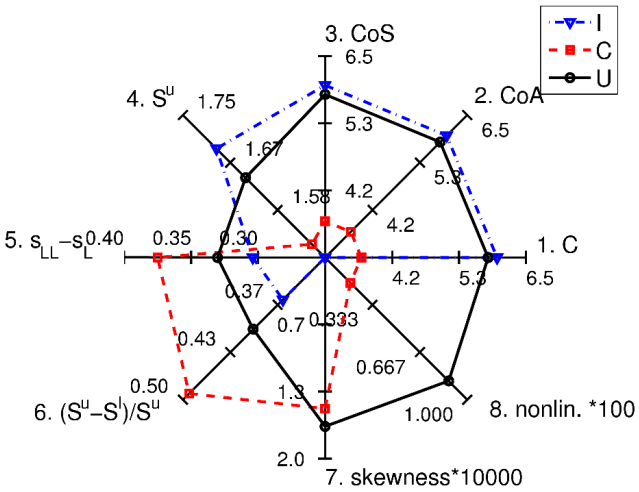

Figure 5.17.: Radar charts for minimal mass designs - mass

For crisp optimization only a few very lightweight designs are restricted by basic geometric considerations or by stresses in the temperature load case, all other designs are restricted by compression strength for buckling in the plate part of profile 1 or 2. For optimal designs with manufacturing uncertainties only very few solutions are restricted by stress constraints. For lightweight designs the position of the reinforcing elements is critical due to deflection during the extrusion process. The most critical limitation are minimal wall thicknesses.

The ratio of the plate thicknesses p^1_{pt} and p^2_{pt} is analyzed in figure 5.18. It is shown on the left hand side in figure 5.18a over mass. For crisp optimization the spread of different ratios is high especially for lightweight designs. In figure 5.18b p^1_{pt}/p^2_{pt} is shown over the ratio of the plate widths p^1_{pw}/p^2_{pw}. It can be seen that crisp optimal designs have very small outer profiles compared to the middle one ($p^1_{pw}/p^2_{pw} < 0.6$). No clear trend can be identified. For included manufacturing aspects, the plate widths are more similar $p^1_{pw}/p^2_{pw} > 0.6$ and optimal designs with $p^1_{pt}/p^2_{pt} \approx p^1_{pw}/p^2_{pw} \approx 1$ are present.

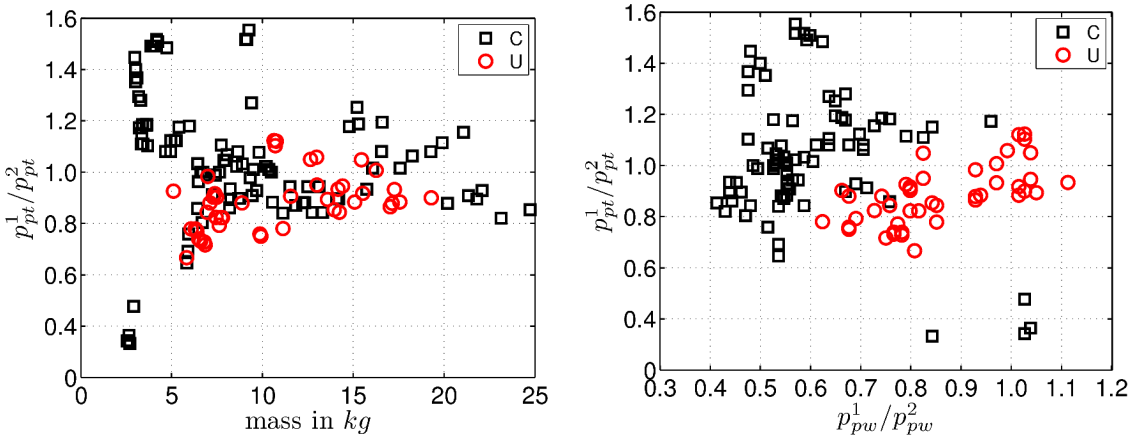

(a) over mass (b) over ratio of plate widths

Figure 5.18.: Ratio of plate thicknesses

The number of stringers over their height is displayed in figure 5.19a for the first profile and in figure 5.19b for the second profile. For both optimization formulations the first profile has fewer and smaller stringers. For crisp optimization the second profile has more stringers, most of them at the upper variable boundary $p^2_{sh} = 80\ mm$. Optimal designs with uncertainties use fewer stringers with less height. This is due to the limitation of minimal wall thickness with respect to CCDi, which increases with higher p^2_{sh}.

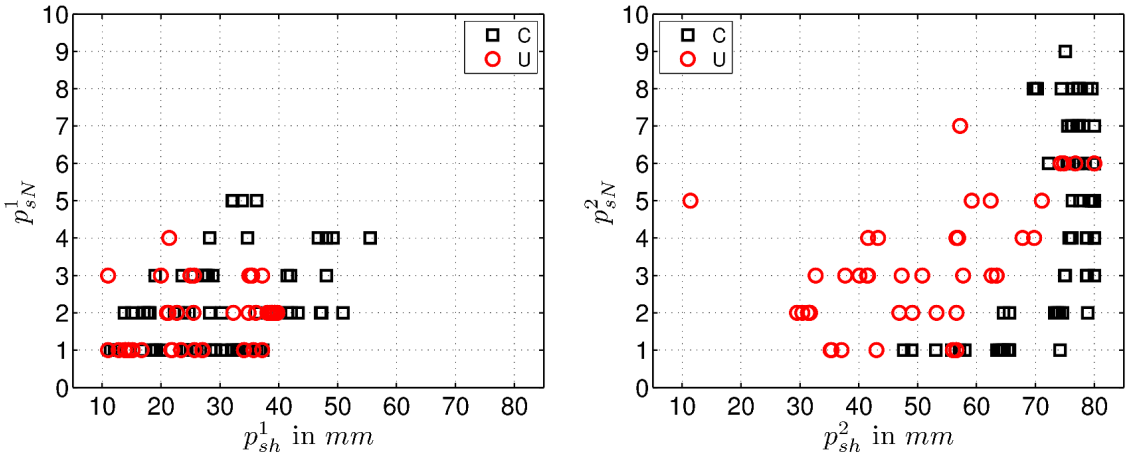

(a) for profile 1 (b) for profile 2

Figure 5.19.: Number and height of stringer

Differences in design can also be found for reinforcing elements. In figure 5.20 the diameter of reinforcing elements is shown over plate mass. For the first profile a maximum diameter of 3 mm is chosen in crisp optimization. For optimization with uncertainties this also holds for lightweight plates. For heavier plates with more than 15 kg reinforcing wires with higher diameter are selected. The second profile is analyzed in figure 5.20b. Crisp designs show a wide range of reinforcing diameters whereas big reinforcements are selected for lightweight designs in the presence of uncertainties.

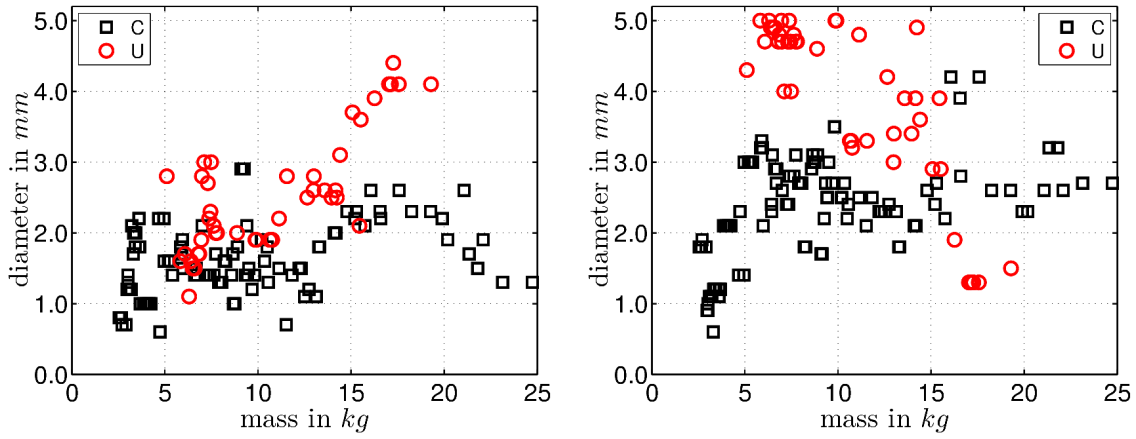

(a) profile 1 (b) profile 2

Figure 5.20.: Diameter of reinforcing elements over mass

5.3.6. Summary of TR10 plate optimization

This example is focused on design consequences from manufacturing aspects. The uncertainty based optimal designs have quite different design parameters but comparable structural properties. From investigation of different design parameters and their ratios design rules can be drawn. It is important to note, that these design rules were not introduced to the problem directly by FRBS but are results of the uncertainty based optimization procedure.

5.4. Summary of chapter

The methods presented in chapters 2 to 4 are successfully utilized for engineering optimization problems. Optimal designs computed by opTUM-II with respect to design parameter. Design rules described by ratios of different dimensional parameters change due to uncertainties. Also the distribution and dimension of reinforcing elements is influenced by manufacturing aspects.

6. Optimization of a sandwich beam for a satellite antenna model

Modern communication and earth observation satellites use large deployable antenna reflectors (LDRs) for receiving and sending signals. An antenna with parabolic surface shape is used. The shape of the antenna in orbit should not change due to dynamic or thermal loads.
A new concept called shell membrane antenna reflector technology (SMART) has been developed at Institute for Lightweight Structures - Technische Universität München (LLB) for several years now. It is based on the innovative carbon fiber reinforced silicone (CFRS) shell membrane technology. For details please refer to Datashvili et al. (2006). A challenging task in the development of LDRs is testing the surface accuracy on ground in 1 g conditions. Due to the lightweight character of deployable designs the earths gravity introduces high deformation of the reflecting surface and the backside structure which leads to disturbances typical for membranes such as buckling, waving and wrinkling. These highly nonlinear effects make simulation of the surface deflection in 1 g complicated and time consuming. An additional source of error are manufacturing uncertainties, especially for the backside structure. Even small forces introduced by deviations from the exact shape into the membrane can cause the effects already mentioned.
To verify the concept of CFRS a laboratory test model called Flexible Antenna Membrane Experiment (FLAME) with 1.6 m diameter and a focal length of f_P=1.2 m was built with a simplified umbrella like backside structure. Twelve sandwich beams following an exact parabola with given focal length are connected via an aluminum central unit. These beams have to be lightweight and stiff in order to maintain the parabolic shape also in 1 g conditions. To overcome gravity introduced surface errors the laboratory model was tested under 0 g conditions during the 8th Parabolic Flight Campaign of Deutsches Zentrum für Luft- und Raumfahrt - German Aerospace Center (DLR). Therefore the backside structure also has to withstand given loads during take-off and landing.
The reflector has two configurations leading to different orientation of the beams. The first one is the stored configuration shown in figure 6.1a, the second one deployed configuration in figure 6.1b

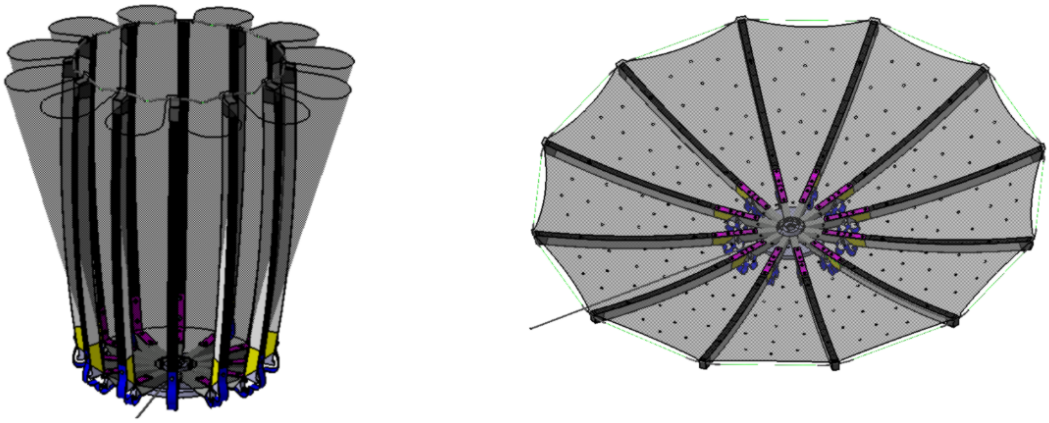

(a) stored (b) deployed

Figure 6.1.: FLAME configurations

In section 6.1 the design and manufacturing of the sandwich beams is described, load cases are addressed in 6.2. The modeling and the evaluation of the initial design follows in 6.3 and 6.4, respectively. Finally, the optimization task is defined in 6.5 and the results are discussed in 6.6.

6.1. Description of sandwich beam design

Twelve sandwich beams provide the two main features of FLAMEs backside structure. First the parabolic shape and second the deployment and folding kinematics. One complete beam assembly is shown in figure 6.2a. In this example only the outer part consisting of CFRP box, top and bottom face sheet, foam core and the interface to the deployment mechanism is of interest.
The top and bottom face sheet have two layers of unidirectional prepreg laminate each which gives a very high bending stiffness. The torsional stiffness is low which results in high deformations and rotation of the beam in case of loads in y_{beam} direction. The dimensions are given in figure 6.2b. The beam is built from a CFRP box made from T300 carbon fibers, a foam core and M40J face sheets. Detailed material characteristics can be found in appendix A.5.1. Unidirectional laminate layers are oriented in length direction of the sandwich beam with a nominal orientation angle of $\beta_i^{FST} = \beta_i^{FSB} = 0°$. Top an bottom face sheets have two layers each. The CFRP box is made from a fabric tube.

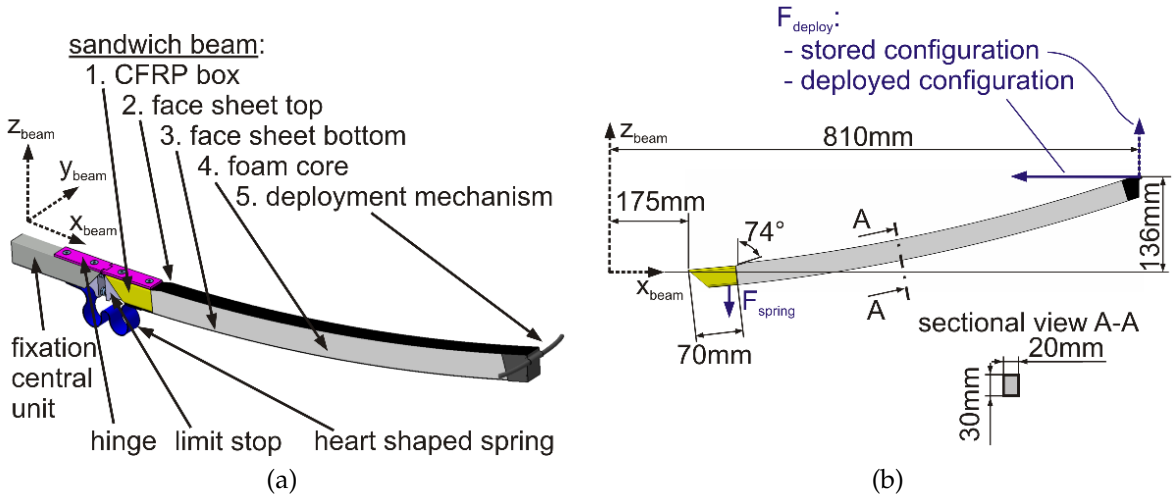

Figure 6.2.: FLAME sandwich beam description and dimensions

Forces on the beam are introduced by:

- reflecting surface:
  The reflecting surface of FLAME has a mass of m_{RS}=0.3 kg. It is attached to the twelve beams via thin layers of silicon by a given attachment area pattern.
- heart shaped spring:
  The spring provides the energy to deploy the beam and hold it in the deployed configuration. The spring characteristic is given in figure 6.3 for one spring and several test runs. The springs degrade at the beginning and provide a constant moment after 10 to 20 loading cycles. The force on the beam is computed with the distance from the hinge to the fixation point in z_{beam} direction. The run with the highest moment is used in this example.

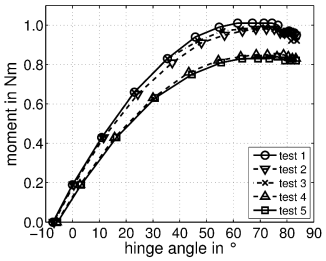

Figure 6.3.: Characteristic of heart shaped spring

- deployment mechanism:
  Two forces are introduced by the deployment mechanism in stored and deployed configuration. The first is needed to fold the reflector in the deployed configuration. To overcome the holding force of the limit stop, 12 N are necessary in negative x_{beam} direction at the right tip. This value was measured. The second force acts in the y_{beam} direction and is introduced by friction in the deployment mechanism. Also this force

is very small with approximated 1 N the resulting bending moment is significant. Additionally, a mass of 0.01 kg is added at the tip of the sandwich beam for the guiding tube and bonding measures.

6.2. Load cases

The requirements of FLAME's reflector are determined by laboratory testing, transport and parabolic flight. The mass of the reflecting surface m_{RS}=0.3 kg is distributed between the twelve beams together with the weight of each beam. The loads during the parabolic flight maneuver range from 0 g to 1.8 g according to Ceglia (2005). From the design requirements provided by NOVESPACE in Novespace (1999) test equipment has to withstand loads up to 9 g in different directions also for the failure of certain structural parts.

6.2.1. FLAME - load case 1

In order to evaluate the root mean square error (RMS) with respect to the given exact parabola a 1 g acceleration in z_{beam} direction is applied. The mass of the reflecting surface m_{RS} is distributed to twelve beams. The loads are summarized in appendix A.5.2 in table A.2. The root mean square error (RMS) value is computed according to Lang (2009).

6.2.2. FLAME - load case 2

The twelve beams are oriented at different angles with respect to the coordinate system of the aircraft. The relevant acceleration loads are listed in table 6.1. For the deployed configuration six load cases for all beam orientations are merged to just one by assuming that the highest possible acceleration in x_{beam} and y_{beam} direction occur simultaneously. High forces from the deployment mechanism F_{deploy} act at the tip and the spring force F_{spring} is active. The mass of the reflecting surface m_{RS} is distributed only to two beams assuming a partial failure of the backside structure. The loads are summarized in table A.3. The maximum and minimum strain in the face sheets is the limiting factor in this load case.

Table 6.1.: Design loads in ZERO-G coordinates, Novespace (1999)

axis	direction	acceleration	unit
X_{ZERO-G}	+	9.0	g
	-	1.5	g
Y_{ZERO-G}	+	3.0	g
	-	3.0	g
Z_{ZERO-G}	+	4.2	g
	-	7.3	g

6.2.3. FLAME - load case 3

The stored configuration is basically subjected to the same accelerations with changed coordinates. F_{deploy} in z_{beam} direction is very small in the stored configuration, see also figure 6.2b. The spring moment M_{spring} is very high in this configuration and so is the resulting F_{spring}. The loads are summarized in table A.4. The maximum and minimum strain in the face sheets is the limiting factor in this load case.

6.3. Design parameters and performance measure

In this section a short overview of the parameters including uncertain ones and their modeling and performance measures are given in more detail.

6.3.1. Design parameters and uncertain parameters

The most important design parameters of the sandwich beam are the dimensions of the cross section B and H, the number and fiber angle of layer i in each face sheet (β_i^{FSB}, β_i^{FST}) and the slope angle of the top face sheet for the hinge γ^{FST}. Uncertainties in the loads origin from the spring force, the forces from the deployment mechanism, acceleration loads and the distribution of the reflecting surface loads. Uncertainties in material properties are not considered in this example.
Fuzzy numbers for those parameters are derived from expert knowledge. The resulting FOU for twelve fuzzy numbers used in opTUM-II for uncertainty modeling are shown in figure 6.4 on page 101 and in figure 6.5 on page 102. A short explanation for the chosen shape of the inputs is given in the following:

- H and B: The height (figure 6.4a) and width (figure 6.4b) of the beam depends on the manufacturing accuracy of the foam core. Milling and cutting operations have to be considered. For curing the top face sheet is pressed against a mold via pressure applied to the bottom face sheet. This adds additional uncertainties to the beam height H.

- β_i^{FSB} and β_i^{FST}: The fiber angles (figure 6.4c) can vary due to prepreg, cutting and lay up tolerances. The single layers are independent from each other.

- γ^{FST}: This angle (figure 6.4d) is crucial for structural failure of the sandwich beam. Direction of loads change in the top face sheet resulting in stress concentrations. γ^{FST} was changed several times during development and is accurate once it is set in the mold within tight boundaries. Nevertheless an influence analysis is interesting from point of structural performance.

- M_{spring}: The properties of the spring are highly uncertain due to manual lay up. In the deployed configuration shown in figure 6.4e a minimum moment has to be provided resulting in a non symmetrical fuzzy number. In the stored configuration in figure 6.4f similar influences hold with symmetrical uncertainties.

- F_{deploy}: In the deployed configuration displayed in figure 6.5a the force necessary for folding is highly uncertain due to friction effects in the deployment mechanism. In the stored configuration in figure 6.5b a minimum force has to be provided. The vector of F_{deploy} in y_{beam} direction in figure 6.5c is based on the same assumptions.
- a_x and a_z: The given acceleration loads in figure 6.5d and 6.5e are the minimum value. An uncertainty of up to 2 g is assumed for both.
- m_{RS} division factor: Depending on the structural damage to the twelve sandwich beams during an emergency, only one beam may have to support the reflecting surface. The wide FOU represents the missing knowledge about the failure state of the reflector.

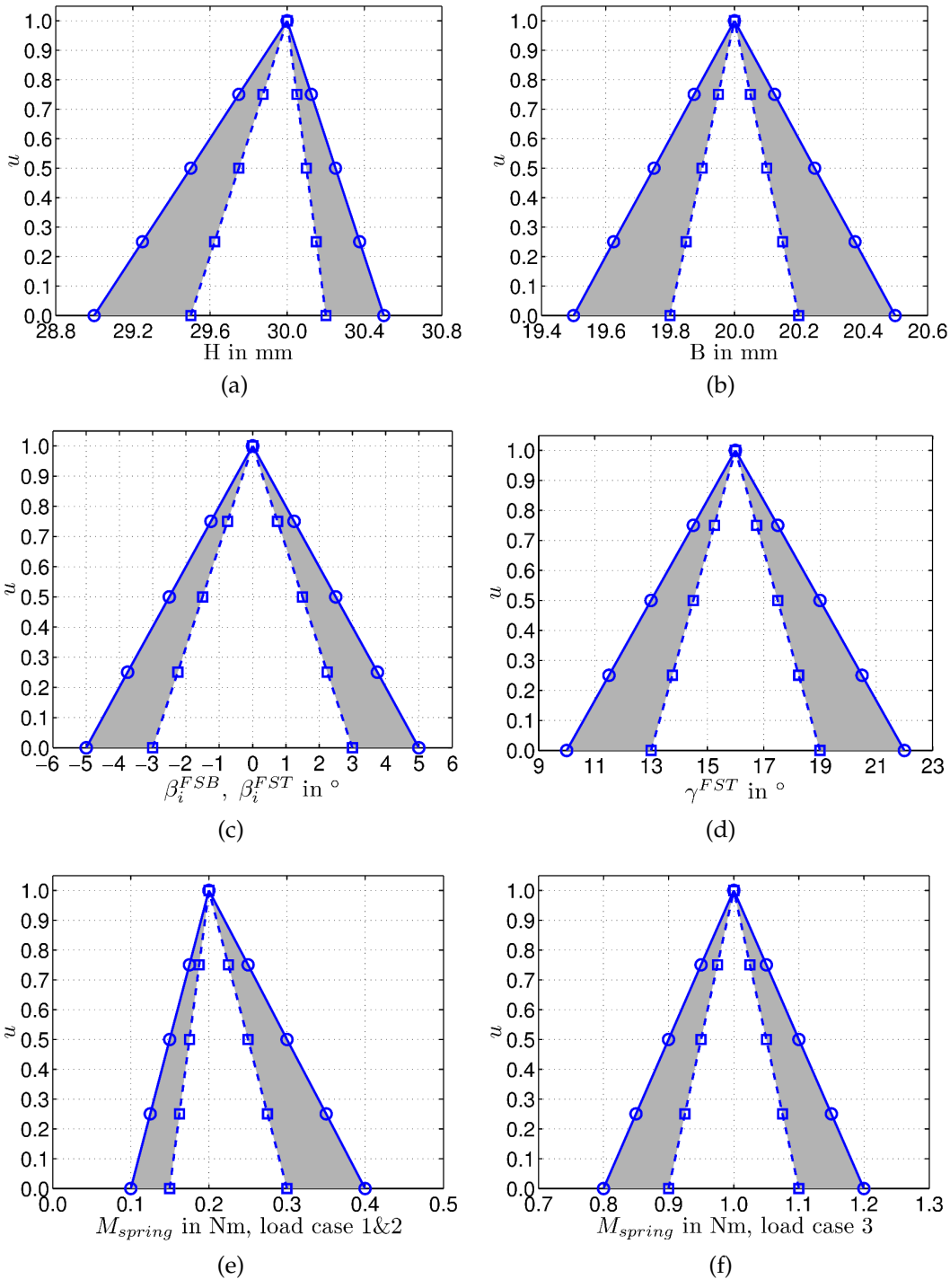

Figure 6.4.: Uncertain input parameters - 1

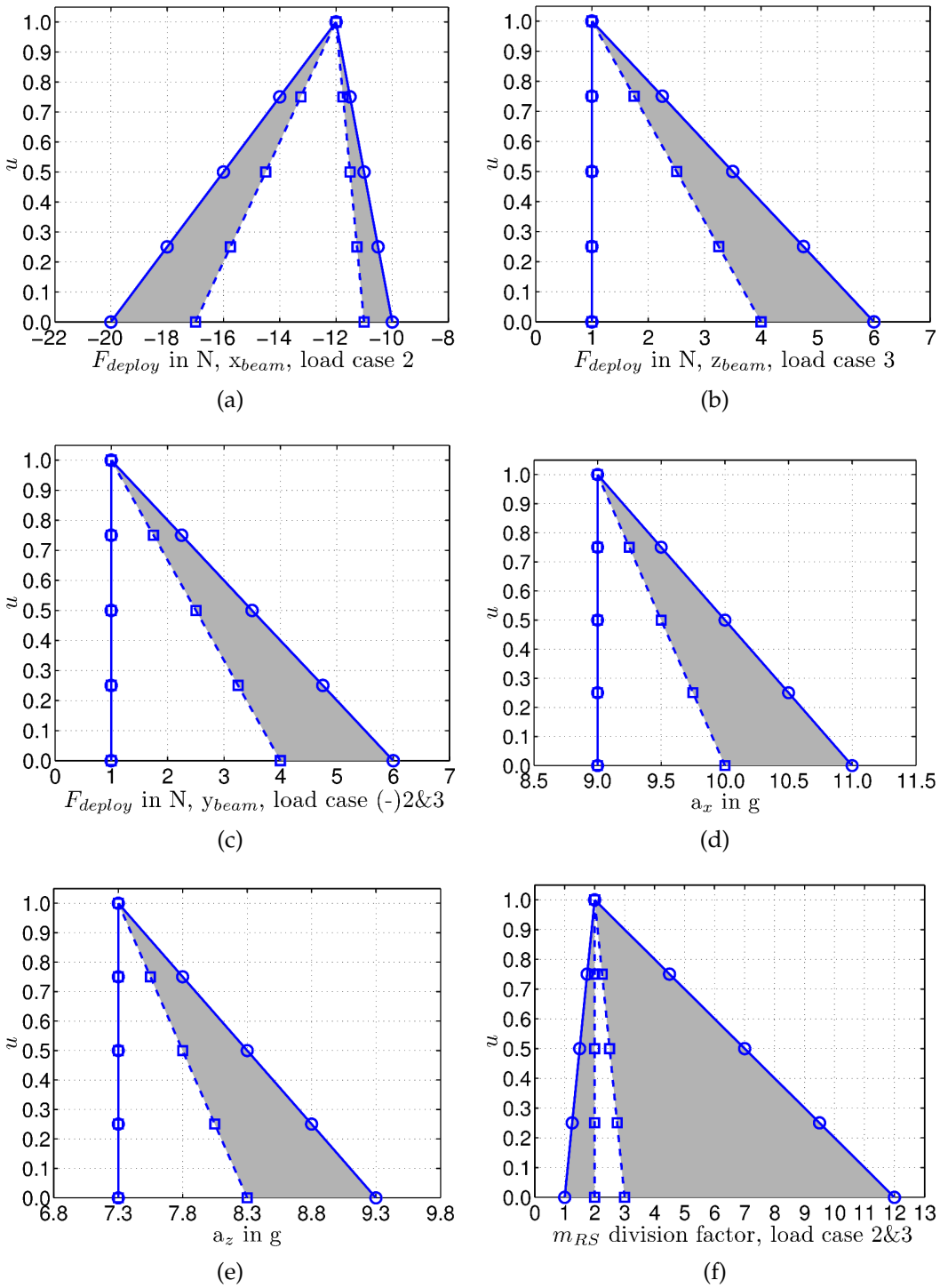

Figure 6.5.: Uncertain input parameters - 2

6.3.2. Performance measures

The evaluation of FLAME focuses on the structural performance. The following measures will be used to characterize the design.

- mass of beam m_B: The mass of the sandwich beam should be as low as possible.
- root mean square error (RMS): The surface accuracy of the beam under 1 g conditions is assessed. The RMS is computed according to Lang (2009) with the difference from the reference surface u and N nodes in the finite element mesh.

$$RMS = \sqrt{\sum_{i=1}^{N} w_i * u_i^2} \tag{6.1a}$$

$$w_i = \frac{A_i}{\sum_{i=1}^{N} A_i} \tag{6.1b}$$

  RMS should be as small as possible in order to assure good measuring results under laboratory conditions.
- inverse of Tsai-Wu strength ratio index failure criterion (iTWFC): Failure criterion for anisotropic composites provided in ANSYS®. iTWFC is evaluated for top and bottom face sheet for load cases 2 and 3 leading to four performance measures iTWFC_2^{FSB}, iTWFC_3^{FSB}, iTWFC_2^{FST} and iTWFC_3^{FST}. The foam core and the CFRP box are not considered in this example. The box is intentionally overdimensioned and a local failure of the core does not pose problems as long as the face sheets are intact in load case 2 and 3.
- deformation **u**: The deformation at the beam tip is a measure for nonlinearity of the model under load. As mass and stiffness are conflicting objectives the minimum mass design has also a very low stiffness for which nonlinear deformations can be critical. Six performance measures are computed for loadcase 2 and 3: u_2^x, u_2^y, u_2^z, u_3^x, u_3^y, u_3^z.

6.4. Evaluation of initial design

The initial design with H=30 mm, B=20 mm, β_i^{FSB}=β_i^{FST}=0 and γ^{FST}=16 is evaluated and the results are listed in table 6.2. The bottom face sheet is not critical and the failure criteria are nearly the same for load case 2 and 3. The top face sheet has a much higher but still feasible failure criteria which differs approximately 22% between load case 2 and 3.

Table 6.2.: Performance measures for initial design

m_B	RMS	iTWFC_2^{FSB}	iTWFC_3^{FSB}	iTWFC_2^{FST}	iTWFC_3^{FST}
0.0620 kg	0.116 mm	0.155	0.154	0.567	0.483
u_2^x	u_2^y	u_2^z	u_3^x	u_3^y	u_3^z
0.13 mm	-11.97 mm	-1.32 mm	0.53 mm	11.73 mm	-3.16 mm

Consequences for optimization. Several changes to the problem result from the evaluation of the initial design. One of the most important is to assign just one fiber angle to the top and bottom face sheet. The second layer will have the symmetrical value, for example $\beta_i^{FST} = [+3, -3]\,;\ i = 1, 2$. Also γ^{FST} will be fixed to its lower bound of 10° which was actually used in the manufactured reflector. This design has initial RMS=0.095 mm and reduces the number of design variables to four.
One of the most important changes is the uncertainty for m_{RS} division factor. The large FOU would lead to very wide fuzzy system answers. The boundaries are therefore changed to a minimum of 1.5 (instead of 1.0) and the maximum value to 4.0 (instead of 12.0).
Crisp optimization runs are performed for different safety factor settings and single and multiple objectives. Also nominal and maximum values are used for uncertain parameters to gain optimal design for both conditions. For optimization runs based on opTUM-II different evaluation methods for fuzzy numbers will be tested. The optima of crisp and uncertain runs are compared with each other.

6.5. Definition of optimization task

The most important property of lightweight structures is, of course, the mass. Minimization of mass is necessary for performance enhancement and even feasibility of the design. The first goal in this example is the mass of a single beam m_B. With decreasing mass the performance measure for shape accuracy RMS will increase due to lower stiffness of the beam. This leads to the second goal of simultaneous minimization of RMS. These two goals are conflicting and have to be handled via multiobjective optimization approaches. A typical Pareto-front is generated representing optimal compromises between m_B and RMS. The design variables are H, B, β_i^{FSB}, and β_i^{FST}. Especially H will influence RMS. The load cases are the same as for the initial design.
The design is limited by maximum allowed deformation and maximum allowed failure criteria. The first has to be limited in order to prevent catastrophic collision between parts of the reflectors structure. The latter guarantees that no structural failure occur which would lead to fragmentation of the sandwich beam. iTWFC is also subjected to different safety factors in several optimization runs in order to show the influence on the optimal designs.
The mathematical definition of the crisp optimization task is given in equation 6.2 on page 105. The allowed values and safety factors are listed in table 6.3 for three different optimization runs.

Table 6.3.: Crisp constraint limits for different problem formulations

optimization problem	limit for		value	unit	safety factor γ
C1	deformation	u_i^{all}	30.0	mm	1.0
	failure criteria	$iTWFC_i^{all}$	1.0	-	1.0
C2	deformation	u_i^{all}	30.0	mm	1.0
	failure criteria	$iTWFC_i^{all}$	1.0	-	1.5
C3	deformation	u_i^{all}	30.0	mm	1.0
	failure criteria	$iTWFC_i^{all}$	1.0	-	2.0

$$
\begin{aligned}
min \quad & \mathbf{f}(\mathbf{x}) &&= [m_B, RMS] \\
with: \quad & \mathbf{x} &&= [H, B, \beta^{FSB}, \beta^{FST}] \\
subject\ to: \quad & g_1(\mathbf{x}) &&= abs\,(u_2^y) \,/\, (u_2^{all}/\gamma_1^g) - 1 \leq 0 \\
& g_2(\mathbf{x}) &&= abs\,(u_3^y) \,/\, (u_3^{all}/\gamma_2^g) - 1 \leq 0 \\
& g_3(\mathbf{x}) &&= abs\,(iTWFC_2^{FST}) \,/\, (iTWFC_2^{all}/\gamma_3^g) - 1 \leq 0 \\
& g_4(\mathbf{x}) &&= abs\,(iTWFC_3^{FST}) \,/\, (iTWFC_3^{all}/\gamma_4^g) - 1 \leq 0 \\
& g_5(\mathbf{x}) &&= abs\,(iTWFC_2^{FSB}) \,/\, (iTWFC_2^{all}/\gamma_5^g) - 1 \leq 0 \\
& g_6(\mathbf{x}) &&= abs\,(iTWFC_3^{FSB}) \,/\, (iTWFC_3^{all}/\gamma_6^g) - 1 \leq 0 \\
and: \quad & 20\ mm \leq H \leq 50\ mm \\
& 10\ mm \leq B \leq 50\ mm \\
& 0° \leq \beta^{FSB} \leq 90° \\
& 0° \leq \beta^{FST} \leq 90°
\end{aligned}
\tag{6.2}
$$

For optimization with uncertainties the mathematical formulation of the problem changes to the one given in equation 6.3 on page 106. The design variable vector changes to its uncertain equivalent $\tilde{\mathbf{x}}$ and additional uncertain parameters $\tilde{\mathbf{p}}$ are added to the problem formulation. The defuzzification of fuzzy system answers $\tilde{\mathbf{r}}$ is done by CoA and similar results as for crisp optimization are expected. This optimization will be referred to as U1.
The allowed value for constraints $g_1(\tilde{\mathbf{x}}, \tilde{\mathbf{p}})$ and $g_2(\tilde{\mathbf{x}}, \tilde{\mathbf{p}})$ is shown in figure 6.6a, for constraints $g_3(\tilde{\mathbf{x}}, \tilde{\mathbf{p}})$ to $g_6(\tilde{\mathbf{x}}, \tilde{\mathbf{p}})$ in figure 6.6b.

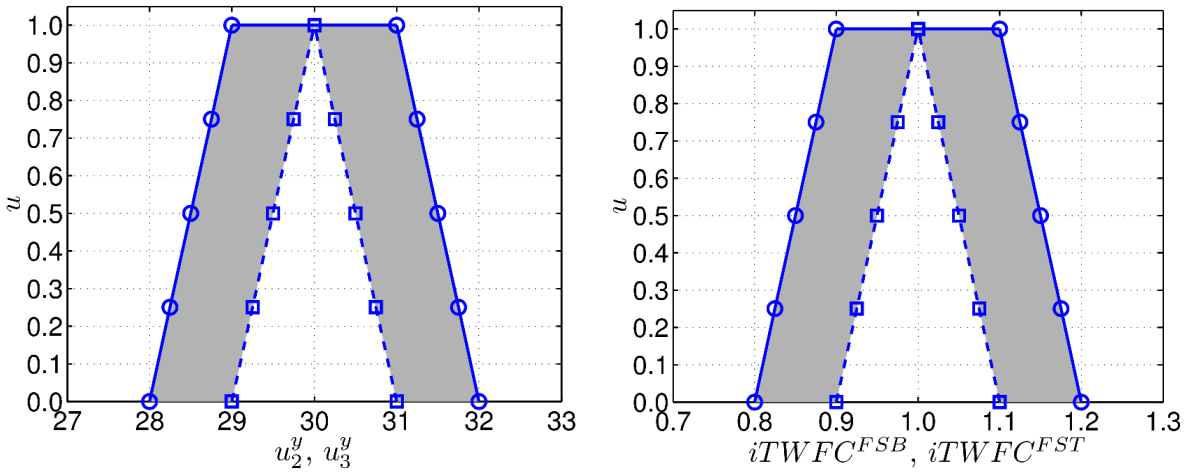

(a) for deformation (b) for failure criteria

Figure 6.6.: Uncertain constraint boundaries

$$
\begin{aligned}
min \quad & \mathbf{f}(\tilde{\mathbf{x}}, \tilde{\mathbf{p}}) &&= [m_B, RMS] && , for\ CoA \\
with: \quad & \tilde{\mathbf{x}} &&= [H, B, \beta^{FSB}, \beta^{FST}] && \\
& \tilde{\mathbf{p}} &&= \left[M_{\text{spring}}, F_{\text{deploy}}, a_{\text{x}}, a_{\text{y}}, a_{\text{z}}, m_{RS}\ \text{div. fact.}\right] && \\
subject\ to: \quad & g_1(\tilde{\mathbf{x}}, \tilde{\mathbf{p}}) &&= abs\left(u_2^y\right) / \left(u_2^{all} / \gamma_1^g\right) - 1 \leq 0 && , for\ CoA \\
& g_2(\tilde{\mathbf{x}}, \tilde{\mathbf{p}}) &&= abs\left(u_3^y\right) / \left(u_3^{all} / \gamma_2^g\right) - 1 \leq 0 && , for\ CoA \\
& g_3(\tilde{\mathbf{x}}, \tilde{\mathbf{p}}) &&= abs\left(iTWFC_2^{FST}\right) / \left(iTWFC_2^{all} / \gamma_3^g\right) - 1 \leq 0 && , for\ CoA \\
& g_4(\tilde{\mathbf{x}}, \tilde{\mathbf{p}}) &&= abs\left(iTWFC_3^{FST}\right) / \left(iTWFC_3^{all} / \gamma_4^g\right) - 1 \leq 0 && , for\ CoA \\
& g_5(\tilde{\mathbf{x}}, \tilde{\mathbf{p}}) &&= abs\left(iTWFC_2^{FSB}\right) / \left(iTWFC_2^{all} / \gamma_5^g\right) - 1 \leq 0 && , for\ CoA \\
& g_6(\tilde{\mathbf{x}}, \tilde{\mathbf{p}}) &&= abs\left(iTWFC_3^{FSB}\right) / \left(iTWFC_3^{all} / \gamma_6^g\right) - 1 \leq 0 && , for\ CoA \\
and: \quad & 20\ mm \leq H \leq 50\ mm && && \\
& 10\ mm \leq B \leq 50\ mm && && \\
& 0° \leq \beta^{FSB} \leq 90° && && \\
& 0° \leq \beta^{FST} \leq 90° && &&
\end{aligned}
\tag{6.3}
$$

To take advantage of additional information generated by uncertainty evaluation with opTUM-II the problem formulation is changed. In equation 6.4 only side constraints are included. The third goals is support S^u_{RMS} of fuzzy response for RMS. From an engineering point of view this reduces changes of RMS due to manufacturing tolerances. The fourth goal represents CWR constraint evaluation described in section 4.2.4 and 4.3.2. The sum for all six constraints g_i in equation 6.3 is computed. The optimization of this goal leads to feasible designs with minimal constraint violation. This is in conflict mainly with mass and RMS goals and allows a trade-off between optimal structural performance and constraint violation. The results of this problem formulation will be referred to as U2.

$$
\begin{aligned}
min \quad & \mathbf{f}(\tilde{\mathbf{x}}, \tilde{\mathbf{p}}) &&= \left[m_B, RMS, S^u_{RMS}, \sum_{i=1}^{6} CWR\,|_{uu} \right] && , for\ CoA \\
with: \quad & \tilde{\mathbf{x}} &&= [H, B, \beta^{FSB}, \beta^{FST}] \\
& \tilde{\mathbf{p}} &&= [M_{\text{spring}}, F_{\text{deploy}}, a_{\text{x}}, a_{\text{y}}, a_{\text{z}}, m_{RS} \text{ div. fact.}] \\
and: \quad & 20\ mm \leq H \leq 50\ mm \\
& 10\ mm \leq B \leq 50\ mm \\
& 0° \leq \beta^{FSB} \leq 90° \\
& 0° \leq \beta^{FST} \leq 90°
\end{aligned}
\tag{6.4}
$$

The settings for the genetic algorithm GAME are given in table 6.4. Due to higher computational effort for opTUM-II evaluation fewer individuals are computed for runs with uncertain design variables and system parameters. High crossover and mutation probabilities are chosen for children generation.

Table 6.4.: Parameter settings for optimization algorithm GAME

GAME parameter	crisp runs C1, C2, C3	fuzzy runs U1, U2[1]
number of generations	30	30
population size	50	20
number of children	100	40
number of elite	0	0
crossover probability in %	50	50
mutation probability in %	80	80
initial standard deviation of mutation in %	20	20
number designs for surrogate	-	50

[1] initial population from all individuals of U1

The smaller amount of evaluated designs in fuzzy optimization runs does not influence convergence. Means for mass and RMS goals are highly improved in the first 10 generations. Afterward only small improvements can be seen in the mean values. The comparison of results is focused on the result space defined by m_B and RMS. Results from four goal optimization are projected into this plane.

6.6. Discussion of optimization results for FLAME

The discussion of results is focused on two main topics. First, designs are evaluated with respect to goals and for optimization with uncertainties with respect to parameters of fuzzy system answers. The classic trade-off between mass and stiffness is shown in figure 6.7 in goal space. The ideal design could be found in lower left corner of the diagrams where the arrow is pointing. Designs which lie beneath the corresponding Pareto-front are infeasible. In general, lower mass of the sandwich beam can be achieved only by non-linearly increasing RMS. The initial design marked with a five-pointed star can be improved with respect to mass and RMS. For higher safety factors the Pareto-front is shifted nearly in parallel in the direction of the upper right corner. With a safety factor of $\gamma = 2$ for C3 improvements are still achievable with respect to the initial design. In figure 6.7a results for optimization runs with uncertainties U1 are shown together with S^u_{mass} and in figure 6.7b together with S^u_{RMS} for selected designs. Variation in mass due to manufacturing tolerances are nearly constant for all Pareto-optimal solutions. Variation in RMS in the right hand diagram increases with lower mass.

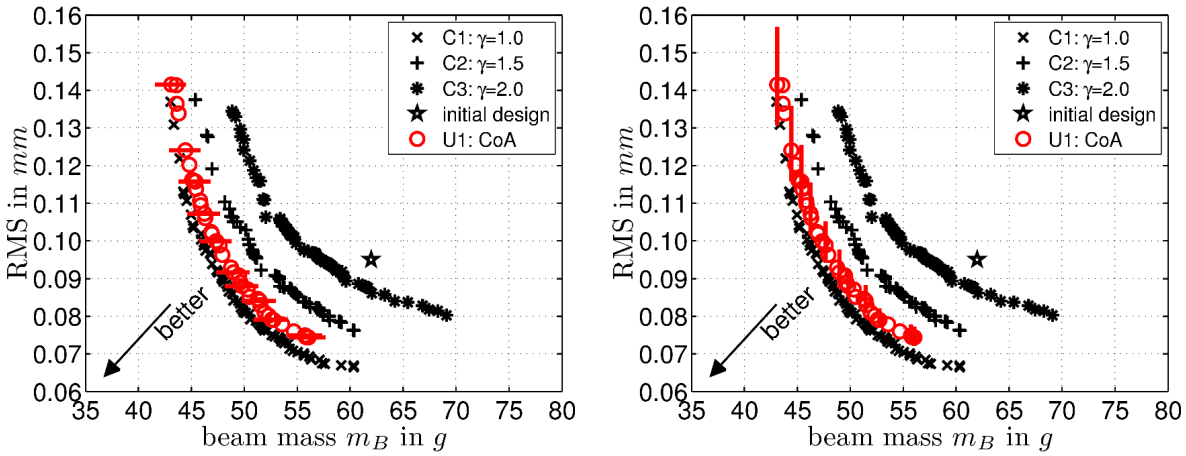

(a) Pareto-front with uncertainty for mass

(b) Pareto-front with uncertainty for RMS

Figure 6.7.: Pareto-front for crisp and fuzzy optimization

Design variables for minimum mass and minimum RMS designs are listed in table 6.5. For minimum mass designs higher safety factors for runs C2 and C3 are satisfied via higher width B of the sandwich beam. Height H is at its lower boundary of 20 mm. The minimum mass design with uncertainties for run U1 is very similar to the crisp design from run C1. For minimal RMS high H are chosen by the optimizer. For run C1 the upper boundary of 50 mm is almost reached. Again higher safety factors are satisfied by higher width B. Contrary to minimum mass design the optimal design with uncertainties for run U1 is quite

different in height H compared to the optimal C1 design.

Table 6.5.: Optimal designs for FLAME

minimal goal	optimization run	mass g	RMS mm	H mm	B mm	β_i^{FSB} °	β_i^{FST} °
mass	C1	43.06	0.137	20.25	14.35	1.01	0.00
	C2	45.36	0.138	20.00	15.64	7.23	0.53
	C3	48.85	0.134	20.00	17.45	0.00	2.48
	U1	43.12	0.142	20.00	14.52	0.00	0.00
RMS	C1	60.35	0.066	49.42	13.99	5.13	0.00
	C2	60.38	0.076	38.94	16.47	0.00	1.60
	C3	69.09	0.080	41.66	19.21	0.00	0.00
	U1	56.05	0.074	39.63	14.56	0.04	2.42

The interpretation of fiber angles β_i^{FSB} and β_i^{FST} is not obvious from the results in table 6.5. Therefore, the mean values for all Pareto-optimal solutions are evaluated and listed in table 6.6. Designs are further distinguished with respect to mean mass of optimal design solutions. Mean fiber angle values are given for heavy ($m_i \geq \bar{m}_{sol}$) and light ($m_i < \bar{m}_{sol}$) designs, respectively. No obvious order can be seen for β_i^{FSB}, but for β_i^{FST} higher safety factors are satisfied by higher fiber angles especially for designs with small mass for C1, C2 and C3. Optimal designs for U1 are not necessarily in between results for C1 and C2.

Table 6.6.: Optimal mean fiber angles for FLAME

	designs $m_i < \bar{m}_{sol}$		designs $m_i \geq \bar{m}_{sol}$	
optimization run	mean $\bar{\beta}_{FSB}$ in °	mean $\bar{\beta}_{FST}$ in °	mean $\bar{\beta}_{FSB}$ in °	mean $\bar{\beta}_{FST}$ in °
C1	2.27	0.62	1.26	0.52
C2	2.53	1.44	0.67	0.54
C3	0.75	2.14	1.03	1.46
U1	1.89	0.90	0.80	1.33

Now fuzzy properties for optimal solutions of optimization run U1 are evaluated. In figure 6.8 different properties of fuzzy system answers $\tilde{\tilde{r}}_{RMS}$ are shown over mass and RMS. First is support S^u_{RMS}. From figure 6.8a and 6.8b it can be seen that S^u_{RMS} increases with smaller mass and high RMS. Whereas the correlation is nearly linear for RMS it is non-linear for mass. In addition to U1 results minimum mass and minimum RMS results for C1-C3 are evaluated with opTUM-II and shown also. Those designs are mostly to the right of optimal designs from the U1 run in figure 6.8a. In figure 6.8b designs from crisp runs are in good accordance with fuzzy ones except the initial design. The latter is fully in feasible design space in an area with favorable properties of fuzzy responses.
Skewness measures are displayed in figure 6.8c and 6.8d. A similar behavior as for S^u_{RMS} can be observed. This holds also for designs from crisp runs.

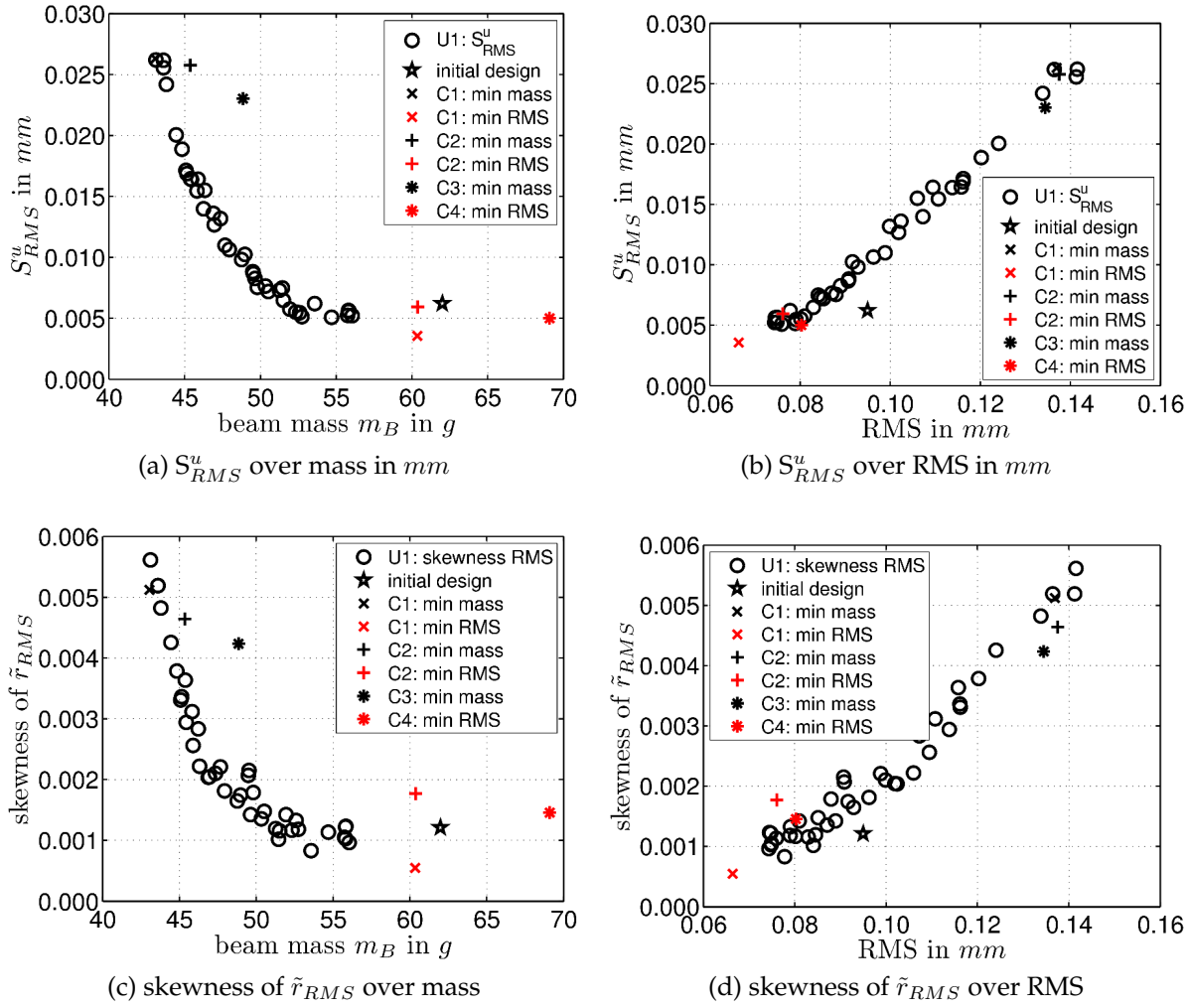

(a) S^u_{RMS} over mass in mm

(b) S^u_{RMS} over RMS in mm

(c) skewness of $\tilde{r}_{RMS}$ over mass

(d) skewness of $\tilde{r}_{RMS}$ over RMS

Figure 6.8.: Selected properties of fuzzy system answers

The results from run U2 were not discussed till now. For better comparison optimal designs are shown in figure 6.9 in two dimensional design space for mass and RMS. The size of the markers for single designs of U2 in figure 6.9a reflects the third goal S^u_{RMS}. The bigger the marker the higher S^u_{RMS}. The fourth goal $\sum CWR\,|_{uu}$ is coded by the color of the marker. The brighter the marker face, the bigger $\sum CWR\,|_{uu}$. Dark and very dark markers lie within crisp feasible design space (for $\gamma = 1$).
From figure 6.9a designs with better goals than designs from the crisp run C1 can be chosen with respect to uncertainty in the second goal S^u_{RMS} and constraint violation. For beam mass $m_B \in [44, 60]\ g$ improvements for goals mass and RMS can be achieved with low constraint violation. For beams with $m_B < 44\ g$ such improvements lead to much higher constraint violation. Also the increasing uncertainty in S^u_{RMS} for lightweight beams is confirmed by these results. It is interesting to note that S^u_{RMS} increases also for very low RMS. This can be seen from slightly bigger markers in figure 6.9a for RMS$\approx 0.07\ mm$.
In figure 6.9b the contours of an approximation for the fourth goal $\sum CWR\,|_{uu}$ are given. The Pareto-fronts of crisp runs C1, C2 and C3 nearly lie on top of contours for $\sum CWR\,|_{uu}$= $[4, 3, 2]$. This allows the engineer to do a trade-off between constraint violation and goal enhancement. For example a decrease in mass of $\approx 5\%$ from 47.5 g to 45 g for RMS=0.09 mm needs the same increase in constraint violation as a decrease of RMS from 0.09 mm to

0.08 mm for m_B = 47.5 g. The latter is an enhancement of 11%.

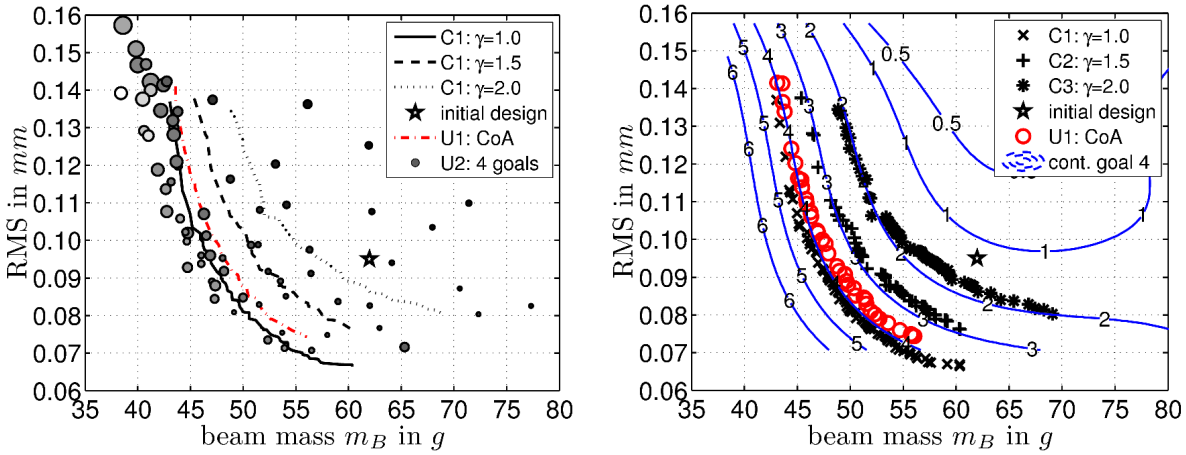

(a) optimal designs for four goals

(b) contour of fourth goal

Figure 6.9.: Pareto-front for crisp and fuzzy optimization with results for four goals

In optimization run U2 S^u_{RMS} is also optimized. A comparison for selected optimal designs from U2 with U1 solutions is shown in figure 6.10. Designs are chosen so that $\sum CWR\,|_{uu} \in [3.6, 4.4]$ is still reasonable and masses are similar to U1 results. In figure 6.10a S^u_{RMS} is plotted over mass. Pareto-optimal designs from U1 are black circles, selected optimal designs from U2 are blue squares. Designs from U1 with similar mass to a U2 design are displayed with filled markers.
With the same mass much smaller S^u_{RMS} can be achieved compared to Pareto-optimal designs from U1. The most important change in design variables are a bigger height H and smaller width B for U2 designs. H is ≈1.7 to 4.5 mm bigger, B ≈0.7 to 1.3 mm smaller. Changes of S^u_{RMS} due to manufacturing tolerances are smaller if H is bigger.
In figure 6.10b S^u_{RMS} is shown over RMS. For the chosen designs of U2 with restricted constraint violations and maximum mass no improvement of S^u_{RMS} is possible for a given RMS.

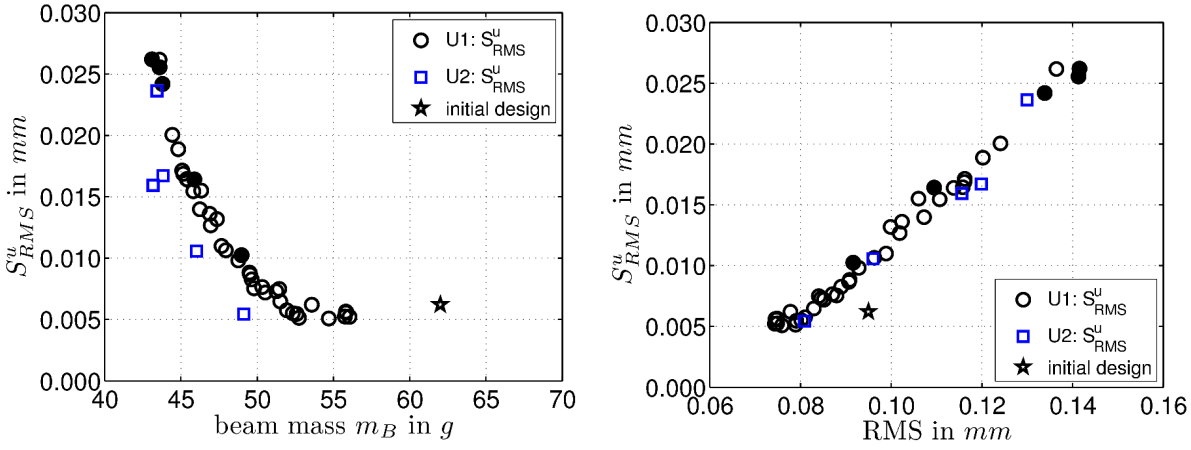

(a) S^u_{RMS} over mass in mm

(b) S^u_{RMS} over RMS in mm

Figure 6.10.: Selected properties of fuzzy system answers for optimization runs U1 and U2

Finally, five designs are evaluated in order to make a design decision. The picked designs are highlighted in figure 6.11. Design number 1 has minimum mass of 47.04 g and lies slightly left of the Pareto-front for C1. Designs 2 and 3 are nearly exactly on Pareto-front for C2. Design 4 is situated in between Pareto-fronts for C2 and C3. Finally design 5 has a lower RMS.

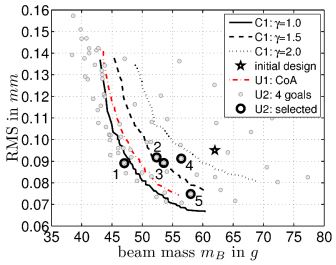

Figure 6.11.: Selected designs for detailed evaluation

Design variables and goals are listed in table 6.7. Mass increases from design 1 to 5. RMS for design 1 to 4 is ≈ 0.090 mm. Design 5 has a much smaller RMS of 0.075 mm. Also S^u_{RMS} is lowest for design 5. The constraint violation is summarized in $\sum CWR\,|_{uu}$. Design 1 and 3 have the highest values followed by design 5, 2 and 4. The initial design has even lower $\sum CWR\,|_{uu}$. The main difference between initial design and the chosen ones is the width B. Only height of design 5 differs considerably from 30 mm.

Table 6.7.: Properties of selected designs from optimization run U2

design	H mm	B mm	β_i^{FSB} °	β_i^{FST} °	mass g	RMS mm	S^u_{RMS} mm	$\sum CWR\,\|_{uu}$ –
1	30.86	12.99	0.00	2.96	47.04	0.089	0.010	4.60
2	29.63	15.77	0.00	1.56	52.37	0.092	0.008	2.39
3	31.45	15.75	12.67	0.00	53.56	0.089	0.009	3.17
4	30.41	17.38	0.97	0.00	56.45	0.091	0.008	1.88
5	39.88	15.28	0.00	0.00	57.99	0.075	0.004	2.70
initial	30.00	20.00	0.00	0.00	62.00	0.095	0.006	1.32

In order to compare the properties of goals a radar chart for designs 1 to 5 and the initial design is given in figure 6.12. The initial design has favorable properties for fuzzy number of RMS. Design 1 has the most unfavorable properties as can be seen from its high values for axes 4 to 7. Designs 2 to 4 lie in the medium range for fuzzy properties. Design 5 shows most favorable properties for $\tilde{\tilde{r}}_{RMS}$. They are near the center of the radar chart. It has a high value only for nonlinearity which is comparable to the initial design.

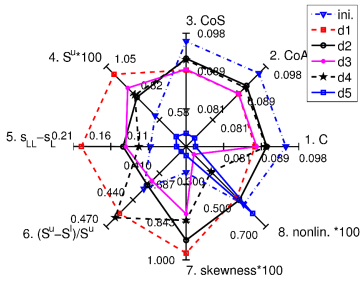

Figure 6.12.: Radar chart for selected designs

From these results a twofold design decision can be made. If uncertainties can not be reduced by quality measures during manufacturing and more precise load estimates, design 4 offers the most promising properties. It stays within the feasible design space for nearly all constraints and constraint violations are very small on the lowest α-cut level. Design 4 has 9% smaller mass and 4% smaller RMS compared to the initial design.
If uncertainties can be reduced to levels at α-cut level $\alpha = 0.5$ design 5 is most promising. Mass is 8% and RMS 21% lower compared to the initial design. Additionally possible changes in RMS due to manufacturing uncertainties are 33% smaller.

6.7. Summary of sandwich beam optimization

In this example the sandwich beam of a laboratory test model for a deployable satellite antenna is optimized. Classic conflicting goals for mass and stiffness are evaluated. Uncertainties arising from manufacturing and loads are handled with opTUM-II. Deterministic optimization for different levels of safety factors provide Pareto-fronts for trade-off leading to lighter and more accurate designs than the initial one. Optimization under uncertainties shows high variations for designs with very small mass. Taking into account constraint handling with a summarized fuzzy approach, optimal designs are found which allow trade-offs for designs which can only be found by several crisp optimizations with different safety factors. The computational effort for uncertainty handling is ≈ 8.3 times higher. This number has to be rated carefully. The most important points are listed in the following.

- Fourteen uncertain parameters have to be considered via approximation models.
- Computations can be parallelized easily.
- No advanced scheme for sample exchange between parallelized design evaluations is utilized.
- Information gained is much greater than by gradient evaluation.

Finally, two designs are chosen for further investigation and development. Those two designs are 9% and 8% lighter with 4% and 21% lower RMS, respectively.

7. Conclusion and outlook

In this thesis a new approach for the integration of qualitative manufacturing knowledge into structural optimization is developed. The main goal was to include qualitative expert knowledge in a multidisciplinary problem formulation. Two main methods of fuzzy logic are the basis of the approach. First, type-2 fuzzy rule-based system are used to generate knowledge-based models from qualitative expert knowledge. Second, system answers for uncertain - fuzzy - input parameters of numerical models are computed by α-cut level optimization. The latter is extended in this thesis for the use with type-2 fuzzy set in the the algorithm for optimization with type-2 fuzzy uncertainties (opTUM-II). This algorithm takes advantage of response surface approximation together with optimization algorithms in order to generate fuzzy system responses.
System answers with uncertainties described by fuzzy numbers have to be transformed in order to be used together with optimization algorithms. Different methods have been evaluated for goal and constraint evaluation. From an analytical example, center of area for type-2 fuzzy sets is identified as the method of choice for goal evaluation. For constraints Chen-Wang ranking for fuzzy numbers is chosen for engineering examples due to flexible handling of decision maker's preferences and numerical properties. Distance of center of areas between system answer and allowed value is utilized for constraint handling, if the decision maker's preference is not taken into account for constraint evaluation.
Two formulations for type-2 fuzzy sets have been investigated. First, general type-2 fuzzy sets, and second interval type-2 fuzzy sets. The latter are implemented in the engineering examples due to a good balance between knowledge representation and computational efficiency.
In the first and second engineering example, extruded profiles are investigated with respect to different manufacturing aspects and available manufacturing knowledge. In the first example mechanical properties of the profile as a result of the manufacturing process are mapped to a qualitative performance number. The results allow for a trade-off between structural performance and manufacturability. It also reflects the manufacturing effort with respect to the manufacturing process.
In the second example a plate made from two different extruded profiles is optimized. Minimal wall thicknesses as well as deviation of reinforcing elements from designed position due to the extrusion process are taken into account. Design rules are derived from optimized designs, for example the ratio between the number of stringers and their height. The optimal ratio changes if uncertainties are present in the problem formulation.
The third engineering example is focused on a sandwich beam with design parameter uncertainties and load uncertainties. Compared with deterministic optimization results, optimal designs with uncertainty considerations are more conservative in this example. The uncertainties in the goal mass are nearly constant for optimal solutions whereas uncertainties for surface accuracy increase with decreasing mass. Finally, two designs are chosen for further investigations which are 9% and 8% lighter with 4% and 21% lower RMS compared to the initial design.

The afore mentioned examples showed the applicability and advantages of the implemented methods. Surrogate models reduce the computational effort. Fuzzy constraints provide information on the feasibility of designs with respect to the decision maker's preference.
Future research potential for opTUM-II is identified for better parallelized response surface approximation computation. A central data pool of designs together with nearest neighbor search can enhance computation time.
Another source of data based models with uncertainties which often cannot be described by statistics are derived from data mining methods. Data mining can help to gather information and generate more accurate models in the course of project development. This can be used to update type-2 fuzzy rule-based systems models describing qualitative information. A comparison between designs found in early development stages with designs in later stages of the project reflects increasing knowledge.
The methods presented in this work can easily include aspects from other disciplines in structural optimization. Also the type of numerical models used to generate response surface approximation for α-cut level optimization is not limited to structural finite element method. The proposed methodology provides a new approach for the quantification of qualitative manufacturing knowledge with type-2 fuzzy sets and the usage of this knowledge in structural optimization.

A. Appendix

A.1. Definition of type-2 fuzzy sets

In figure A.1a and A.1b the parameters for Gaussian and in figure A.1c and A.1d for trapezoidal type-2 fuzzy sets are given for the primary MF. The former needs an additional parameter $p_{u=0}$ which defines the point $u = 0$. This is necessary, because the spread of the Gaussian primary MF has to be limited for reasonable computation limits of the αCLO. In figure A.1e the parameters p_1 and p_2 for the secondary MF are given. $p_1, p_2 \in [0, 1]$ determine the position of secondary MF core as ratio of FOU width.

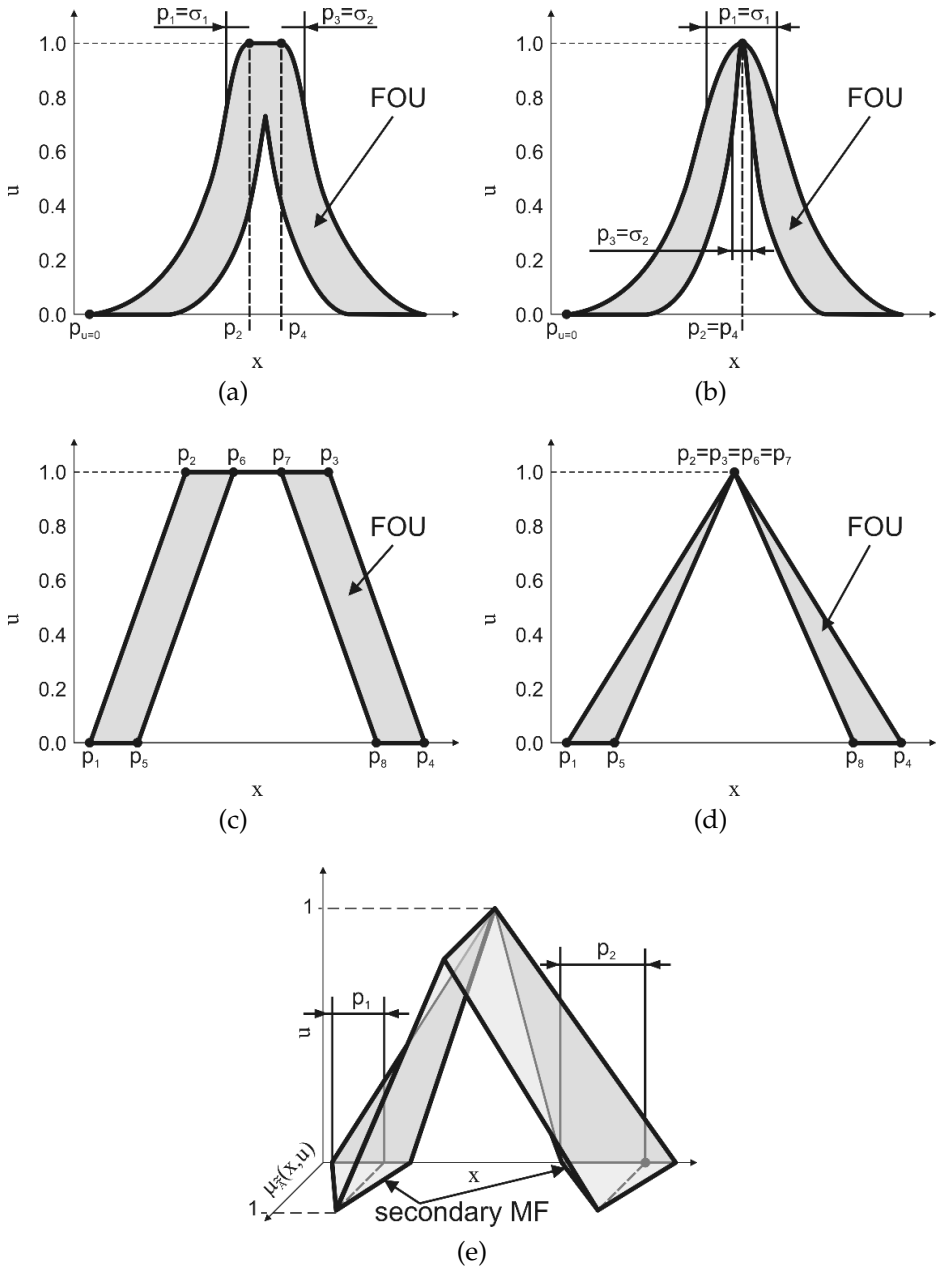

Figure A.1.: Type-2 fuzzy set parameters in opTUM-II

A.2. Knowledge-based models for minimum wall thickness

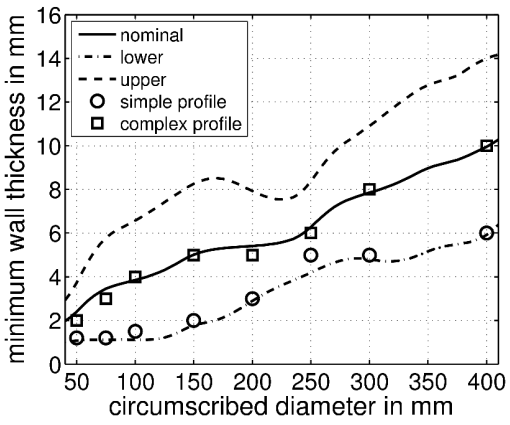

(a) EN AW 2017 and EN AW 2024

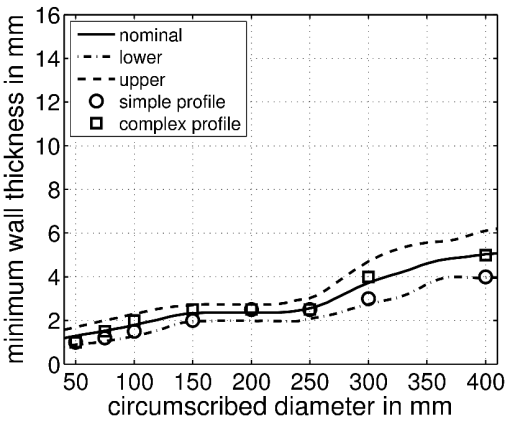

(b) EN AW 6060

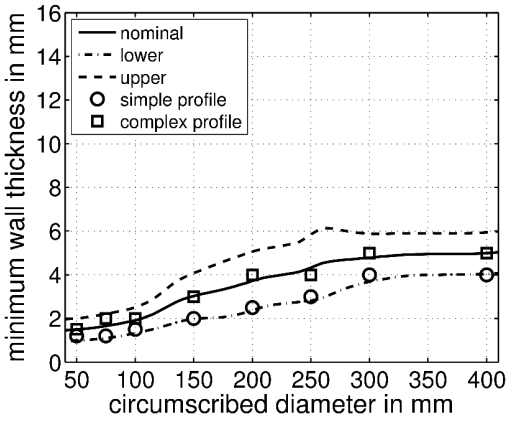

(c) EN AW 6082

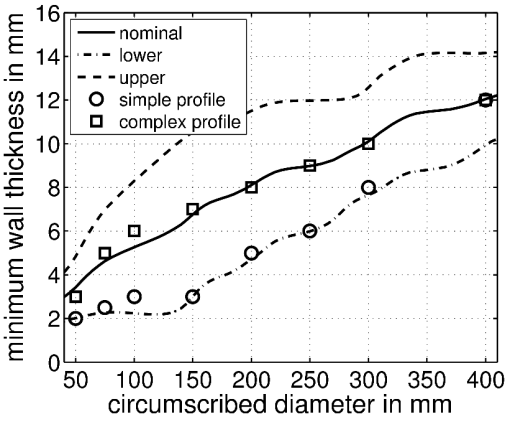

(d) EN AW 7075

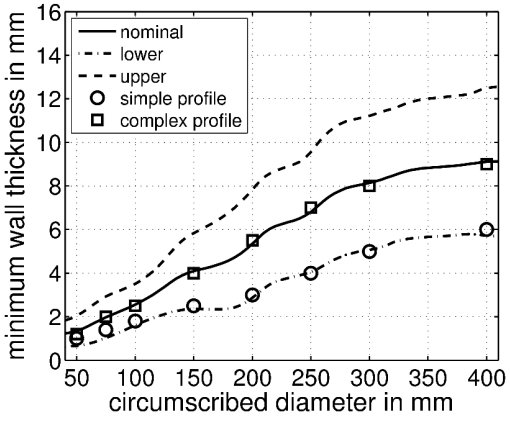

(e) AZ31B

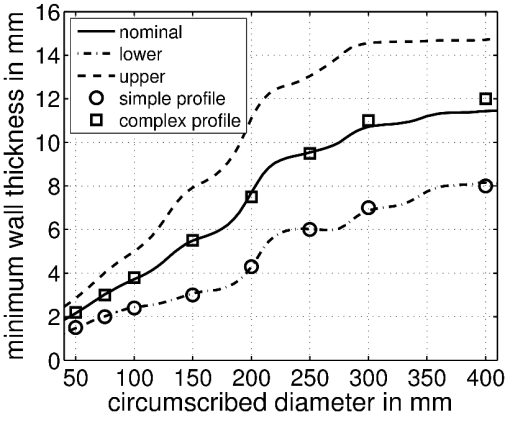

(f) AZ61A

Figure A.2.: Minimum wall thickness

A.3. Evaluation of methods for goal handling in analytical example

A.3.1. Support S^u

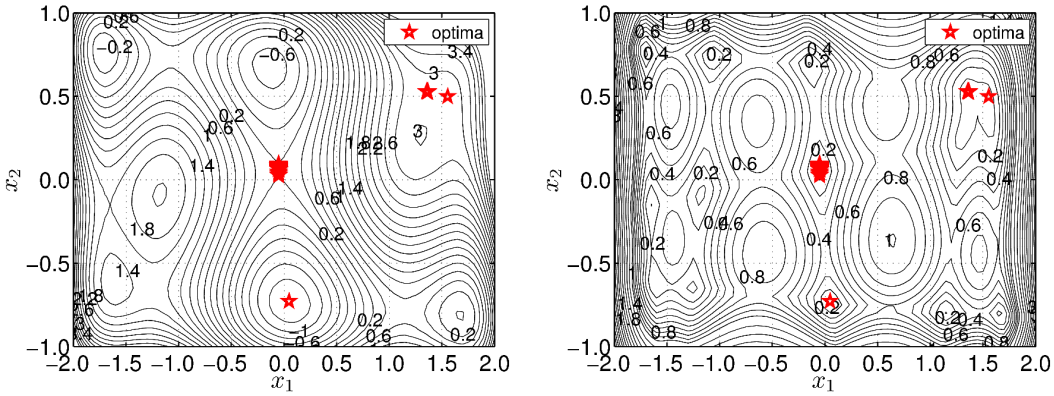

(a) $S^u(\tilde{x})$ = 4%, goal=CoA

(b) $S^u(\tilde{x})$ = 4%, goal=S^u

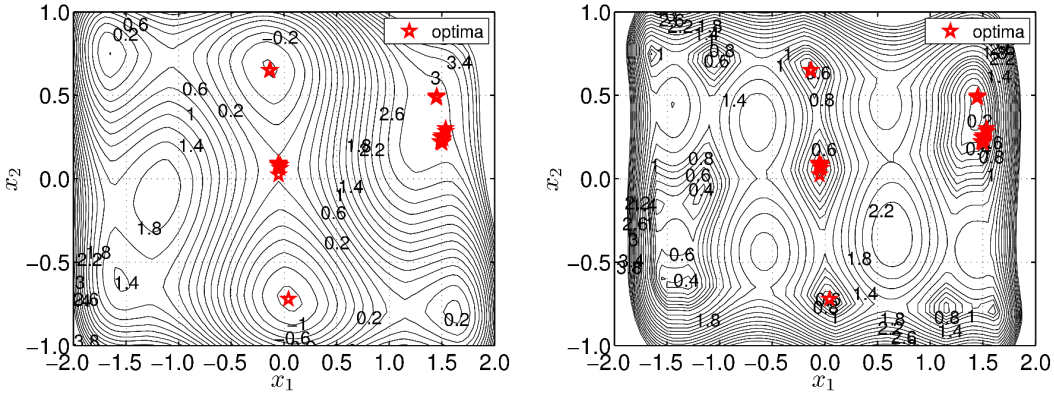

(c) $S^u(\tilde{x})$ = 10%, goal=CoA

(d) $S^u(\tilde{x})$ = 10%, goal=S^u

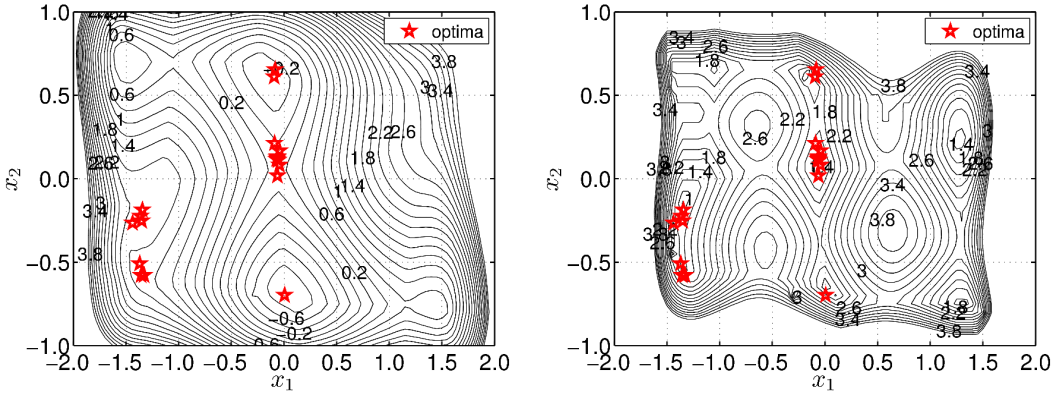

(e) $S^u(\tilde{x})$ = 20%, goal=CoA

(f) $S^u(\tilde{x})$ = 20%, goal=S^u

Figure A.3.: Goals CoA and S^u

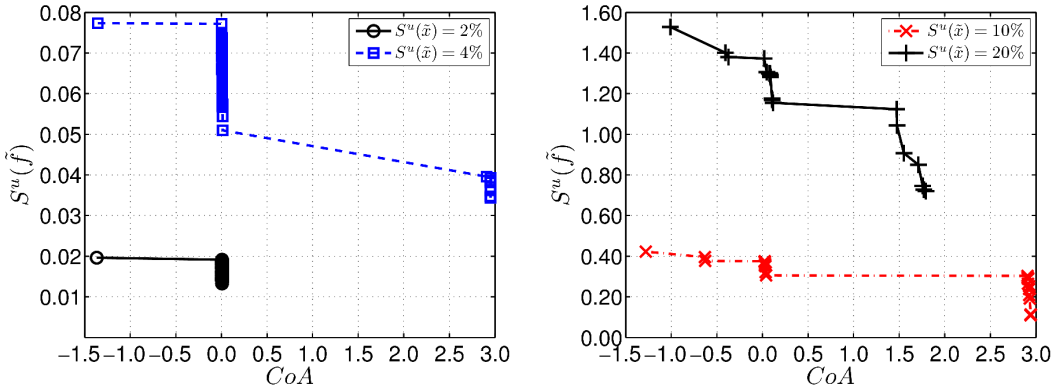

(a) small $S^u(\tilde{x})$ (b) high $S^u(\tilde{x})$

Figure A.4.: Pareto-front for CoA and S^u for different levels of uncertainty

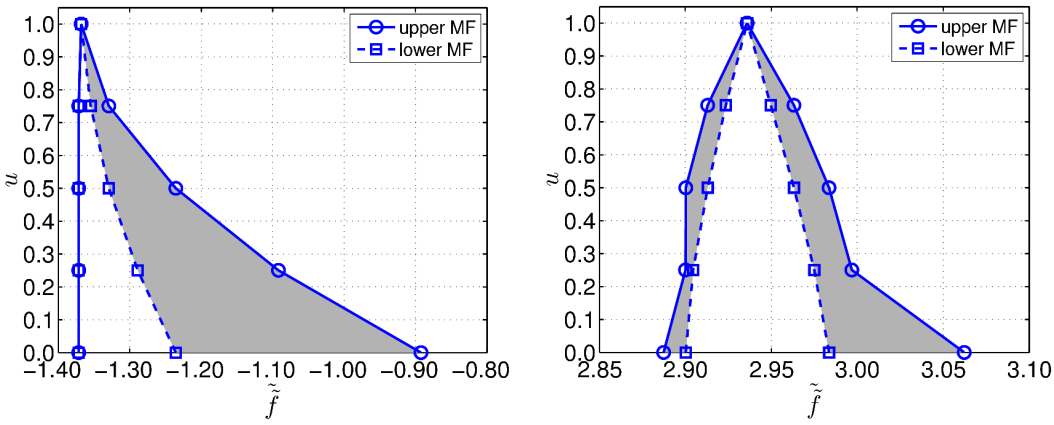

(a) design with minimum CoA (b) design with minimum S^u

Figure A.5.: System answer f for selected optimal designs

A.3.2. Difference $S^u - S^l$

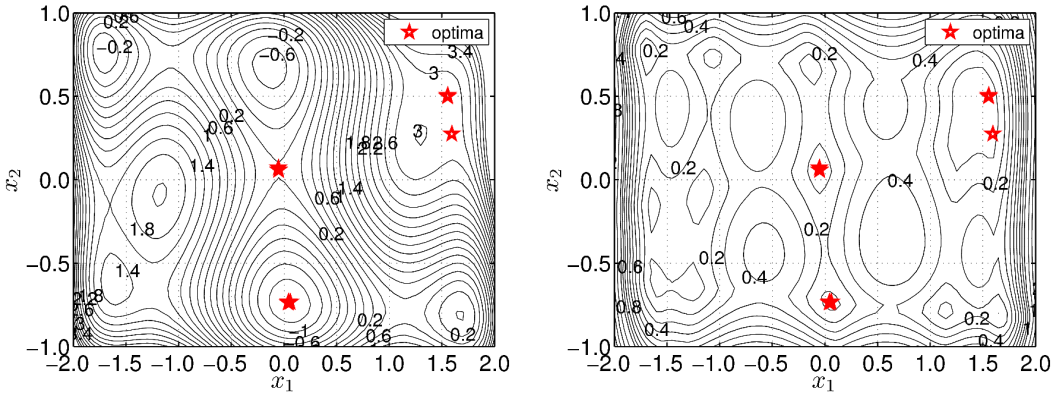

(a) $S^u(\tilde{x})$ = 4%, goal=CoA (b) $S^u(\tilde{x})$ = 4%, goal=$S^u - S^l$

Figure A.6.: Goals CoA and $S^u - S^l$ - 1

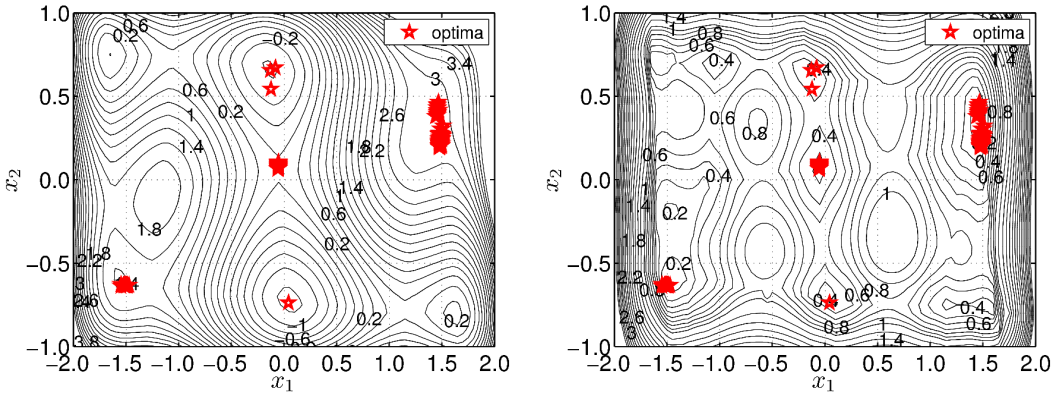

(a) $S^u(\tilde{x})$ = 10%, goal=CoA (b) $S^u(\tilde{x})$ = 10%, goal=$S^u - S^l$

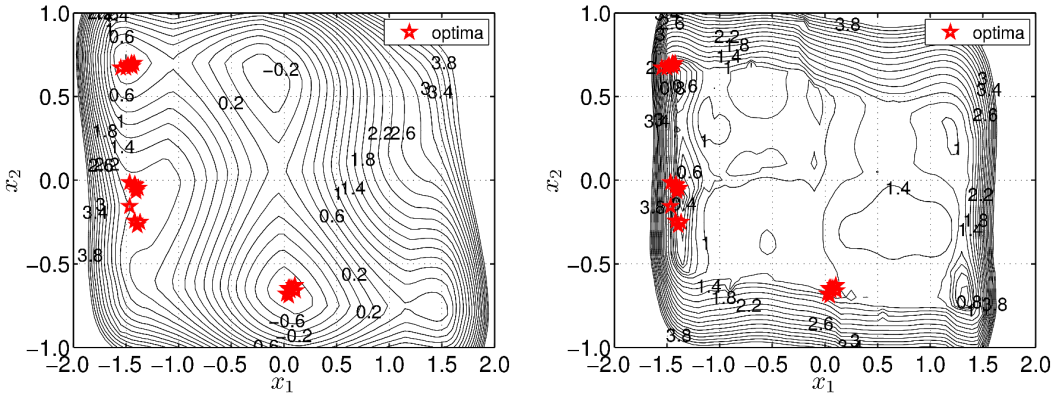

(c) $S^u(\tilde{x})$ = 20%, goal=CoA (d) $S^u(\tilde{x})$ = 20%, goal=$S^u - S^l$

Figure A.7.: Goals CoA and $S^u - S^l$ - 2

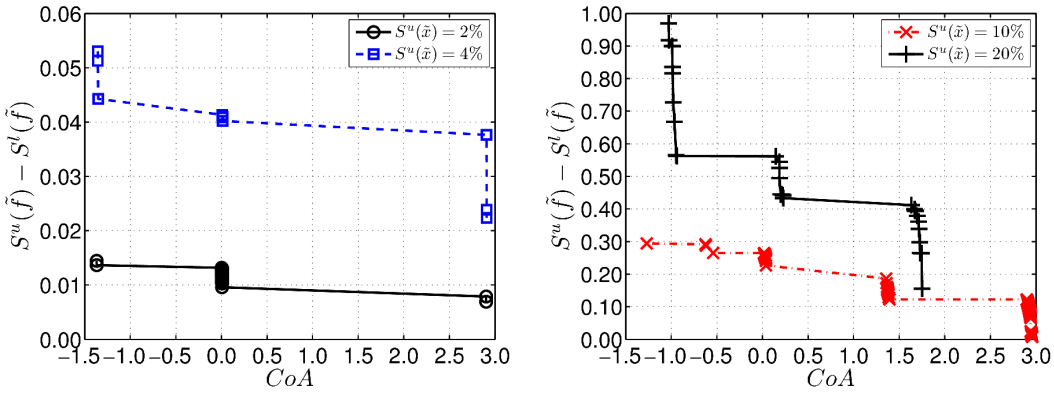

(a) small $S^u(\tilde{x})$ (b) high $S^u(\tilde{x})$

Figure A.8.: Pareto-front for CoA and $S^u - S^l$ for different levels of uncertainty

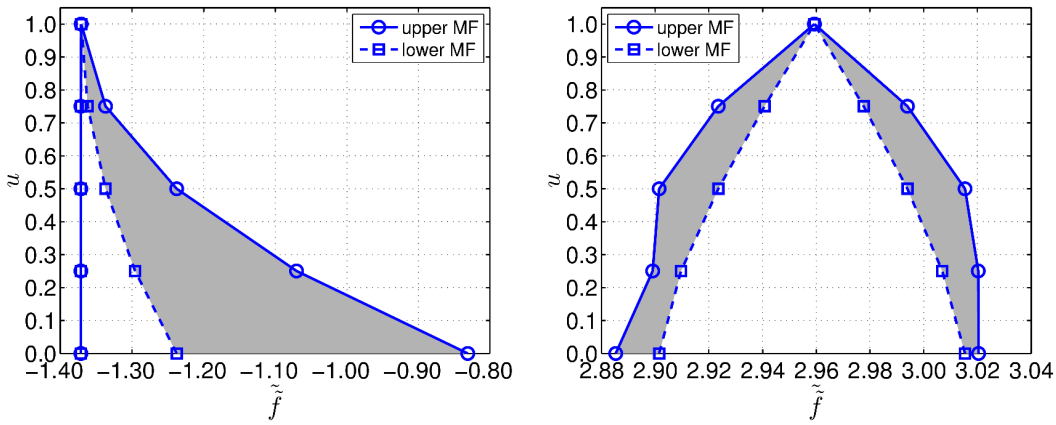

(a) design with minimum CoA (b) design with minimum $S^u - S^l$

Figure A.9.: System answer f for selected optimal designs

A.3.3. Relative difference $(S^u - S^l)/S^u$

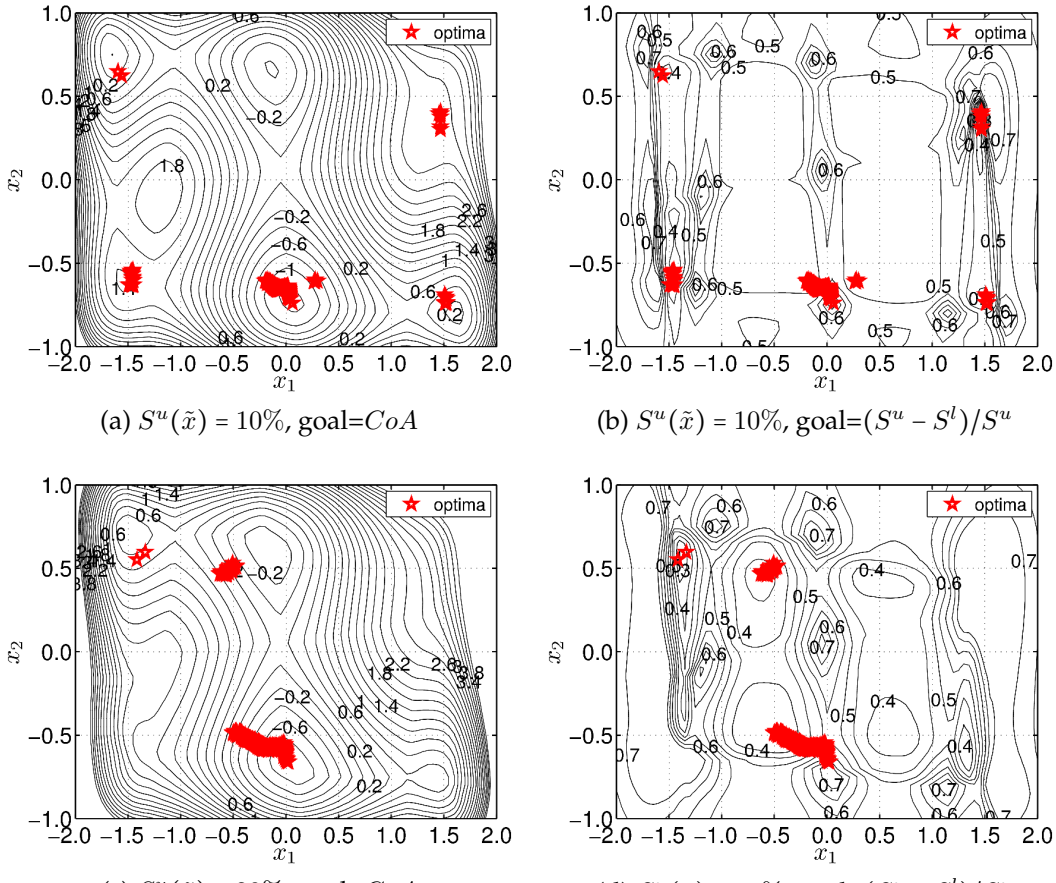

(a) $S^u(\tilde{x}) = 10\%$, goal=CoA (b) $S^u(\tilde{x}) = 10\%$, goal=$(S^u - S^l)/S^u$

(c) $S^u(\tilde{x}) = 20\%$, goal=CoA (d) $S^u(\tilde{x}) = 20\%$, goal=$(S^u - S^l)/S^u$

Figure A.10.: Goals CoA and $(S^u - S^l)/S^u$

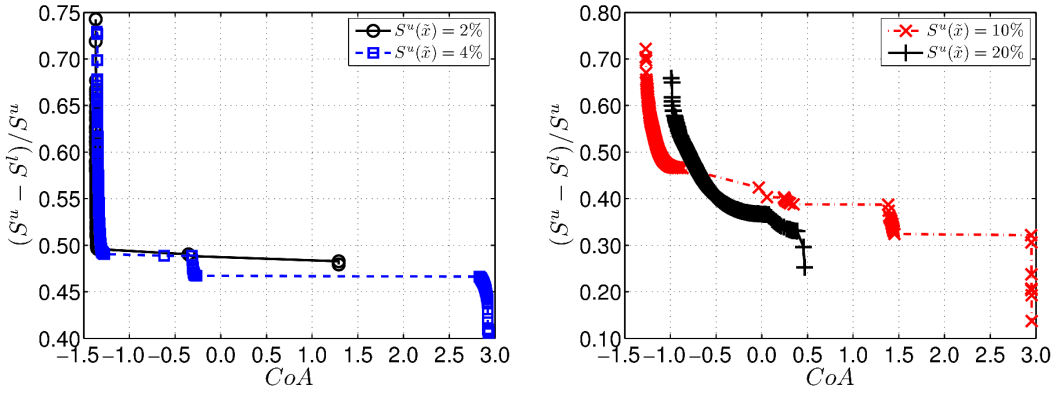

(a) small $S^u(\tilde{x})$ (b) high $S^u(\tilde{x})$

Figure A.11.: Pareto-front for CoA and $(S^u - S^l)/S^u$ for different levels of uncertainty

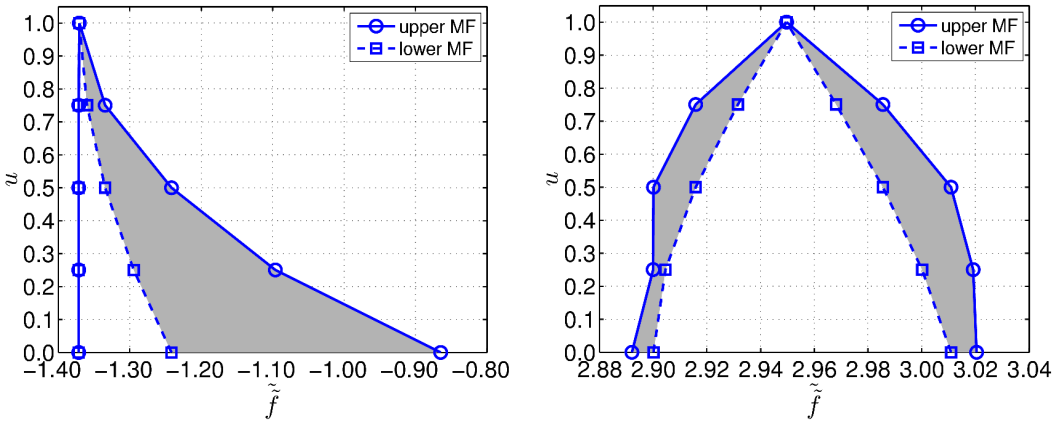

(a) design with minimum CoA (b) design with minimum $S^u - S^l$

Figure A.12.: System answer f for selected optimal designs

A.3.4. Distance $\sum d_{L\mu} + \sum d_{R\mu}$

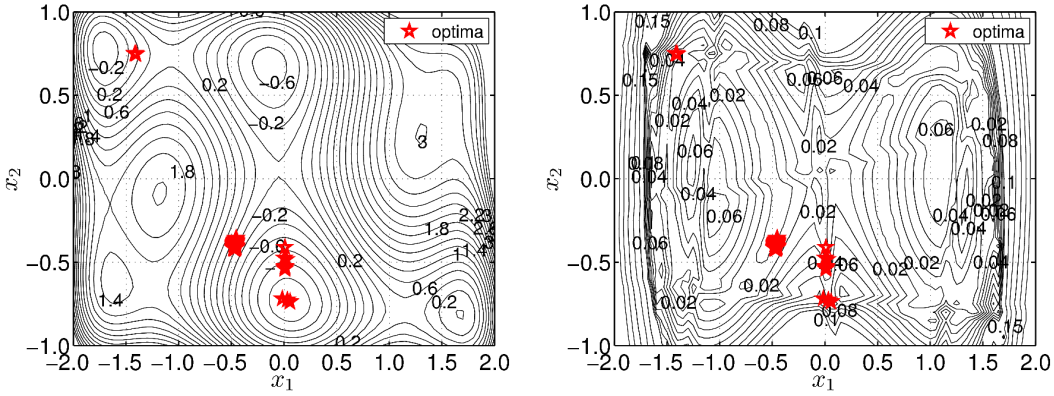

(a) $S^u(\tilde{x})$ = 4%, goal=CoA (b) $S^u(\tilde{x})$ = 4%, goal=$\sum d_{L\mu} + \sum d_{R\mu}$

Figure A.13.: Goals CoA and $\sum d_{L\mu} + \sum d_{R\mu}$ - 1

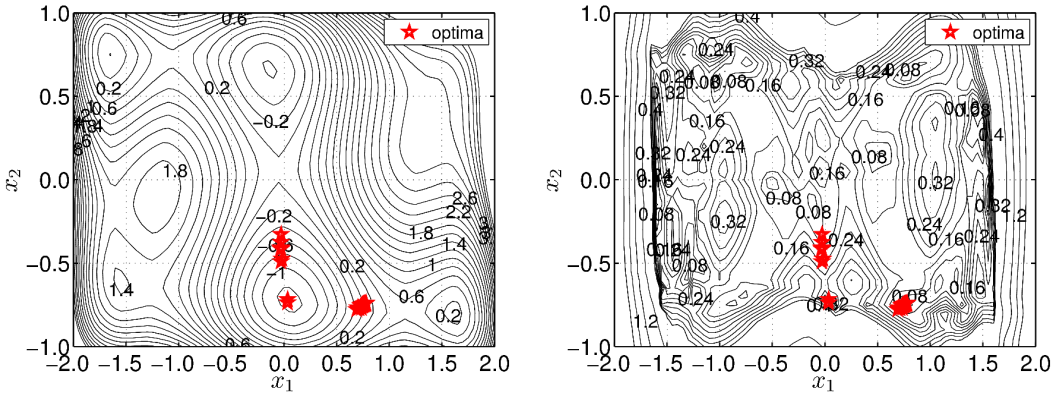

(a) $S^u(\tilde{x})$ = 10%, goal=CoA (b) $S^u(\tilde{x})$ = 10%, goal=$\sum d_{L\mu} + \sum d_{R\mu}$

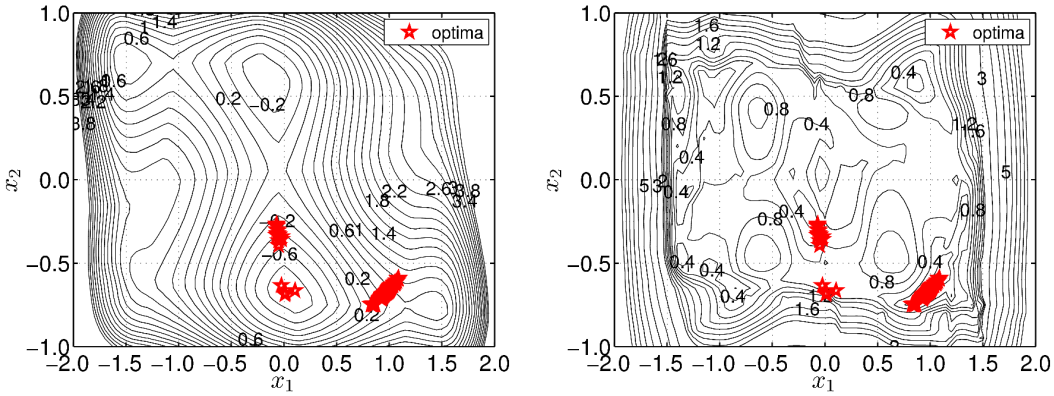

(c) $S^u(\tilde{x})$ = 20%, goal=CoA (d) $S^u(\tilde{x})$ = 20%, goal=$\sum d_{L\mu} + \sum d_{R\mu}$

Figure A.14.: Goals CoA and $\sum d_{L\mu} + \sum d_{R\mu}$ - 2

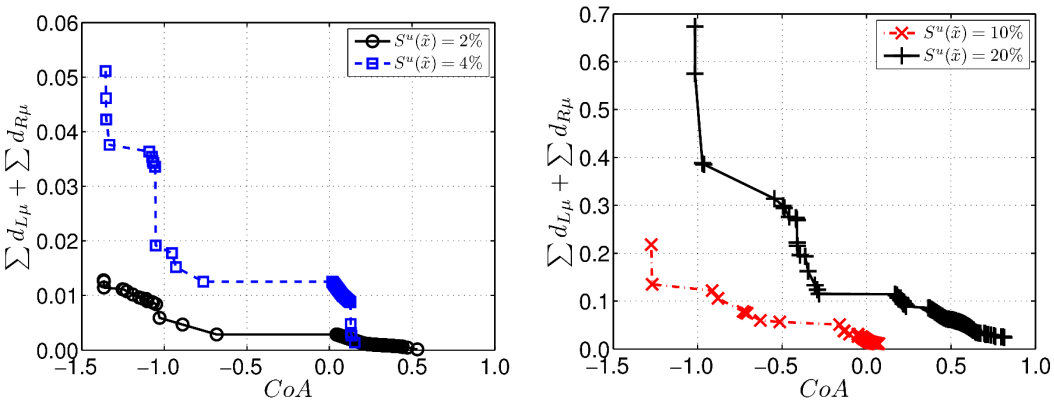

(a) small $S^u(\tilde{x})$ (b) high $S^u(\tilde{x})$

Figure A.15.: Pareto-front for CoA and $\sum d_{L\mu} + \sum d_{R\mu}$ for different levels of uncertainty

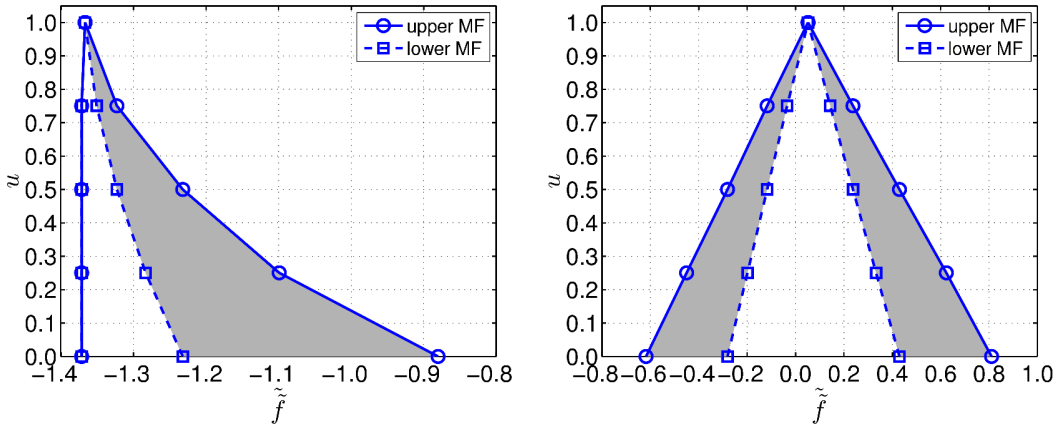

(a) design with minimum CoA (b) design with minimum $\sum d_{L\mu} + \sum d_{R\mu}$

Figure A.16.: System answer f for selected optimal designs

A.3.5. Distance $abs(CoS|_{S^u} - CoS|_{S^l})$

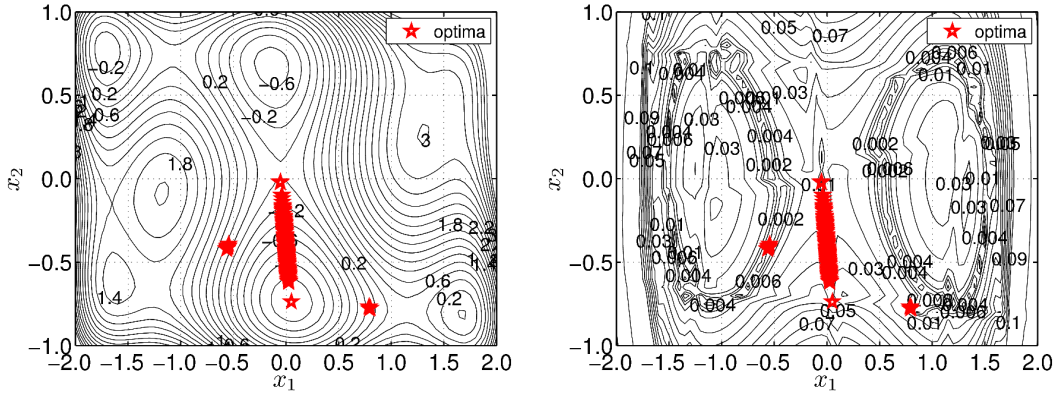

(a) $S^u(\tilde{x})$ = 4%, goal=CoA (b) $S^u(\tilde{x})$ = 4%, goal=$abs(CoS|_{S^u} - CoS|_{S^l})$

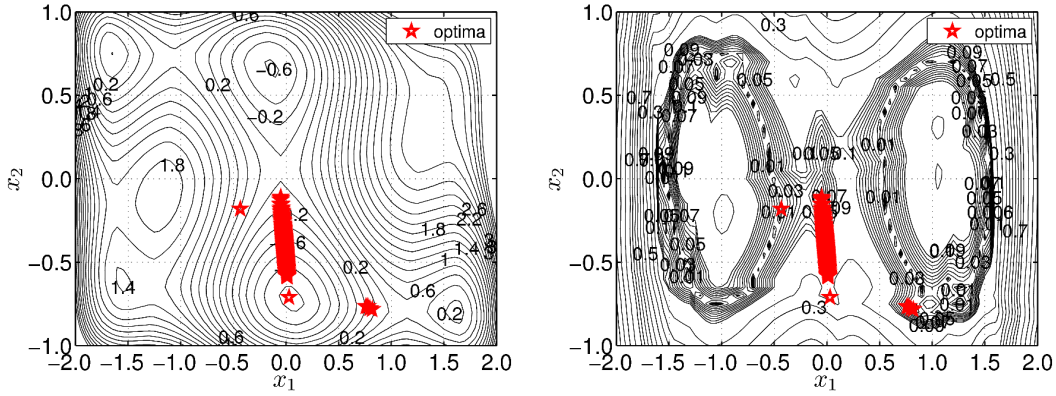

(c) $S^u(\tilde{x})$ = 10%, goal=CoA (d) $S^u(\tilde{x})$ = 10%, goal=$abs(CoS|_{S^u} - CoS|_{S^l})$

Figure A.17.: Goals CoA and $abs(CoS|_{S^u} - CoS|_{S^l})$ - 1

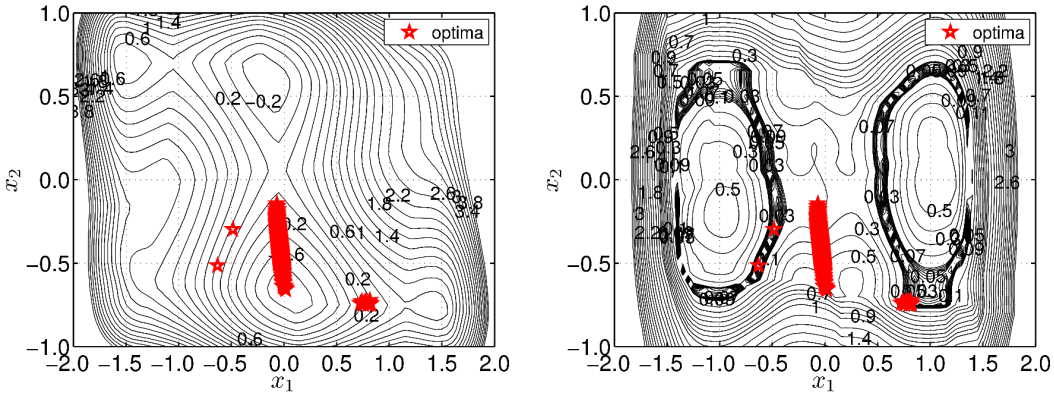

(a) $S^u(\tilde{x})$ = 20%, goal=CoA (b) $S^u(\tilde{x})$ = 20%, goal=$abs(CoS|_{S^u} - CoS|_{S^l})$

Figure A.18.: Goals CoA and $abs(CoS|_{S^u} - CoS|_{S^l})$ - 2

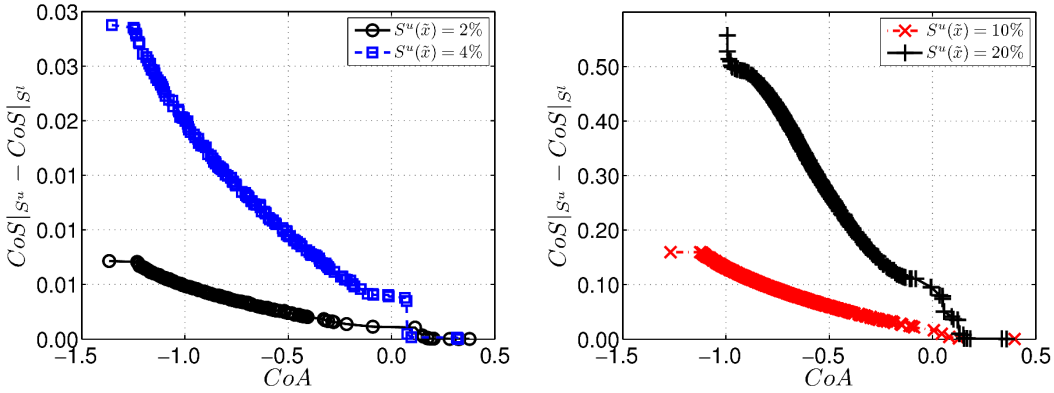

(a) small $S^u(\tilde{x})$ (b) high $S^u(\tilde{x})$

Figure A.19.: Pareto-front for CoA and $abs(CoS|_{S^u} - CoS|_{S^l})$ for different levels of uncertainty

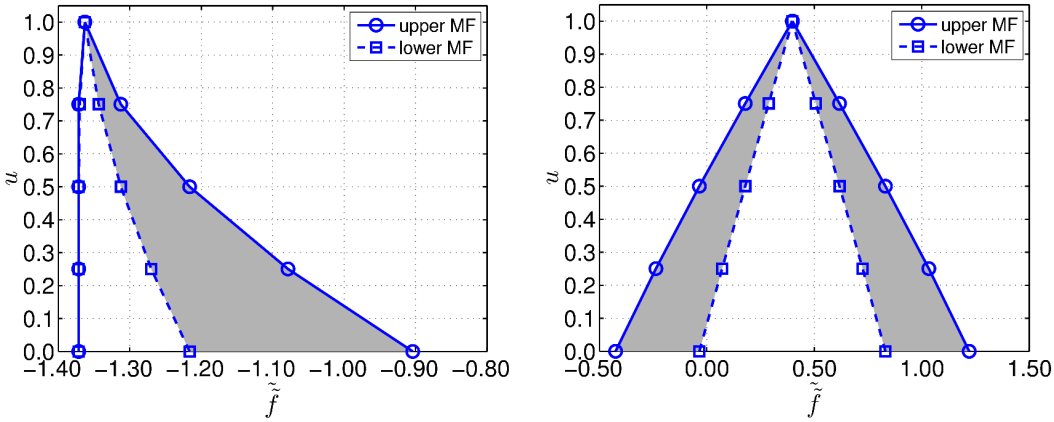

(a) design with minimum CoA (b) design with minimum $abs(CoS|_{S^u} - CoS|_{S^l})$

Figure A.20.: System answer f for selected optimal designs

A.3.6. Skewness evaluation

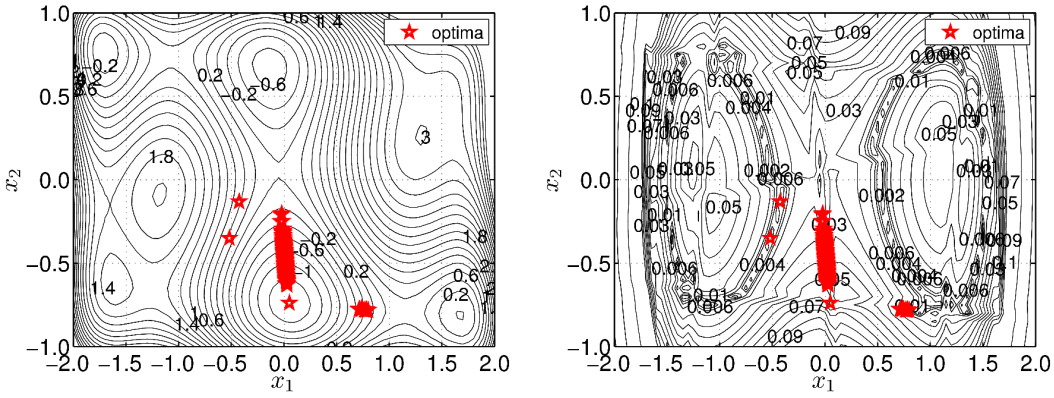

(a) $S^u(\tilde{x})$ = 4%, goal=CoA

(b) $S^u(\tilde{x})$ = 4%, goal=$abs(C - CoS|_{S^l})$

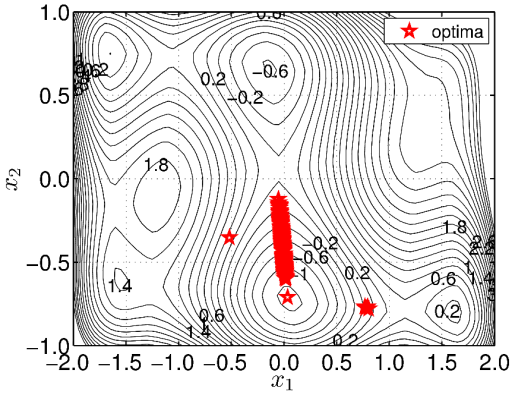

(c) $S^u(\tilde{x})$ = 10%, goal=CoA

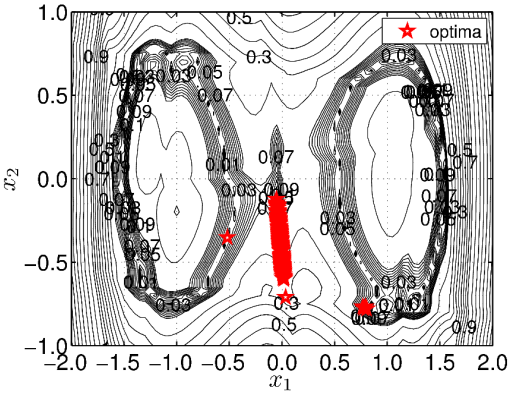

(d) $S^u(\tilde{x})$ = 10%, goal=$abs(C - CoS|_{S^l})$

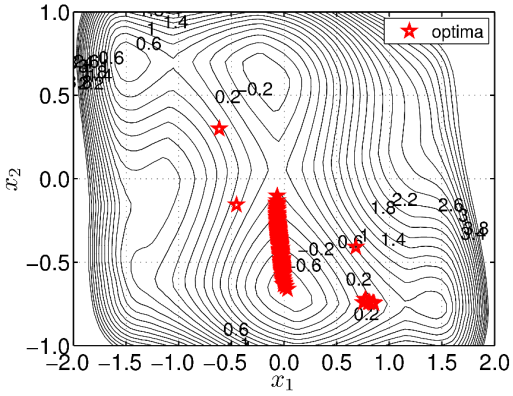

(e) $S^u(\tilde{x})$ = 20%, goal=CoA

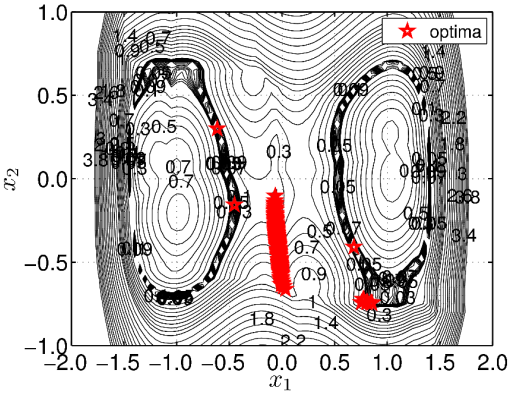

(f) $S^u(\tilde{x})$ = 20%, goal=$abs(C - CoS|_{S^l})$

Figure A.21.: Goals CoA and $abs(C - CoS|_{S^l})$

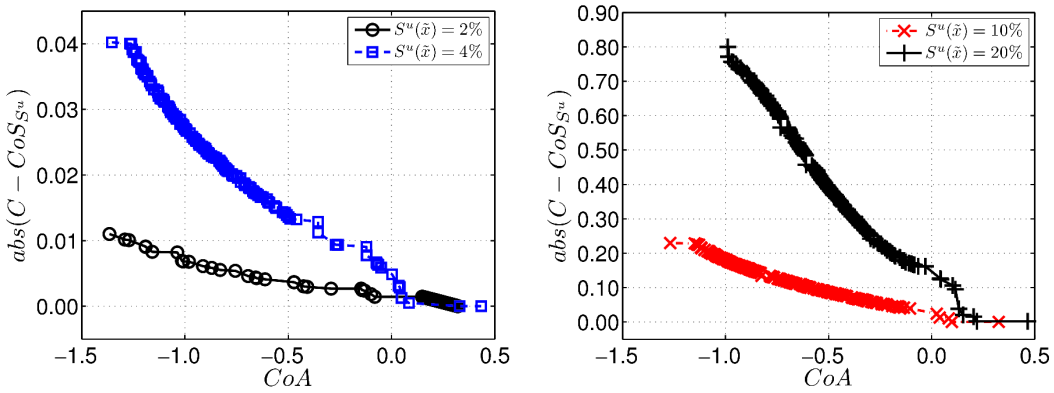

(a) small $S^u(\tilde{x})$ (b) high $S^u(\tilde{x})$

Figure A.22.: Pareto-front for CoA and $abs(C - CoS|_{S^l})$ for different levels of uncertainty

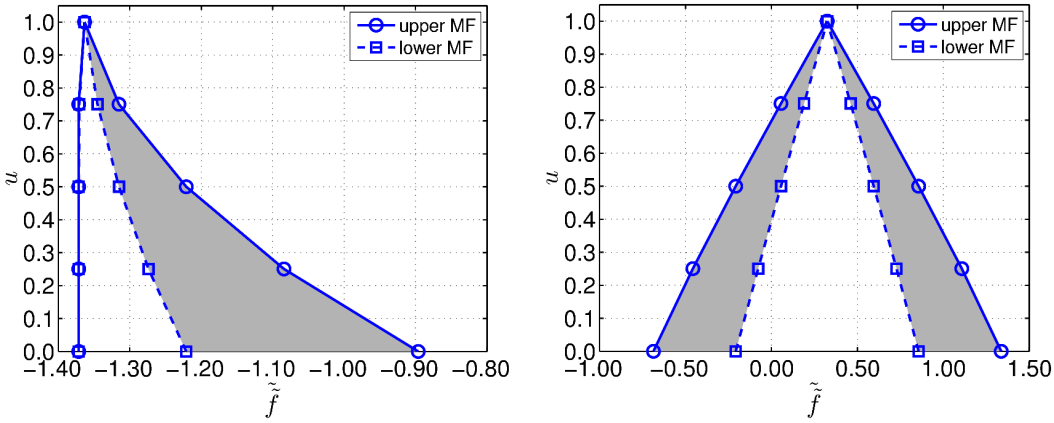

(a) design with minimum CoA (b) design with minimum $abs(C - CoS|_{S^l})$

Figure A.23.: System answer f for selected optimal designs

A.4. Constraint evaluation for analytical example

A range of different combinations of DPR for T2 FS is available. First basic measures are evaluated such as mean and maximum value of DPR on n_α^{II} levels. Second sums of measures are evaluated.
In figure A.24 results for secondary MF parameters $p_1 = 1.0, p_2 = 0.0$ of inputs are displayed. The mean value is evaluated on the left hand side, the maximum for all n_α^{II} levels on the right hand side. For comparison CoA results of IT2 FS already shown in figure 4.9c are also displayed. Different version of allowable fuzzy sets described in table 4.3 are summarized, version 1 in figures A.24a and A.24b, version 2 in A.24c and A.24d and version 3 in A.24e and A.24f.
The first two versions of allowable fuzzy values show the same behavior with different absolute values. Compared to CoA different sensitivities of the constraint function have much higher influences on the shape of the boundary. The mean value on the left side provides a better spread for different settings of fuzzy allowed values.
A different characteristic is generated by version 3 in figures A.24e and A.24f. The settings

A,B and C for fuzzy allowed values show marginal influence on the boundary. Also the fuzzy boundary lies completely in original feasible design space.
In figure A.25 results for secondary MF parameters $p_1 = 0.5, p_2 = 0.5$ of inputs are shown. Those are shifted slightly compared to the ones in figure A.24. The evaluation of the maximum is more influenced by the change in parameters than the mean value.

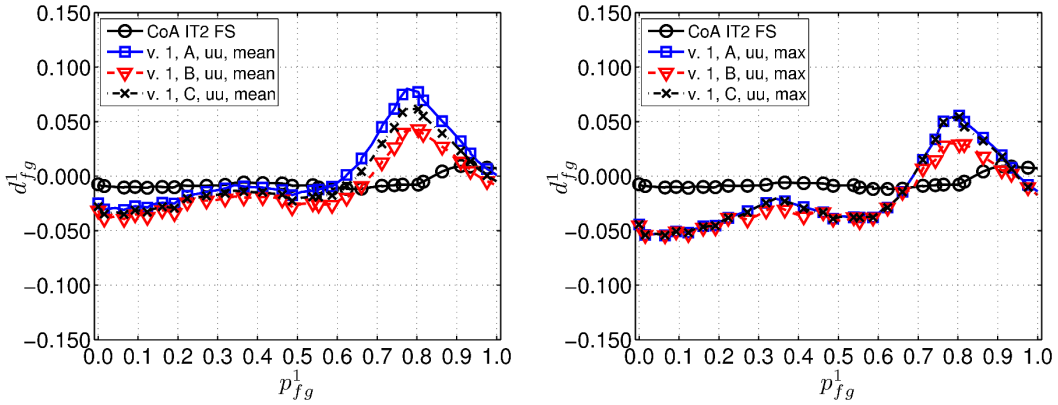

(a) version 1, mean

(b) version 1, max

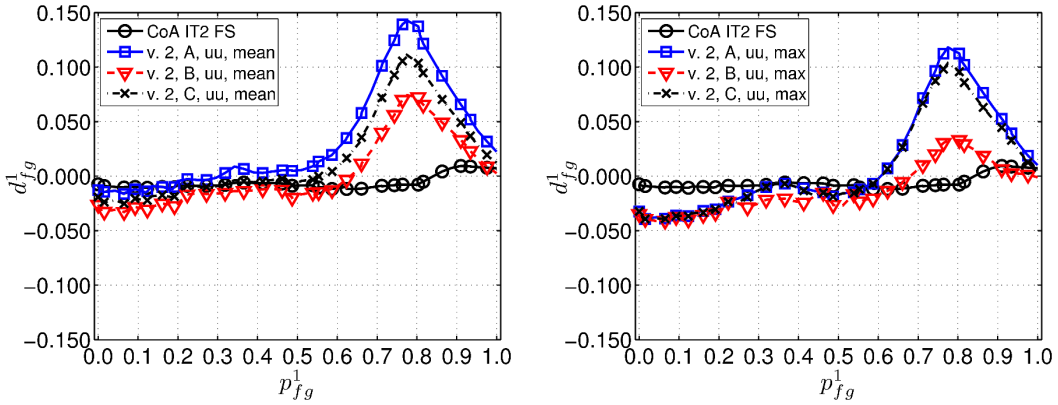

(c) version 2, mean

(d) version 2, max

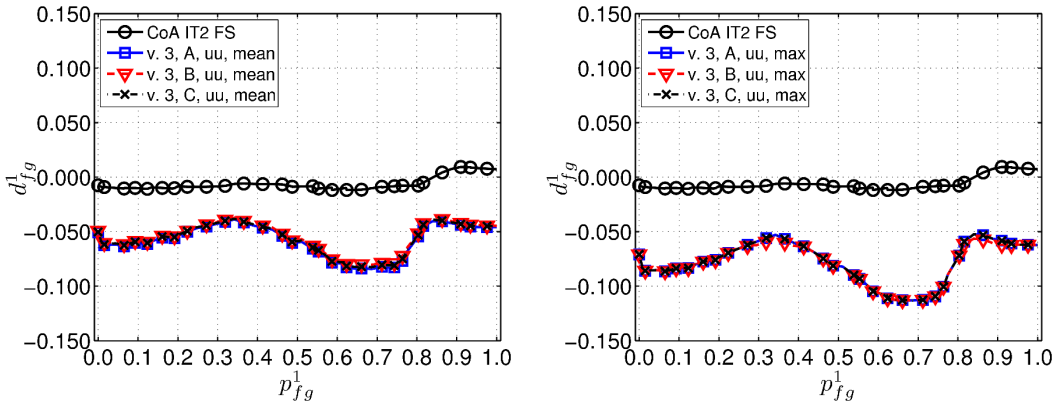

(e) version 3, mean

(f) version 3, max

Figure A.24.: Mean and maximum DPR PSD for upper MFs of T2 FS and $q_{DPR} = 0.5$, input parameter second MF $p_1 = 1.0, p_2 = 0.0$

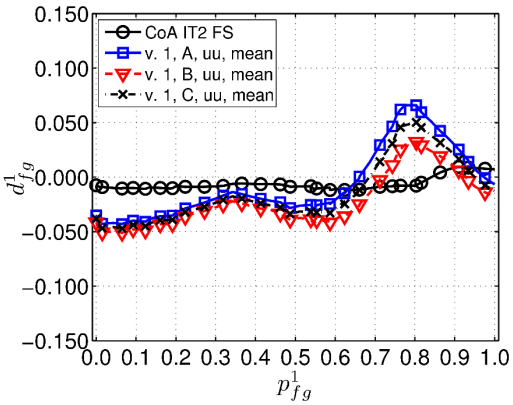

(a) version 1, mean

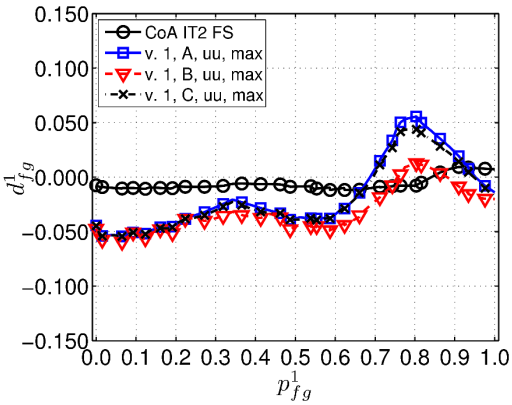

(b) version 1, max

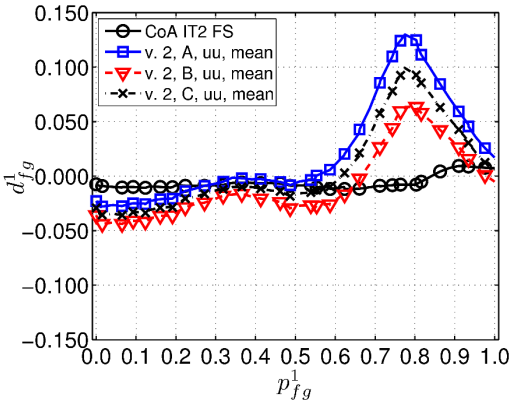

(c) version 2, mean

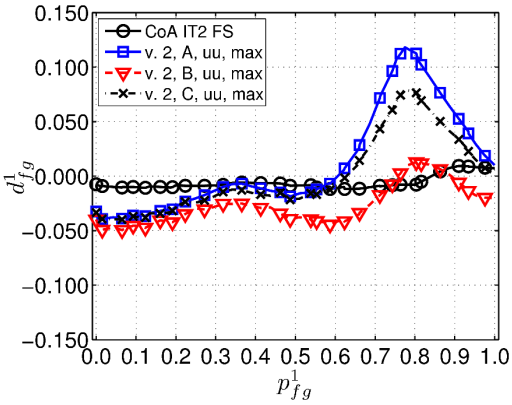

(d) version 2, max

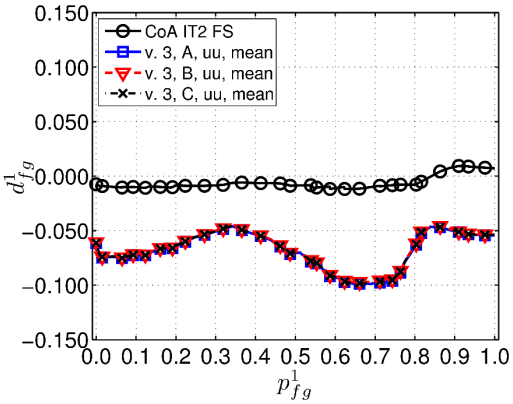

(e) version 3, mean

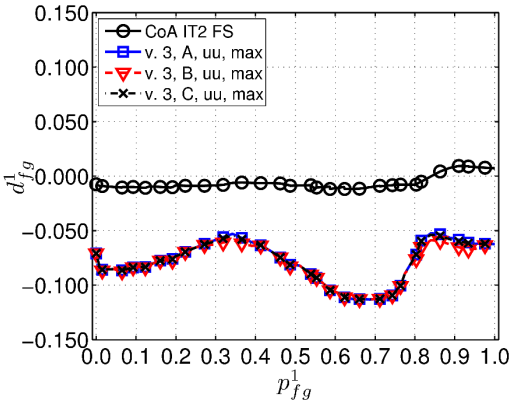

(f) version 3, max

Figure A.25.: Mean and maximum DPR PSD for upper MFs of T2 FS and $q_{DPR} = 0.5$, input parameter second MF $p_1 = 0.5, p_2 = 0.5$

A.5. Example FLAME beam

A.5.1. Materials

Table A.1.: Material parameters of sandwich beam (single layer properties for composites)

face sheet top/bottom				
material	φ in %	property	unit	value
M40J/Epoxy 2500	60	E_{c11}	MPa	215000
		E_{c22}	MPa	7800
		E_{c33}	MPa	7800
		G_{c12}	MPa	5000
		G_{c13}	MPa	5000
		G_{c23}	MPa	2786
		ν_{c12}	-	0.3
		ν_{c13}	-	0.3
		ν_{c23}	-	0.5
		ρ_c	kg/m^3	1580
CFRP box				
T300/Epoxy 924	60	E_{c11}	MPa	132525
		E_{c22}	MPa	8440
		E_{c33}	MPa	8440
		G_{c12}	MPa	4219
		G_{c13}	MPa	4219
		G_{c23}	MPa	2910
		ν_{c12}	-	0.34
		ν_{c13}	-	0.34
		ν_{c23}	-	0.40
		ρ_c	kg/m^3	1580
foam core				
Rohacell®51A	-	E	MPa	70
		G	MPa	20
		ν	-	0.3
		ρ	kg/m^3	52

A.5.2. Load cases

Table A.2.: FLAME beam - load case 1

load	direction	value	unit
M_{spring}	-	0.2	Nm
F_{deploy}	x_{beam}	0.0	N
F_{deploy}	y_{beam}	0.0	N
a_x	x_{beam}	0.0	g
a_y	y_{beam}	0.0	g
a_z	z_{beam}	1.0	g
m_{RS} division factor	-	12.0	-

Table A.3.: FLAME beam - load case 2

load	direction	value	unit
M_{spring}	-	0.2	Nm
F_{deploy}	x_{beam}	-12.0	N
F_{deploy}	y_{beam}	-1.0	N
a_x	x_{beam}	9.0	g
a_y	y_{beam}	9.0	g
a_z	z_{beam}	7.3	g
m_{RS} division factor	-	2.0	-

Table A.4.: FLAME beam - load case 3

load	direction	value	unit
M_{spring}	-	1.0	Nm
F_{deploy}	z_{beam}	1.0	N
F_{deploy}	y_{beam}	1.0	N
a_x	x_{beam}	7.3	g
a_y	y_{beam}	-9.0	g
a_z	z_{beam}	9.0	g
m_{RS} division factor	-	2.0	-

A.5.3. Influence of uncertain parameters

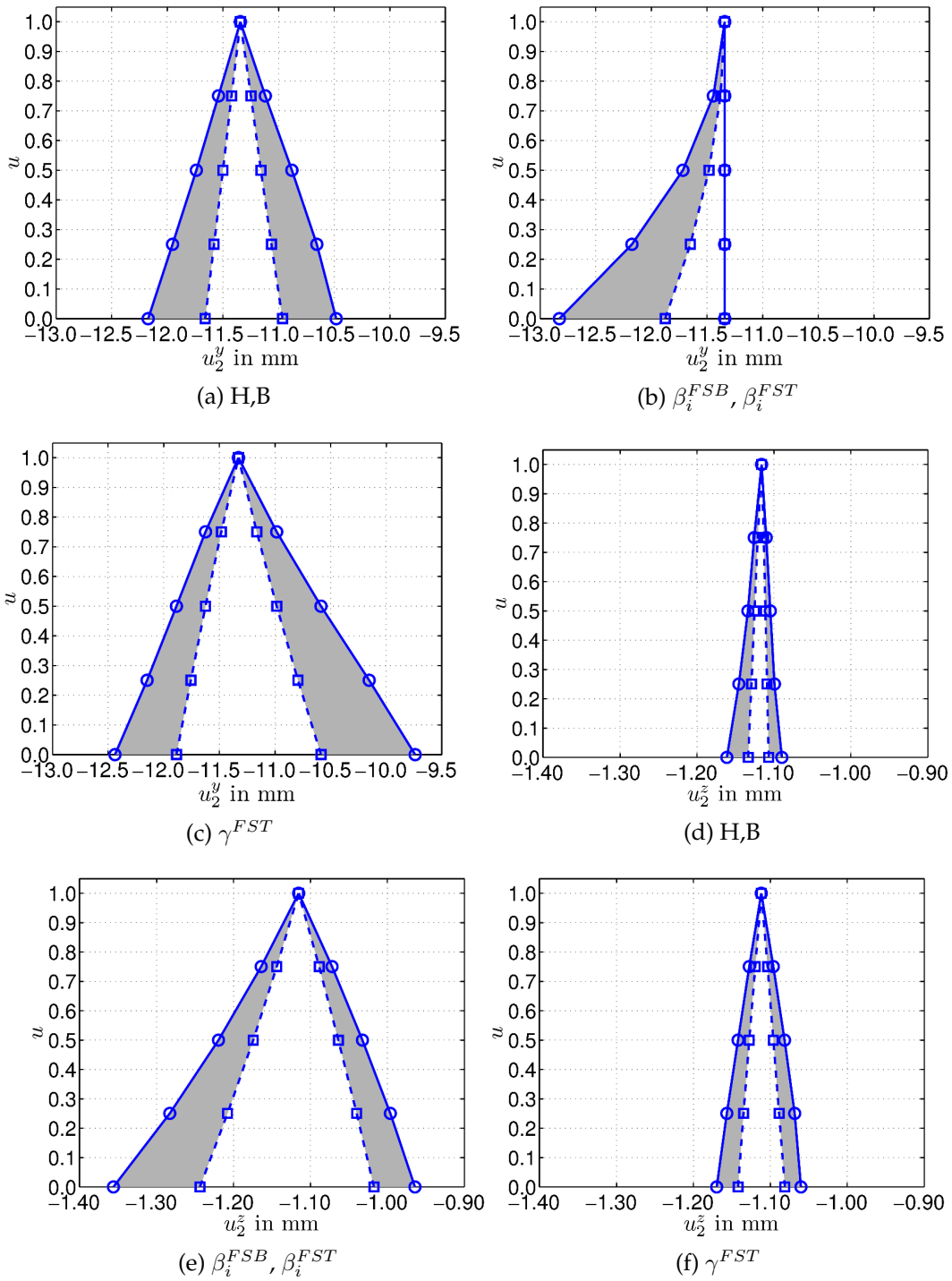

(a) H,B (b) β_i^{FSB}, β_i^{FST}

(c) γ^{FST} (d) H,B

(e) β_i^{FSB}, β_i^{FST} (f) γ^{FST}

Figure A.26.: u_2^y and u_2^z with respect to design uncertainties

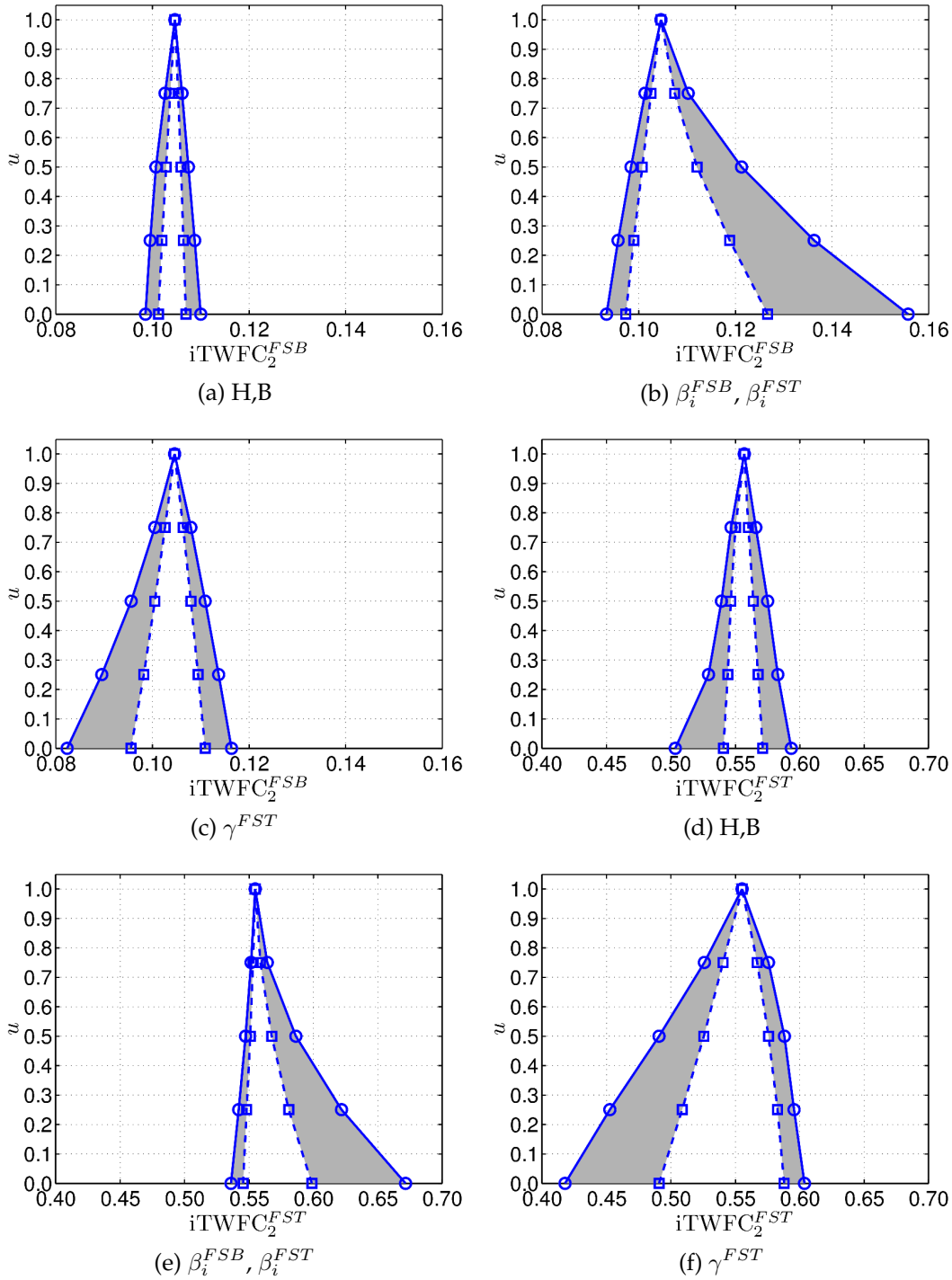

(a) H,B (b) β_i^{FSB}, β_i^{FST}

(c) γ^{FST} (d) H,B

(e) β_i^{FSB}, β_i^{FST} (f) γ^{FST}

Figure A.27.: iTWFC$_2^{FSB}$ and iTWFC$_2^{FST}$ with respect to design uncertainties

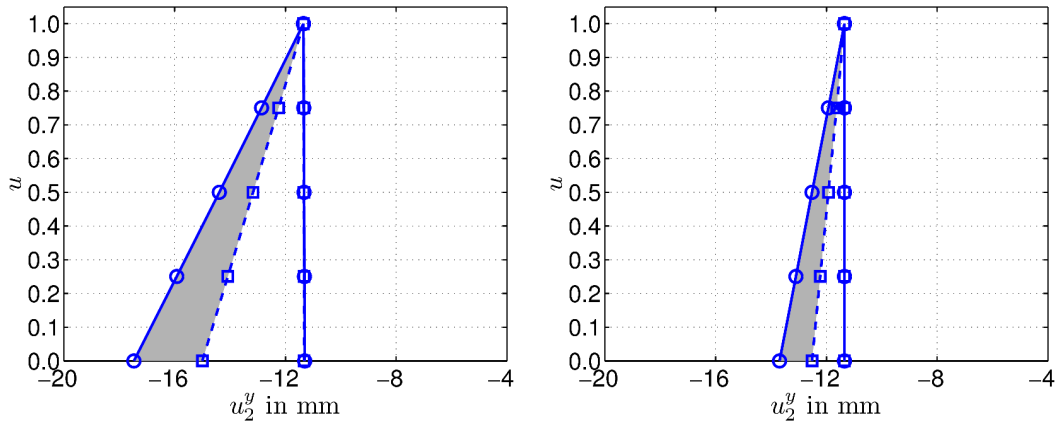

(a) F, M

(b) a_x, a_y, a_z

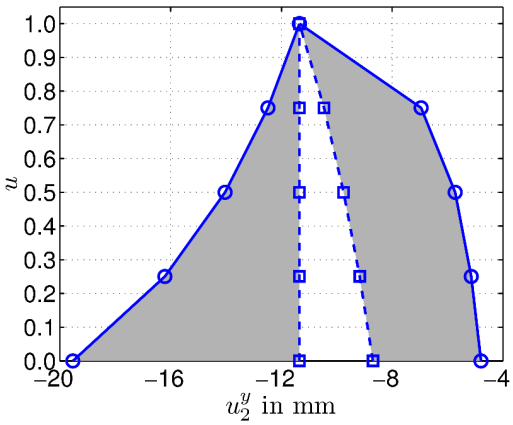

(c) m_{RS} div. fact.

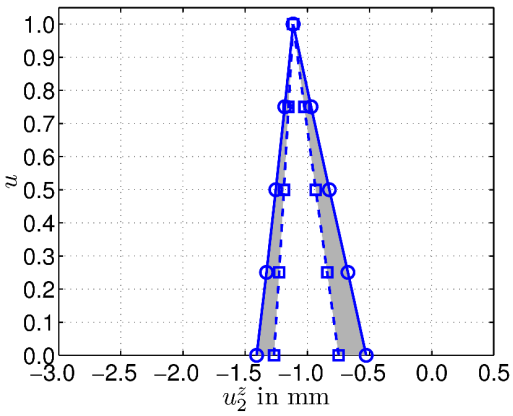

(d) F, M

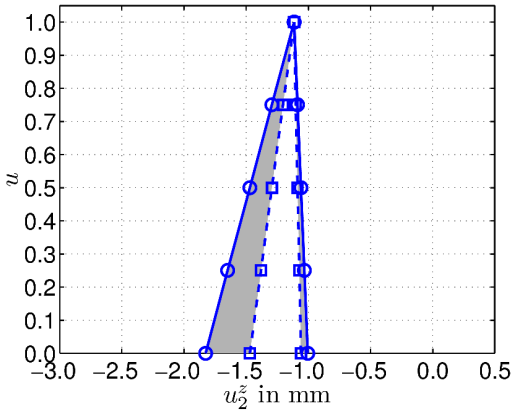

(e) a_x, a_y, a_z

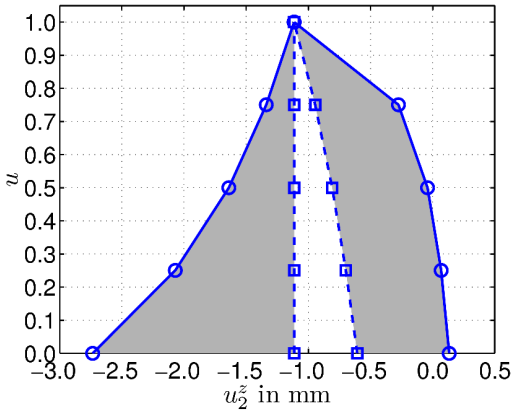

(f) m_{RS} div. fact.

Figure A.28.: u_2^y and u_2^z with respect to load uncertainties

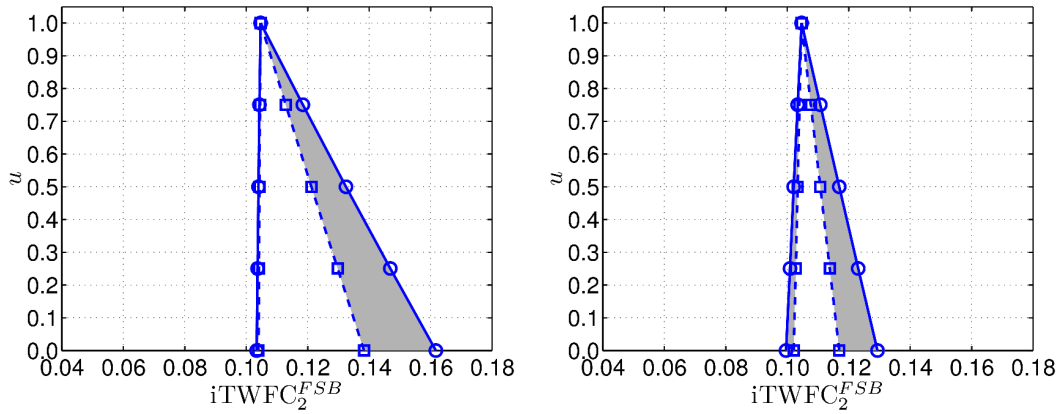

(a) F, M

(b) a_x, a_y, a_z

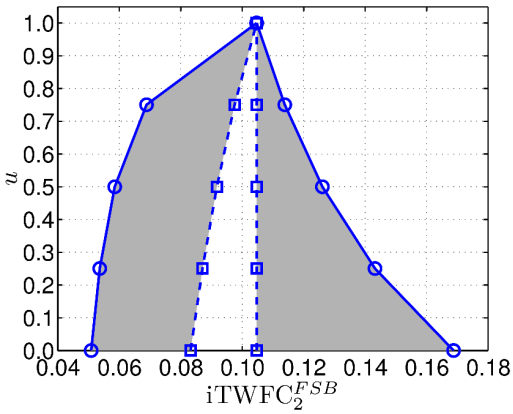

(c) m_{RS} div. fact.

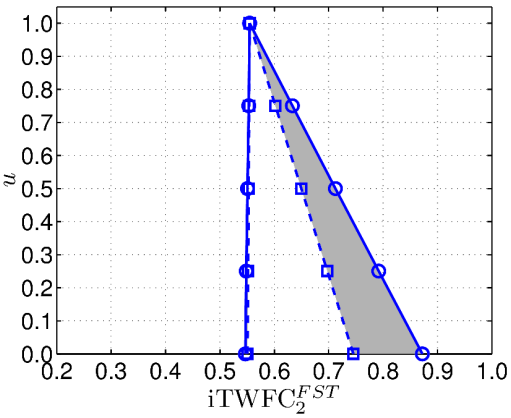

(d) F, M

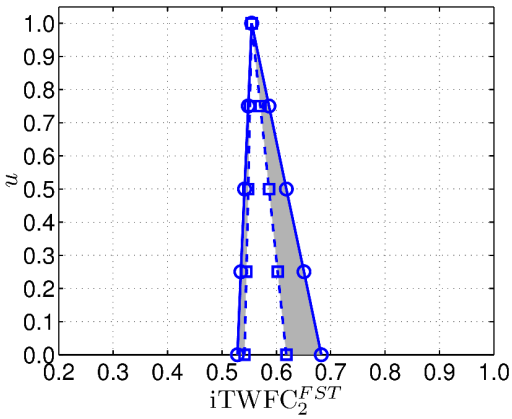

(e) a_x, a_y, a_z

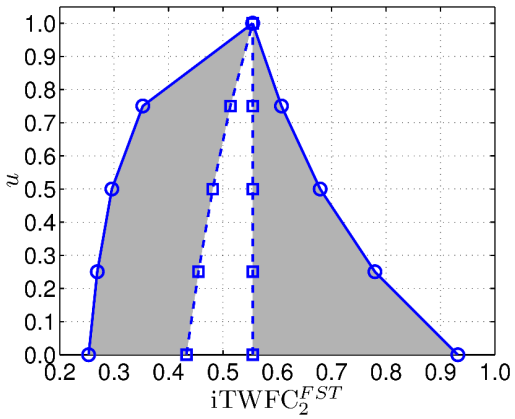

(f) m_{RS} div. fact.

Figure A.29.: iTWFC$_2^{FSB}$ and iTWFC$_2^{FST}$ with respect to load uncertainties

A.6. Example stringer stiffened, metal matrix composite plate

A.6.1. Literature review for joining

For FSW of EN AW-7075 T651 a 35% loss in yield strength and 15% loss in ultimate strength compared to base material is discussed in Mahoney et al. (1998). An aging treatment was performed after welding. FSW of dissimilar aluminum alloys EN AW-6082 and EN AW-6061 is reported in Moreira et al. (2008) resulting in approximately 50% lower yield strength than the unaffected weaker base material. The tested base material was in T6 condition and no heat treatment was performed after FSW. Joining of EN AW-5083 and EN AW-6061 aluminum is evaluated in Shigematsu et al. (2003). The FSW joined specimens reach approximately 63% of tensile strength of the weaker base material. It is not clear if aging treatment was performed on the tensile test specimens. For comparison FSW was performed for joining two specimens of the same alloy which resulted in nearly no reduction of tensile strength for EN AW-5083 and a 38% loss for EN AW-6061. Amancio-Filho et al. (2008) shows that a FSW joint for EN AW-2024 T351 and EN AW-6056 T4 can reach 90% of the yield strength of the weaker base material without aging after welding. EN AW-2024 T3 and EN AW-7075 T6 is joined in Cavaliere et al. (2005). Without an aging treatment after welding a yield strength of approximately 86% compared to weaker base material is achieved.
Together with FSW mainly AZ31B is investigated for magnesium, for example in Esparza et al. (2002), Afrin et al. (2008) and Commin et al. (2009). The latter two authors found a reduction of yield stress of approximately 45% due to FSW for AZ31B specimens. Also dissimilar welds between magnesium and aluminum can be found in literature. For extruded EN AW-1060 and AZ31B alloy Yan et al. (2005) found a tensile strength of approximately 82 MPa for joined specimens which is 67% of the tensile strength of the weaker aluminum alloy. Zettler et al. (2006) finds an ultimate tensile strength for EN AW-6040 and AZ31B FSW weld of approximately 189 MPa which is 88% of the ultimate strength of weaker EN AW-6040 FSW weld. For EN AW-6063 and AZ31B Venkateswaran et al. (2009) reports a maximum transverse tensile strength of the weld of 68% of the EN AW-6063 base metal.
Laser beam welding offers similar possibilities for joining of different alloys and even materials. In SFB-TR10 BHLS is used to join plates and profiles made of EN AW-6060. Details can be found in Trautmann and Zäh (2006), Zäh et al. (2008) and Zäh et al. (2009). Other aluminum alloys are investigated in for example in El-Batahgy and Kutsuna (2009). Depending on the alloy the welded joint has nearly the same strength properties as the base materials after aging treatment. A broad overview for different alloys is also given in Cao et al. (2003b) and Cao et al. (2003a).
Also magnesium can be joined by laser beam welding. Basic research without mechanical properties can be found for example in Leong et al. (1998) and Watkins (2003). Cao et al. (2006) provides several literature sources with tensile test results. Yield strength of the joints is between 65% and 100% of the base material depending on the alloy, welding parameters and aging treatment after welding. Coelho et al. (2008) reports different changes in yield strength depending on the loading dircetion for AZ31B laser welds of rolled plates. In welding direction a yield strength of approximately 92% of the base material can be achieved without aging treatment. Quan et al. (2008b) show similar results for AZ31B. Tensile properties for laser welded joints of dissimilar magnesium alloys can be found in Quan et al. (2008a) for AZ31B, AM60 and ZK60 and in Kolodziejczak and Kalita (2009) for AM50 and

AZ91. The strength of the weaker alloy in the joint is always reached or exceeded.
Also examples for laser welding of dissimilar materials can be found for magnesium and aluminum joints. In Liu et al. (2007) results for a lap joint between AZ31B and EN AW-6061 with and without additional adhesive are presented. With welding only very low strength can be achieved. Borrisutthekul et al. (2005) give results for a lap joint without adhesive and two different welding configurations (center-line and edge-line). The reported strength properties are well below the ones known for FSW joints for this material combination.

A.6.2. Evaluation of initial design

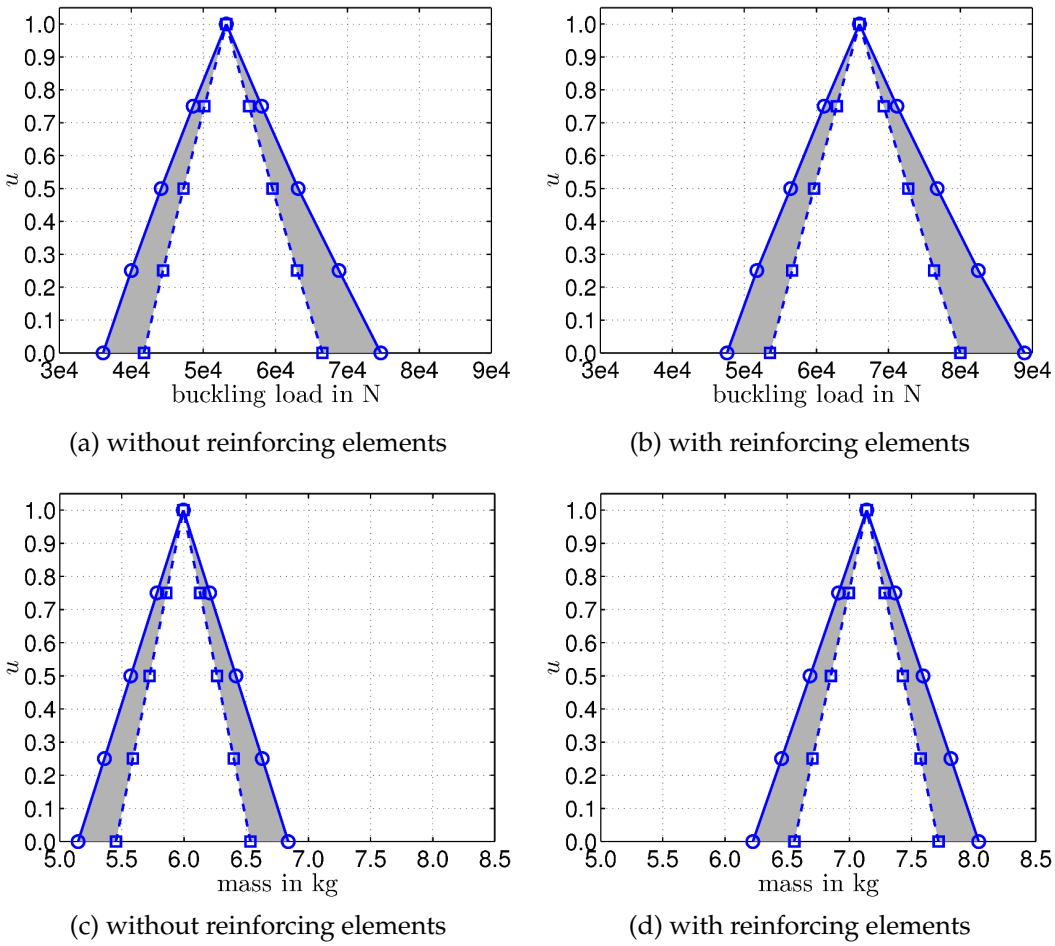

(a) without reinforcing elements

(b) with reinforcing elements

(c) without reinforcing elements

(d) with reinforcing elements

Figure A.30.: Selected properties of fuzzy system answers

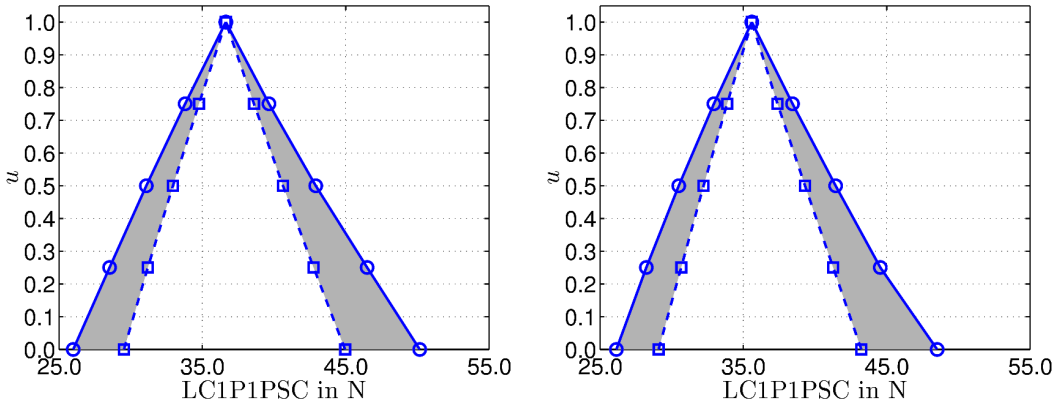

(a) without reinforcing elements

(b) with reinforcing elements

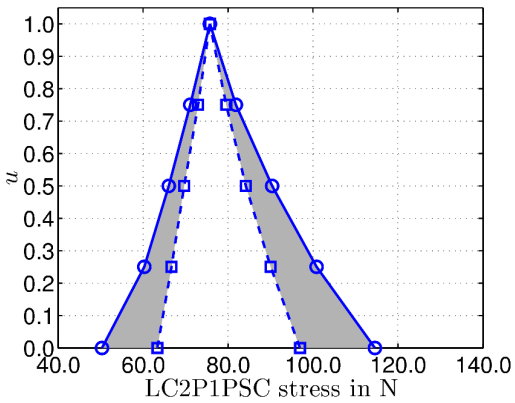

(c) without reinforcing elements

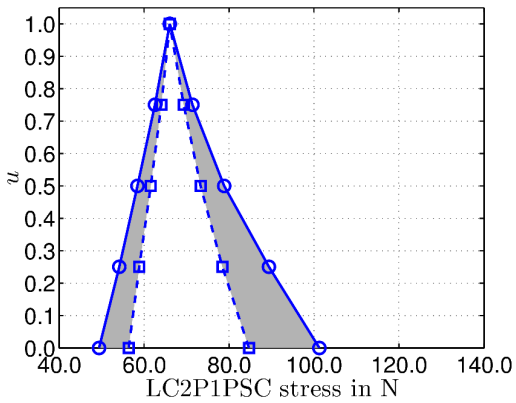

(d) with reinforcing elements

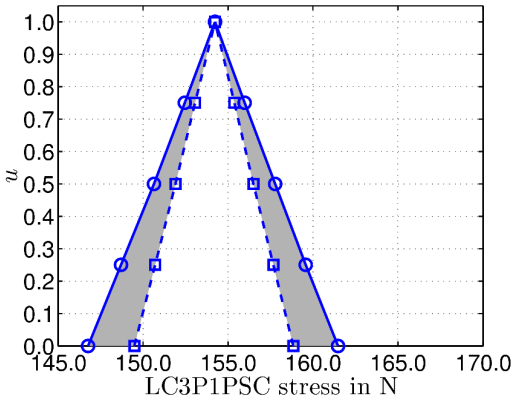

(e) without reinforcing elements

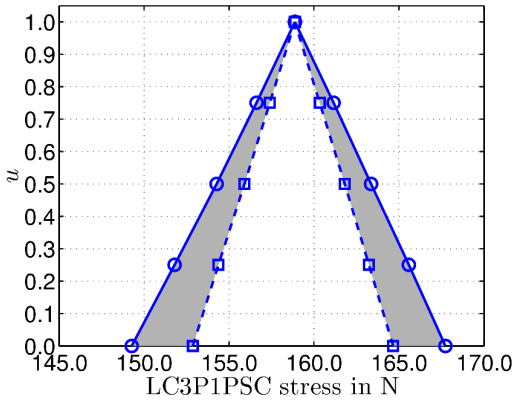

(f) with reinforcing elements

Figure A.31.: Selected properties of fuzzy system answers

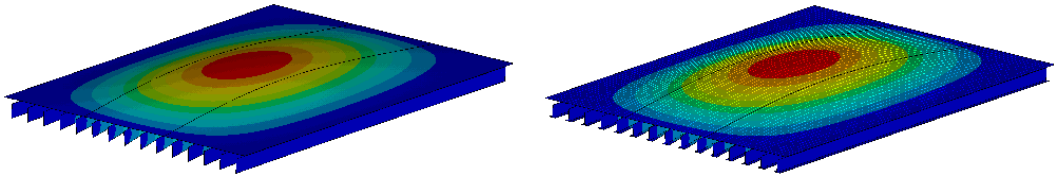

(a) deformation first buckling mode, simple plate

(b) deformation first buckling mode, with I-stringer and reinforcements

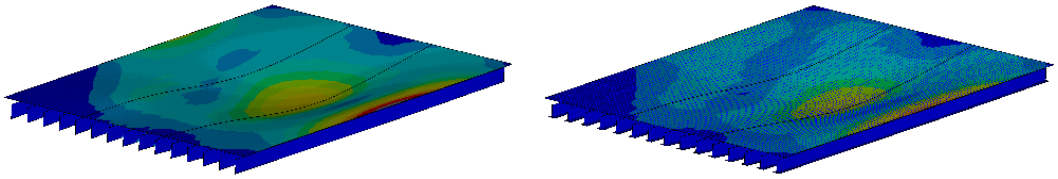

(c) von Mises stress pothole load case, simple plate

(d) von Mises stress pothole load case, with I-stringer and reinforcements

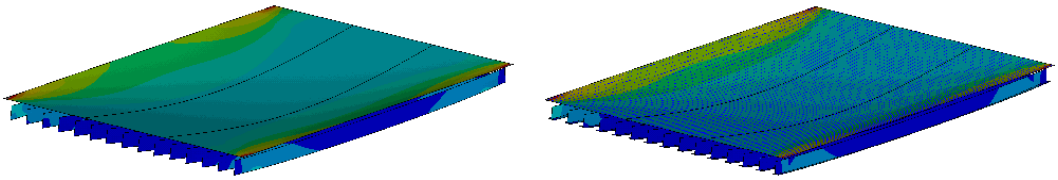

(e) von Mises stress temperature load case, simple plate

(f) von Mises stress temperature load case, with I-stringer and reinforcements

Figure A.32.: Deformation plots for load cases of TR10 example

B. Bibliography

N. Afrin, D.L. Chen, X. Cao, and M. Jahazi. Microstructure and tensile properties of friction stir welded az31b magnesium alloy. *Materials Science and Engineering A*, 472:179–186, 2008.

N. Alberti, R. Di Lorenzo, F. Micari, R. Teti, P. Buonadonna, and A. Manzoni. Intelligent computation techniques for process planning of cold forging. *Journal of Intelligent Manufacturing*, 9(4):353–359, August 1998. ISSN 0956-5515 (Print) 1572-8145 (Online). doi: 10.1023/A:1008982910847. URL http://www.springerlink.com/content/w334522137v755m1/.

S.T. Amancio-Filho, S. Sheikhi, J.F. dos Santos, and C. Bolfarini. Preliminary study on the microstructure and mechanical properties of dissimilar friction stir welds in aircraft aluminium alloys 2024-t351 and 6056-t4. *Journal of Materials Processing Technology*, 206:132–142, 2008.

M.F. Amateau. Progress in the development of graphite-aluminum composites using liquid infiltration technology. *Journal of Composite Materials*, 10(4):279–296, 1976. doi: 10.1177/002199837601000402.

Erik K. Antonsson (ed.). Imprecision in engineering design. Technical report, Engineering Design Research Laboratory, Division of Engineering and Applied Science, California Institute of Technology, Pasadena, 2001. URL http://www.design.caltech.edu/Research/Imprecise/Reading_List/Imprecision_Book.pdf.

Bilal M. Ayyub. *Elicitation of expert opinions for uncertainty and risk*. CRC Press LLC, June 2001. ISBN 978-0849310874.

Horst Baier, Martin Huber, gmundur Petersson, and Erich Wehrle. Multidisciplinary design optimization, 2008. URL http://www.llb.mw.tum.de. Lecture Notes – Institute for Lightweight Structures, Technische Universität München.

H.P. Bao and J.A. Samareh. Affordable design - a methodology to implement process-based manufacturing cost models into the traditional performance-focused multidisciplinary design optimization. In *Proceedings of 8th AIAA/USAF/NASA/ISSMO Symposium on Multidisciplinary Analysis and Optimization*, Long Beach, CA, USA, September 6-8 2000. AIAA-2000-4839.

Michael Beer and Martin Liebscher. Designing robust structures - a nonlinear simulation based approach. *Computers & Structures*, 86(10):1102–1122, 2008. ISSN 0045-7949. doi: 10.1016/j.compstruc.2007.05.037. URL http://www.sciencedirect.com/science/article/B6V28-4P53RK0-2/2/9836b4536130bbf51d264b788e63f4a4. Uncertainty in Structural Analysis - Their Effect on Robustness, Sensitivity and Design.

Richard Ernest Bellman, Robert E. Kalaba, and Lotfi A. Zadeh. Abstraction and pattern classification. Technical report, RAND Corporation (Research ANd Development), October 1964. Memorandum RM-4307-PR.

Hans-Georg Beyer and Bernhard Sendhoff. Robust optimization - a comprehensive survey. *Computer Methods in Applied Mechanics and Engineering*, 196(33-34):3190–3218, 2007. ISSN 0045-7825. doi: 10.1016/j.cma.2007.03.003. URL http://www.sciencedirect.com/science/article/B6V29-4NCSGJK-5/2/5dd8b5afb6be64ceaf371667122d5932.

D. Biermann, K. Weinert, A. Zabel, T. Engbert, and J. Rautenberg. Machining of lightweight frame components. *Advanced Materials Research*, 43:37–46, 2008. doi: 10.4028/www.scientific.net/AMR.43.37. Flexible Manufacture of Lightweight Frame Structures - Phase II: Integration.

A.W. Blom, J. List, P.B. Stickler, and Z. Gürdal. Optimization of a composite cylinder under bending by tailoring stiffness properties in circumferential direction. In *Proceedings of EngOpt 2008 - International Conference on Engineering Optimization*, Rio de Janeiro, Brazil, June 1-5 2008.

J.T. Blucher, U. Narusawa, M. Katsumata, and A. Nemeth. Continuous manufacturing of fiber-reinforced metal matrix composite wires - technology and product characteristics. *Composites: Part A*, 32:1759–1766, 2001.

Rattana Borrisutthekul, Yukio Miyashita, and Yoshiharu Mutoh. Dissimilar material laser welding between magnesium alloy AZ31B and aluminum alloy A5052-O. *Science and Technology of Advanced Materials*, 6(2):199–204, 2005. ISSN 1468-6996. doi: 10.1016/j.stam.2004.11.014. 21st Century COE Program, Nagaoka University of Technology, Hybridized Materials with Super Functions 2005.

Vincent Braibant, Adrien Oudshoorn, Chris Boyer, and Franck Delcroix. Nondeterministic "possibilistic" approaches for structural analysis and optimal design. *AIAA Journal*, 37 (10):1298–1303, 1999.

X. Cao, W. Wallace, J.P. Immarigeon, and C. Poon. Research and progress in laser welding of wrought aluminum alloys. ii. metallurgical microstructures, defects, and mechanical properties. *Materials and Manufacturing Processes*, 18(1):23–49, 2003a. doi: 10.1081/AMP-120017587.

X. Cao, W. Wallace, C. Poon, and J.P. Immarigeon. Research and progress in laser welding of wrought aluminum alloys. i. laser welding processes. *Materials and Manufacturing Processes*, 18(1):1–22, 2003b. doi: 10.1081/AMP-120017586.

X. Cao, M. Jahazi, J.P. Immarigeon, and W. Wallace. A review of laser welding techniques for magnesium alloys. *Journal of Materials Processing Technology*, 171(2):188–204, 2006. ISSN 0924-0136. doi: 10.1016/j.jmatprotec.2005.06.068.

Oscar Castillo and Patricia Melin. *Type-2 Fuzzy Logic: Theory and Applications*. Studies in Fuzziness and Soft Computing. Springer, 1 edition, 2 2008. ISBN 9783540762836.

P. Cavaliere, E. Cerri, and A. Squillace. Mechanical response of 2024-7075 aluminium alloys joined by friction stir welding. *Journal of Materials Science*, 40:3669–3676, 2005.

Enrico Ceglia. European users guide to low gravity platforms, September 2005. URL http://www.spaceflight.esa.int/users/index.cfm?act=default.page&level=1c&page=adv-ug. Erasmus User Centre and Communication Office, ESA.

O. L. Cetin and K. Saitou. Decomposition-based assembly synthesis for structural modularity. *Journal of Mechanical Design*, 126(2):234–243, 2004. doi: 10.1115/1.1666890. URL http://link.aip.org/link/?JMD/126/234/1.

Onur L. Cetin and Kazuhiro Saitou. Decomposition-based assembly synthesis of multiple structures for minimum manufacturing cost. *Journal of Mechanical Design*, 127(4):572–579, 2005. doi: 10.1115/1.1897409. URL http://link.aip.org/link/?JMD/127/572/1.

Shyi-Ming Chen and Chih-Huang Wang. Fuzzy risk analysis based on ranking fuzzy numbers using [alpha]-cuts, belief features and signal/noise ratios. *Expert Systems with Applications*, 36(3, Part 1):5576–5581, 2009. ISSN 0957-4174. doi: 10.1016/j.eswa.2008.06.112.

Sophie Qinghong Chen. *Comparing Probabilistic and Fuzzy Set Approaches for Design in the Presence of Uncertainty*. PhD thesis, Virginia Polytechnic Institute and State University, Blacksburg, 2000. URL http://scholar.lib.vt.edu/theses/available/etd-09122000-00170009/unrestricted/Sophie.pdf.

Wei Chen, Atul Sahai, Achille Messac, and Glynn J. Sundararaj. Exploration of the effectiveness of physical programming in robust design. *Journal of Mechanical Design*, 122(2):155–163, 2000. doi: 10.1115/1.533565. URL http://link.aip.org/link/?JMD/122/155/1.

Kyung Choi, Liu Du, and Byeng Youn. A new fuzzy analysis method for possibility-based design optimization. In *Proceedings of 10th AIAA/ISSMO Multidisciplinary Analysis and Optimization Conference*, Albany, NY, USA, August 30- September 1 2004. AIAA-2004-4585.

Seung-Kyum Choi, Ramana V. Grandhi, and Robert A. Canfield. *Reliability-based Structural Design*. Springer, 1 edition, 10 2006. ISBN 9781846284441. URL http://www.springerlink.com/content/978-1-84628-444-1.

R. Filomeno Coelho and Ph. Bouillard. A multicriteria evolutionary algorithm for mechanical design optimization with expert rules. *International Journal for Numerical Methods in Engineering*, 62(4):516–536, 2005. doi: 10.1002/nme.1198.

Rajan Filomeno Coelho. *Multicriteria Optimization with Expert Rules for Mechanical Design*. PhD thesis, Facult des Sciences Appliques, Universit Libre de Bruxelles, 2004. URL http://www.lania.mx/~ccoello/EMOO/thesis_coelho.pdf.gz.

R.S. Coelho, A. Kostka, H. Pinto, S. Riekehr, M. Koak, and A.R. Pyzalla. Microstructure and mechanical properties of magnesium alloy az31b laser beam welds. *Materials Science and Engineering: A*, 485(1-2):20 – 30, 2008. ISSN 0921-5093. doi: 10.1016/j.msea.2007.07.073.

L. Commin, M. Dumont, J.E. Masse, and L. Barrallier. Friction stir welding of az31 magnesium alloy rolled sheets: Influence of processing parameters. *Acta Materialia*, 57:326–334, 2009. doi: 10.1016/j.actamat.2008.09.011.

Simon Coupland and Robert John. A fast geometric method for defuzzification of type-2 fuzzy sets. *IEEE Transaction on fuzzy systems*, 16(4):929–941, 2008. ISSN 1063-6706. doi: 10.1109/TFUZZ.2008.924345.

Nick Cristello and Il Yong Kim. Multidisciplinary design optimization of a zero-emission vehicle chassis considering crashworthiness and hydroformability. *Proceedings of the Institution of Mechanical Engineers, Part D: Journal of Automobile Engineering*, 221(5):511–526, 2007. doi: 10.1243/09544070JAUTO440. URL http://journals.pepublishing.com/content/v1531773v3t79884.

R. Curran, S. Raghunathan, and M. Price. Review of aerospace engineering cost modelling: The genetic causal approach. *Progress in Aerospace Sciences*, 40(8):487–534, 2004. doi: 10.1016/j.paerosci.2004.10.001.

R. Curran, A. K. Kundu, J. M. Wright, S. Crosby, M. Price, S. Raghunathan, and E. Benard. Modelling of aircraft manufacturing cost at the concept stage. *The International Journal of Advanced Manufacturing Technology*, 31(3-4):407–420, November 2006a. ISSN 0268-3768 (Print) 1433-3015 (Online). doi: 10.1007/s00170-005-0205-8. URL http://www.springerlink.com/content/q66m57r8nx1j0186/.

Richard Curran, Alan Rothwell, and Sylvie Castagne. Numerical method for cost-weight optimization of stringer-skin panels. *Journal of Aircraft*, 43(1):264–274, 2006b. doi: 10.2514/1.13225.

Charalambos Daniilidis. Erstellung qualitativer Modelle zur Beschreibung innovativer Fertigungsprozesse in der Strukturauslegung. term paper: TUM-MW65/0649-SA, 2007.

L. Datashvili, M. Lang, M. Huber, and H. Baier. Accuracy study of a space deployable antenna reflecting surface under 0g and 1g conditions. In *DGLR Jahrbuch Band III 2006*, pages 1685–1693, Braunschweig, Germany, November 6-9 2006. DGLR-2006-044.

Hilde De Gersem, David Moens, Wim Desmet, and Dirk Vandepitte. A fuzzy finite element procedure for the calculation of uncertain frequency response functions of damped structures: Part 2–numerical case studies. *Journal of Sound and Vibration*, 288(3):463–486, 2005. ISSN 0022-460X. doi: 10.1016/j.jsv.2005.07.002. URL http://www.sciencedirect.com/science/article/B6WM3-4H16P3S-7/2/2bdf2b9cfd38897b2fdf970d67713de1. Uncertainty in structural dynamics.

Daan Degrauwe. *Uncertainty propagation in structural analysis by fuzzy numbers*. PhD thesis, Department of Civil Engineering, Katholieke Universiteit Leuven, 2007. URL http://www.kuleuven.be/bwm/papers/phd-daan-07a.pdf.

Anoop K. Dhingra, Singiresu S. Rao, and Virendra Kumar. Nonlinear membership functions in multiobjective fuzzy optimization of mechanical and structural systems. *AIAA Journal*, 30(1):251–260, 1992.

DIN. Strangpressprofile aus Magnesium: Gestaltung, 9711-2. released 1963.

DIN. Strangpressprofile aus Magnesium: Zulässige Abweichungen, 9711-3. released 1963.

S. Donders, D. Vandepitte D, J. Van de Peer, and W. Desmet. The short transformation method to predict the frf of dynamic structures subject to uncertainty. In *Proceedings of*

International Conference on Noise & Vibration Engineering 2004, pages 3043–3054, Leuven, Belgium, September 20-22 2004. URL http://www.isma-isaac.be/publications/PMA_MOD_publications/ISMA2004/3043_3054.pdf.

W. M. Dong and H. C. Shah. Vertex method for computing functions of fuzzy variables. *Fuzzy Sets and Systems*, 24(1):65 – 78, 1987. ISSN 0165-0114. doi: 10.1016/0165-0114(87)90114-X. URL http://www.sciencedirect.com/science/article/B6V05-4C7WMVP-5/2/5061b1e09822217a84a07c08ab29065d.

W. M. Dong and F. S. Wong. Fuzzy weighted averages and implementation of the extension principle. *Fuzzy Sets and Systems*, 21(2):183–199, 1987. ISSN 0165-0114. doi: 10.1016/0165-0114(87)90163-1. URL http://www.sciencedirect.com/science/article/B6V05-4D8W91Y-11/2/5d9dd1f7f502e3672053baf9db87c7d1.

Didier Dubois and Henri Prade. Ranking fuzzy numbers in the setting of possibility theory. *Information Sciences*, 30(3):183–224, 1983. ISSN 0020-0255. doi: 10.1016/0020-0255(83)90025-7.

K. Duran, H. Bernal, and M. Melgarejo. Improved iterative algorithm for computing the generalized centroid of an interval type-2 fuzzy set. In *Fuzzy Information Processing Society, NAFIPS 2008.*, pages 1–5, New York City, NY, May 19–22, 2008. doi: 10.1109/NAFIPS.2008.4531244.

John Durkin. *Expert Systems: Design and Development*. Macmillan, 1st edition, January 1994. ISBN 0023309709.

A. El-Batahgy and M. Kutsuna. Laser beam welding of AA5052, AA5083, and AA6061 aluminum alloys. *Advances in Materials Science and Engineering*, 2009, 2009. doi: 10.1155/2009/974182.

I. Elishakoff. Essay on uncertainties in elastic and viscoelastic structures: From a. m. freudenthal's criticisms to modern convex modeling. *Computers & Structures*, 56(6):871–895, September 1995. doi: {10.1016/0045-7949(94)00499-S}. URL http://dx.doi.org/10.1016/0045-7949(94)00499-S.

I. Elishakoff, R. T. Haftka, and J. Fang. Structural design under bounded uncertainty–optimization with anti-optimization. *Computers & Structures*, 53(6):1401–1405, December 1994. doi: 10.1016/0045-7949(94)90405-7. URL http://dx.doi.org/10.1016/0045-7949(94)90405-7.

Isaac Elishakoff and Yongjian Ren. The bird's eye view on finite element method for structures with large stochastic variations. *Computer Methods in Applied Mechanics and Engineering*, 168(1-4):51 – 61, 1999. ISSN 0045-7825. doi: 10.1016/S0045-7825(98)00133-9. URL http://www.sciencedirect.com/science/article/B6V29-3W28VR6-5/2/27807c2126c17b13c6bc9b2ec8c3a051.

Isaac Elishakoff and Yongjian Ren. *Finite Element Methods for Structures with Large Stochastic Variations (Oxford Texts in Applied and Engineering Mathematics, 7)*. Oxford University Press, USA, 9 2003. ISBN 9780198526315.

DIN EN. Aluminium und Aluminiumlegierungen - Stranggepresste Präzisionsprofile aus Legierungen EN AW-6060 und EN AW-6063 - Teil 2: Grenzabmaße und Formtoleranzen, 12020-2. released 2008.

DIN EN. Aluminium und Aluminiumlegierungen - Stranggepresste Stangen, Rohre und Profile - Teil 8: Mit Kammerwerkzeug stranggepresste Rohre, Grenzabmaße und Formtoleranzen, 755-9. released 2008.

J.A. Esparza, W.C. Davis, E.A. Trillo, and L.E. Murr. Friction-stir welding of magnesium alloy az31b. *Journal of Materials Science Letters*, 21:917–920, 2002.

European Aluminium Association. aluselect homepage. http://aluminium.matter.org.uk/aluselect/, 2009.

Horst E. Friedrich and Barry L. Mordike. *Magnesium technology: metallurgy, design, data, applications*. Springer, 1 edition, January 2006. ISBN 978-3540205999.

K. Gantois and A.J. Morris. The multi-disciplinary design of a large-scale civil aircraft wing taking account of manufacturing costs. *Structural and Multidisciplinary Optimization*, 28 (1):31–46, 2004. doi: 10.1007/s00158-004-0427-7. URL http://dx.doi.org/10.1007/s00158-004-0427-7.

R. Gleichmar. *Approximationen und paralleles Rechnen bei der multidisziplinären Strukturoptimierung*. PhD thesis, Institute for Lightweight Structures - Technische Universität München, 2004. URL http://nbn-resolving.de/urn/resolver.pl?urn:nbn:de:bvb:91-diss20050628-1119013588.

Sarah Greenfield, Robert John, and Simon Coupland. A novel sampling method for type-2 defuzzification. In *Proceedings of 5th annual UK Workshop on Computational Intelligence (UKCI) 2005*, pages 120–127, London, UK, September 5-7 2005. URL http://www.dcs.bbk.ac.uk/ukci05/ukci05proceedings.pdf.

Wang Guang-Yuan and Wang Wen-Quan. Fuzzy optimum design of structures. *Engineering Optimization*, 8(4):291–300, 1985. ISSN 0305-215X. URL http://www.informaworld.com/10.1080/03052158508902491/.

M. Güden, O. Akil, A. Tasdemirci, M. Ciftcioglu, and I.W. Hall. Effect of strain rate on the compressive mechanical behavior of a continuous alumina fiber reinforced ZE41A magnesium alloy based composite. *Materials Science and Engineering A*, 425:145–155, 2006.

Satyandra K. Gupta, William C. Regli, Diganta Das, and Dana S. Nau. Automated manufacturability analysis: A survey. *Research in Engineering Design*, 9(3):168–190, September 1997. ISSN 0934-9839 (Print) 1435-6066 (Online). doi: 10.1007/BF01596601. URL http://www.springerlink.com/content/p8p5516251023777/.

Hussam Hamrawi and Simon Coupland. Type-2 fuzzy arithmetic using alpha-planes. In *Proceedings of IFSA-EUSFLAT 2009*, pages 606–611, Lisbon, Portugal, July 20-24 2009. ISBN: 9789899507968.

Michael Hanss. The transformation method for the simulation and analysis of systems with uncertain parameters. *Fuzzy Sets and Systems*, 130(3):277–289, 2002. ISSN 0165-0114. doi: 10.1016/S0165-0114(02)00045-3. URL http://www.sciencedirect.com/science/article/B6V05-45G00MM-4/2/46193dea3d4b57268d67467a84c65b37.

G.J. Hayes, D.D. Edie, and J.M. Kennedy. The recoil compressive strength of pitch-based carbon fibres. *Journal of Materials Science*, 28:3247–3257, 1993.

Li-Ping He and Fu-Zheng Qu. Possibility and evidence theory-based design optimization: an overview. *Kybernetes*, 37(9/10):1322–1330, 2008. ISSN 0368-492X. doi: 10.1108/03684920810907616. URL http://www.emeraldinsight.com/10.1108/03684920810907616.

Robert R. Hoffman, Nigel R. Shadbolt, A. Mike Burton, and Gary Klein. Eliciting knowledge from experts: A methodological analysis. *Organizational Behavior and Human Decision Processes*, 62(2):129–158, May 1995. doi: 10.1006/obhd.1995.1039. URL http://dx.doi.org/10.1006/obhd.1995.1039.

Martin Huber and Horst Baier. Qualitative knowledge and manufacturing considerations in multidisciplinary structural optimization of hybrid material structures. *Advanced Materials Research*, 10:143–152, 2006. doi: 10.4028/www.scientific.net/AMR.10.143. Flexible Manufacture of Lightweight Frame Structures.

Martin Huber, Ögmundur Petersson, and Horst Baier. Knowledge-based modeling of manufacturing aspects in structural optimization problems. *Advanced Materials Research*, 43:111–122, 2008. doi: 10.4028/www.scientific.net/AMR.43. Flexible Manufacture of Lightweight Frame Structures - Phase II: Integration.

Martin Huber, Erich Wehrle, and Horst Baier. Entwurfsoptimierung. In A. Erman Tekkaya, Horst Baier, Dirk Biermann, Detlef Löhe, Volker Schulze, Michael Zäh, and Michael Marré, editors, *Integration von Umformen, Trennen und Fügen für die flexible Fertigung von leichten Tragwerkstrukturen; Zwischenbericht Phase 2; 1. Januar 2007 - 31. Dezember 2008*, pages 257–274. VDI Verlag, 2009. ISBN 978-3-18-366802-1. Fortschritt-Berichte Fertigungstechnik, Band Nr. 668.

Martin Huber, Daniel Neufeld, Joon Chung, Horst Baier, and Kamran Behdinan. Data mining based mutation function for engineering problems with mixed continuous-discrete design variables. *Structural and Multidisciplinary Optimization*, 41(4):589–604, 2010. ISSN 1615-147X (Print) 1615-1488 (Online). doi: 10.1007/s00158-009-0439-4.

W. Hufnagel. *Aluminium-Taschenbuch*. Aluminium-Verlag Düsseldorf, 14 edition, 1984. ISBN 3-87017-169-3.

B. Hug, H. Baier, and R. Füssinger. Neuere Auslegungsmethoden und Werkstoffe bei der Entwicklung hochmobiler Brücken. *Der Stahlbau*, 3(52):85–89, 1983. URL http://www.ernst-und-sohn.de/zeitschriften/artikelrecherche/artikel.php?ID=3992.

Hector A. Jensen. Structural optimal design of systems with imprecise properties: a possibilistic approach. *Advances in Engineering Software*, 32(12): 937–948, 2001. ISSN 0965-9978. doi: 10.1016/S0965-9978(01)00038-2. URL http://www.sciencedirect.com/science/article/B6V1P-45461HY-7/2/fd0c385c82d8a46146884efe193689f4.

C. Jiang, X. Han, and G.R. Liu. Optimization of structures with uncertain constraints based on convex model and satisfaction degree of interval. *Computer Methods in Applied Mechanics and Engineering*, 196(49-52):4791–4800, November 2007. doi: 10.1016/j.cma.2007.03.024. URL http://dx.doi.org/10.1016/j.cma.2007.03.024.

C. Jiang, X. Han, and G.P. Liu. A sequential nonlinear interval number programming method for uncertain structures. *Computer Methods in Applied Mechanics and Engineering*, 197(49-50):4250–4265, September 2008. doi: 10.1016/j.cma.2008.04.027. URL http://dx.doi.org/10.1016/j.cma.2008.04.027.

R. Jin, X. Du, and W. Chen. The use of metamodeling techniques for optimization under uncertainty. *Structural and Multidisciplinary Optimization*, 25(2):99–116, July 2003. ISSN 1615-147X (Print) 1615-1488 (Online). doi: 10.1007/s00158-002-0277-0. URL http://www.springerlink.com/content/ll4xa5t7fe9qm0br/.

Florian Jurecka. *Robust Design Optimization Based on Metamodeling Techniques*. Schriftenreihe des Lehrstuhls fr Statik TU München. Shaker Verlag, 2007. ISBN 978-3-8322-6390-4. PhD thesis.

K.U. Kainer. *Magnesium alloys and technology*. Wiley-VCH, 1 edition, 2003. ISBN 978-3527305704.

Nilesh N. Karnik and Jerry M. Mendel. Centroid of a type-2 fuzzy set. *Information Sciences*, 132(1-4):195–220, 2001. ISSN 0020-0255. doi: 10.1016/S0020-0255(01)00069-X.

Christos Kassapoglou. Simultaneous cost and weight minimization of composite-stiffened panels under compression and shear. *Composites Part A: Applied Science and Manufacturing*, 28(5):419–435, 1997. ISSN 1359-835X. doi: {10.1016/S1359-835X(96)00141-8}. URL http://dx.doi.org/10.1016/S1359-835X(96)00141-8.

Christos Kassapoglou. Minimum cost and weight design of fuselage frames: Part a: design constraints and manufacturing process characteristics. *Composites Part A: Applied Science and Manufacturing*, 30(7):887–894, July 1999a. ISSN 1359-835X. doi: {10.1016/S1359-835X(98)00190-0}. URL http://dx.doi.org/10.1016/S1359-835X(98)00190-0.

Christos Kassapoglou. Minimum cost and weight design of fuselage frames : Part b: cost considerations, optimization, and results. *Composites Part A: Applied Science and Manufacturing*, 30(7):895–904, July 1999b. ISSN 1359-835X. doi: {10.1016/S1359-835X(98)00191-2}. URL http://dx.doi.org/10.1016/S1359-835X(98)00191-2.

Matthias Kleiner, Alexander Klaus, and Michael Schomäcker. Composite extrusion determination of the influencing factors on the positioning of the reinforcing elements. *Advanced Materials Research*, 10:13–22, 2006. doi: 10.4028/www.scientific.net/AMR.10.13.

Andreas Klimke. An efficient implementation of the transformation method of fuzzy arithmetic (extended preprint version). Technical Report Preprint 2003/009, Institute for Applied Analysis and Numerical Simulation (IANS) - University of Stuttgart, 2003. URL http://preprints.ians.uni-stuttgart.de/downloads/2003/2003-009.pdf.

Andreas Klimke. *Uncertainty modeling using fuzzy arithmetic and sparse grids*. PhD thesis, Institut fr Angewandte Analysis und Numerische Simulation, Fakultät Mathematik und Physik, Universität Stuttgart, 2006. URL http://www.ians.uni-stuttgart.de/nmh/publications/download/klimke_thesis.pdf.

Andreas Klimke. Sparse grid surrogate functions for nonlinear systems with parameter uncertainty. In *Proceedings of the 1st International Conference on Uncertainty in Structural Dynamics*, pages 159–168, Sheffield, UK, June 11-13 2007. URL http://www.ians.uni-stuttgart.de/nmh/publications/download/USD2007-Klimke-v2.pdf.

Andreas Klimke and Barbara Wohlmuth. Algorithm 847: spinterp: piecewise multilinear hierarchical sparse grid interpolation in matlab. *ACM Transactions on Mathematical Software (TOMS)*, 31(4):561–579, 2005. ISSN 0098-3500. doi: http://doi.acm.org/10.1145/1114268.1114275.

Andreas Klimke, Kai Willner, and Barbara Wohlmuth. Uncertainty modeling using fuzzy arithmetic based on sparse grids: applications to dynamic systems. *International Journal of Uncertainty, Fuzziness & Knowledge-Based Systems*, 12(6):745–759, 2004. ISSN 02184885.

Andreas Klimke, Ronaldo F. Nunes, and Barbara I. Wohlmuth. Fuzzy arithmetic based on dimension-adaptive sparse grids: a case study of a large-scale finite element model under uncertain parameters. *International Journal of Uncertainty, Fuzziness & Knowledge-Based Systems*, 14(5):561–577, 2006. ISSN 02184885. URL http://search.ebscohost.com/login.aspx?direct=true&db=buh&AN=22673713&site=ehost-live.

George J. Klir. On fuzzy-set interpretation of possibility theory. *Fuzzy Sets and Systems*, 108 (3):263–273, 1999. ISSN 0165-0114. doi: DOI:10.1016/S0165-0114(97)00371-0.

T. Kloppenborg, M. Schikorra, and A.E. Tekkaya. Optimization of the reinforcement position in aluminum composite extrusion. In *Proceedings of the 11th International Conference on Aluminium Alloys*, volume 2, pages 1345–1352, Aachen, Germany, September 22-26 2008a.

T. Kloppenborg, N.B. Khalifa, and A.E. Tekkaya. Accurate welding line prediction in extrusion processes. *Key Engineering Materials*, 424:87–95, 2009. ISSN 1013-9826. doi: 10.4028/www.scientific.net/KEM.424.87.

Thomas Kloppenborg, Thilo Hammers, Marco Schikorra, Eberhard Kerscher, A.E. Tekkaya, and Detlef Löhe. Prototype manufacturing of extruded aluminum aircraft stringer profiles with continuous reinforcement. *Advanced Materials Research*, 43:167–174, 2008b. doi: 10.4028/www.scientific.net/AMR.43.167.

Patrick Koch, Oleg Golovidov, and Brett Wujekand Timothy Simpson. Facilitating probabilistic multidisciplinary optimization using kriging approximation models. In *Proceedings of 9th AIAA/ISSMO Symposium on Multidisciplinary Analysis and Optimization*, Atlanta, GA, USA, September 4-6 2002. URL http://edog.mne.psu.edu/pdfs/AIAA-2002-5415.pdf. AIAA-2002-5415.

Pawel Kolodziejczak and Wojciech Kalita. Properties of co2 laser-welded butt joints of dissimilar magnesium alloys. *Journal of Materials Processing Technology*, 209(2):1122 – 1128, 2009. ISSN 0924-0136. doi: DOI:10.1016/j.jmatprotec.2008.03.072.

P. Kumar and P. Bauer. Progressive design methodology for complex engineering systems based on multiobjective genetic algorithms and linguistic decision making. *Soft Computing - A Fusion of Foundations, Methodologies and Applications*, 13(7):649–679, May 2009. ISSN 1432-7643 (Print) 1433-7479 (Online). doi: 10.1007/s00500-008-0371-3. URL http://www.springerlink.com/content/47gk67jp341842j3/.

Ajoy Kundu, Richard Curran, S. Crosby, and Srinivasan Ragunathan. Rapid cost modelling at the conceptual stage of aircraft design. In *Proceedings of AIAA's Aircraft Technology, Integration, and Operations (ATIO) 2002 Technical Forum*, Los Angeles, CA, USA, October 1-3 2002. AIAA-2002-5853.

Michael Lang. *Integrierte Modellierung für Strukturentwurf und thermoelastische Auslegung von Satellitenreflektoren*. PhD thesis, Institute for Lightweight Structures - Technische Universität München, 2009. URL http://nbn-resolving.de/urn/resolver.pl?urn:nbn:de:bvb:91-diss-20081218-680432-1-4.

Harald Langer. *Extended Evolutionary Algorithms for Multiobjective and Discrete Design Optimization of Structures*. PhD thesis, Institute for Lightweight Structures - Technische Universität München, 2005. URL http://nbn-resolving.de/urn/resolver.pl?urn:nbn:de:bvb:91-diss20061108-1512163206.

William Sauway Law. *Evaluating imprecision in engineering design*. PhD thesis, California Institute of technology, Pasadena, 1996. URL http://www.design.caltech.edu/Research/Imprecise/Papers/wslthes.pdf.

Stuart M. Lee. *Handbook of composites reinforcements*. Wiley-VCH, 1 edition, November 1992. ISBN 978-0-471-18861-2.

K.H. Leong, G. Komecki, P.G. Sanders, and J.S. Keske. Laser beam welding of AZ31B-H24 magnesium alloy. In *Proceedings of 17th International Congress on Applications of Lasers and Electro-Optics (ICALEO '98)*, Orlando, USA, September 16–19 1998. URL http://www.osti.gov/bridge/servlets/purl/10805-fDzLFJ/webviewable/.

D. Y. Li, Y. H. Peng, and J. L. Yin. Optimization of metal-forming process via a hybrid intelligent optimization technique. *Structural and Multidisciplinary Optimization*, 34(3):229–241, September 2007. ISSN 1615-147X (Print) 1615-1488 (Online). doi: 10.1007/s00158-006-0075-1. URL http://www.springerlink.com/content/a66466g784161632/.

Feilong Liu. An efficient centroid type-reduction strategy for general type-2 fuzzy logic system. *Information Sciences*, 178(9):2224–2236, 2008. ISSN 0020-0255. doi: 10.1016/j.ins.2007.11.014.

Liming Liu, Heng Wang, Gang Song, and Jianan Ye. Microstructure characteristics and mechanical properties of laser weld bonding of magnesium alloy to aluminum alloy. *Journal of Materials Science*, 42(2):565–572, 2007. ISSN 1573-4803. doi: 10.1007/s10853-006-1068-6. URL http://www.springerlink.com/content/n00r1t4042820w12/.

Qing Liu and Singiresu S. Rao. Fuzzy finite element approach for analysis of fiber-reinforced laminated composite beams. *AIAA Journal*, 43(3):651–661, 2005. doi: 10.2514/1.940.

Wenli Liu and Richard Butler. Optimum buckling design for composite wing cover panels with manufacturing constraints. In *Proceedings of 48st AIAA/ASME/ASCE/AHS/ASC Structures, Structural Dynamics, and Materials Conference and Exhibit*, Honolulu, Hawaii, USA, April 23-26 2007. AIAA-2007-2215.

Marco Lombardi and Raphael T. Haftka. Anti-optimization technique for structural design under load uncertainties. *Computer Methods in Applied Mechanics and Engineering*, 157(1-2):

19–31, April 1998. doi: {10.1016/S0045-7825(97)00148-5}. URL http://dx.doi.org/10.1016/S0045-7825(97)00148-5.

S.N. Lophaven, H.B. Nielsen, and J. Søndergaard. DACE - a matlab kriging toolbox, version 2.0. Technical Report Report IMM-TR-2002-12, Department of Informatics and Mathematical Modelling - Technical University of Denmark, 2002a. URL http://www2.imm.dtu.dk/$\sim$hbn/dace/dace.pdf.

S.N. Lophaven, H.B. Nielsen, and J. Søndergaard. Aspects of the matlab toolbox DACE. Technical Report Report IMM-REP-2002-13, Department of Informatics and Mathematical Modelling - Technical University of Denmark, 2002b. URL http://www.imm.dtu.dk/$\sim$hbn/publ/TR0213.ps.

Naesung Lyu and Kazuhiro Saitou. Decomposition-based assembly synthesis of a three-dimensional body-in-white model for structural stiffness. *Journal of Mechanical Design*, 127 (1):34–48, 2005. doi: 10.1115/1.1799551. URL http://link.aip.org/link/?JMD/127/34/1.

M.W. Mahoney, C.G. Rhodes J.G. Flintoff, R.A. Spurling, and W.H. Bingel. Properties of friction-stir-welded 7075 t651 aluminum. *Metallurgical and Materials Transactions A*, 29A: 1955–1964, 1998.

Michael P. Martinez, Achille Messac, and Masoud Rais-Rohani. Manufacturability-based optimization of aircraft structures using physical programming. *AIAA Journal*, 39(3):517–525, 2001.

F. Massa, T. Tison, and B. Lallem. A fuzzy procedure for the static design of imprecise structures. *Computer Methods in Applied Mechanics and Engineering*, 195(9-12):925–941, February 2006. doi: 10.1016/j.cma.2005.02.015. URL http://dx.doi.org/10.1016/j.cma.2005.02.015.

F. Massa, K. Ruffin, T. Tison, and B. Lallem. A complete method for efficient fuzzy modal analysis. *Journal of Sound and Vibration*, 309(1-2):63–85, 2008. doi: 10.1016/j.jsv.2007.06.004. URL http://dx.doi.org/10.1016/j.jsv.2007.06.004.

F. Massa, B. Lallem, and T. Tison. Fuzzy multiobjective optimization of mechanical structures. *Computer Methods in Applied Mechanics and Engineering*, 198(5-8):631–643, 2009. doi: 10.1016/j.cma.2008.09.010. URL http://dx.doi.org/10.1016/j.cma.2008.09.010.

Tadashi Matsunaga, Kenji Matsuda, Tomei Hatayama, Kenji Shinozaki, and Makoto Yoshida. Fabrication of continuous carbon fiber-reinforced aluminummagnesium alloy composite wires using ultrasonic infiltration method. *Composites: Part A*, 38:1902–1911, 2007.

Stewart McWilliam. Anti-optimisation of uncertain structures using interval analysis. *Computers & Structures*, 79(4):421–430, February 2001. doi: {10.1016/S0045-7949(00)00143-7}. URL http://dx.doi.org/10.1016/S0045-7949(00)00143-7.

M. Melgarejo. A fast recursive method to compute the generalized centroid of an interval type-2 fuzzy set. In *North American Fuzzy Information Processing Society, NAFIPS 2007.*, pages 190–194, San Diego, CA, June 24–27, 2007. doi: 10.1109/NAFIPS.2007.383835.

J. M. Mendel and Feilong Liu. On new quasi-type-2 fuzzy logic systems. In *Fuzzy Systems, 2008. FUZZ-IEEE 2008. (IEEE World Congress on Computational Intelligence). IEEE International Conference on*, pages 354–360, Hong Kong, June 1–6, 2008. doi: 10.1109/FUZZY.2008.4630390.

J. M. Mendel, F. Liu, and D. Zhai. Alpha-plane representation for type-2ffuzzy sets: Theory and applications. *IEEE Transactions on Fuzzy Systems: Accepted for future publication*, 2009. ISSN 1063-6706. doi: 10.1109/TFUZZ.2009.2024411.

Jerry M. Mendel. *Uncertain Rule-Based Fuzzy Logic Systems: Introduction and New Directions*. Prentice Hall PTR, 1 2001. ISBN 9780130409690.

Jerry M. Mendel. On a 50% savings in the computation of the centroid of a symmetrical interval type-2 fuzzy set. *Information Sciences*, 172(3-4):417–430, 2005. ISSN 0020-0255. doi: 10.1016/j.ins.2004.04.006.

Thomas Menzel. *Wissensbasierte Methoden für die rechnergestützte Charakterisierung und Bewertung innovativer Fertigungsprozesse*. Bericht aus dem Lehrstuhl für Fertigungstechnologie. Meisenbach Verlag, Bamberg, Germany, 2001. ISBN 3875251423. PhD thesis.

Matthias Merzkirch, Kay Weidenmann, Eberhard Kerscher, and Detlef Löhe. Werkstoffsysteme für verstärkte Leichtbauprofile. In A. Erman Tekkaya, Horst Baier, Dirk Biermann, Detlef Löhe, Volker Schulze, Michael Zäh, and Michael Marré, editors, *Integration von Umformen, Trennen und Fügen für die flexible Fertigung von leichten Tragwerkstrukturen; Zwischenbericht Phase 2; 1. Januar 2007 - 31. Dezember 2008*, pages 45–64. VDI Verlag, 2009. ISBN 978-3-18-366802-1. Fortschritt-Berichte Fertigungstechnik, Band Nr. 668.

Achille Messac. Physical programming: Effective optimization for computational design. *AIAA Journal*, 34(1):149–158, 1996.

Achille Messac and Amir Ismail-Yahaya. Multiobjective robust design using physical programming. *Structural and Multidisciplinary Optimization*, 23(5):357–371, June 2002. ISSN 1615-147X (Print) 1615-1488 (Online). doi: 10.1007/s00158-002-0196-0. URL http://www.springerlink.com/content/0k1x0twrpff3k1jg/.

D. Moens and D. Vandepitte. Recent advances in non-probabilistic approaches for non-deterministic dynamic finite element analysis. *Archives of Computational Methods in Engineering*, 13(3):389–464, September 2006. ISSN 1134-3060 (Print) 1886-1784 (Online). doi: 10.1007/BF02736398. URL http://www.springerlink.com/content/15736572654407t2/.

David Moens and Dirk Vandepitte. A survey of non-probabilistic uncertainty treatment in finite element analysis. *Computer Methods in Applied Mechanics and Engineering*, 194(12-16):1527–1555, 2005a. ISSN 0045-7825. doi: 10.1016/j.cma.2004.03.019. URL http://www.sciencedirect.com/science/article/B6V29-4DS9CKN-1/2/f61085634e641be21071e824136d551c. Special Issue on Computational Methods in Stochastic Mechanics and Reliability Analysis.

David Moens and Dirk Vandepitte. A fuzzy finite element procedure for the calculation of uncertain frequency-response functions of damped structures: Part 1–procedure. *Journal of Sound and Vibration*, 288(3):431–462, 2005b. ISSN 0022-460X. doi: 10.1016/j.jsv.2005.07.001. URL http://www.sciencedirect.com/science/

article/B6WM3-4GXVG98-4/2/56fa9cc30754924aa645e17892884f4d. Uncertainty in structural dynamics.

Bernd Möller and Michael Beer. *Fuzzy Randomness: Uncertainty in Civil Engineering and Computational Mechanics*. Springer, 1 edition, 3 2004. ISBN 9783540402947.

P. Moreira, T. Santos, S. Tavares, V. Richter-Trummer, P. Vilaca, and P. de Castro. Mechanical characterization of friction stir welds of two dissimilar aluminium alloys of the 6xxx series. *Materials Science Forum*, 587–588:430–434, 2008.

Zissimos P. Mourelatos and Jun Zhou. Reliability estimation and design with insufficient data based on possibility theory. *AIAA Journal*, 43(8):1696–1705, 2005.

Zissimos P. Mourelatos and Jun Zhou. Non-probabilistic design optimization with insufficient data using possibility and evidence theories. In Yiannis Tsompanakis, Nikkos D. Lagaros, and Manolis Papadrakakis, editors, *Structural Design Optimization Considering Uncertainties: Vol.1., Structures & Infrastructures Series*, part 10, pages 247–279. Taylor & Francis, 1 edition, 3 2008. ISBN 9780415452601.

Eric Neussl, Peter R. Sahm, and Harvey M. Flower. Continuous fiber reinforced aluminum matrix composites - influence of the alloy composition on the mechanical properties. *Advanced Engineering Materials*, 2(9):587–592, 2000.

Adnan Niazi, Jian S. Dai, Stavroula Balabani, and Lakmal Seneviratne. Product cost estimation: Technique classification and methodology review. *Journal of Manufacturing Science and Engineering*, 128(2):563–575, 2006. doi: 10.1115/1.2137750. URL http://link.aip.org/link/?MAE/128/563/1.

Efstratios Nikolaidis, Dan M. Ghiocel, and Suren Singhal, editors. *Engineering Design Reliability Handbook*. CRC Press, 1 edition, 7 2005. ISBN 9780849311802.

Novespace. Parabolic flight campaign with a300 zero-g user's manual, July 1999. URL http://www.novespace.fr/en,home.html.

R.F. Nunes, A. Klimke, and J.R.F. Arruda. On estimating frequency response function envelopes using the spectral element method and fuzzy sets. *Journal of Sound and Vibration*, 291(3-5):986 – 1003, 2006. ISSN 0022-460X. doi: 10.1016/j.jsv.2005.07.024. URL http://dx.doi.org/10.1016/j.jsv.2005.07.024.

Qi Pan. Realization of soft restrictions with the help of fuzzy numbers, 2009. term thesis TUM-MW65/0815-SA.

Sp.G. Pantelakis, Ch.V. Katsiropoulos, G.N. Labeas, and H. Sibois. A concept to optimize quality and cost in thermoplastic composite components applied to the production of helicopter canopies. *Composites Part A: Applied Science and Manufacturing*, 40 (5):595–606, May 2009. ISSN 1359-835X. doi: 10.1016/j.compositesa.2009.02.012. URL http://dx.doi.org/10.1016/j.compositesa.2009.02.012.

Gyung-Jin Park, Tae-Hee Lee, Kwon Hee Lee, and Kwang-Hyeon Hwang. Robust design: An overview. *AIAA Journal*, 44(1):181–191, 2006.

Yajie Quan, Zhenhua Chen, Xiaosan Gong, and Zhaohui Yu. Co2 laser beam welding of dissimilar magnesium-based alloys. *Materials Science and Engineering: A*, 496(1-2):45 – 51, 2008a. ISSN 0921-5093. doi: DOI:10.1016/j.msea.2008.04.065.

Y.J. Quan, Z.H. Chen, X.S. Gong, and Z.H. Yu. Effects of heat input on microstructure and tensile properties of laser welded magnesium alloy az31. *Materials Characterization*, 59(10): 1491–1497, 2008b. ISSN 1044-5803. doi: 10.1016/j.matchar.2008.01.010.

M. Rais-Rohani and M.N. Singh. Comparison of global and local response surface techniques in reliability-based optimization of composite structures. *Structural and Multidisciplinary Optimization*, 26(5):333–345, March 2004. ISSN 1615-147X (Print) 1615-1488 (Online). doi: 10.1007/s00158-003-0353-0. URL http://www.springerlink.com/content/lfyk0h79hetxy1wj/.

Masoud Rais-Rohani. Manufacturing and cost considerations in multidisciplinary aircraft design. Technical Report NASA/CR-96-206151, NASA, 1996. URL http://ntrs.nasa.gov/archive/nasa/casi.ntrs.nasa.gov/19970040675_1997087421.pdf. NASA Grant NAG1-1716.

Masoud Rais-Rohani. A framework for preliminary design of aircraft structures based on process information - part 1 & 2. Technical report, NASA, 1998. URL http://ntrs.nasa.gov/archive/nasa/casi.ntrs.nasa.gov/19990018151_1999007106.pdf. NASA Grant NAG1-1716, only Part 1 is available online, Part 2 was provided personally by Mr. Rais-Rohani.

Masoud Rais-Rohani and Zhaohui Huo. Analysis and optimization of primary aircraft structures based on strength, manufacturability, and cost requirements. In *Proceedings of AIAA/ASME/ASCE/AHS/ASC Structures, Structural Dynamics, and Materials Conference and Exhibit*, volume 2, St. Louis, MO, USA, April 12-15 1999. AIAA-1999-1328.

Masoud Rais-Rohani and Qiulin Xie. Probabilistic structural optimization under reliability, manufacturability, and cost constraints. *AIAA Journal*, 43(4):864–873, 2005. doi: 10.2514/1.2048.

Singiresu S. Rao and L. Berke. Analysis of uncertain structural systems using interval analysis. *AIAA Journal*, 35(4):727–735, 1997. doi: 10.2514/2.164.

Singiresu S. Rao and Lingtao Cao. Fuzzy boundary element method for the analysis of imprecisely defined systems. *AIAA Journal*, 39(9):1788–1797, 2001. doi: 10.2514/2.1510.

Singiresu S. Rao and Qing Liu. Fuzzy approach to the mechanics of fiber-reinforced composite materials. *AIAA Journal*, 42(1):159–167, 2004. doi: 10.2514/1.9039.

Singiresu S. Rao and James P. Sawyer. Fuzzy finite element approach for analysis of imprecisely defined systems. *AIAA Journal*, 33(12):2364–2370, 1995. doi: 10.2514/3.12910.

Singiresu S. Rao, Li Chen, and Eric Mulkay. Unified finite element method for engineering systems with hybrid uncertainties. *AIAA Journal*, 36(7):1291–1299, 1998. doi: 10.2514/2.513.

S.S. Rao. Multi-objective optimization of fuzzy structural systems. *International Journal for Numerical Methods in Engineering*, 24(6):1157–1171, 1987. URL http://dx.doi.org/10.1002/nme.1620240608.

S.S. Rao and Li Chen. Generalized hybrid method for fuzzy multiobjective optimization of engineering systems. *AIAA Journal*, 34(8):1709–1717, 1996.

Mark Russell-Stevens, Richard Todd, and Maria Papakyriacou. The effect of thermal cycling on the properties of a carbon fibre reinforced magnesium composite. *Materials Science and Engineering A*, 397:249–256, 2005.

Kazuhiro Saitou, Kazuhiro Izui, Shinji Nishiwaki, and Panos Papalambros. A survey of structural optimization in mechanical product development. *Journal of Computing and Information Science in Engineering*, 5(3):214–226, 2005. doi: 10.1115/1.2013290. URL http://link.aip.org/link/?CIS/5/214/1.

Marco Schikorra and Matthias Kleiner. Seam weld positioning for composite extrusion. *Advanced Materials Research*, 10:101–110, 2006. doi: 10.4028/www.scientific.net/AMR.10.101.

G.I. Schuëller and H.A. Jensen. Computational methods in optimization considering uncertainties - an overview. *Computer Methods in Applied Mechanics and Engineering*, 198(1):2–13, 2008. ISSN 0045-7825. doi: 10.1016/j.cma.2008.05.004. URL http://www.sciencedirect.com/science/article/B6V29-4SHF4D2-1/2/341eb6c39a7902978a343732782ac295.

Gerd Schumacher. *Multidisziplinäre, fertigungsgerechte Optimierung von Faserverbund-Flächentragwerken*. PhD thesis, Uni-GH Siegen, 1995. FOMAAS Bericht Nr. T07-03.95.

Atanu Sengupta and Tapan Kumar Pal. On comparing interval numbers. *European Journal of Operational Research*, 127(1):28–43, 2000. ISSN 0377-2217. doi: 10.1016/S0377-2217(99)00319-7.

A. B. Shaibu and Byung Rae Cho. Another view of dual response surface modeling and optimization in robust parameter design. *The International Journal of Advanced Manufacturing Technology*, 41(7-8):631–641, April 2009. ISSN 0268-3768 (Print) 1433-3015 (Online). doi: 10.1007/s00170-008-1509-2. URL http://www.springerlink.com/content/78527t7717105475/.

Srinivasa R. Shankar and David G. Jansson. A generalized methodology for evaluating manufacturability. In Hamid R. Parsaei and William G. Sullivan, editors, *Concurrent Engineering, Contemporary Issues and Modern Design Tools*, chapter 13, pages 248–263. Chapman & Hall, 1. edition, 1993.

E. Shehab and H. Abdalla. An intelligent knowledge-based system for product cost modelling. *The International Journal of Advanced Manufacturing Technology*, 19(1):49–65, January 2002. ISSN 0268-3768 (Print) 1433-3015 (Online). doi: 10.1007/PL00003967. URL http://www.springerlink.com/content/vwmxrqt9raqbmyrw/.

I. Shigematsu, Y.J. Kwon, K. Suzuki, T. Imai, and N. Saito. Joining of 5083 and 6061 aluminum alloys by friction stir welding. *Journal of Materials Science Letters*, 22:353–356, 2003.

C.J. Shih and H.W. Lee. Modified double-cuts approach in 25-bar and 72-bar fuzzy truss optimization. *Computers & Structures*, 84(29-30):2100–2104, November 2006. doi: 10.1016/j.compstruc.2006.08.017. URL http://dx.doi.org/10.1016/j.compstruc.2006.08.017.

C.J. Shih, C.C. Chi, and J.H. Hsiao. Alternative α-level-cuts methods for optimum structural design with fuzzy resources. *Computers & Structures*, 81(28-29):2579–2587, November 2003. doi: 10.1016/S0045-7949(03)00331-6. URL http://dx.doi.org/10.1016/S0045-7949(03)00331-6.

S.A. Smith, T. Krishnamurthy, and B.H. Mason. Optimized vertex method and hybrid reliability. In *Proceedings of 43rd AIAA/ASME/ASCE/AHS/ASC Structures, Structural Dynamics and Materials Conference*, Denver, CO, USA, April 22-25 2002. URL http://hdl.handle.net/2060/20030005805. AIAA-2002-1465.

George Stefanou. The stochastic finite element method: Past, present and future. *Computer Methods in Applied Mechanics and Engineering*, 198(9-12):1031–1051, 2009. ISSN 0045-7825. doi: 10.1016/j.cma.2008.11.007. URL http://www.sciencedirect.com/science/article/B6V29-4TYR04S-4/2/302f17bbb1353d59667a1677993c806b.

P. Subasic and M. Nakatsuyama. A new representational framework for fuzzy sets. In *Fuzzy Systems, 1997., Proceedings of the Sixth IEEE International Conference on*, volume 3, pages 1601–1606, Jul 1997. doi: 10.1109/FUZZY.1997.619780.

Bala L. Subramaniam and Karl T. Ulrich. Producibility analysis using metrics based on physical process models. *Research in Engineering Design*, 10(4):210–225, December 1998. ISSN 0934-9839 (Print) 1435-6066 (Online). doi: 10.1007/s001639870002. URL http://www.springerlink.com/content/n1fb3ggam52h2fvq/.

Bruno Sudret and Armen Der Kiureghian. Stochastic finite element methods and reliability: a state-of-the-art report. Technical report, Dept. of Civil and Environmental Engineering, University of California, Berkeley, 2000. URL http://nisee.berkeley.edu/elibrary/Text/1293213. UCB/SEMM-2000/08.

J. Swiostek. *Erweiterung der Prozessgrenzen beim Strangpressen von Magnesiumlegierungen der AZ-Reihe durch das hydrostatische Strangpressverfahren*. PhD thesis, Institut für Werkstoffkunde - Technische Universität Hamburg-Harburg, 2008. Helmholtz Gemeinschaft GKSS 2008/5, ISSN 0344-9629.

Fulvio Tonon, Alberto Bernardini, and Isaac Elishakoff. Hybrid analysis of uncertainty: probability, fuzziness and anti-optimization. *Chaos, Solitons & Fractals*, 12(8):1403–1414, June 2001. doi: {10.1016/S0960-0779(00)00103-X}. URL http://dx.doi.org/10.1016/S0960-0779(00)00103-X.

Andreas Trautmann and Michael Zäh. Laser bifocal hybrid welding of aluminum. *Advanced Materials Research*, 10:65–79, 2006. doi: 10.4028/www.scientific.net/AMR.10.65.

Nikos Tsangarakis and Barmac Taleghani. Mechanical properties of several magnesium and aluminum composites. Technical Report ARL-TR-34, Army Research Laboratory, 1992. URL http://www.dtic.mil/cgi-bin/GetTRDoc?AD=ADA262481&Location=U2&doc=GetTRDoc.pdf.

Yiannis Tsompanakis, Nikkos D. Lagaros, and Manolis Papadrakakis, editors. *Structural Design Optimization Considering Uncertainties: Vol.1., Structures & Infrastructures Series*. Taylor & Francis, 1 edition, 3 2008. ISBN 9780415452601.

P. Venkateswaran, Z.H. Xu, X. Li, and A.P. Reynolds. Determination of mechanical properties of almg alloys dissimilar friction stir welded interface by indentation methods. *Journal of Materials Science*, 44:4140–4147, 2009. doi: 10.1007/s10853-009-3607-4.

C. Wagner and H. Hagras. zslices towards bridging the gap between interval and general type-2 fuzzy logic. In *Fuzzy Systems (FUZZ-IEEE) 2008*, pages 489–497, Hong Kong, June 1–6, 2008. doi: 10.1109/FUZZY.2008.4630413.

William P. Wagner and Michael L. Zubey. Knowledge acquisition for marketing expert systems based upon marketing problem domain characteristics. *Marketing Intelligence & Planning*, 23(4):403–416, 2005. ISSN 0263-4503. doi: 10.1108/02634500510603500.

K.G. Watkins. Laser welding of magnesium alloys. In *Magnesium Technology 2003: Proceedings of the jointly sponsored by the Magnesium Committee of the Light Metals Division (LMD) and the Solidification Committee of the Materials Processing and Manufacturing Division of The Minerals, Metals & Materials Society (TMS) with the International Magnesium Association held during the 2003 TMS Annual Meeting*, San Diego, USA, March 2–6 2003. URL http://iweb.tms.org/Mg/magtech2003/153.pdf/.

Erich Wehrle. Robust structural optimization using possibility theory to model uncertainties. Master's thesis, Institute for Lightweight Structures - Technische Universität München, 2008. TUM–MW65/0772–MT.

K.A. Weidenmann, C. Fleck, V. Schulze, and D. Löhe. Materials selection process for compound-extruded aluminium matrix composites. *Advanced Engineering Materials*, 7(12): 1150–1155, 2005a.

K.A. Weidenmann, M. Schomäcker, E. Kerscher, D. Löhe, and M. Kleiner. Composite extrusion of aluminium matrix specimens reinforced with continuous ceramic fibres. *Light Metal Age*, 63(5):6–10, 2005b.

K. Weinert, J. Fleischer, A. E. Tekkaya, M. Zäh, and M. Schikorra. Flexible manufacturing of lightweight frame structures. *Advanced Materials Research*, 43:1–174, 2008. doi: 10.4028/www.scientific.net/AMR.43. Phase II: Integration.

Kristin L. Wood, Kevin N. Otto, and Erik K. Antonsson. Engineering design calculations with fuzzy parameters. *Fuzzy Sets and Systems*, 52(1):1–20, 1992. ISSN 0165-0114. doi: http://dx.doi.org/10.1016/0165-0114(92)90031-X.

D. Wu and J. M. Mendel. Enhanced karnik-mendel algorithms. *IEEE Transactions on : Accepted for future publication Fuzzy Systems*, 2008. ISSN 1063–6706. doi: 10.1109/TFUZZ.2008.924329.

Dongrui Wu and Jerry M. Mendel. Uncertainty measures for interval type-2 fuzzy sets. *Information Sciences*, 177(23):5378–5393, 2007. ISSN 0020-0255. doi: 10.1016/j.ins.2007.07.012.

Jiuchun Yan, Zhiwu Xu, Zhiyuan Li, Lei Li, and Shiqin Yang. Microstructure characteristics and performance of dissimilar welds between magnesium alloy and aluminum formed by friction stirring. *Scripta Materialia*, 53:585–589, 2005. doi: 10.1016/j.scriptamat.2005.04.022.

Ji-Long Yin, Da-Yong Li, Ying-Chung Wang, and Ying-Hong Peng. Knowledge discovery from finite element simulation data. In *Proceedings of 2004 International Conference on Machine Learning and Cybernetics*, volume 3, pages 1335–1340, Shanghai, China, August 6-29 2004. doi: 10.1109/ICMLC.2004.1381980.

Ji-Long Yin, Da-Yong Li, and Ying-Hong Peng. Knowledge acquisition from metal forming simulation. *The International Journal of Advanced Manufacturing Technology*, 29(3-4):279–286, June 2006. ISSN 0268-3768 (Print) 1433-3015 (Online). doi: 10.1007/s00170-005-2521-4. URL http://www.springerlink.com/content/f026j48m8q227265/.

Jun Sun Yoo. *Adaptation of soft computing methods in multidisciplinary and structural optimization*. PhD thesis, Rensselaer Polytechnic Institute - Troy, New York, 2000. URL http://nbn-resolving.de/urn/resolver.pl?urn:nbn:de:bvb:91-diss20061108-1512163206.

Byeng Dong Youn, K.K. Choi, Liu Du, and David Gorsich. Integration of possibility-based optimization to robust design for epistemic uncertainty. In *Proceedings of 6th World Congresses of Structural and Multidisciplinary Optimization*, Rio de Janeiro, Brazil, May 30 - June 3 2005. URL http://www.wcsmo6.org/papers/442.pdf.

Lotfi Asker Zadeh. Fuzzy sets. *Information and Control*, 3(8):338–353, 1965.

Michael Zäh, Markus Ruhstorfer, Sonja Huber, and Michael Kronthaler. Fügezentrum zur Integration dreidimensionaler Naht- und Stogeometrien in Aluminiumtragwerksstrukturen. In A. Erman Tekkaya, Horst Baier, Dirk Biermann, Detlef Löhe, Volker Schulze, Michael Zäh, and Michael Marré, editors, *Integration von Umformen, Trennen und Fügen für die flexible Fertigung von leichten Tragwerkstrukturen; Zwischenbericht Phase 2; 1. Januar 2007 - 31. Dezember 2008*, pages 149–180. VDI Verlag, 2009. ISBN 978-3-18-366802-1. Fortschritt-Berichte Fertigungstechnik, Band Nr. 668.

Michael F. Zäh, Paul Gebhard, Sonja Huber, and Markus Ruhstorfer. Bifocal hybrid laser beam welding and friction stir welding of aluminium extrusion components. *Advanced Materials Research*, 43:69–80, 2008. doi: 10.4028/www.scientific.net/AMR.43.69. Flexible Manufacture of Lightweight Frame Structures - Phase II: Integration.

R. Zettler, A. da Silva, S. Rodrigues, A. Blanco, and J. dos Santos. Dissimilar Al to Mg alloy friction stir welds. *Advanced Engineering Materials*, 8(5):415–421, 2006. doi: 10.1002/adem.200600030.

Jun Zhou and Zissimos P. Mourelatos. Design under uncertainty using a combination of evidence theory and a bayesian approach. In *3rd International Workshops on Reliable Engineering Computing*, Savannah, GA, USA, February 20-22 2008. URL http://www.gtsav.gatech.edu/workshop/rec08/documents/REC2008Proceedings.pdf.